An Investigation of the Kinetics of Thermophilic Microbial Ferrous Iron Oxidation in Continuous Culture

By

Giles E. Searby

Thesis presented for the Degree of
DOCTOR OF PHILOSOPHY
In the Department of Chemical Engineering
UNIVERSITY OF CAPE TOWN
December 2006

An Investigation of the Kinetics of Thermophilic Microbial Ferrous Iron Oxidation in Continuous Culture

Giles Edward Searby

Department of Chemical Engineering, University of Cape Town, Private Bag Rondebosch, 7700

November 2006

Abstract

The potential of thermophilic micro-organisms to bioleach primary copper sulfides and other minerals has led to the need to develop a fundamental understanding of the mechanistic processes involved. Ferrous iron oxidation has been established as a key step in bioleaching and is understood to be achieved largely by microbial action. The objective of this work was to determine an appropriate set of kinetic expressions that describe the rates of microbial growth and ferrous iron oxidation of a thermophilic archaeal culture grown in continuous culture on ferrous iron between 60 and 80°C.

A review of rate equations developed to describe mesophilic ferrous iron oxidation established that the system could be modelled by adopting an unstructured approach that did not require in-depth knowledge of the precise metabolic pathway. This approach allows the development of models that are not species-specific.

Sterile tests showed that the competing chemical oxidation reaction by molecular oxygen was significant at elevated temperatures and high ferrous iron concentrations. The abiotic iron oxidation rate was found to be second order with respect to the ferrous iron concentration and this rate was deducted from the overall measured rate in the ensuing microbial investigation.

The ferrous iron utilisation rate was determined, via a degree-of-reduction balance, from the measured change in the oxygen and the carbon dioxide concentration in the off-gas stream. The observed kinetics were described by a Michaelis-Menten-type rate equation, describing the specific rate of iron utilisation as a function of the ferric/ferrous-iron ratio, coupled to a yield expression describing energy utilisation in terms of a maximum microbial yield and a maintenance coefficient. The resultant model was able to predict growth rate, iron utilisation rate and cell concentration over the range of temperatures and solution conditions tested.

DECLARATION

I declare that this thesis is my own, unaided work. It is being submitted for the Degree of Doctor of Philosophy in the University of Cape Town. It has not been submitted before for any degree or examination in any other university.

Signed by candidate

23rd day of December 2006

Summary

The potential of various thermophilic archaeal species to bioleach primary copper sulfides and other minerals has led to the need to develop a fundamental understanding of the mechanistic processes involved. Ferrous iron oxidation has been established as a key step in bioleaching and is understood to be largely achieved by microbial action. The objective of this work was to formulate an appropriate rate equation to describe the kinetics of microbial ferrous iron oxidation under thermophilic bioleaching conditions. This was achieved by critically reviewing rate equations proposed for mesophilic iron oxidation kinetics and by applying that knowledge to an experimental investigation of thermophilic microbial iron oxidation performed in continuous culture.

A review of bioleaching literature established the existence of a number of thermophilic ferrous-iron-oxidising micro-organisms. These micro-organisms are archaea, phylogenetically distinct from the bacteria that predominate at lower temperatures, yet performing the same role with similar thermodynamic constraints.

Parameters influencing the rate of oxidation were discussed with respect to their observed effect on mesophilic iron oxidation systems and their implied effect on thermophilic ferrous iron oxidation. The concentrations of ferrous and ferric iron and the ratio of the two were found to be key parameters in controlling the rate of growth and oxidation. These findings are in accord with the chemiosmotic mechanism proposed for energy assimilation. Other parameters of interest were O_2 and CO_2 availability, pH, and temperature.

A number of unstructured models have been developed to describe mesophilic microbial ferrous iron oxidation. The nature of these models, based on following the macroscopic oxidation reaction and transfer of energy to a generalised growth reaction rather than individual biochemical pathways allow the models to be transferred to the thermophilic regime. The unstructured model proposed involves the two macroscopic reactions of iron oxidation and microbial growth, generating and consuming energy respectively. This is best described in terms of a Michealis-Menten-form rate expression for the specific rate of iron oxidation, coupled to the rate of growth via some expression of the growth yield, energy utilisation, efficiency and cell maintenance.

Kinetic data and rate equations for the microbial oxidation of ferrous iron under mesophilic conditions were re-evaluated. Conversion factors were collated from sources published in the literature and were used to convert all kinetic constants and data to a common basis, evaluating all

rates in terms of moles per hour, and evaluating cell concentrations in terms of moles of carbon present. This allowed direct comparison of published results, both in terms of the kinetic data presented and the capacity of each rate equation to predict reaction rates over a wide range of conditions.

This comparison showed that the mode of operation chosen in the design of the experiments influenced the results produced. Studies have been done using many different modes of operation: including continuous stirred tank reactors, batch experiments in both stirred reactors and shake flasks, oxygen uptake experiments and controlled potential experiments. The disparate results of continuous and discontinuous experiments both in terms of the influence of reaction conditions and of the kinetic constants generated for similar models confirms that batch experiments are an unreliable way of generating kinetic data as the rapid change in solution conditions does not allow for a true response from the organisms.

While a large number of rate equations have been presented for microbial ferrous iron oxidation, the majority of results from studies in continuous culture have been fitted to relatively simple unstructured kinetic models. The data scatter in the results further discourages attempts to fit more complicated models.

Analysis of the linear transforms of common simple rate equations shows similarities in the response to changes in both the ferrous iron concentration and the ferric/ferrous-iron ratio. This similarity means that the goodness of fit to a set of data obtained under a single set of experimental conditions does not imply the appropriateness of the model, and cannot be used to choose between models. Further analysis of transforms of the continuous data over a range of total iron concentrations shows that microbial ferrous iron oxidation is best described by a rate equation derived from Michaelis-Menten reaction kinetics with competitive product inhibition, and that this rate equation may be simplified to a Monod-form equation in terms of the ferric/ferrous-iron ratio at total iron concentrations found in commercial bioleaching stirred tank reactor systems.

The competing abiotic oxidation of ferrous iron by molecular oxygen was most often deemed negligible under conditions of mesophilic temperatures, ambient pressure and low pH. As chemical reaction rates increase exponentially with increasing temperature, this assumption was considered unwise in the thermophilic temperature regime and the contribution of the abiotic reaction to thermophilic ferrous iron oxidation was investigated. Abiotic ferrous iron oxidation was found to be significant at high ferrous iron concentrations only, corresponding to conditions in the biotic

$$-r_{Fe^{2+}}\Big|_{Bio} = -r_{Fe^{2+}}\Big|_{Total} - k_0[Fe^{2+}]^2 e^{-\frac{E_{a,1}}{RT}} \quad [5.3]$$

Where $k_0 = 7.58 \times 10^5$ mM $Fe^{2+}.h^{-1}$
$E_{a,1} = 65.5$ kJ.mol^{-1}

The microbial oxidation of ferrous iron by a thermophilic archaeal culture was studied in continuous culture in a well-mixed, well-aerated, pH-controlled system (pH 1.5) over a temperature range of 60 to 80°C, at dilution rates between 0.015 and 0.09h^{-1} and at ferrous iron concentrations between 0.0525 and 0.210mM. The experiments were performed in continuous stirred tank reactors, stirred at 400rpm and sparged with air at between 300 and 400mL.min^{-1}. The microbial culture used was a mixed culture taken from a chalcopyrite concentrate test column, which was then grown for an extended period on ferrous sulphate to allow the system to select its dominant iron oxidising culture before starting kinetic studies. The dominant iron oxidiser was later identified to be a *Metallosphaera* species, most likely *M. hakonensis*.

The reaction kinetics were followed by analysis of the off-gas oxygen and carbon dioxide concentrations and the measured redox potential. The rate of ferrous iron oxidation was determined from the gas utilisation rates via the degree-of-reduction balance. A comparison of this ferrous iron oxidation rate with rates determined from the iron mass balance showed good agreement, confirming the validity of the methodology.

The observed kinetics could be described by a rate equation describing the specific iron utilisation rate in terms of the ferric/ferrous-iron ratio (Boon, 1996), coupled to a yield expression in terms of a maximum yield and a constant maintenance coefficient (Pirt, 1965).

$$q_{Fe^{2+}} = \frac{q_{Fe^{2+}}^{max}}{1 - K_{Fe^{2+}} \frac{[Fe^{3+}]}{[Fe^{2+}]}} \quad [2.14]$$

$$q_{Fe^{2+}} = -\frac{\mu}{Y_{SX}^{max}} + m_S \quad [2.33]$$

The effect of temperature on the system could be described by simple functions of the kinetic constants determined for each data set. Both the maximum specific iron utilisation rate, q_{Fe2+}^{max}, and the maintenance coefficient, m_S, increased exponentially with temperature and could be described by Arrhenius functions, whilst K_{Fe2+} and Y_{SX}^{max} could be replaced by linear functions of temperature. This allows Equations 2.14 and 2.33 to be replaced by

$$q_{Fe^{2+}} = \frac{q_0 e^{-E_{a2}/RT}}{1 + (aT - b)\frac{[Fe^{3+}]}{[Fe^{2+}]}} \quad [6.11]$$

$$q_{Fe^{2+}} = \frac{\mu}{Y_{SX}^{max}{}_0 - cT} + m_{S0} e^{-E_{a3}/RT} \quad [6.13]$$

where $q_0 = 2.22 \times 10^9$ molFe^{2+}.molC^{-1}.h^{-1}
$E_{a2} = 48.0$ kJ.mol^{-1}
$a = 1.39 \times 10^{-3}$ T^{-1}
$b = 0.457$
$c = 1 \times 10^{-4}$ T^{-1}
$Y_{SX}^{max}{}_0 = 0.0418$
$m_{S0} = 7.97 \times 10^7$ molFe^{2+}.molC^{-1}.h^{-1}
$E_{a3} = 51.9$ kJ.mol^{-1}

producing a model that describes thermophilic microbial ferrous iron oxidation as a function of the ferric/ferrous-iron ratio over a range of temperature from 60-80°C.

Acknowledgements

I would like to take this opportunity to thank my supervisor Prof Geoff Hansford for his boundless enthusiasm and wise advice, and for giving me this life-changing experience.

I would like to acknowledge the National Research Foundation, BiominE, Prof Geoff Hansford and Prof Sue Harrison for the generous funding that made this work possible.

Thank you to Dr Rob van Hille and Dr Nicolette Coram for their expertise in identifying the culture used in this investigation.

Thanks are also due to Peter Dobias and Joachim Macke in the Mechanical workshop for their prompt and craftsman-like repairs every time an impeller shaft seized or baffle dissolved in front of my eyes, and to Helen Divey in the Main Lab, for always knowing what to do with endless buckets of waste.

Thank you to all denizens of the former Biomin Lab for the camaraderie and long discussions on the road to understanding bioleaching, and to the inhabitants of the new shiny Fe/S lab for taking the torch further.

Thank you to my friends and family for your love, unwavering support, and remarkable restraint in biting back the question "Is it finished yet?" for so long.

giles

To mon petit chou,

for life isn't worth living without a healthy supply of leafy greens...

Publication Declaration

Searby GE, Hansford GS. 2003. The Kinetics of Thermophilic Ferrous Iron Oxidation. In: Proceedings of IBS 2003: 15th International Biohydrometallurgy Symposium; Athens, Greece; September 2003

Ojumu TV, Petersen J, Searby GE, Hansford GS. 2006. A review of rate equations proposed for microbial ferrous-iron oxidation with a view to application to heap bioleaching. Hydrometallurgy 83(1-4): 21-28.

Table of Contents

List of Figures

List of Tables

Nomenclature

a	constant in Equation 6.11	K^{-1}
b	constant in Equation 6.11	dimensionless
b	constant in Ratkowsky equation	$h^{-0.5}.K^{-0.5}$
c	constant in Equation 6.13	mol C.(mol Fe^{2+}.K)$^{-1}$
C_X	concentration of bacteria	mM C.
D	dilution rate	h^{-1}
E	redox potential of the solution (Pt-Ag/AgCl)	mV
E^0	standard electrode potential	mV
E_a	activation energy	$kJ.mol^{-1}$
F	Faraday's constant	$C.mol^{-1}$
$[Fe]_T$	total iron concentration	mM Fe
$[Fe^{2+}]$	concentration of ferrous iron	mM Fe^{2+}
$[Fe^{2+}]_{IN}$	concentration of ferrous iron entering a continuous reactor	mM Fe^{2+}
$[Fe^{2+}]_{OUT}$	concentration of ferrous iron leaving a continuous reactor	mM Fe^{2+}
$[Fe^{2+}]_{threshold}$	threshold ferrous iron concentration	mM Fe^{2+}
$[Fe^{3+}]$	concentration of ferric iron	mM Fe^{3+}
k	rate constant for abiotic ferrous iron oxidation	(mM Fe^{2+})$^{-1}$.h^{-1}
k_e	frequency factor for abiotic ferrous iron oxidation	(mM Fe^{2+})$^{-1}$.h^{-1}
K_{Fe2+}	ferrous-iron based kinetic constant in Equation 2.14	dimensionless
K_i	Michaelis-Menten product (ferric-iron) inhibition constant	mM Fe^{3+}
k_La	overall mass transfer coefficient	h^{-1}
K_m	Monod equation substrate (ferrous-iron) saturation constant	mM Fe^{2+}
K_s	Michaelis-Menten substrate affinity constant	mM Fe^{2+}
K_{Si}	Michaelis-Menten substrate (ferrous iron) inhibition constant	mM Fe^{2+}
m	mass	kg
m_s	maintenance coefficient	mol Fe^{2+}.(mol C)$^{-1}$.h^{-1}
m_{so}	frequency factor for maintenance	mol Fe^{2+}.(mol C)$^{-1}$.h^{-1}
m_s^v	growth-rate-dependent maintenance coefficient	mol Fe^{2+}.(mol C)$^{-1}$.h^{-1}
ORP	oxidation reduction potential (redox)	mV
OTR	oxygen transfer rate	mM O_2.h^{-1}
OUR	oxygen utilisation rate	mM O_2.h^{-1}
p_{O2}	partial pressure of oxygen	atm
q_{i0}	frequency factor for specific iron utilisation rate	mol Fe^{2+}.(mol C)$^{-1}$.h^{-1}
q_{Fe2+}	bacterial specific ferrous iron utilisation rate	mol Fe^{2+}.(mol C)$^{-1}$.h^{-1}
$q_{Fe^{2+}}^{max}$	maximum bacterial specific ferrous iron utilisation rate	mol Fe^{2+}.(mol C)$^{-1}$.h^{-1}
q_{O2}	bacterial specific oxygen utilisation rate	mol O_2.(mol C)$^{-1}$.h^{-1}
$q_{O_2}^{max}$	maximum bacterial specific oxygen utilisation rate	mol O_2.(mol C)$^{-1}$.h^{-1}
R	universal gas constant	$kJ.K^{-1}.mol^{-1}$
R^2	correlation coefficient	dimensionless

r_i	rate of production of compound i	mM $i.h^{-1}$
$-r_i$	rate of utilisation of compound i	mM $i.h^{-1}$
$-r_{CO2}$	carbon dioxide utilisation rate	mM $CO_2.h^{-1}$
$-r_{Fe2+}$	ferrous-iron utilisation rate	mM $Fe^{2+}.h^{-1}$
$-r_{Fe2+}\|_{abiotic}$	contribution of abiotic iron oxidation to the overall rate	mM $Fe^{2+}.h^{-1}$
$-r_{Fe2+\|Bio}$	contribution of microbial iron oxidation to the overall rate	mM $Fe^{2+}.h^{-1}$
$-r_{Fe2+\|total}$	the overall rate of iron oxidation	mM $Fe^{2+}.h^{-1}$
$-r_{O2}$	oxygen utilisation rate	mM $O_2.h^{-1}$
r_X	biomass production rate	mM $C.h^{-1}$
S	Substrate concentration	mM
SSE	sum of the squared error	dimensionless
T	absolute temperature	K
T_{opt}	optimum temperature	K
V	volume	m^3
x_i	mole fraction of component i	dimensionless
Y_{SX}	bacterial yield on substrate (ferrous iron)	mol $C.(mol\ Fe^{2+})^{-1}$
Y_{SX}^{max}	maximum bacterial yield on substrate (ferrous iron)	mol $C.(mol\ Fe^{2+})^{-1}$
$Y_{SX}^{max}{}_{II}$	constant in Equation 6.13	mol $C.(mol\ Fe^{2+})^{-1}$
y_{mean}	mean value of data set y	-
y_{reg}	predicted value of y determined by regression	-
z	number of electrons in a reaction	-

Greek Symbols

γ_i	degree-of-reduction of component i	-
μ	specific rate of growth	h^{-1}
μ_d	specific rate of cell death	h^{-1}
μ_{max}	maximum specific rate of cell growth	h^{-1}
Φ	volumetric gas flow rate	$L.h^{-1}$
ρ	density	$kg.m^{-3}$
τ_{res}	residence time	h

Chapter 1

Introduction

Bioleaching is industrially recognised as a pre-treatment for refractory gold ores and for the commercial processing of secondary copper sulfide ores. Bioleaching of the primary copper sulfide, chalcopyrite, has proved unsuccessful, with slow leach rates and incomplete extraction (Olson *et al.*, 2003). A number of different technologies have been developed to best exploit this process for different grades of mineral, from stirred tank reactor systems for finely milled flotation concentrates, to carefully engineered heaps for low grade concentrates and whole ores, to irrigated mine dumps for marginal-grade run-of-mine ores (Brierley & Brierley, 2001).

Bioleaching is understood to involve a number of key intermediate steps as illustrated in Figure 1: a primary chemical leach by acid and ferric iron, producing ferrous iron and releasing the sulfide mineral as metal and a variety of reduced sulfur compounds. This is followed by the microbial oxidation of ferrous iron to ferric iron and the microbial oxidation of the reduced sulfur compounds to elemental sulfur or to sulfate (Boon, 1996; Schippers & Sand, 1999). It can be seen that bioleaching micro-organisms play an important role in maintaining the concentration of the primary leaching agent and thereby promoting continued leaching.

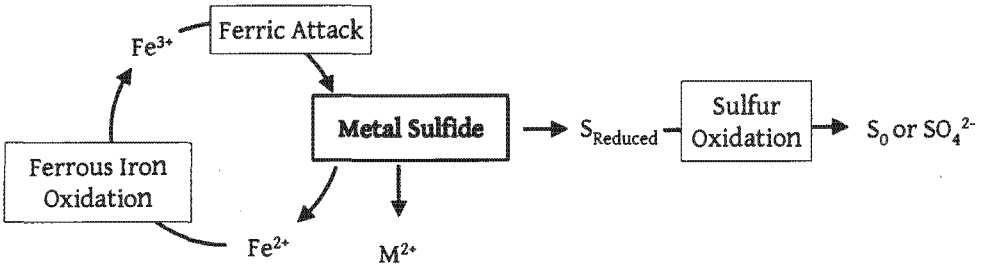

Figure 1.1 A simple diagram of the key mechanistic sub-processes in bioleaching

The microbial oxidation of ferrous iron is thus an integral part of the bioleaching process, and a fundamental understanding of the mechanism and the kinetics of the reaction will provide a basis for the development of a predictive model for bioleaching to aid further process design and optimisation.

Conventional bioleaching is facilitated by acidophilic iron and sulfur oxidising micro-organisms that operate at ambient temperatures (mesophiles). As the bioleaching reaction is exothermic, the poor heat transfer in bioleach heaps causes the core temperature to rise beyond the maximum temperature that the micro-organisms could withstand (Brierley, 1978). This, along with the recalcitrance of chalcopyrite to effective bioleaching at ambient temperatures, led to the investigation of the potential of selected thermophilic micro-organisms, micro-organisms that are capable of living and thriving at extraordinarily high temperatures.

Table 1.1 Definition of temperature ranges used in this work.

Temperature Range	Designation
< 45 °C	mesophiles
45-60 °C	moderate thermophiles
60-80 °C	thermophiles
> 80 °C	extreme thermophiles

Comparison of chalcopyrite bioleaching with mesophilic, moderately thermophilic, and extremely thermophilic cultures indicated that the efficiency of copper extraction increased proportionately with temperature up to 80°C (Norris *et al.*, 1990; Norris & Owen, 1993). This has produced the need to elucidate the mechanism and kinetics of thermophilic bioleaching. BHP Billiton's BioCop™ process has already shown that thermophilic bioleaching of copper sulfide mineral concentrates is commercially viable (Batty & Rorke, 2006), however this commercial exploitation would be greatly facilitated by the development of a fundamental understanding of the mechanism and the kinetics of a thermophilic bioleaching system: the chemical and biochemical reactions that occur, the roles and identities of the various micro-organisms involved and how they all combine. This understanding is emerging, but requires further elucidation of mechanism and an evaluation of kinetic parameters and rate equations.

Preliminary investigations indicate that the multiple sub-process mechanism is still appropriate at elevated temperature and hence that microbial ferrous iron oxidation is still a crucial sub-process.

Many rate equations and kinetic models have been proposed for mesophilic ferrous iron oxidation, deduced from numerous experiments conducted under a range of experimental conditions, using a

variety of different techniques. Little kinetic work has yet been performed in thermophilic iron systems, and few kinetic models have been proposed.

1.1 Objectives of this Study

This investigation was undertaken to establish a description of the kinetics of the oxidation of ferrous iron under thermophilic bioleaching conditions, with a view to developing a model of the process that can be incorporated later into a general model of thermophilic bioleaching.

This was achieved by

- critically reviewing rate equations proposed for mesophilic ferrous iron oxidation, and establishing similarities and differences between the results published and
- performing a rigorous investigation of the kinetics of ferrous iron oxidation by a thermophilic bioleaching culture, and proposing an appropriate rate equation for the process based on the experimental results observed and the knowledge gleaned from the examination of the mesophilic results.

1.2 Scope and Limitations

This investigation was focussed on the oxidation of ferrous iron, and did not include the possible interactions of iron and sulfur-oxidising species. The iron oxidation and growth kinetics were examined in continuous culture using an originally mixed thermophilic culture, grown on a chalcopyrite concentrate. The system was allowed ample time to select for its dominant iron oxidising species but no attempt was made to maintain sterility, the low pH and high temperature being considered sufficient to prevent contamination from the surroundings. The system was studied at temperatures between 60 and 80°C, running separate reactors at constant temperature and varying the feed flow rate to produce different steady state ferric and ferrous iron concentrations.

1.3 Thesis Outline

This thesis will start with a review of the relevant literature. This will be introduced by a brief description of the historical development of bioleaching, from its origins to current industrial practices and further to processes under development. The current understanding of bioleaching will be established, including the reaction mechanism, and characteristics of the relevant micro-organisms, highlighting the central role of microbial ferrous iron oxidation. Factors influencing the rate of ferrous iron oxidation will be discussed, emphasising areas that may be more significant at

elevated temperature. The extent of research reported on thermophilic ferrous iron oxidation will also be discussed. This will be followed by a brief history describing the development of models for microbial iron oxidation. While this will be focussed mainly on mesophilic iron oxidation by *Acidithiobacillus ferrooxidans*, as the majority of previous kinetic studies have been performed on this species, the resultant models are unstructured and hence should be applicable or at least adaptable to describe the kinetics of other iron oxidisers.

This will be followed in Chapter 3 by a critical review of published kinetic data and rate equations, to attempt to reconcile the different continuous data presented and the equations proposed.

The experimental methodology followed, including a description of how microbial kinetics can be monitored by off-gas analysis, will be presented in Chapter 4.

The experimental results are presented and discussed in Chapters 5 and 6. The contribution of abiotic ferrous iron oxidation is studied in Chapter 5, and the growth and oxidation data from the microbial investigation in Chapter 6. The data was fitted to the most appropriate model available, following the discussion of models in Chapters 2 and 3, and the model and its associated constants will also be presented here.

Chapter 7 will bring together the pertinent questions raised and answers produced in the course of this investigation and will present the conclusions that can be drawn from this work, including the value of this investigation to the overall quest to fully understand bioleaching.

Chapter 2

Literature Review

The purpose of this review is to establish what is known about iron oxidation by acidophilic microbial cultures, and to use this knowledge as a framework upon which a model for thermophilic ferrous iron oxidation can be built.

Microbial iron oxidation will be placed in context by a brief overview of bioleaching; industrial applications, the micro-organisms involved in the process and the current understanding of the mechanisms proposed for the bioleaching of sulfide minerals. Little is known about how any micro-organism other than *Acidithiobacillus ferrooxidans* oxidises ferrous iron, and so the current understanding of the mechanism of mesophilic ferrous iron oxidation and the development of mesophilic microbial ferrous iron oxidation models have been reviewed in order to determine the most useful models and to understand the assumptions that were required to produce them: biochemical mechanisms; the influence of physico-chemical parameters and microbial physiology.

These assumptions will be re-evaluated in terms of thermophilic iron-oxidising archaea and the results used to determine whether the models and methodologies used to describe mesophilic systems can be transferred to the thermophiles studied here.

2.1 Background

Bioleaching is a natural process that has been found to have commercial application. Whilst it is often referred to as an emerging technology, it has been used, if unwittingly, for the extraction of metals for millennia. Bioleaching was employed in China before the start of the current era (Rossi, 1990), copper was extracted from the Rio Tinto mine, Spain, in Roman times, and actively heap leached during and after the Moorish conquest. Large amounts of copper have also been leached

from Falun, Sweden since 1687 (Ehrlich, 2001). All of these processes were run without any understanding of the role of microbial action in the leaching process.

Four configurations are generally used in modern bioleaching; dump leaching, heap leaching, *in-situ* leaching and stirred tank reactors. In dump and heap leaching, mineral is piled in heaps and irrigated with leach liquor, leaching is allowed to continue relatively uncontrolled within the heaps and dissolved metals are recovered from the leachate from the bottom of the heap. In *in-situ* leaching, the leach liquor is pumped into a blast-fractured ore body and then pumped out and metals recovered. In stirred tank systems, finely-milled mineral concentrates are leached in agitated, aerated, temperature-controlled reactors.

The modern exploitation of bioleaching began in the 1950s with the dump leaching of sub-marginal-grade run-of-the-mine material from the Kennecott Copper Mine (Brierley & Brierley, 2001). Early dumps were simply irrigated waste rock heaps, not optimised to encourage microbial activity, leading to slow reaction rates. The low costs of dump leaching make it useful for scavenging copper from material of such low grade that it cannot be obtained economically by any other method (Brierley & Brierley, 2001).

Heap leaching is a more structured approach to bioleaching, in which milled mineral is agglomerated and stacked on impermeable pads, often with active aeration built into the heap. The material is stacked evenly to ensure uniform fluid and heat flows through the heap. The first bioheap leach process was initiated at Lo Aguirre in 1980 by SML (Sociedad Minera Pudahuel) using a thin layer leaching process to leach mixed and secondary copper sulfides (Bustos *et al.*, 1993). Another example is the Quebrada Blanca project in Chile, that processes 17 300 tonnes ore/day, the ore is crushed, agglomerated with sulfuric acid and hot water and stacked on drainage pads in 6 - 6.5 m heaps and aerated (Brierley & Brierley, 2001). Further examples are given in Table 2.1.

Table 2.1 Industrial examples of chalcocite (Cu_2S) heap leaching operations (adapted from Olson *et al.*, 2003).

Plant and Location	Throughput tonnes ore/day	Years in Operation
Lo Aquirre, Chile	16000	1980-1996
Mt Leyson, Australia	1370	1992-1997
Cerro Colorado, Chile	16000	1993-
Girilambone, Australia	2000	1993-
Ivan-Zar, Chile	1500	1994
Quebrada Blanca, Chile	17300	1994-
Andacollo, Chile	10000	1996-
Dos Amigos, Chile	3000	1996-

Plant and Location	Throughput tonnes ore/day	Years in Operation
Cerro Verde, Peru	32000	1996-
Zaldivar, Chile	20000	1998-
S & K Copper, Myanmar	18000	1998-
Equatorial Tonopah, Nevada, USA	24500	2000-2001

Heap leaching is not restricted to copper leaching. Newmont Mining has run demonstration scale heaps for the heap biooxidation of refractory gold ores (Brierley, 1997), and ran a commercial scale operation at Quarry Mine, Carlin, Nevada (Bhakta & Arthur, 2001). Geobiotics, LLC's GEOCOAT process of coating support rock with gold concentrate and then heap leaching has been adopted by African Pioneer Mining at the Agnes Mine, South Africa (Harvey & Bath, 2003).

The use of stirred tank reactors was pioneered in 1986 at the Fairview gold mine, where the BIOX® process was developed for the pre-treatment of refractory gold ores. There are now numerous commercial plants in operation (see Table 2.2), most using the BIOX® technology, others using a Mintek/Bactech process developed using moderately thermophilic bacteria.

Table 2.2 Industrial examples of commercial stirred tank reactor bioleaching operations (adapted from Olson *et al.*, 2003, and Rawlings *et al.*, 2003).

Plant and Location	Technology	Throughput tonnes concentrate/day	Years in Operation
Fairview, South Africa	BIOX®	14	1986-
		35	(expanded 1991)
		55	(expanded 1999)
Sao Bento, Brazil	BIOX®	150	1991-
		300	(expanded 1994)
		300	(expanded 1998)
Wiluna, Australia	BIOX®	115	1993-
		154	(expanded 1996)
Youanmi, Australia	BacTech	120	1994-1998
Ashanti-Sansu, Ghana	BIOX®	720	1994-
		960	(expanded 1995)
Tamboraque, Peru	BIOX®	60	1998-
Beaconsfield, Tasmania	Mintek-BacTech	68	2000-
Laizhou, China	Mintek-BacTech	100	2001-
Perseverance, Australia	BIOX®	126	2005-
Amantaytau, Uzbekistan			

Stirred tank technology is currently being extended to process base metals. BRGM developed a plant for Kasese Cobalt to process a cobaltiferous sulfide concentrate, this ran successfully from 1999 until the low cobalt price made the process unsustainable in 2002 (Morin *et al.*, 2003). The plant reopened following a recovery in the cobalt price in 2004 (www.thecdi.com/cdi/images/news_pdf/Cobalt_News_April_06.pdf). Copper and nickel processing plants have been run at pilot scale (Dew *et al.*,1999). Thermophilic bioleaching demonstration plants for the processing of chalcopyrite have been built, Alliance Copper Ltd.'s (BHP Billiton/Codelco) BioCOP™ plant in Chuquicamata, Chile (Batty & Rorke, 2006), and PBM's (Peñoles/Bactech/Mintek) plant in Monterrey, Mexico (Rawlings *et al.*, 2003). PBM have recently announced the successful production of commercial cathode copper from their process (http://www.engineeringnews.co.za/eng/features/environment/?show=13436).

2.2 Bioleaching Micro-organisms

The first micro-organism identified as involved in bioleaching was *Thiobacillus ferrooxidans* (since reclassified as *Acidithiobacillus ferrooxidans* (Kelly & Wood, 2000)), isolated in 1951 (Temple & Colmer, 1951), triggering a disproportionate research focus on this micro-organism despite the growing realisation that other micro-organisms play far more significant roles in many systems (Rawlings 2002; Johnson, 1998).

Bioleaching micro-organisms are phylogenetically diverse, consisting of members of two domains, bacteria and archaea. The dominant species share the characteristics of being acidophilic, iron and/or sulfur-oxidising chemolithotrophs, and are generally found in consortia with different species being dominant under different prevailing conditions (Rohwerder *et al.*, 2003). The dominant species can be changed by changing the reaction temperature. Increasing the temperature leads to the dominance of thermotolerant, moderately thermophilic and eventually extremely thermophilic micro-organisms.

Under mesophilic conditions (T < 40°C), the predominant leaching micro-organisms are autotrophic bacteria: *Acidithiobacillus ferrooxidans, At. thiooxidans, At. caldus, Leptospirillum ferrooxidans* and *L. ferriphilum*. *L. ferriphilum* and *At. caldus* have been observed to predominate in commercial stirred tank bioleaching reactors (Rawlings *et al.*,1997).

The *Acidithiobacilli* are Gram-negative, obligately autotrophic Proteobacteria. *At. ferrooxidans* is preferentially aerobic, utilising oxygen as electron acceptor and either ferrous iron or reduced sulfur as electron donor. It can also grow anaerobically, utilising ferric iron as the electron acceptor reducing it to ferrous iron, and oxidising reduced sulfur compounds as the electron donors. It is capable of rapid growth at temperatures between 20 and 35°C in the presence of abundant substrate.

This, along with its flexibility in potential substrate, make it an important micro-organism in acid mine drainage (Johnson, 2005). *At. thiooxidans* and *At. caldus* are obligate aerobes restricted to reduced sulfur as electron donor. Both of these species are extremely acid tolerant, capable of growing at pH below 1. *At. caldus* is moderately thermotolerant, with an optimum growth temperature of 45°C, and has been found to be the dominant sulfur oxidiser over the temperature range from 35 to 50°C (Rawlings, 2002; Rawlings *et al.*, 1999).

L. ferrooxidans belongs to the division Nitrospira rather than Proteobacteria (Hugenholtz *et al.*, 1998) and is an obligately aerobic autotroph restricted to ferrous iron as electron donor (Hallmann *et al.*, 1992). It is acid tolerant and is relatively less inhibited by ferric iron than *At. ferrooxidans* and thus is able to out-compete *At. ferrooxidans* in ferrous iron-limited systems. This explains why *L. ferrooxidans* is the dominant iron oxidiser in commercial stirred tank bioleaching reactors (Rawlings *et al.*, 1999). Several isolates of *L. ferrooxidans* have been differentiated by genomic G+C ratio and varying thermotolerance into putative separate species: *L. ferrooxidans*, *L. thermoferrooxidans*, and *L. ferriphilum*. *L. ferriphilum* is the strain that has been identified as the dominant species in South African commercial bioreactors (Coram & Rawlings, 2002).

Several mesophilic archaea have also been identified that respire solely on iron. *Ferroplasma acidophilus* was isolated from a pilot plant reactor in Kazakhstan (Golyshina *et al.*, 2000) and *Ferroplasma acidarmanus* from Iron Mountain, California (Edwards *et al.*, 2000; Dopson *et al.*, 2004), both are pleomorphic micro-organisms lacking cell walls, and characterised by capacity to operate at extremely low pH. Recently another isolate, *Ferroplasma cupricumulans*, has been isolated from a copper heap in Myanmar (Hawkes *et al.*, 2006).

If the temperature is increased to between 45 and 60°C, the mesophiles are superseded by moderate thermophiles. The most studied group of moderate thermophiles is the genus *Sulfobacillus*. Culture analysis at 50°C indicated that the dominant species was still *At. caldus*, followed by *Acidimicrobium ferrooxidans*, and then only *Sulfobacillus* (Norris *et al.*, 2000). *Sulfobacillus* species are Gram-positive, endospore-forming bacteria and have been isolated from mineral waste heaps and bioleaching operations. *Sulfobacillus thermosulfidooxidans* oxidises iron and mineral, while *Sulfobacillus acidophilus* is primarily a sulfur oxidiser. Both are facultative aerobes and can grow either autotrophically or heterotrophically, but are poor carbon dioxide fixers and most often grow in close association with *Acidimicrobium ferrooxidans* (Clark & Norris, 1996b). *A. ferrooxidans* is a Gram-positive rod-shaped bacterium, capable of autotrophic growth on ferrous iron, but more effective growing heterotrophically. Mixed cultures of *A. ferrooxidans* and *Sulfobacillus* species exhibited a greater iron-oxidising capacity than any of the individual constituent species in pure culture (Clark & Norris, 1996b).

No bacteria are found at temperatures above 60°C, this temperature regime is dominated by thermophilic archaea of the order *Sulfolobales*, including members of the genera *Sulfolobus*, *Acidianus*, *Metallosphaera*, and *Sulfosphaera* (Norris *et al.*, 2000). *Sulfolobus* and *Sulfolobus*-like cultures were isolated from acidic continental solfatara fields; in copper mine drainage and from self-heated coal spoil heaps (Brock, 1978; Gomez *et al.*, 1993; Marsh & Norris, 1983). The isolates were coccoid cells, between 0.8 – 2 μm in diameter, and showed the capacity for growth on iron, sulfur and mineral sulfides. Classification is currently organised by 16S rRNA phylogeny (Itoh, 2003), a feature which has necessitated the re-classification of a number of previously classified species.

Important thermophilic archaea include *Sulfolobus metallicus* (originally studied as *Sulfolobus* BC (Norris, 1997)), an obligately aerobic autotroph, capable of oxidising ferrous iron, reduced sulfur and sulfide ores, with an optimum temperature of 68°C; *Metallosphaera sedula*, another obligate aerobe and iron- and sulfur-oxidising chemolithoautotroph, with an optimum temperature between 80 and 85°C; *Acidianus brierleyi* (originally *Sulfolobus brierleyi* (Brierley, 1978)), a mixotroph capable of autotrophic growth on ferrous and reduced sulfur and heterotrophic growth on complex organics; and a number of *Sulfolobus*-like and *Metallosphaera*-like organisms that show capacity for efficient oxidation of sulfide ores.

The archaeal cells differ structurally from bacterial cells. Where bacteria possess a cell wall consisting of a rigid peptidoglycan layer and a cell membrane formed from a bilayer of ester-linked phospholipids and sterols, to maintain the cell's integrity and provide protection from its environment, archaeal cell walls consist of one or two surface layers (S-layers) of protein or glycoprotein subunits (Konig, 1988; Baumeister & Lembke, 1992), closely associated with the cell membrane, which is formed from ether-linked branched hydrocarbons (Van de Vossenberg *et al.*, 1998; De Rosa *et al.*, 1991). This lack of structural rigidity allows the cell to adapt the fluidity of its cell membrane to cope with elevated temperature and extreme acidity (Van de Vossenberg *et al.*, 1998) but renders it susceptible to damage by mechanical shear stresses (Raja, 2005), limiting the maximum solids loading that the system can tolerate (Le Roux & Wakerley, 1988; Clark & Norris, 1996a). The common iron- and sulfur-oxidising species identified in bioleaching environments, or identified to have potential in bioleaching, are reviewed in Table 2.3.

Table 2.3 Iron- and/or sulfur-oxidising micro-organisms used in, or with potential for, biomining.

Micro-organism	Domain	Metabolism	Substrate	Reference
Mesophile (20 – 45°C)				
Acidiphilium acidophilum	Bacteria	aerobic, A, M, H	RSC, excreted organic compounds	Hiraishi *et al.*, 1998; Rohwerder & Sand, 2003
Acidithiobacillus caldus	Bacteria	aerobic, A, M	S_0, RSC, yeast, glucose	Hallberg & Lindstrom, 1994
Acidithiobacillus ferrooxidans	Bacteria	facultative aerobic, A	Fe^{2+} RSC	Temple & Colmer, 1951; Kelly & Wood, 2000
Acidithiobacillus thiooxidans	Bacteria	aerobic, A	RSC	Kelly & Wood, 2000; Rawlings, 2002,
Ferroplasma acidarmanus	Archaea	aerobic, M	Fe^{2+}	Dopson *et al.*, 2004; Edwards *et al.*, 2000
Ferroplasma acidiphilum	Archaea	aerobic, A	Fe^{3+}	Golyshina *et al.*, 2000
Ferroplasma cyprexacervatum	Archaea	aerobic	Fe^{2+}, RSC	Hawkes *et al.*, 2005
Leptospirillum ferrooxidans	Bacteria	aerobic, A	Fe^{2+}	Hippe, 2000
Leptospirillum thermoferrooxidans	Bacteria	aerobic, A	Fe^{2+}	Golovacheva *et al.*, 1992
Leptospirillum. ferriphilum	Bacteria	aerobic, A	Fe^{2+}	Coram & Rawlings, 2002
Moderate Thermophile (45 – 60°C)				
Acidimicrobium ferrooxidans	Bacteria	aerobic, A, H	Fe^{2}, yeast extract	Clark & Norris, 1996b
Acidithiobacillus caldus	Bacteria	aerobic, A, M	S_0, RSC, yeast, glucose	Hallberg & Lindstrom, 1994
Sulfobacillus acidiphilus	Bacteria	aerobic, A, M, H	Fe^{2+}, S_0	Norris *et al.*, 1996
Sulfobacillus thermosulfidooxidans	Bacteria	aerobic, A, M, H	Fe^{2+}, S_0, RSC	Golovacheva & Karavaiko, 1978; Norris *et al.*, 1996

Where A – Autotroph, M – Mixotroph, H – Heterotroph; and Fe^{2+} - ferrous iron, RSC – reduced sulfur compounds, and S_0 – elemental sulfur

Micro-organism	Domain	Metabolism	Substrate	Reference
		Thermophile (60 – 80°C)		
Acidianus ambivalens	Archaea	facultative aerobe, A, M, H	RSC	Fuchs *et al.*, 1996
Acidianus brierleyi	Archaea	facultative aerobe, A, H	Fe^{2+}; RSC, complex organics	Segerer *et al.*, 1986; Rawlings, 2002
Acidianus infernus	Archaea	aerobic anaerobic	S_0, RSC S_0	Segerer *et al.*, 1986
Acidianus tengchongensis	Archaea	aerobic, A, H	S_0, sugars	He *et al.*, 2004
Metallosphaera hakonensis	Archaea	aerobic, facultative A	Fe^{2+}, S_0, RSC	Kurosawa *et al.*, 2003
Metallosphaera prunae	Archaea	aerobic		Fuchs *et al.*, 1995
Metallosphaera sedula	Archaea	aerobic, facultative A	Fe^{2+}, RSC, S_0, complex organics	Huber *et al.*, 1989
Sulfolobus acidocaldarius	Archaea	aerobic, facultative A	Fe^{2+}; RSC	Brock *et al.*, 1972
Sulfolobus solfaraticus	Archaea	aerobic, facultative A	Fe^{2+}; RSC	Zillig *et al.*, 1980
Sulfolobus metallicus	Archaea	aerobic, A	Fe^{2+}, S_0, RSC	Huber & Stetter, 1991
Sulfolobus shibatae	Archaea	aerobic, A	Fe^{2+}, S_0, RSC	Grogan *et al.*, 1990
Sulfolobus yangmingensis	Archaea	aerobic, facultative A	S_0, RSC	Jan *et al.*, 1999
Sulfurococcus mirabilis	Archaea	aerobic, facultative A	S_0	Golovacheva *et al.*, 1987
Sulfurococcus yellowstonensis	Archaea	aerobic, facultative A	Fe^{2+}, S_0, sulphide	Karavaiko *et al.*, 1994
Thermoplasma thiooxidans	Archaea	aerobic, facultative A	S_0	Li *et al.*, 1994

Where A – Autotroph, M – Mixotroph, H – Heterotroph; and Fe^{2+} - ferrous iron, RSC – reduced sulfur compounds, and S_0 – elemental sulphur

2.3 The Mechanism of Bioleaching

The idea that bioleaching is effected by a direct enzymatic attack is no longer supported, and there is a general consensus that bioleaching occurs via a multiple sub-process mechanism (illustrated in Figure 1.1) consisting of an initial abiotic ferric or acid leach step followed by microbial oxidation of the iron and sulfur products released, regenerating the primary leach agents (Sand *et al.*, 2001; Hansford & Vargas, 2001; Tributsch, 2001).

Distinction is now made between the "contact" and "non-contact mechanisms", which stress the importance of the attachment of cells to the mineral surface. In the non-contact mechanism, planktonic cells grow and oxidise soluble substrate available in the bulk liquid phase. In the contact

mechanism, cells attach to the mineral surface, and oxidise substrate available at the surface. The rates of growth and oxidation of attached cells are dependent on the concentrations of substrate and other physicochemical conditions under the cells excreted extracellular polysaccharide (EPS) layer, rather than those of the bulk liquid (Schippers & Sand, 1999). Both planktonic and attached cells are found in bioleaching systems so both mechanisms undoubtedly occur, it is their contribution to the overall leach rate that is unclear.

Two mechanistic pathways, illustrated in Figure 2.1, have been proposed that describe the oxidation of the sulfur moiety released by the ferric leach (Schippers & Sand, 1999). The pathway followed depends on the properties of the mineral. Sulfides such as pyrite (FeS_2), molybdenite (MoS_2), and tungstenite (WS_2), whose valence bands are derived from the metal atom orbitals only, are acid insoluble and are leached via the thiosulfate pathway.

Sulfides such as sphalerite (ZnS), galena (PbS), arsenopyrite (FeAsS), chalcopyrite ($CuFeS_2$) and hauerite (MnS_2), have valence bands derived from both the metal and the sulfide orbitals, are acid-soluble, and are leached via the polysulfide pathway (Schippers & Sand, 1999).

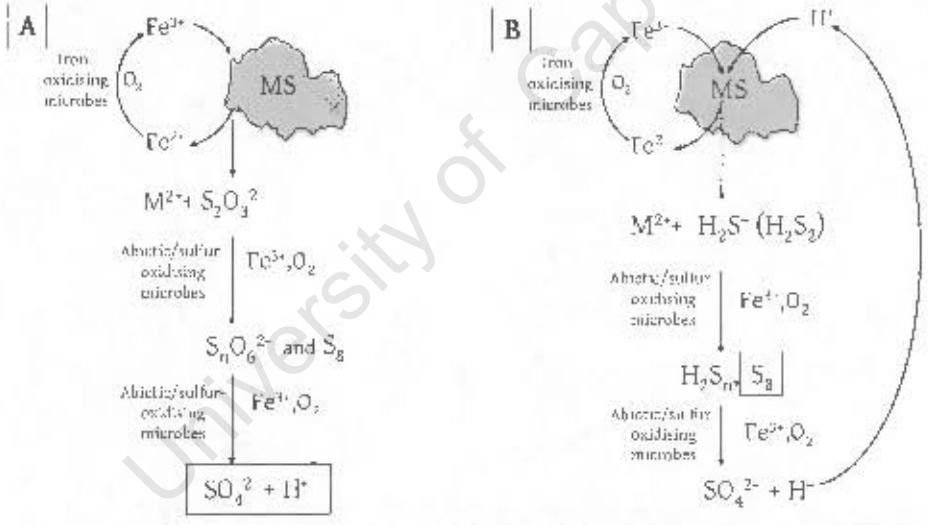

Figure 2.1 Schematic representations of [A] the thiosulfate pathway, and [B] the polysulfide pathway proposed by Schippers & Sand (1999) for the bioleaching of a metal sulfide (MS), showing the cycling of the primary leach agents and the consequent breakdown of the sulfur intermediates released. The main oxidising agents for the reactions are shown to the right of the arrows. The main products are boxed. Adapted from Rohwerder *et al.*(2003).

In the thiosulphate mechanism, there are six individual ferric leach steps, transferring valence band electrons to ferric ions, producing ferrous iron and releasing thiosulfate. The thiosulfate is oxidised via tetrathionate and other polythionates to sulfate. The oxidation may stop at elemental sulfur if no sulfur oxidising micro-organisms are present.

In the polysulfide mechanism, the mineral is dissolved by the combination of ferric and proton attack. In the absence of ferric iron, two protons break the bond between the metal and the sulfur moiety, releasing hydrogen sulfide, H_2S. In the presence of ferric iron, the sulfur moiety is oxidised concomitantly with the proton attack, producing ferrous iron and the sulfide cation, H_2S^*. H_2S^* spontaneously dimerises to free sulfide, H_2S_2, and is further oxidised to elemental sulfur via higher polysulfides and polysulfide radicals (Steudel, 1996). The sulfur produced can then be oxidised to sulfate by sulfur-oxidising micro-organisms. In the absence of sulfur-oxidisers, more than 90% of sulphur is transformed to elemental sulfur (Schippers & Sand, 1999).

In both mechanisms, the main role of the micro-organisms present is the regeneration of ferric iron (Rohwerder *et al.*, 2003), and hence the investigation of the kinetics of microbial ferrous iron oxidation becomes important.

2.3.1 The Mechanism of Microbial Ferrous Iron Oxidation

Mitchell (1966) presented a chemiosmotic mechanism for energy generation. The mechanism involves the coupling of the transfer of electrons across an energy-transducing membrane to the production of energy-rich molecules. This chemiosmotic theory was used by Ingledew (1982) to develop a model to explain the bioenergetics of ferrous iron oxidation by *At. ferrooxidans*.

In this model, the oxidation reaction

$$4Fe^{2+} + O_2 + 4H^+ \rightarrow 4Fe^{3+} \cdot 2H_2O \qquad [2.1]$$

is split into its constituent redox half reactions which are separated by the cell membrane. The iron (electron donor) half reaction occurs outside the membrane,

$$Fe^{2+} \rightarrow Fe^{3+} + e^- \qquad [2.2]$$

where ferrous iron in solution (pH ~ 2) is oxidised by ferric iron bound in the cell wall. The electron passes through a poly-nuclear ferric complex in the cell wall to the periplasm (pH ~ 3.5). Here the electron is transferred via c-type cytochromes and a copper-containing protein, rusticyanin, to a cytochrome a_1-type oxidase buried in the cell membrane, and then passed to the final electron acceptor, O_2, in the cytoplasm (pH ~ 6.5).

$$2H^+ + \tfrac{1}{2}O_2 + e^- \rightarrow H_2O \qquad [2.3]$$

The consumption of protons combined with the pH difference between the cytoplasm and the bulk solution generates the proton gradient that drives the formation of adenosine triphosphate (ATP).

This is achieved by the cell membrane being impermeable to protons apart from proton channels that are associated with ATPase.

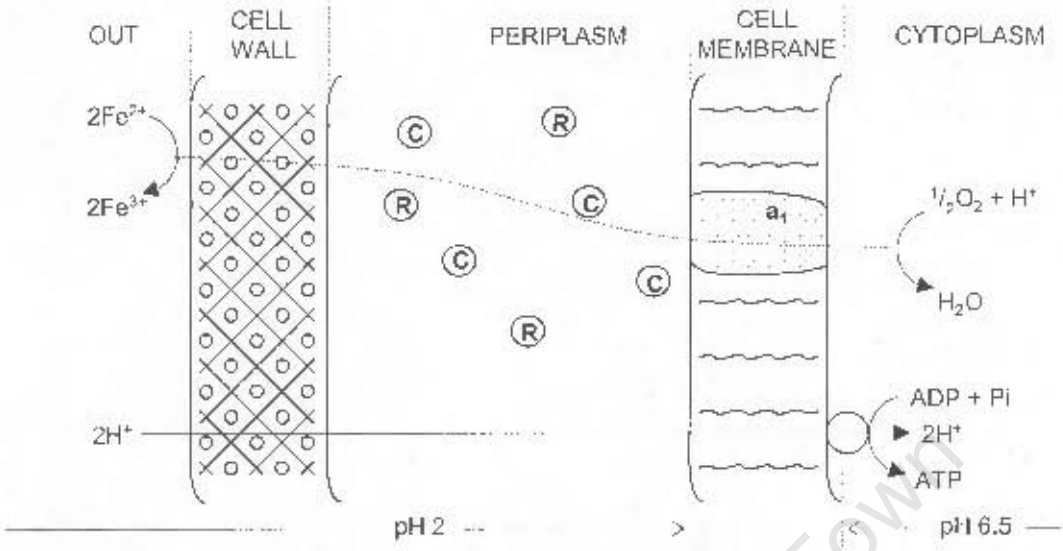

Figure 2.2 The possible arrangement of the electron transport chain of *At. ferrooxidans* (adapted from Ingledew, 1982 and Ingledew, 1986) where C denotes cytochrome C, R denotes rusticyanin, and a_1 an a_1-type cytochrome oxidase.

Further work on the components of the electron chain of *At. ferrooxidans* have identified a high molecular weight c-type cytochrome (Cyc2) bound in the outer membrane (cell wall) that acts as the primary electron acceptor (Yarzábal *et al.*, 2002a), the electron is passed to a second cytochrome (Cyc1) in the periplasm, possibly via rusticyanin (Giudici-Orticoni *et al.*, 1999), and then on to a cytochrome oxidase.

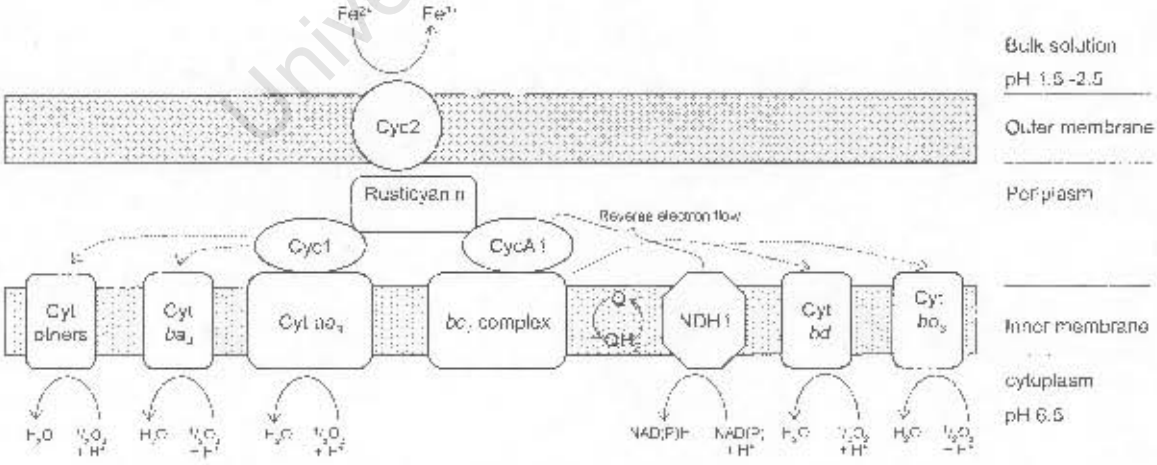

Figure 2.3 A model of a number of possible electron transfer chains for *At. ferrooxidans*, showing electron transfer generating a proton gradient, and reverse electron transfer for the formation of NADH (Rawlings, 2005).

A number of cytochrome oxidases have been identified (Brasseur *et al.*, 2004), the most common in iron-grown cells is an aa_3-type cytochrome oxidase embedded in the cell membrane, which facilitates the oxygen half reaction. Another uphill pathway that the electrons may follow is via a c4-type cytochrome for the formation of NAD(P)H in the cytoplasm for the fixation of CO_2 for cell growth (Rawlings, 2005).

The role of rusticyanin has not yet been resolved. It has been proposed to act as an electron reservoir, maintaining the primary electron acceptor in its fully oxidised state, and hence capable of operating at maximum efficiency (Rohwerder *et al.*, 2003).

This level of mechanistic information is only available for *At. ferrooxidans*. Investigations of other micro-organisms have identified individual cytochromes, but insufficient to postulate complete electron transfer chains.

Leptospirillum ferrooxidans, moderately thermophilic bacteria and extremely thermophilic archaea were all investigated to see what their iron oxidation systems consisted of and whether any evolutionary links could be drawn (Barr *et al.*, 1990, Blake & McGinness, 1993). They were found to contain a variety of cytochromes linked to iron oxidation, with insufficient similarity to indicate common ancestry, inferring that the ability to respire on iron evolved separately in each case.

Work on *Sulfolobus acidocaldarius* (Anemüller *et al.*, 1985), grown on sulfur, suggested that the generation of ATP is membrane linked and achieved by chemiosmotic oxidative phosphorylation. This was backed by the finding that ATP generation was linked to the chemiosmotic cycling of protons across the archaeon's plasma membrane (Moll & Schafer, 1988). Peeples and Kelly (1995) measured proton motive force in *Metallosphaera sedula* and noted that cells under nutritional and/or thermal stress showed a reduction in the proton motive force and a consequent lack of metabolic activity.

Another investigation of a number of thermophilic archaea: *Sulfolobus*, *Acidianus* and *Metallosphaera* species, found that the production of an identical novel membrane-bound cytochrome was induced when the micro-organisms were grown on ferrous iron. Another cytochrome similar to cytochrome aa_3 found in *Sulfolobus acidicaldarius* was also discovered (Norris, 1992).

2.3.2 Carbon Dioxide Fixation

The iron-oxidising micro-organisms studied are predominantly autotrophs, obtaining the carbon required in their cellular structure by assimilating atmospheric carbon dioxide. This is achieved by different mechanisms in different species.

Carbon dioxide fixation in bacteria such as *At. ferrooxidans* and *L. ferrooxidans* occurs via the Calvin-Benson cycle, catalysed by a ribulose 1,5-biphosphate carboxylase, consuming 3 ATP molecules and 2 NADH molecules per molecule of CO_2 fixed (Rawlings, 2005). The NADH is thought to be formed by reverse electron transport through the membrane as described in Figure 2.3. *At. ferrooxidans* also possesses a glycolytic pathway and an incomplete citric acid cycle, but it not known whether these influence CO_2 assimilation.

The archaea do not fix CO_2 via the Calvin-Benson cycle, and the pathway that does operate is not yet fully understood, but was first thought to involve either the reductive citric acid cycle or the reductive malonyl-Coenzyme A (CoA) pathway (Kandler, 1992). Work on *Acidianus brierleyi* indicated the operation of a modified 3-hydroxypropionate pathway (Ishii, 1996), a pathway later extended to *Metallosphaera sedula* and *Sulfolobus metallicus* (Menendez *et al.*,1999).

The modified 3-hydroxypropionate pathway is catalysed by acetyl CoA carboxylase and propionyl CoA carboxylase. CO_2-limited growth of *S. metallicus* induced expression of a biotin carboxylase and a biotin-carboxyl-carrier protein complex, this complex is encoded by a gene adjacent to that encoding a putative propionyl CoA carboxyl transferase, (Burton *et al.*, 1999) suggesting that CO_2 fixation in at least *S. metallicus* follows the modified 3-hydroxypropionate pathway. Biotin carboxylases have also been found in *M. sedula* (Hugler *et al.*, 2003).

2.4 Physicochemical Parameters that Affect Microbial Iron Oxidation

A number of parameters that influence the rates of microbial iron oxidation and microbial growth have been studied: pH, temperature, iron concentration, availability of O_2 and CO_2, inhibition by other metals, ionic speciation, precipitation and competing reactions. The effects of the parameters have been investigated by researchers approaching the topic from a chemiosmotic mechanism, enzyme inhibition and a microbial physiology point of view. Most have been studied with respect to iron oxidation by *At. ferrooxidans*. The main findings will be reviewed here, with the emphasis on how these parameters will affect thermophilic microbial iron oxidation. The incorporation of the effects of these parameters into kinetic models will be discussed in Section 2.5.

2.4.1 The Effect of Solution pH

Changes in the pH of the bulk solution will affect the metabolic activity of the cell directly, as the chemiosmotic mechanism of energy generation depends on the maintenance of a pH gradient across the cell membrane.

The effect of pH on mesophilic microbial ferrous iron oxidation is characterised by a region around the observed optimum where there is limited effect of pH (Lacey & Lawson, 1970; Pesic *et al.*, 1989; Gomez & Cantero, 1998; Halfmeier *et al.*, 1993), and reduced growth at pH below and above the optimum (MacDonald & Clark, 1970; Crundwell, 1997; Gomez & Cantero, 1998).

A variety of pH optima have been presented for *At. ferrooxidans* ranging from pH 2 to 2.3 (Jensen & Webb, 1994) ascribing differences to different strains. *L. ferrooxidans* has a much lower reported optimum of pH 1.7 (Norris & Johnson, 1998), whilst amongst the archaea, *Ferroplasma* species have been found to grow at pH ~0 to 2.5, with an optimum at 1.2 (Dopson *et al.*, 2004), and *Sulfolobus metallicus* and *Metallosphaera sedula* at pH 1 to 4 (Norris, 1997; Itoh, 2003). The differences in pH-tolerance may be explained by structural differences in the cell membrane affecting ion permeability, archaeal membranes containing tetraether lipids which reduce ion permeability allowing the micro-organism to tolerate much lower pH (Macalady *et al.*, 2004).

The solution pH also affects the system indirectly. Ferric iron is sparingly soluble and precipitates with increasing pH (MacDonald & Clark, 1970; Lacey & Lawson, 1970), this precipitation releases protons, buffering the solution weakly at pH 2.3. Precipitation will be discussed further in Section 2.4.3. Increasing pH also favours the competing chemical oxidation of ferrous iron by molecular oxygen, overtaking microbial oxidation above pH 5 (Meruane & Vargas, 2003). pH also affects the iron speciation. At low pH, uncomplexed ferrous and ferric iron ions are dominant, as pH increases, hydroxide and sulfate complexes become more prevalent. This may change the amount of substrate available to the micro-organisms. Breed & Hansford (1999) found that the threshold concentration, limiting iron oxidation, with *L. ferrooxidans*[*] decreased with decreasing pH and ascribed this to speciation.

2.4.2 The Effect of Temperature

The effect of temperature can be described with reference to a culture-specific optimum temperature, T_{opt}. As illustrated in Figure 2.4, below T_{opt}, increasing temperature causes an increase in growth and substrate utilisation rates. Above T_{opt}, further increases of temperature causes a rapid reduction in microbial activity.

[*] Breed & Hansford, 1999 and Breed *et al.* 1999 identified their culture as *Leptospirillum ferrooxidans*, however the work presented in Coram & Rawlings 2002 indicates that the culture was most likely *L. ferriphilum*

limiting iron oxidation, with *L. ferrooxidans*[*] decreased with decreasing pH and ascribed this to speciation.

2.1.1 The Effect of Temperature

The effect of temperature can be described with reference to a culture-specific optimum temperature, T_{opt}. As illustrated in Figure 2.4, below T_{opt}, increasing temperature causes an increase in growth and substrate utilisation rates. Above T_{opt}, further increases of temperature causes a rapid reduction in microbial activity.

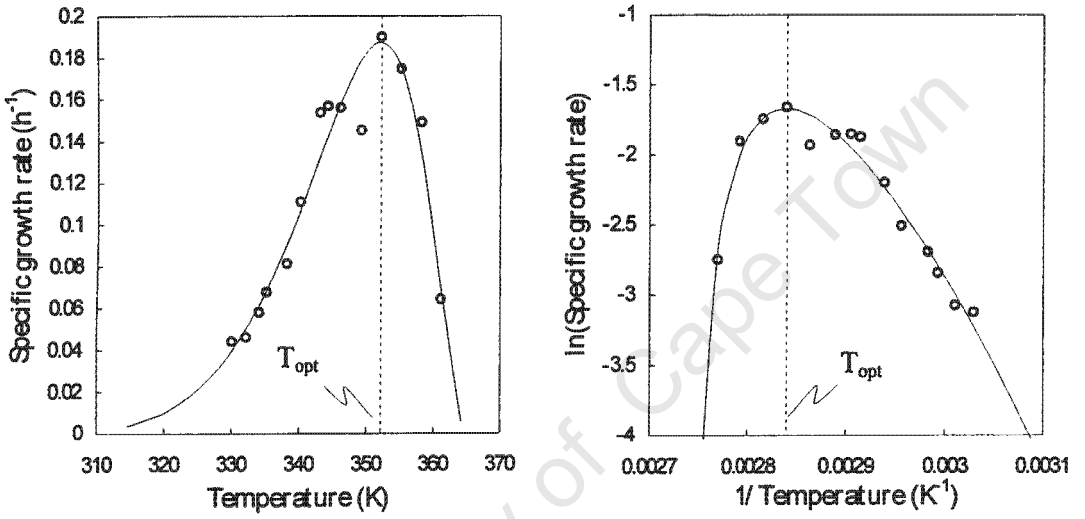

Figure 2.4 An example of the effect of temperature on specific growth rate. Data taken from Plumb et al. (2002) investigating the effect of temperature on the heterotrophic growth of a *Sulfolobus* strain JP2.

Thermotolerance is related primarily to the ion permeability of the cellular membrane and also to the thermal stability of enzymes and other macromolecules required for cellular metabolism (van de Vossenberg *et al.*, 1998). Archaeal cell membranes contain ether lipids that are more resistant to high temperature than bacterial ester lipids. Archaea respond to high temperature by the cyclization of fatty acyl chains, moving from ether, to diether, to tetraether lipids (De Rosa *et al.*, 1991). These membrane-spanning lipids make the membrane nearly impermeable to ions and protons, countering the increased diffusivity with increased temperature. Archaea respond to low temperature by unsaturation of the lipids (Nichols & Franzmann, 1992).

[*] Breed & Hansford, 1999 and Breed *et al.* 1999 identified their culture as *Leptospirillum ferrooxidans*, however the work presented in Coram & Rawlings 2002 indicates that the culture was most likely *L. ferriphilum*

Many models describe the effect of temperature as a modulation of the maximum rate. Temperature also affects other parameters: substrate affinity coefficients K_s and other analogous constants; yield coefficients and cell maintenance parameters. K_s has been reported to be affected by temperature (Topiwala & Sinclair, 1971; Breed *et al.*, 1999), although its effect on the overall rate is not as pronounced as the maximum specific growth rate. Breed *et al.* (1999) found that K_{Fe2+} was a linear function of temperature, but subsequently found that the influence of temperature on K_{Fe2+} was not significant (Breed & Hansford, 1999).

A number of researchers have studied the effect of temperature on mesophilic microbial ferrous iron oxidation. Growth at low temperature has been studied (Ahonen & Tuovinen, 1989). This study was necessary as low temperatures may be experienced in some *in situ* bioleaching operations or in European heap operations during winter or at high altitudes. Growth under these conditions was found to be slow but not stopped.

Many studies have been focussed on finding the optimum temperature for growth of different species, mostly *Acidithiobacillus ferrooxidans*, and on describing the effect of temperature near the optimum. The optimum temperature for *At. ferrooxidans* was found to be pH-dependent (MacDonald & Clark, 1970) as would be expected as both parameters affect the membrane permeability.

The effect of temperature was most often described as a simple Arrhenius function, describing increased activity with increased temperature, or by a Ratkowsky equation (Ratkowsky *et al.*, 1983) for more extended temperature ranges. These and other functions describing the effect of temperature are discussed in Section 2.5.5. Activation energies published or derived from published data are tabulated below.

Table 2.4 Activation energies describing the effect of temperature on a selection of bioleaching micro-organisms.

Researchers	Species	Temperature range studied (°C)	E_a (kJ.mol^{-1})
Smith *et al.*, 1988	*Acidithiobacillus ferrooxidans*	20 - 30	-
Lacey & Lawson, 1970	*At. ferrooxidans*	20 - 30	33.9
Nemati and Webb, 1997	*At. ferrooxidans*	20 - 35	68.4
Ahonen & Tuovinen, 1989	*At. ferrooxidans*	10 - 46	80.0
MacDonald & Clark, 1970	*At. ferrooxidans*	20 - 40	51.2[a]
Okereke & Stevens, 1991	*At. ferrooxidans*	10 - 30	47.2[b]
Franzmann *et al.*, 2005	*At. ferrooxidans*	10 - 55	62
Breed *et al.*, 1999	*Leptospirillum ferrooxidans*	30 - 40	35.63
Franzmann *et al.*, 2005	*L. ferrooxidans*	8 - 55	80
Franzmann *et al.*, 2005	*L. ferriphilum*	15 - 58	89
Han *et al.*, 1997	*M. sedula*	74 - 81	-
Franzmann *et al.*, 2005	*Sulfobacillus thermosulfooxidans*	27 - 65	51

The most common measured variable in iron oxidation experiments is the concentration of the substrate, ferrous iron, as the rate of oxidation is strongly influenced by the availability of substrate (Silverman & Lundgren, 1959).

Threshold concentrations below which no growth is observed have been proposed for both *At. ferrooxidans* (Braddock *et al.*, 1984; Boon *et al.*, 1999) and *L. ferrooxidans* (Breed & Hansford, 1999), representing the limit at which the available substrate does not contain sufficient free energy to sustain the culture.

At the other end of the spectrum, excessive amount of substrate may cause substrate inhibition. Substrate inhibition has been explained in terms of a Michaelis-Menten reaction mechanism, where high substrate concentration causes the binding of a second substrate molecule to the substrate-enzyme-complex, thereby inactivating it (Nemati & Webb, 1997). Jones & Kelly (1983) report substrate inhibition for *At. ferrooxidans* above 100mM Fe^{2+} but note that it is difficult to separate from product inhibition in growing cultures. Barron & Lueking (1990) found a decrease in specific growth rate at ferrous iron concentrations above 70 mMFe^{2+}. Nemati & Webb (1997) found the onset in substrate inhibition to be affected by the cell concentration. Nikolov & Karamanev (1992) studied an *At. ferrooxidans* culture resuspended from a biofilm and found that it was unaffected by ferrous iron concentrations up to the solubility limit near 1250 mMFe^{2+}.

The product of the oxidation reaction, ferric iron, has been found to inhibit growth of *At. ferrooxidans* (Kelly & Jones, 1978). This inhibition has been studied repeatedly with many researchers finding that ferric iron inhibits the growth competitively (Kelly & Jones, 1978; Liu *et al.*, 1988; Norris *et al.*, 1988; Gomez *et al.*, 1996; Nyavor *et al.*, 1996; Harvey & Crundwell, 1997; Boon *et al.*, 1999; Kawabe *et al.*, 2003). In competitive inhibition, ferric iron binds to the active site on the cell membrane, obstructing the attachment of ferrous iron for oxidation. Jones & Kelly (1983) found that ferric inhibition could be either competitive or non-competitive depending on the reaction conditions. Nemati & Webb (1998) also found that the inhibition observed was non-competitive. Shrihari & Gandhi (1990) described the phenomenon as ferric poisoning, where the ferric iron poisoned cells reducing the apparent growth rate, but did not explain how the poisoning was achieved.

Product (ferric iron) inhibition models have also been applied to other iron-oxidising species. Norris *et al.* (1988) determined inhibition constants for *At. ferrooxidans* , *L. ferrooxidans* , *Sulfobacillus* and *Sulfolobus* species. Inhibition constants and substrate affinity constants are presented in Table 2.5. A comparison of mesophilic species showed that *L. ferrooxidans* proved to be much less inhibited by ferric iron than *At. ferrooxidans*.

Table 2.5 A comparison of published affinity coefficients and ferric inhibition constants for a number of common iron-oxidising species.

Organism		K_s ($mMFe^{2+}$)	K_i ($mMFe^{3+}$)	Reference
At. ferrooxidans	30°C	1.3	3.1	Norris, 1992
	30°C	1.31	2.04	Meruane *et al.*, 2002
	35°C	4.62	36.89	Nemati & Webb, 1998
	30°C	0.788-0.895	1-2	Jones & Kelly, 1983
	30°C	0.2	5	Boon *et al.*, 1999a
L. ferrooxidans	30°C	0.25	42.8	Norris, 1992
Sulfolobus BC	68°C	0.4	1.7	Norris, 1992
S. metallicus	70°C	3.65	0.95	Meruane *et al.*, 2003
Acidianus brierleyi	68°C	0.4	1.9	Norris, 1992
Metallosphaera sedula	68°C	1.0	1.0	Norris, 1992

The ferric/ferrous-iron ratio can be linked to the solution ORP via the Nernst equation, and its controlling influence on microbial kinetics is consistent with the chemiosmotic theory of microbial chemotrophic metabolism. Huberts (1994) found that perceived ferric inhibition could be removed by adding ferrous iron and concluded that the kinetics were more strongly affected by the ferric/ferrous-iron ratio than its individual constituents. This finding was used to develop a novel mode of operation for an electro-chemical cell, running oxidation experiments at constant redox potential and hence a constant ferric/ferrous-iron ratio (Harvey & Crundwell, 1997). Michaelis-Menten-form kinetic rate equations were proposed where specific substrate utilisation rates vary as a function of the ferric/ferrous-iron ratio, rather than as a function of ferrous iron (Boon, 1996; Hansford, 1997). This form of rate equation was found to be appropriate for following *L. ferrooxidans* growth as well (van Scherpenzeel *et al.*, 1998; Breed *et al.*, 1999; Breed & Hansford, 1999). Meruane *et al.* (2002) developed a rate equation controlled by the solution ORP from reversible Michaelis-Menten enzyme kinetics.

2.4.4 The Effect of Oxygen and Carbon Dioxide Limitation

As the system is aerobic and autotrophic; using oxygen as the final electron acceptor and fixing carbon dioxide as the carbon source for producing cell mass, these components need to be freely available so as not to constrain the system. Two forms of limitation are possible, gas-liquid mass transfer limitation, and a reduction of the growth rate caused by a low liquid phase O_2 or CO_2 concentration. Both are referred to as O_2 and/or CO_2-limitation and this adds to the conflicting results of the concentration at which the growth and oxidation kinetics are affected by O_2 and CO_2.

Studies on *At. ferrooxidans* indicate that no growth occurs below dissolved oxygen concentrations of 0.2mg.l^{-1}, growth is oxygen-limited between 0.29 and 0.7 mg.l^{-1} and unaffected by oxygen at higher concentrations (Liu *et al.*, 1988). Boon (1996) found a similar oxygen threshold at 0.5mM, and an oxygen affinity coefficient at 10% of the saturation concentration at 30°C. A more relevant measure of oxygen-limitation, is the rate of gas-liquid transfer, Savic *et al.* (1998) found the critical oxygen transfer rate to be 1.8mM.h^{-1}.

The low concentration of CO_2 in normal air, combined with its low solubility in acidic media makes CO_2-limitation more likely than O_2-limitation (Liu *et al.*, 1988; Mandl, 1984), leading some researchers to consider CO_2-supplemented air. Barron & Lueking (1990) reported maximum growth after supplementing with 7-8% CO_2, however their maximum specific growth rate of 0.11h^{-1} was achieved by MacDonald & Clark (1970) without supplemented air and who concluded that while the cell yield could be improved, the specific growth rate was unaffected by CO_2 supplementation.

As the solubility of O_2 and CO_2 are strongly affected by temperature, gas-liquid mass transfer limitations were expected to play an even greater role under thermophilic bioleaching conditions. The reduced gas solubility, coupled with the increased water partial pressure in the gas phase, reduces the potential maximum transfer rate. This is offset by a concomitant increase in the overall transfer coefficient, k_La (Boogerd *et al.*, 1990). Studies on tap water between 20 and 55°C indicated that the oxygen transfer rate was constant over this range (Vogelaar *et al.*, 2000). The transfer coefficient, k_La, is strongly affected by the reactor configuration, degree of mixing, and impeller type, as well as being a weak function of temperature. This makes comparisons between different experimental designs difficult.

The effects of elevated O_2 and CO_2 concentrations were studied in batch experiments oxidising ferrous iron with *Sulfolobus* (de Kock *et al.*, 2004). An optimum dissolved O_2 region of between 1.5 and 4.1mg.L^{-1} was found. At higher O_2 concentrations, increased formation of free radicals proved detrimental to microbial activity, whilst at lower concentrations, O_2 was growth-limiting. The optimum CO_2 concentration was found to be between 7 and 17%. These experiments were performed in a vessel stirred by a magnetic stirrer, and it is unknown whether similar results would be observed in a baffled bioreactor, sparged from below the impeller.

2.4.5 The Effect of the Precipitation of Iron Compounds

The iron oxidation reaction produces ferric iron and consumes acid. Ferric iron is only sparingly soluble and precipitates readily as hydroxide, oxyhydroxide and jarosite compounds. This releases protons, buffering the solution weakly at pH 2.3. Precipitation is minimal at pH 1.6, but increases with increasing pH (MacDonald & Clark, 1970; Lacey & Lawson, 1970). Precipitation is linked to a

drop in activity as it may cause diffusion barriers hampering oxidation (Pesic *et al.*, 1989; Meruane & Vargas, 2003). It also affects the system by blinding reaction surfaces, reducing free ferric iron for continued leaching and blocking pumps, pipes and valves (Nemati *et al.*, 1998). Iron-hydroxy compounds have been linked to the passivation of chalcopyrite in bioleaching systems (Stott *et al.*, 2000). The removal of iron from solution also complicates the measurement of iron oxidation kinetics.

The initial hydrolysis reaction forms ferric hydroxide.

$$Fe^{3+} + 3H_2O \leftrightarrow Fe(OH)_3 + 3H^+ \quad [2.4]$$

In the presence in excess sulphate, and suitable cations, e.g. K^+, Na^+, NH_4^+, and H_3O^+, a competing precipitation reaction forms ferric hydroxysulfates.

$$3Fe^{3+} + M^+ + 2HSO_4^- + 6H_2O \leftrightarrow MFe_3(SO_4)_2(OH)_6 + 8H^+ \quad [2.5]$$

These hydroxysulfates can be amorphous or crystalline (jarosite). The formation of the hydroxysulfate compounds is stimulated by the high sulfate concentration found in bioleaching systems. The type of compound is dependent on the availability of suitable cations, if they are present, crystalline jarosite is formed, if absent, then amorphous compounds predominate (Lazaroff *et al.*, 1982). Toro *et al.* (1988) found that in batch microbial oxidation systems, hydroxide precipitates form first, followed by jarosite, and that by the end of the batch the precipitate was predominantly jarosite. The nature can also be affected by the pH, Eneroth & Koch (2004) found that iron oxidation by *At. ferrooxidans* produced well-formed crystals of ammonium jarosite at pH 1.6, and a mixture of ammonium jarosite and schwertmannite at pH between 1.6 and 3.2. Increasing temperature to the thermophilic range leads to increased jarosite formation (Gomez *et al.* 1996, Norris and Barr, 1985).

2.4.6 The Contribution of Abiotic Oxidation of Ferrous Iron

Iron will oxidise from ferrous to ferric in the presence of oxygen without microbial assistance. This abiotic iron oxidation competes with microbial oxidation for available ferrous iron and oxygen in solution. In a mesophilic bioleaching environment, the rate of abiotic iron oxidation is negligibly slow, up to 500 000 times slower than the corresponding rate of oxidation by *Acidithiobacillus ferrooxidans* (Lacey and Lawson, 1970) and most researchers have neglected the effect of abiotic oxidation altogether. Increasing the temperature to the thermophilic range will produce a corresponding increase in the competing abiotic rate. Norris (1991) found iron oxidation rates of 1.5 $mMFe^{2+}.h^{-1}$ in his sterile controls whilst studying thermophilic iron oxidation. The contribution of

abiotic ferrous iron oxidation to thermophilic microbial ferrous iron oxidation will be investigated further in this work, and the results and appropriate rate equations will be discussed in Chapter 5.

2.4.7 Experimental Technique used to Follow Kinetics

Microbial iron oxidation has been investigated in a number of ways including batch culture, continuous culture, initial rate experiments (both oxygen uptake and iron oxidation experiments) and controlled potential experiments and the mode of operation chosen has been found to affect the kinetic constants derived (Dempers, 2000).

Kinetic constants determined for *At. ferrooxidans* (McDonald & Clark, 1970) and *L. ferrooxidans* (Dempers, 2000) showed marked differences between those determined from batch experiments and those from continuous experiments. Furthermore Dempers (2000) found that trends observed when varying temperature and pH differed between batch and continuous systems. Boon (1996) found that initial rate experiments also differed from continuous results. These differences are likely to result from the dependence of discontinuous experiments on the initial conditions used and the inoculum history (growth rate, substrate availability, metabolic activity) (Kovarova-Kovar & Egli, 1998; Liu, 1998) and the uncoupling of the rates of iron oxidation and microbial growth that may occur in the rapidly changing conditions at the beginning of a batch (Jones & Kelly, 1983). Hence batch and initial rate experiments are of limited use for the purposes of determining kinetic constants. Published kinetic constants derived from data produced by all of the above-mentioned experimental techniques will be compared and discussed in Chapter 3.

2.4.8 Other Parameters Affecting Iron Oxidation Systems

Other factors which have been identified as having an influence on the microbial oxidation of ferrous iron include inhibition by heavy metals, inhibition by other cells, and the ionic strength of the solution.

Growth of *At. ferrooxidans* was found to be inhibited by the presence of heavy metals in solution. Leaching of arsenopyrite to expose refractory gold, leads to the release of arsenic which inhibits microbial growth. Arsenic toxicity and microbial resistance has been studied in *At. ferrooxidans* (Tuovinen *et al.*, 1971), *At. caldus* (Hallberg, 1995), *L. ferrooxidans* (Breed, 2000) and *Sulfolobus* BC (Clark & Norris, 1996a). Similarly, the influence of copper, nickel and uranium in solution on the leaching of their respective ores is of interest. Silver was found to catalyze the ferric leaching of chalcopyrite (Miller & Portillo, 1981), but this benefit is offset by the toxic effect of silver on microbial growth (Mier *et al.*, 1996).

Varying effects of copper concentration on *At. ferrooxidans* growth have been reported, from inhibition at 0.45g.L^{-1} (Imai *et al.*, 1975) to unaffected at 10.1g.L^{-1} (Leduc & Ferroni, 1994). Similar tolerances and inhibitions were determined for thermophiles (Miller *et al.*, 1992; Mier *et al.*, 1996). Increased tolerance can be developed by progressive adaption, Le Roux & Wakerley (1988) adapted the copper tolerance of a *Sulfolobus* BC culture from 3g.L^{-1} to 27g.L^{-1} over 18 months.

High concentrations of cells have been found to inhibit the oxidation rate in *At. ferrooxidans.* This inhibition was found to be either competitive (Suzuki *et al.*, 1989, Nemati & Webb, 1997) or synergistic with ferric inhibition (Lizama and Suzuki, 1989). These conclusions were drawn from initial rate studies, using cell concentrations far higher than those found in common bioleaching systems and may be an artefact of the experimental apparatus and conditions chosen.

It has been suggested that increasing ionic strength will affect the growth kinetics of *At. ferrooxidans* both directly, by altering the osmotic pressure and the transmembrane potential, and indirectly, by altering the equilibrium speciation of the iron present (Blight & Ralph, 2004).

2.5 The Development of Kinetic Models to describe Microbial Ferrous Iron Oxidation

The gaps in the knowledge of the electron transfer chain and the overall complexity of modelling the number of intermediate kinetic reactions does not allow for the development of a completely structured model. Structured models restricted to *At. ferrooxidans* have been proposed. Huberts *et al.* (1994) developed a mechanistic model based on Ingledew's (1982) chemiosmotic theory, producing a set of five rate expressions dependent on which step is rate-limiting. Nagpal (1997) produced a structured model in which the cell mass was divided into three non-interchangeable portions, one comprising the cell components responsible for iron oxidation, one comprising the components for CO_2-assimilation, and the third , energy storage compounds. The split of the total cell mass into the three portions was achieved by assumed yield parameters. The model then produced fourteen cellular reactions that could be solved simultaneously to describe the overall reaction kinetics.

An alternative approach is the use of unstructured models, ignoring the intermediate reaction steps and treating a microbial cell as a macroscopic black box, with a fixed composition, that consumes substrate and produces product and more cells. The rates of microbial growth and substrate utilisation can thus be related to measurable extra-cellular conditions, like substrate concentration, pH, temperature, concentration of inhibitory substances, etc., and followed by completing elemental and charge balances (Roels, 1983).

Using this technique, microbial iron oxidation is characterised by two main reactions: iron oxidation:

$$4Fe^{2+} + 4H^{+} + O_2 \xrightarrow{\text{micro-organisms}} 4Fe^{3+} + 2H_2O \qquad [2.1]$$

and cell synthesis, where cells are assumed to possess typical cell stoichiometry $CH_{1.8}O_{0.5}N_{0.2}$ (Roels, 1983):

$$CO_2, H_2O, NH_4^{+} \longrightarrow CH_{1.8}O_{0.5}N_{0.2} \qquad [2.6]$$

and can be modelled by following the fate of the constituents of these reactions.

The reactions represent the generation and use of energy, and hence the rates of the two reactions are linked via a growth yield, or some expression of how the micro-organism uses the energy generated. A rigorous list of published rate equations for iron oxidation by *At. ferrooxidans* and *L. ferrooxidans* can be found in Tables 3.8-9.

2.5.1 Growth Rate Models

The most common unstructured model for microbial growth is the Monod equation (Monod, 1949) empirically linking the specific growth rate (μ) to the concentration of the limiting substrate.

$$\mu = \frac{\mu_{max}[Fe^{2+}]}{K_m + [Fe^{2+}]} \qquad [2.7]$$

where μ = the specific growth rate (h^{-1})
μ_{max} = the theoretical maximum specific growth rate (h^{-1})
K_m = the saturation constant (mM Fe^{2+})

This rate equation was used to describe both batch and continuous ferrous iron oxidation experiments with *At. ferrooxidans* (MacDonald & Clark, 1970; Lacey & Lawson, 1970; Kelly & Jones, 1978; Guay *et al.*, 1977; Smith *et al.*, 1988).

Whilst the Monod equation is an empirical model, an identical relation can be derived by assuming that the system follows a reaction mechanism analogous to Michaelis-Menten enzyme kinetics. In this mechanism the substrate (reactant) binds to an active site on the surface of the cell (enzyme), reacts, and the product is released, leaving the site free to react again. This reaction mechanism can be modified to account for inhibitory effects, producing different kinetic models.

Inhibition by ferric iron is most commonly described by a competitive product inhibition model (Kelly & Jones, 1978; Liu *et al.*, 1988; Norris *et al.*, 1988; Gomez *et al.*, 1996; Nyavor *et al.*, 1996; Harvey & Crundwell, 1997; Kawabe *et al.*, 2003).

$$\mu = \frac{\mu_{max}}{1 + \frac{K_S}{[Fe^{2+}]} + \frac{K_S}{K_I}\frac{[Fe^{3+}]}{[Fe^{2+}]}} \quad [2.8]$$

where K_S = the substrate affinity coefficient (mM Fe^{2+})
K_I = the ferric inhibition constant (mM Fe^{3+})

Jones & Kelly (1983) found that at least some portion of the inhibitory effect of ferric iron was non-competitive, modifying the observed μ_{max} value rather than the substrate affinity.

$$\mu = \frac{\mu_{max}}{\left(1 + \frac{[Fe^{3+}]}{K_I}\right)\left(\frac{K_s}{[Fe^{2+}]} + 1\right)} \quad [2.9]$$

Excessively high ferrous iron concentrations were found to induce substrate inhibition (Nikolov & Karamanev, 1992), this could be modelled by adding a $[Fe^{2+}]/K_{SI}$ term. Equation 2.10 also includes a term to account for simultaneous competitive product inhibition.

$$\mu = \frac{\mu_{max}}{1 + \frac{K_S}{[Fe^{2+}]} + \frac{K_S}{K_I}\frac{[Fe^{3+}]}{[Fe^{2+}]} + \frac{[Fe^{2+}]}{K_{SI}}} \quad [2.10]$$

where K_{Si} = the substrate inhibition coefficient ((mM Fe^{2+})$^{-1}$)

Braddock *et al.* (1984) modified the Monod equation adding a threshold ferrous iron concentration to account for the lack of growth at very low but non-zero iron concentrations

$$\mu = \frac{\mu_{max}([Fe^{2+}] - [Fe^{2+}]_t)}{K_m + ([Fe^{2+}] - [Fe^{2+}]_t)} \quad [2.11]$$

where $[Fe^{2+}]_t$ = the threshold ferrous iron concentration (mM Fe^{2+})

2.5.2 Specific Iron Utilisation Rate Models

One of the earliest studies on microbial ferrous iron oxidation, followed the kinetics of the iron oxidation reaction, and then related the results back to a specific growth rate equation via a growth yield (Lacey & Lawson, 1970).

$$\mu = \frac{\mu_{max}[Fe^{2+}]}{Y_{sx}(K_m + [Fe^{2+}])} \quad [2.12]$$

where Y_{sx} = the growth yield (molC.(mol Fe^{2+})$^{-1}$)

The derivation of the Michaelis-Menten mechanism follows the fate of the iron species, and the reaction implied is the iron oxidation reaction. This is related to the growth kinetics by assuming some yield relation. The specific iron utilisation rate can therefore also be described by a Michaelis-

Menten expression. Modified models including ferric inhibition, and threshold terms were re-developed in terms of the specific iron, or oxygen, utilisation rate (Kelly & Jones, 1978; Boon, 1996).

Boon (1996) used a competitive ferric inhibition model to describe her data and then showed that the substrate affinity term, K_s, could be neglected, producing a Michaelis-Menten-form rate equation that gave specific oxygen utilisation rates as a function of the ferric/ferrous-iron ratio, rather than as a function of ferrous iron.

$$q_{O_2} = \frac{q_{O_2}^{max}}{1 + \frac{K_S}{K_i}\frac{[Fe^{3+}]}{[Fe^{2+}]}} \qquad [2.13]$$

where q_{O2} = the specific oxygen utilisation rate ($molO_2.(molC.h)^{-1}$)
q_{O2}^{max} = the maximum specific oxygen utilisation rate ($molO_2.(molC.h)^{-1}$)

This equation was used by Hansford (1997) who argued that the analogous specific iron utilisation rate would also be a function of the ferric/ferrous-iron ratio, and that this was consistent with the chemiosmotic theory of microbial chemotrophic metabolism (Ingledew, 1982).

$$q_{Fe^{2+}} = \frac{q_{Fe^{2+}}^{max}}{1 + K_{Fe^{2+}}\frac{[Fe^{3+}]}{[Fe^{2+}]}} \qquad [2.14]$$

where q_{Fe2+} = the specific iron utilisation rate ($molFe^{2+}.(molC.h)^{-1}$)
q_{Fe2+}^{max} = the maximum specific iron utilisation rate ($mol\ Fe^{2+}.(molC.h)^{-1}$)
K_{Fe}^{2+} = the affinity coefficient with respect to the ferric/ferrous-iron ratio (-)

This rate equation was found to be appropriate for following *L. ferrooxidans* growth (Breed *et al.*, 1999; Breed & Hansford, 1999).

Meruane *et al.* (2002) developed a rate equation in terms of the ferric/ferrous-iron ratio by assuming reversibility of all reaction steps in the Michaelis-Menten reaction mechanism.

$$q_{Fe^{2+}} = \frac{q_{max} - K_2\frac{[Fe^{3+}]}{[Fe^{2+}]}}{1 + \frac{K_s}{[Fe^{2+}]} + K_I\frac{[Fe^{3+}]}{[Fe^{2+}]}} \qquad [2.15]$$

where K_2 ($molFe^{2+}.(molC.h)^{-1}$), K_s ($molFe^{2+}.L^{-1}$), and K_i (-) are constants derived from the defined reaction mechanism.

They also incorporated the Nernst equation to express their rate equation in terms of the solution redox potential.

$$q_{Fe^{2+}} = \frac{K_1^* \exp\left[\frac{nF}{2RT}\left(E^m - E_h^0\right)\right]\left\{1 - \exp\left[\frac{nF}{RT}\left(E^m - E\right)\right]\right\}}{1 + \frac{K_2^*}{[Fe^{2+}]} + K_3^* \exp\left[\frac{nF}{RT}\left(E_h - E_h^0\right)\right]} \quad [2.16]$$

where K_1^* ($molFe^{2+}.(molC.h)^{-1}$), K_2^* ($molFe^{2+}.L^{-1}$), and K_3^* (-) are equivalent to K_2, K_s and K_i respectively.

A novel model was developed focussing on the generation of energy across a membrane by using the analogy of a fuel cell circuit (Crundwell, 1997). The rate equation developed greatly resembles the ferric inhibition model raised to the power of one half. This one half power is a result of the assumption that the rate-limiting steps are electrochemical in nature and that the charge-transfer coefficients are close to one half.

$$q_{Fe^{2+}} = k\left(\frac{[Fe^{2+}]}{K_{Fe^{2+}} + [Fe^{2+}] + K_I[Fe^{3+}]}\right)^{0.5}\left(\frac{p_{O_2}}{k_B + p_{O_2}}\right)^{0.5} \quad [2.17]$$

where k = a constant, equivalent to q_{Fe2+}^{max} ($mMFe^{2+}.(cell.h)^{-1}$)
K_{Fe2+} = the substrate affinity coefficient, equivalent to K_S (mM Fe^{2+})
K_I = the ferric inhibition constant, equivalent to K_S/K_i (-)
k_B = the oxygen affinity coefficient (atm)
p_{O2} = the partial pressure of oxygen (atm)

2.5.3 Incorporating the Effects of Oxygen Concentration

Monod kinetics describe the specific growth rate in terms of the concentration of the growth-limiting reagent. Liu *et al.* (1988) studied a system that was designed to be limited by the dissolved oxygen concentration only.

$$\mu = \frac{\mu_{max}(DO - DO_\infty)}{K_S + (DO - DO_\infty)} \quad [2.18]$$

where DO = the dissolved oxygen concentration (mMO_2)
DO_∞ = the minimum dissolved oxygen concentration capable of sustaining growth (mMO_2)
K_S = the oxygen affinity coefficient (mMO_2)

In the case where more than one reagent is growth-limiting, the final rate can be determined by multiplying Monod terms. Huberts (1994) added a term to account for the effect of changing oxygen concentration.

$$q_{Fe^{2+}} = a_1\left(\frac{p_{O_2}}{k_B + p_{O_2}}\right)\left(\frac{[Fe^{2+}]}{[Fe^{2+}] + K_{Fe^{2+}}\left(1 + \frac{[Fe^{3+}]}{K'}\right)}\right) \quad [2.19]$$

where a_1 = constant, equivalent to q_{Fe2+}^{max}
K_{Fe2+} = the substrate affinity coefficient, equivalent to K_S ($mMFe^{2+}$)

K' = the ferric inhibition constant ($mMFe^{3+}$)
k_b = the oxygen affinity coefficient (atm)
p_{O2} = the partial pressure of oxygen (atm)

2.5.4 Incorporating the Effect of pH

Whilst many researchers have presented pH optima for their system, very few have attempted to explain how the system responds to conditions away from the optimum.

Breed & Hansford (1999) studied *L. ferrooxidans* over a range of pH values 1.3 – 1.7 and found competitive inhibition, with the pH affecting the observed affinity coefficient but not the maximum utilisation rate. The effect of pH could be modelled by modifying their K_{Fe2+} term by a linear function of pH.

$$q_{Fe^{2+}} = \frac{q^{max}_{Fe^{2+}}}{1+(0.0048pH-0.0043)\frac{[Fe^{3+}]}{[Fe^{2+}]}} \qquad [2.20]$$

Kelly and Jones (1978) found that the inhibiting effect of pH on *At. ferrooxidans* was purely non-competitive, affecting the maximum growth rate only.

Shrihari *et al.* (1990) studied *At. ferrooxidans* in shake flasks and found that pH had a severe effect, and modelled it as an exponential decrease in the rate away from the optimum. This can be related to rapid ferric precipitation at the pH studied (2.2-2.5) rather than a direct effect of the pH.

$$\frac{dN}{dt} = \frac{\mu_{mo} e^{\left(-K(pH-pH_o)^2\right)}[Fe^{2+}]}{K_s+[Fe^{2+}]}N - \mu_d[Fe^{3+}]^2 N \qquad [2.21]$$

where N = cell concentration ($molC.L^{-1}$)
μ_{mo} = the maximum growth rate under optimum conditions (h^{-1})
K = a constant modulating μ_{mo} to account for pH (-)
pH_o = optimum pH
μ_d = the specific death rate (h^{-1})

In contrast, Pesic *et al.* (1989) found no effect of pH on *At. ferrooxidans* iron oxidation below pH 2.0, and found a linear relation above pH 2.2

$$-\frac{d[Fe^{2+}]}{dt} = 1.62\times10^{11} C_{bact}[H^+][Fe^{2+}]pO_2 e^{-\left(\frac{58.77}{RT}\right)} \qquad [2.22]$$

where C_{bact} = cell concentration ($molC.L^{-1}$)
pO_2 = the partial pressure of oxygen (atm)

Crundwell (1997) extended his rate equation to account for pH by the formation of a reactive $FeOH^+$ species which adsorbs to the reactive sites on the cell membrane.

$$q_{Fe^{2+}} = k\left(\frac{[Fe^{2+}]/[H^+]}{K_{Fe^{2+}} + [Fe^{2+}]/[H^+] + K_1[Fe^{3+}]}\right)^{0.5}\left(\frac{p_{O_2}}{k_B + p_{O_2}}\right)^{0.5} \quad [2.23]$$

2.5.5 Effect of Temperature

Over the temperature ranges investigated, the effect of temperature on the maximum specific rate was often accounted for by an Arrhenius function (Lacey & Lawson, 1970; MacDonald & Clark, 1970; Breed *et al.*, 1999; Nemati & Webb, 1997; Han *et al.*, 1997).

$$\mu_{max} = k_0 \exp\left(\frac{-E_a}{RT}\right) \quad [2.24]$$

where k_0 = frequency factor (h^{-1})
E_a = Activation energy or temperature characteristic ($J.mol^{-1}$)

This function describes the effect of temperature below T_{opt}, as illustrated in Figure 2.4, where $\ln(\mu_{max})$ is a linear function of T^{-1}. As it is increasingly difficult to perform meaningful continuous experiments in the temperature-inhibited region above T_{opt}, the Arrhenius function is often sufficient to describe the effect of temperature in continuous systems.

Since microbial growth is undoubtedly more complicated than a simple chemical reaction, E_a no longer represents the activation energy of any given reaction and becomes a curve-fitting parameter.

Another function that describes the viable growth temperature region was proposed by Ratkowsky *et al.* (1982), who used a square-root function.

$$\sqrt{\mu_{max}} = b(T - T_0) \quad [2.25]$$

where T_0 = the temperature at which appreciable growth ceases

Comparisons between the Arrhenius and the Ratkowsky functions result in little statistical difference in fit (Ratkowsky *et al.*, 1982).

The Ratkowsky equation was later extended to cover the full biokinetic temperature range (Ratkowsky *et al.*, 1983), accounting for decreasing rates both above and below the optimal temperature region of growth.

$$\sqrt{\mu_{max}} = b(T - T_{min})\left\{1 - \exp^{d(T - T_{max})}\right\} \quad [2.26]$$

where T_{min} and T_{max} are the temperatures above and below the optimum at which the predicted rate is zero.

This function was successfully used to describe the growth of two extremely thermophilic *Sulfolobus*-like cultures (Plumb *et al.*, 2002) and for a range of common iron- and sulfur-oxidising Bacteria and Archaea (Franzmann *et al.*, 2005).

Zwietering *et al.* (1991) noted that the Ratkowsky equation predicted positive rates above the T_{max} as a consequence of the square root function, and suggested a modification

$$\mu_{max} = [b(T - T_{min})]^2 \left\{1 - \exp^{d(T-T_{max})}\right\} \quad [2.27]$$

which predicts negative rates above T_{max}.

A number of functions were proposed by analogy with the effect of temperature on enzymes. This is in agreement with the analogy of using Michaelis-Menten kinetics to describe the overall microbial kinetics. In these reaction schemes, the increase in the growth reaction with temperature remains modelled by either an Arrhenius or an Eyring-type function, and the overall rate is modified by a simultaneous temperature-related denaturing or deactivation reaction, reducing the fraction of the enzyme (cell mass) that remains viable.

MacDonald & Clark (1970) studied *At. ferrooxidans* at temperatures between 20 and 40°C, and attempted to fit the resultant μ_{max} values to one such function, developed for the effect of temperature on enzymes based on absolute reaction rates (Koffler *et al.*, 1947)

$$I = \frac{C\,T \exp^{-\frac{\Delta H_1}{RT}}}{1 + \exp^{\frac{\Delta H_2}{RT}} \exp^{\frac{\Delta S}{R}}} \quad [2.28]$$

where I = enzyme activity or cell activity or specific rate
C = a constant
ΔH_1 = the activation energy of the enzyme-catalysed reaction
ΔH_2 = the heat of reaction of the enzyme denaturation equilibrium
ΔS = the entropy of the denaturation equilibrium

A simpler form of this function was presented by Esener *et al.* (1983), based on the same dual reaction scheme

$$\mu_{max} = \frac{A \exp^{-\frac{\Delta H_1^*}{RT}}}{1 + K \exp^{\frac{\Delta H_2}{RT}}} \quad [2.29]$$

Both forms are flawed in that they present thermal deactivation as a reversible reaction, when in truth it is at least partially irreversible. Hinshelwood and Dean (1966) proposed a function assuming complete irreversibility of the denaturation reaction.

$$\mu_{max} = A \exp^{\left(\frac{-E_a}{RT}\right)} - B \exp^{\left(\frac{-E_b}{RT}\right)} \quad [2.30]$$

where A = frequency factor of growth reaction (h^{-1})
E_a = activation energy of growth reaction ($J.mol^{-1}$)
B = frequency factor of the denaturation reaction (h^{-1})
E_b = the activation energy of the denaturation reaction ($J.mol^{-1}$)

This function was used by Gomez and Cantero (1998) to describe the effect of temperature on *At. ferrooxidans* in batch culture.

Another function accounting for both hot and cold deactivation of the cell was presented by Schoolfield *et al.* (1981), who modified the parameters of a previously published function to reduce correlation between parameters.

$$\mu_{max} = \frac{\mu_{25} \frac{T}{298} \exp\left[\frac{H_a}{R}\left(\frac{1}{298} - \frac{1}{T}\right)\right]}{1 + \exp\left[\frac{H_l}{R}\left(\frac{1}{T_l} - \frac{1}{T}\right)\right] + \exp\left[\frac{H_h}{R}\left(\frac{1}{T_h} - \frac{1}{T}\right)\right]} \quad [2.31]$$

where μ_{25} = specific growth rate at 25°C
H_a = enthalpy of activation
T_l = temperature at which the enzyme (cell) is de-activated due to low temperature
H_l = enthalpy of de-activation due to low temperature
T_h = temperature at which the enzyme (cell) is de-activated due to high temperature
H_h = enthalpy of de-activation due to high temperature

Ratkowsky *et al.* (2005) noted the similarity between how cells and globular proteins react to temperature and concluded that the similarity is mechanistic, and proposed

$$r = \frac{cT \exp^{\frac{\Delta H_1}{RT}}}{1 + \exp^{-n\frac{\left(\Delta H^* - T\Delta S^* + \Delta C_p\left[(T - T_H^*) - T\ln\frac{T}{T_S^*}\right]\right)}{RT}}} \quad [2.32]$$

where r = reaction rate
ΔH_1 = enthalpy of activation
ΔH^* = enthalpy change at T_H
T_H^* = convergence temperature for enthalpy
ΔS^* = entropy change at T_S
T_S^* = convergence temperature for entropy
ΔC_p = heat capacity change between the native and denatured enzyme states
n = number of amino acid residues in the protein

Thus a number of equations have been proposed, with a variety of numbers of parameters. While many of the parameters purport to possess some physical meaning, they tend to be individually immeasurable, and so can only be determined by regression of the observed rate. Therefore the function chosen is dependent on the number of points available for regression and the temperature region in which the data fall, if no data were captured at temperatures where the rate was

noticeably inhibited by high temperature, then it is unlikely that meaningful predictions of T_{max} or the rate of thermal deactivation can be made and other functions should be used. Comprehensive models are only valuable if there is a comprehensive data set to be modelled.

2.5.6 Yield and Maintenance

The rate of substrate utilisation and the consequent rate of microbial growth can be coupled by some accounting of how a cell uses the energy produced. The simplest coupling is by assuming a constant yield (Monod, 1949), where the rate of growth is directly proportional to the rate of substrate utilisation. This has been found to be inadequate to explain observed trends in microbial growth and has been modified to include features like endogenous respiration (Herbert *et al.*, 1958), or the use of existing cell mass as additional substrate, and cell maintenance (Pirt, 1965), acknowledging that some portion of energy acquired is used to maintain the integrity of existing cells instead of generating new ones.

Following proposing the concept of maintenance energy as an additional avenue for energy consumption, Pirt developed a model of the relationship between microbial growth and substrate consumption, assuming that the energy required for cell maintenance remained constant (Pirt, 1965)

$$q_{Fe^{2+}} = \frac{\mu}{Y_{SX}^{max}} + m_s \qquad [2.33]$$

where Y_{SX}^{max} = the theoretical maximum yield
m_s = the maintenance coefficient

This assumption was challenged by several researchers who reported varying cell yield and maintenance requirements under different stresses (Neijssel & Tempest, 1976; Kuenen, 1979). Neijssel & Tempest (1976) proposed a modified relationship adding a term to account for increased maintenance energy requirement at low growth rates.

$$q_{Fe^{2+}} = \frac{\mu}{Y_{SX}^{max}} + m_s + cm_s\mu \qquad [2.34]$$

Where c = a constant governing the growth-rate-dependent portion of the maintenance energy

Pirt (1982) modified his model to include growth-rate-dependent maintenance, assuming that the growth rate dependent portion of the maintenance energy requirement decreases to zero as μ approached μ_{max}.

$$q_{Fe^{2+}} = \frac{\mu}{Y_{SX}^{max}} + m_s + m_s^v(1-k\mu) \qquad [2.35]$$

Where m_s = the constant maintenance energy coefficient

m_s^v = the growth-rate-dependent maintenance energy coefficient

Differences in yield have been found between substrate-limited and substrate-sufficient cultures. This has been linked to the uncoupling of growth and substrate utilisation and the dissipation of the non-growth energy in "futile cycles", operating inefficient biochemical pathways, wasting ATP (Tempest, 1978; Liu, 1998). This adds an additional component to the substrate balance.

$$\Delta Substrate = \Delta Substrate_{growth} + \Delta Substrate_{maintenance} + \Delta Substrate_{waste} \quad [2.36]$$

In iron oxidation systems, few researchers have attempted to account for non-growth energy usage. Much initial work was performed assuming a constant growth yield (Lacey & Lawson, 1970; MacDonald & Clark, 1970; Liu *et al.*, 1988; Shrihari *et al.*, 1990). Kelly & Jones (1978) noted that growth and substrate utilisation can be uncoupled in batch cultures and that *At. ferrooxidans* has the capacity to dissipate energy generated in the absence of growth.

Microbial maintenance requirements have been described by the constant maintenance Pirt equation (Equation. 2.33). Jones & Kelly (1983) found that this equation predicts different results for cultures experiencing competitive or non-competitive product inhibition. Boon (1996) attempted to model the bioenergetics of both batch and continuous cultures and found that only the continuous cultures could be modelled with the Pirt equation. Breed *et al.* (1999) and Breed and Hansford (1999) used the constant maintenance Pirt equation for continuous cultures run at varying temperature and pH, and found that the scattering of the results was too great to propose any effect of the parameters varied on the bioenergetics observed.

Heijnen & van Dijken (1992) developed a black box description of the theoretical maximum yield possible for a system, based on the dissipation of available Gibbs free energy. In this system, a macrochemical balance for microbial growth is set up from the simultaneous solution of the individual element and charge balances. This produces coefficients in terms of the substrate yield Y_{sx}. The macrochemical balance is used to determine the Gibbs free energy of reaction, which is in turn equal to the Gibbs free energy dissipated. The energy dissipated has two components, one growth related and the other maintenance related.

$$\left(\frac{D_S^{01}}{r_x}\right) = \left(\frac{D_S^{01}}{r_x}\right)_{growth} + \frac{m_E}{\mu} \quad [2.37]$$

Where D_s^{01}/r_x = the dissipation of Gibbs energy needed to produce 1 C-mol of biomass from a given carbon source (kJ. molC^{-1})

m_E = the specific rate of consumption of maintenance energy (kJ.(molC.h)$^{-1}$)

For autotrophic growth with reverse electron transfer D_s^{01}/r_{ax} = 3500 kJ/molC, and the maintenance requirement can be determined from the correlation (Tijhuis *et al.*, 1993).

$$m_E = 5.7 \exp\left\{\frac{-6.94\times10^4}{R}\left(\frac{1}{T}-\frac{1}{298}\right)\right\} \quad [2.38]$$

2.6 Thermophilic Ferrous Iron Oxidation Kinetics

Little quantitative kinetic data has been published on thermophilic microbial ferrous iron oxidation. Earlier studies focussed on establishing which microbial strains were capable of growth on ferrous iron and whether that growth was autotrophic (Brierley *et al.*, 1978, Marsh *et al.*, 1983, Norris & Barr, 1985; Brock *et al.*, 1976; Wood & Kelly, 1983; De Rosa *et al.*, 1975).

Comparative studies were performed, comparing overall iron consumption rates between different isolates (Marsh *et al.*, 1983) and between thermophile and mesophile (Nemati & Harrison, 2000). These are of limited use as the overall consumption rate is strongly dependent on the cell concentration, and direct comparison is difficult without sufficient cell concentration and growth rate data.

Specific iron utilisation rates can be extrapolated from published specific growth rates and cell yields. Nemati & Harrison (2000) measured the iron oxidation rates of *A. brierleyi* in batch culture over varying initial ferrous iron concentrations and found that below iron concentrations of 5.8g.L^{-1}, the maximum specific growth rate (μ_{max}) was 0.043h^{-1} and the growth yield was 2.2 x 10^{14}cells/kgFe^{2+}, this implies a maximum specific iron utilisation (q_{max}) of 0.55 molFe^{2+}.(molC.h)$^{-1}$. This is significantly lower than Konishi *et al.* (1995) who produced a q_{max} of 8.2 molFe^{2+}.(molC.h)$^{-1}$ (from Y_{sx} = 2.05 x 10^{13}cells/kgFe^{2+}, and μ_{max} = 0.06, re-calculated from the exponential growth phase of the ferrous iron oxidation batch growth curve). Nemati & Harrison (2000) also found that the growth yield dropped with an increase in the initial ferrous iron concentration, and that growth was completely inhibited above 7.5 g.L^{-1}.

Kinnunen *et al.* (2003) investigated ferrous iron oxidation of moderate thermophiles over a range of temperatures, noting increasing oxidation rates up to 60°C, significantly above the observed optimum temperature for growth of 50°C. This is in agreement with the results of Brierley *et al.* (1978) who studied the isolate Thiobacillus TH1 (later identified as *Sulfobacillus thermosulfooxidans* (Bridge & Johnson, 1998)). Brierley *et al.* (1978) found that in oxygen uptake experiments, the maximum specific oxygen utilisation rate (V_{max}) increased up to 60°C, with the effect of temperature described by an Arrhenius term with E_a = 36 kJ.mol^{-1}. The kinetics were described by a competitive product inhibition model. The constants are presented in Table 2.6.

Table 2.6 Published kinetic constants for thermophilic ferrous iron oxidation, converted to a common unit basis.

Micro-organism	μ_{max} (h^{-1})	q_{max} ($molFe^{2+}.(molC.h)^{-1}$)	K_s ($mMFe^{2+}$)	K_i ($mMFe^{3+}$)	Author
A. brierleyi	0.04	0.53-4.1[a]	-	-	Nemati & Harrison, 2000
A. brierleyi	0.06[b]	8.2[c]	-	-	Konishi *et al.*, 1995
A. brierleyi	0.073	4.2	0.4	1.9	Norris, 1992
M. sedula	0.139	11.9	1.0	1.0	Norris, 1992
S. metallicus		5.04	3.646	0.95	Meruane *et al.*, 2003
S. metallicus (BC)	0.082	9.9	0.4	1.7	Norris, 1992
Sulfobacillus thermosulfooxidans	0.18	10.96	7.3	2.9	Brierley *et al.*, 1978

a - q_{max} determined from μ and the cell yield given as $2.2 \times 10^{14} - 5.3 \times 10^{13}$ cells.$(kgFe^{2+})^{-1}$
b - μ re-calculated from presented iron oxidation batch data
c - q_{max} determined from μ and the cell yield given as 2.05×10^{13} cells.$(kgFe^{2+})^{-1}$

The ferrous iron oxidation kinetics of extreme thermophiles have also been studied in oxygen uptake experiments (Norris, 1992) and in an electrochemical cell (Meruane *et al.*, 2003). Both concluded that a competitive product inhibition model (Equation. 2.10) was appropriate to describe the results.

The metabolic activity of the thermophiles, as indicated by their specific substrate utilisation rate, was found to be similar to that of mesophilic ferrous iron oxidisers (Nemati & Harrison, 2000; Norris, 1992), leading to the conclusion that it is not their superior iron-oxidising capacity that gives thermophiles their advantage in the oxidation of mineral sulfides.

2.7 Conclusions

The review of the available literature has revealed that a number of thermophilic micro-organisms have been identified that have shown the capacity for ferrous iron oxidation. Information on the oxidation kinetics of these micro-organisms is limited.

A number of unstructured models have been developed to describe mesophilic microbial ferrous iron oxidation. The nature of these models, based on following the macroscopic oxidation reaction and transfer of energy to a generalised growth reaction rather than individual biochemical pathways allow the models to be transferred to the thermophilic regime. The models and kinetic constants produced for *At. ferrooxidans* and *L. ferrooxidans* will be compared and discussed further in Chapter 3.

The unstructured model proposed involves the two macroscopic reactions of iron oxidation and microbial growth, generating and consuming energy respectively. This is best described in terms of a Michealis-Menten-form rate expression for the specific rate of iron oxidation, coupled to the rate of growth via some expression of the growth yield, energy utilisation , efficiency and cell

maintenance. This is preferred to a Michaelis-Menten-form expression for cell growth, as the rate of iron oxidation is directly affected by the rate-determining parameters, whereas the rate of cell growth is affected primarily by the availability of energy for growth and only indirectly affected by the conditions outside the cell.

Parameters influencing the rate of oxidation were discussed with respect to their observed effect on mesophilic iron oxidation systems and their implied effect on thermophilic ferrous iron oxidation. The concentrations of ferrous and ferric iron and the ratio of the two were found to be key parameters in controlling the rate of growth and oxidation. These findings are in accord with the chemiosmotic mechanism proposed for energy assimilation.

In mesophilic systems, the contribution of the competing (abiotic) oxidation of ferrous iron by molecular oxygen is negligible. Increased temperature will result in an increased rate of abiotic oxidation and its contribution to the overall iron oxidation rate under thermophilic conditions will need to be quantified, so that the microbial contribution may be assessed.

The decreased solubility of oxygen and carbon dioxide in water at elevated temperature, though partially offset by the concomitant increase in the overall gas-liquid mass transfer coefficient implies that caution is necessary in the design and operation of kinetic experiments performed at elevated temperature to avoid gas-liquid mass transfer limitations.

Chapter 3

A Re-evaluation of Published Mesophilic Microbial Iron Oxidation Data and Rate Equations

A number of unstructured models of varying complexity have been proposed to describe the kinetics of the oxidation of ferrous iron by *Acidithiobacillus ferrooxidans* and other mesophilic bioleaching micro-organisms observed over a range of experimental conditions, using a variety of experimental techniques. The models include rate equations describing the specific rates of growth and/or substrate utilisation as a function of the reaction conditions. Several comprehensive reviews describe the development of these models (Nemati *et al*, 1998; Jensen & Webb, 1995; Haddadin *et al*, 1995; Boon, 1996). These review what has been published but do not compare models or evaluate each model for incorporation into a general bioleaching model.

As concluded in Chapter 2, the unstructured nature of the kinetic models and the similarity in reaction mechanism between mesophiles and thermophiles suggests that models developed for mesophilic systems may be applied in thermophilic systems. Thus insight gained from close scrutiny of mesophilic rate data and kinetic models may prove useful in choosing appropriate kinetic models to describe the thermophilic rate data presented in Chapter 5.

In this chapter; kinetic data, rate equations and kinetic constants will be compared directly using a defined common basis. The published kinetic data will be examined for similarities and differences. The published rate equations will be evaluated in terms of their general applicability and their responses to changing conditions will be discussed.

3.1 Conversion of Published Units to a Common Basis

One feature which hampers the direct comparison of published data, models and kinetic constants is the great variety of units and measurements used to present experimental results. It is therefore necessary to convert the published data and kinetic constants to a common basis. In this work all units have been converted to a molar basis, in particular, cell concentrations have been expressed in terms of moles carbon present.

These conversions were facilitated by the use of published conversion factors:

Table 3.1 Published quantities and proportions of biomass constituents for *At. ferrooxidans.*

Reference	Published conversion	Units
Silverman & Lundgren, 1959	1.91×10^{-14}	$gN.cell^{-1}$
Lundgren *et al*, 1964	6.1-7.0% 38.1-44%	Nitrogen mass% of dry weight protein mass% of dry weight
Tuovinen & Kelly, 1973	245×10^{-6} 3.9×10^{10} 0.35	$moleCO_2.(g\ Fe^{2+})^{-1}$ $cells.(g\ Fe^{2+})^{-1}$ $g\ dry\ weight.(molFe^{2+})^{-1}$
Gormely & Duncan, 1974	7.67×10^{-11} 1.57×10^{-11}	$mgC.cell^{-1}$ $mgN.cell^{-1}$
Jones & Kelly, 1983	48-66%	protein mass% of dry weight
Moon, 1995	5.30×10^{-11} 1.18×10^{-10} 1.3×10^{-11} 41-48%	$mgC.cell^{-1}$ $g\ dry\ weight.cell^{-1}$ $mgN.cell^{-1}$ protein mass% of dry weight

The complex reactions and reaction mechanisms of microbial life and growth can be avoided by modelling the cell as a unit which can be represented by a single chemical formula consisting of the cell's major elemental constituents in their stoichiometric proportions. These proportions have been measured by direct elemental analysis of the dried cell mass. Elemental analysis determined mass% of carbon, nitrogen and hydrogen, the remainder was assumed to be oxygen. The results for bioleaching micro-organisms were compared in Table 3.2 to the general stoichiometric formula proposed by Roels (1983).

Table 3.2 Stoichiometric formula for biomass determined by elemental analysis.

Reference	Stoichiometric formula	
Roels, 1983	$CH_{1.8}O_{0.5}N_{0.2}$	general
Jones & Kelly, 1983	$CH_{1.77}O_{0.55}N_{0.17}$	*Acidithiobacillus ferrooxidans*
Moon, 1995	$CH_{1.79}O_{0.5}N_{0.2}$	mixed culture

Jones & Kelly (1983) used a pure *At. ferrooxidans* culture, Moon (1995) used a mixed culture from a continuous bioleaching pilot plant operation, most likely pre-dominantly *Leptospirillum ferriphilum*, both show only small variation from the general formula for bioleaching micro-organisms. Hence the general formula will be used in this work.

The most obvious way to quantify the amount of biomass is to count them directly. However this does not account for change in cell size, also cell counting is notoriously inaccurate and is made even more difficult by the presence of solid mineral particles and/or iron precipitates. Conversions from number if cells to moles of carbon present was achieved by finding sources where both had been measured.

Table 3.3 Conversions for moles carbon per cell.

Reference	molC/cell	comment
Tuovinen & Kelly, 1973	6.51×10^{-15}	given yield.cell^{-1} and yield.(mole CO_2)$^{-1}$
Gormely & Duncan, 1974	6.39×10^{-15}	measured
Kelly & Jones, 1978	$4 - 5 \times 10^{-15}$	given dry weight and equivalent cell number
Moon, 1995	4.41×10^{-15}	measured

Measured values of amount of carbon per cell agree to within an order of magnitude, with Tuovinen & Kelly (1973) agreeing closely with that of Gormely & Duncan (1974) and Kelly & Jones (1978). The lower value reported by Moon (1995) is consistent with the lower dry weight per cell observed.

Another common technique used in quantify biomass is measurement of the mass of dried cells. This requires the quantitative separation of the cell mass from all other non-soluble matter in the reactor liquor, without loss of biomass. The amount of carbon in the dried biomass can also be deduced from the stoichiometric formula used to describe the composition of biomass posited by Roels (1983).

Table 3. 4 Amount of carbon present per gram dry cell weight.

Reference	molC/g dry weight	Comment
Tuovinen & Kelly, 1973	4.05×10^{-2}	given yield.(g dry weight)$^{-1}$ and yield.(mole CO_2)$^{-1}$
Jones & Kelly, 1983	4.00×10^{-2}	from elemental analysis
Moon, 1995	3.74×10^{-2} 4.06×10^{-2}	measured dry weight.(cell)$^{-1}$ and molC.(cell)$^{-1}$ from elemental analysis
Roels, 1983	4.06×10^{-2}	from stoichiometric ratio

The values all correspond very closely with that deduced from the general formula. Cell concentrations have also been reported in terms of weight of wet cells per volume, a method which, while possibly internally consistent in the experiments performed, is a dubious method for quantifying

biomass, there is no way of differentiating between liquid inside and outside the cells, and even the liquid inside may vary with the experimental conditions. Proportions of dry weight to wet weight of between 3 – 30% have been reported for a variety of unicellular organisms. A value of 20% has been used to deduce dry weights of *At. ferrooxidans* (Halfmeier *et al*, 1993).

The amount of nitrogen measurable presented in Table 3.5 appeared to be much more variable than other measured elements. This could be attributed to the difficulty in ensuring the complete extraction of nitrogen, or variation in the amount of protein per cell. Most values correspond to nitrogen constituting between 5 -6 mol%, and further conversions will be done using the general stoichiometric formula.

Table 3.5 Amount of carbon present per mole nitrogen.

Reference	molC/molN	Comment
Silverman & Lundgren, 1959	4.68	given mass N.(cell)$^{-1}$
Lundgren *et al.*, 1964	9.32	given % g N.(g dry weight)$^{-1}$
Gormely & Duncan, 1974	5.7	given g N.(cell)$^{-1}$ and g C.(cell)$^{-1}$
Jones & Kelly, 1983	5.85	from elemental analysis
Moon, 1995	4.75 4.95	given g N.(cell)$^{-1}$ and g C.(cell)$^{-1}$ from elemental analysis
Roels, 1983	5.00	from stoichiometric ratio

Measured protein content values published vary even more than nitrogen. This may be due to variable amounts of protein being present per cell under different conditions, or due to difficulties in applying the technique at low pH.

Table 3.6 Amount of cellular carbon present per gram of protein (taking 4.06 x 10^{-2} molC.(g dry weight)$^{-1}$.

Reference	molC/g protein	Mass% of dry weight
Lundgren *et al.*, 1964	0.092	44 %
Jones & Kelly, 1983	0.068 (0.085 - 0.062)	60 % (range 48-66 %)
Moon, 1995	0.099 - 0.085	41-48 %

Jones & Kelly (1983) measured iron oxidation in continuous culture over a range of dilution rate to get an average 60% protein content, the other published values were measuring cells in ore systems. As iron oxidation is the focus of this investigation, the value of 0.068 molC.molN^{-1} will be used further.

It can be seen that despite some variability, the literature reviewed generally agrees on the composition and proportions of cell elements, and it is therefore possible to generate a set of consistent conversion

factors that can be used to compare sets of published data, and to test the general applicability of published models and model constants. The conversions that will be used for the following analysis can be found in Table 3.7.

Table 3.7 Conversions used in this work.

Biomass Element	Conversion	Reference
Biomass stoichiometry	$CH_{1.8}O_{0.5}N_{0.2}$	Roels, 1983
Carbon	6.39×10^{-15} molC.(cell)$^{-1}$	Gormely & Duncan, 1974
Dry Weight	4.06×10^{-2} molC.(g dry weight)$^{-1}$	from $CH_{1.8}O_{0.5}N_{0.2}$
Wet Weight	8.12×10^{-3} molC.(g wet weight)$^{-1}$	Halfmeier *et al*, 1993 (20%)
Nitrogen	5.00 molC.(molN)$^{-1}$	from $CH_{1.8}O_{0.5}N_{0.2}$
Protein	0.068 molC.(g protein)$^{-1}$	Jones & Kelly, 1983 (60%)

3.2 A Comparison of Published Mesophilic Ferrous Iron Oxidation Data in Continuous Culture

Investigations of various features of iron oxidation kinetics have been pursued using a variety of techniques: batch experiments in shake flasks and in stirred tank reactors; continuous culture experiments in stirred tank reactors, initial rate experiments and applied potential experiments in electrochemical cells.

As discussed in Section 2.4.7, cultures behave differently in continuous and discontinuous systems (Kovarova-Kovar & Egli, 1998), as the observed kinetics in discontinuous cultures may be distorted by the inoculum history and by a delay in the response by the culture to adapt to rapidly changing experimental conditions. In iron oxidation systems, it has been shown that the kinetic constants determined for batch experiments differ from those determined in continuous culture (MacDonald & Clark, 1970; Boon *et al.*, 1999a&b; Dempers *et al.*, 2003). The unstructured modelling approach relates the reaction kinetics to measurable bulk solution conditions, this is best observed in continuous culture, where a steady state response to set experimental conditions can be observed. Continuous experiments are also expected to give a more appropriate indication of how the cells will behave in a continuous bioleaching system.

Published continuous rate data were examined to establish commonalities and differences between systems run at temperatures between 22 – 35 °C, and with total iron concentrations between 9 – 210 mM. Data sets were gathered by scanning images from published articles, capturing the data for re-analysis using image analysis software (ScanIt 1.0, www.amsterchem.com/?scanit/). Data sets were collated as sets of steady state specific rates, ferrous iron concentration and the ratio of ferric/ferrous-

iron. Where necessary, the ferric/ferrous-iron ratio was determined from the ferrous iron and the stated total iron concentrations. The rates of growth and specific iron utilisation for published continuous culture experiments were superimposed as a function of the observed ferric/ferrous-iron ratio to see whether the variations in observed rate could be sufficiently explained by changes in the ferrous and ferric iron concentrations.

Steady state specific growth rate data sets for *At. ferrooxidans* were collected from MacDonald & Clark (1970) Figure 6; Braddock *et al.* (1984) Figure 3; Liu *et al.*, (1988) Figure 2; Boon *et al.* (1999a) Figures 2 & 3 combined; Gomez & Cantero (2003) Figure 2; Guay *et al.* (1977) Figure 3; Smith *et al.* (1988) Figure 10; and Jones & Kelly (1983) Figures 6, 8, and 10.

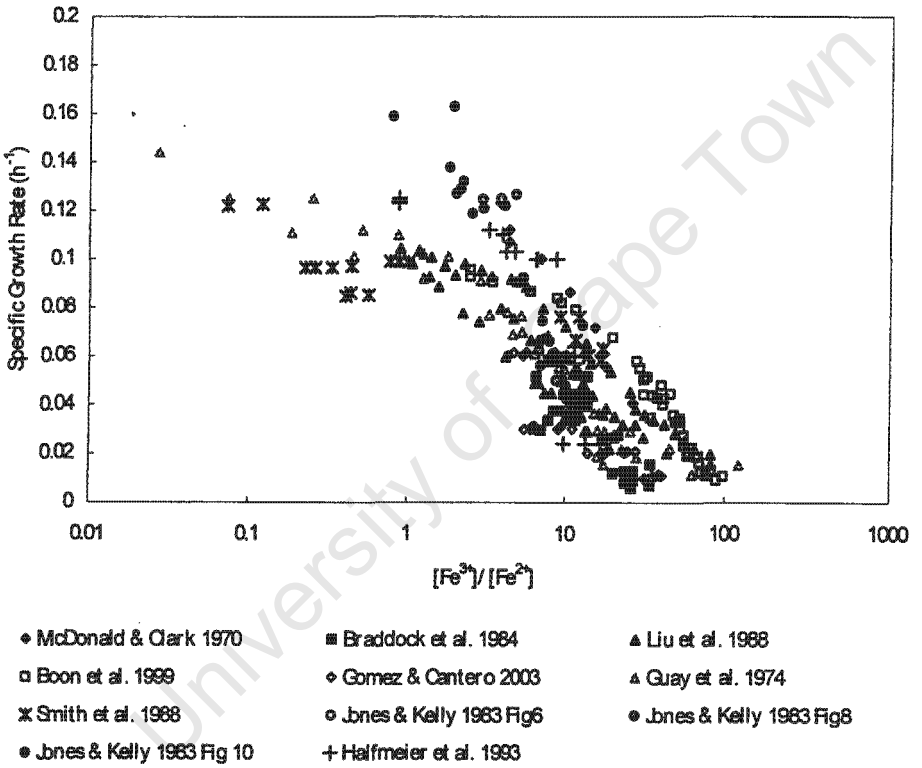

Figure 3.1 A superimposition of published specific growth rates for *At. ferrooxidans* in continuous culture as a function of their ferric/ferrous-iron ratio.

Growth kinetics can be studied in continuous culture without physically measuring the cell concentration as the specific growth rate can be derived from the steady state dilution rate, assuming ideal behaviour in a CSTR. Measurement of the specific substrate utilisation rate is more complicated and necessitates some description of the biomass concentration. Few papers include their cell concentration data and this limits the amount of data that is available for comparison. Specific iron utilisation rate data in continuous culture was collated from MacDonald & Clark (1970) Figure 6; Braddock *et al.* (1984) Figure 9; Boon *et al.* (1999a) Figures 2 & 8 combined and Gomez & Cantero

(2003) Figures 4 & 5 combined. Data from controlled potential experiments: Harvey & Crundwell (1997) Figure 2 and Meruane *et al.* (2002) Figures 2 & 3 were also superimposed.

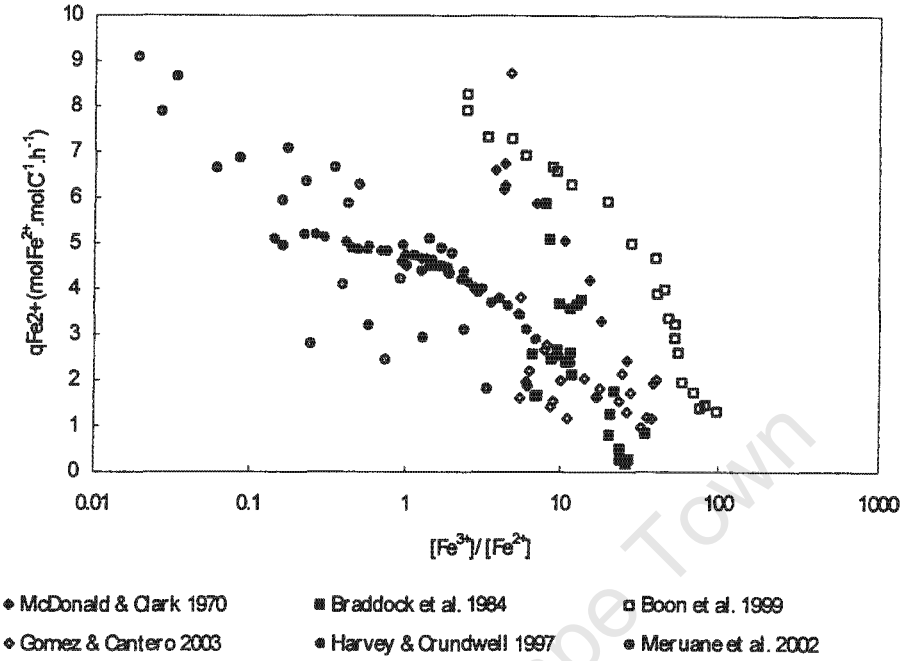

Figure 3.2 A superimposition of published specific iron utilisation rates for *At. ferrooxidans* in continuous culture as a function of their ferric/ferrous-iron ratio.

Figures 3.1 and 3.2 show that trends in specific ferrous iron utilisation rates are very similar to those for specific growth within each data set, indicating that growth and substrate utilisation are tightly coupled in most continuous culture systems.

The similarity in the relationship between the specific iron utilisation rates and the ferric/ferrous iron ratio for the different data sets is less obvious than for the specific growth rates. All systems show high specific rates at low ratios, dropping off with increasing ferric/ferrous-iron ratio, a feature characterised by both increasing ferric concentration and scarcity of substrate, but the point at which this drop-off occurs varies from ferric/ferrous-iron ratios of 1 to 100. This may be due to the lower substrate affinity observed in experiments performed in discontinuous culture (Harvey & Crundwell (1997) and Meruane *et al.* (2002) performed their experiments in redox-controlled batch systems). Microbial cultures grown in continuous systems for extended periods under nutrient–limited conditions have been found to become more efficient at utilising the scarce substrate. This can manifested as either decreased ferric inhibition, or increased affinity for ferrous iron, or both - either effect would produce increased rates at higher ferric/ferrous-iron ratios. This adaption is often a phenotypic change rather than a change in strain or species and may explain differences between continuous results and experiments that do not allow for periods of adaption.

Further variation in substrate affinity may be linked in some part to the difference in the total iron concentration between researchers, as work at higher concentrations Boon *et al.* ([Fe]T = 210 mM) shows a higher affinity than MacDonald & Clark (54 mM), which is in turn higher than Braddock *et al.* (9 – 22 mM).

Some shift in the maximum activity is expected with changes in temperature, thus variation in experimental conditions (from 28°C (Braddock *et al.* (1984) to 35°C Harvey & Crundwell (1997)) may also obscure direct comparison of data. The effect of temperature can be accounted for by the inclusion of an Arrhenius term in the maximum rate constant for both *At. ferrooxidans* (Nemati & Webb, 1997; Smith *et al.*, 1988) and *L. ferrooxidans* (Breed *et al.*, 1999).

Data from experiments run at different total iron concentrations show similar specific rates at common ferric/ferrous-iron ratios, despite the different corresponding ferrous iron concentrations. This indicates that rate equations dependent solely on the substrate concentration will be inadequate over a range of total iron concentrations.

Differences in experimental set-ups, aeration rates, degree of mixing and microbial strain used may also change the precise rates observed, but the results indicate that a kinetic model controlled by the concentration of iron is appropriate in continuous iron oxidation.

3.3 Published Rate Equations for Mesophilic Ferrous Iron Oxidation

A summary of the published rate equations re-evaluated in this work; the conditions under which the experiments were performed; the types of experiments run and the published kinetic constants generated can be found in Table 3.8 - 3.9. The rate equations are arranged chronologically and split according to the method used in the investigation, starting with equations developed from continuous culture experiments, followed by those from a range of discontinuous techniques.

3.3.1 Comparison of Predictions of Independent Continuous Data

Each rate equation in Tables 3.8 and 3.9 describes data captured under a specific set of reaction conditions, or a limited range of reaction conditions, and the kinetic constants generated represent the best fit of the equation to that set of data. This implies only that the mathematical expression of the equation produces an appropriate response to changes in the determining parameter, not that its underlying mechanism is valid, and certainly not that either the mechanism or the rate equation will be appropriate over the full range of conditions that the system might encounter.

Table 3.8 Published rate equations for ferrous iron oxidation with *Acidithiobacillus ferrooxidans*.

Author	Year	Rate Equation	Eqn No.	Conditions	Constants
MacDonald & Clark	1970	$\mu = \frac{\mu_{max} S}{K_m + S}$	[2.7]	Continuous T= 28°C pH =2. 2 $[Fe]_T$ = 53.7 mM	μ^{max} =0.161 h^{-1} K_S = 3.85 mM Y_{SX} =0.0168 molC.$(molFe^{2+})^{-1}$
Guay *et al.*	1977	$D = \frac{K}{1 - \frac{V_{max}}{V}}$	[3.1]	Continuous T= 32°C pH =2.3	V_{max} = 46.51-52.08 mM$Fe^{2+}.h^{-1}$ K = 0.526-0.283 h^{-1}
Jones & Kelly	1983	$\mu = \frac{\mu_{max}}{1 + \frac{K_S}{[Fe^{2+}]} + \frac{K_S [Fe^{3+}]}{K_p [Fe^{2+}]}}$	[2.8]	Continuous competitive inhibition T = 30 °C pH = 1.6 $[Fe]_T$ = 5 – 400mM	μ_{max} = 1.25h^{-1} K_S = 0.8-0.9 mM Fe^{2+} K_p = 1-2 mM Fe^{3+} Y_{SX} = 0.0148 molC.$(molFe^{2+})^{-1}$ m_s = 1 $molFe^{2+}.(molC.h)^{-1}$
Jones & Kelly	1983	$\mu = \frac{\mu_{max}}{\left(1 + \frac{[Fe^{3+}]}{K_p}\right)\left(\frac{K_s}{[Fe^{2+}]} + 1\right)}$	[2.9]	Continuous Non-competitive inhibition T = 30 °C pH = 1.6	μ_{max} = 1.33h^{-1} K_S = 2.4 mM Fe^{2+} K_p = 2.5 mM Fe^{3+} Y_{SX} = 0.041-0.054 molC.$(molFe^{2+})^{-1}$ m_s = 9.36-10.59 $molFe^{2+}.(molC.h)^{-1}$
Jones & Kelly	1983	$\mu = \frac{\mu_{max}}{\frac{K_S}{[Fe^{2+}]}\left(1 + \frac{[Fe^{3+}]}{K_p}\right) + \left(1 + \frac{[Fe^{3+}]}{K_c}\right)}$	[3.2]	Continuous predominantly competitive inhibition T = 30 °C pH = 1.6	μ_{max} = 1.25h^{-1} K_S = 0.8-0.9 mMFe^{2+} K_p = 1.2 mM Fe^{3+} K_c = not determined, assumed v. large Y_{SX} = 0.0148 molC.$(molFe^{2+})^{-1}$ m_s = 1 $molFe^{2+}.(molC.h)^{-1}$
Braddock *et al.*	1984	$\mu = \frac{\mu_{max}(S - S_t)}{K_m + (S - S_t)}$	[2.11]	Continuous T= 22°C $[Fe]_T$ = 9-22mM Isolate AK1	μ_{max} = 0.070h^{-1} K_μ = 0.78mM S_t = 0.25mM Y_{Carbon} = 0.010-0.017 molC.$(molFe^{2+})^{-1}$
Smith *et al.*	1988	$\mu = \frac{YkS}{K_s + S} - b$	[3.3]	Continuous T= 20-30°C pH = 1.8-2.1 $[Fe]_T$ = 0.050 mM	μ_{max} =0.060-0.119 h^{-1} K_S = 3.403 mMFe^{2+} k = 19.7 $molFe^{2+}.molC^{-1}.h^{-1}$ Y_{SX} =0.074 molC.$(molFe^{2+})^{-1}$ b = negligible

Author	Year	Rate Equation	Eqn No.	Conditions	Constants
Liu *et al.*	1988	$\mu = \frac{\mu_{max} S}{S + K_s(1 + K_i\,Pr)}$	[2.8]	Continuous T= 35°C pH = 1.8 $[Fe]_T$ = 9.3-58.9 mM	μ^{max} = 0.12 h^{-1} K_s = 1.594 $mMFe^{2+}$ K_i = 0.024 $(mMFe^{3+})^{-1}$ Y_{SX}= 0.0104 $molC.(molFe^{2+})^{-1}$
Nikolov & Karamanev	1992	$\mu = \frac{\mu_{max} S}{S + K_s + I\frac{K_S}{K_I} + \frac{S^2}{K_{SI}}}$	[2.10]	Continuous T= 29°C pH = 1.8-2.0 $[Fe]_T$ = 35.8 1253.6 mM	μ^{max} = 0.227 h^{-1} K_s = negligible K_S/K_I = 0.939 K_{SI} = 210$mMFe^{2+}$ Y_{SX}= 0.07 $molC.(molFe^{2+})^{-1}$
Boon *et al.*	1999a	$q_{O_2} = \frac{q_{O_2}^{max}}{1 + \frac{K_s}{[Fe^{2+}]-[Fe^{2+}]_t} + \frac{K_s}{K_i}\cdot\frac{[Fe^{3+}]}{[Fe^{2+}]-[Fe^{2+}]_t}}$	[3.4]	Continuous T= 30°C pH = 1.8-1.9 $[Fe]_T$ = 50-360mM	q_{O2}^{max} = 1.9 $molO_2.(molC.h)^{-1}$ $\mu^{washout}$ =0.096 h^{-1} K_s/K_i = 0.04 $[Fe^{2+}]_t$ = 0.5 mM $Y_{Fe^{2+}X}^{max}$=0.012 $molC.(molFe^{2+})^{-1}$ m_O = 0.4 $molFe^{2+}.(molC.h)^{-1}$
Gomez & Cantero	2003	$-r_S = \frac{\mu_{max} S(S_0 - S)}{K_s + S + K_I(S_0 - S)}$	[3.5]	Continuous T= 30°C pH = 1.8 $[Fe]_T$ = 25-150mM	μ^{max} = 0.22 h^{-1} K_s = 16.5$mMFe^{2+}$ K_i = 3.76$mMFe^{2+}$
Lacey & Lawson	1970	$\mu = \frac{\mu_{max} S}{Y_{sx} K_m + S}$	[2.12]	Batch STR T= 25-30 °C pH = 2-2.3 $[Fe]_T$ = 105mM	μ^{max} = 0.15-0.25 h^{-1} K_m = 19.7-18.1 mM
MacDonald & Clark	1970	$\mu = \frac{\mu_{max} S}{K_s + S}$	[2.7]	Batch STR T= 28°C pH = 2.2	μ^{max} = 0.145 h^{-1} K_s = 7.20$mMFe^{2+}$
Kelly & Jones	1978	$\mu = \frac{\mu_{max} S}{K_S + S}$	[2.7]	Batch culture T= 30°C pH =1.6	μ^{max} =0.143 h^{-1} K_S =36 $mMFe^{2+}$ Y_{SX} =0.014 $molC.(molFe^{2+})^{-1}$
Kelly & Jones	1978	$q_{O_2} = \frac{q_{O_2}^{max}[Fe^{2+}]}{[Fe^{2+}] + K_m\left(1 + \frac{[Fe^{3+}]}{K_i}\right)}$	[3.7]	Initial Rate T= 30°C pH =1.6	$q_{O_2}^{max}$ = not determined K_m = 1 $mMFe^{2+}$ K_i = 2.5-28 $mMFe^{3+}$
Norris *et al.*	1988	$\mu = \frac{\mu_{max}}{1 + \frac{K_m}{[Fe^{2+}]} + \frac{K_m}{K_i}\frac{[Fe^{3+}]}{[Fe^{2+}]}}$	[2.8]	Initial Rate T = 30 °C pH = 1.7 $[Fe]_T$ = 50 – 60 mM	K_S = 1.34 $mMFe^{2+}$ K_i = 3.10 $mMFe^{3+}$

Author	Year	Rate Equation	Eqn No.	Conditions	Constants
Lizama & Suzuki	1989	$q_{O_2} = \frac{k_3'}{1+\frac{K_m}{[Fe^{2+}]}\left(1+\frac{[X]}{K_i'}+\frac{[Fe^{3+}]}{K_{if}}+\frac{[X][Fe^{3+}]}{\alpha K_i' K_{if}}\right)}$	[3.7]	Initial Rate T = 25 °C pH = 2.3 $[Fe]_T$ = 100 - 116 mM Isolate SM-4	k_3' = 1.478 $molO_2.(molC.h)^{-1}$ K_m = 0.07 $mMFe^{2+}$ K_i' = 1.1 mM C K_{if} = 0.64 mM Fe^{3+} α = 5
Suzuki *et al.*	1989	$q_{O_2} = \frac{k_3'}{1+\frac{K_m}{[Fe^{2+}]}\left(1+\frac{[X]}{K_i'}\right)}$	[3.8]	Initial Rate T = 25 °C pH = 2.3 $[Fe]_T$ = 80 - 100 mM Isolates SM-4; SM-5	k_3' = 0.924 -1.0567 $molO_2.(molC.h)^{-1}$ K_m = 0.11 - 0.30 $mMFe^{2+}$ K_i' = 13 - 5 mM C
Liu *et al.*	1988	$\mu = \frac{\mu_{max} S}{S + K_S(1 + K_i Pr)}$	[2.8]	Shake Flask T= 35°C pH =1.8 Fe_T = 11.1 – 176.2 mM Fe^{2+}	μ^{max} =0.11 h^{-1} K_S = 0.86 $mMFe^{2+}$ K_i = 126.8 $mMFe^3$ Y_{SX}= 0.0104 $molC.(molFe^{2+})^{-1}$
Shrihari *et al.*	1990	$\frac{dN}{dt} = \frac{\mu_{mo} e^{\left(-K(pH-pH_o)^2\right)} S}{K_s + S} N - \mu_d P^2 N$	[2.21]	Shake Flask T= 30°C pH =2.2 Fe_T = 155.81 – 513.97 mM	μ^{max} =0.183 h^{-1} K_S = 96.24 $mMFe^{2+}$ K = 3.349 μ_d = 1.97 x 10^{-6} h^{-1} Y_{NS}=0.018 $molC.(molFe^{2+})^{-1}$
Nyavor *et al.*	1996	$V = \frac{\beta k_3 [X][S]}{K_m + \left(1+\frac{[I]}{K_i}\right) + [S]}$	[3.9]	Initial Rate T = 27 °C pH = 2.0 Fe_T = 2.69 – 35.82 mM	B = not reported K_3=not reported K_m=0.67 mM K_i= 6.25 mM
Gomez *et al.*	1996	$\mu_c = \frac{\mu_{max}[Fe^{2+}]}{K_s + [Fe^{2+}] + K_i[Fe^{3+}])}$	[2.8]	Shake Flask T = 30 °C pH = 2.0 Fe_T =17.9 – 143.3 mM	μ_c = 0.14 h^{-1} K_S = 16.83 $mMFe^{2+}$ K_i = 2.98
Harvey & Crundwell	1997	$\mu = \frac{\mu_{max}[Fe^{2+}]}{[Fe^{2+}] + K_S(1 + K_i[Fe^{3+}])}$	[2.8]	Electrochemical cell T= 35°C pH = 1.8 Fe_T = 35.8 – 286.5 mM	μ^{max} = 0.16 h^{-1} K_S = 1.31 $mMFe^{2+}$ K_i = 0.072 $(mMFe^{3+})^{-1}$ Y_{SX} = 5.37 x 10^{-4} $molC.(molFe^{2+})^{-1}$
Crundwell	1997	$\mu = k\left(\frac{[Fe^{2+}]/[H^+]}{K_{Fe^{2+}} + [Fe^{2+}]/[H^+] + K_i[Fe^{3+}]}\right)^{0.5}\left(\frac{p_{O_2}}{k_B + p_{O_2}}\right)^{0.5} - m$	[2.23]	fitted to Huberts (1994) data T = 35 °C $[O_2]$ = 0.15 atm	k = 0.152 h^{-1} $K_{Fe^{2+}}$ = 1.486 $mMFe^{2+}$ K_{O_2} = 0.043 atm m = 0.012 h^{-1}

Author	Year	Rate Equation	Eqn No.	Conditions	Constants
Nemati & Webb	1997	$\frac{d[Fe^{2+}]}{dt}=\frac{K_0 e^{\frac{-Ea}{RT}}[C][Fe^{2+}]}{Km'(1+\frac{[C]}{K_I'})+[Fe^{2+}]+1-\left(\frac{[C]}{\beta}\right)\left(\frac{[Fe^{2+}]^2}{\alpha}\right)}$	[3.10]	Initial Rate T = 20-35 °C pH = 2.0 Fe_T = 4.48 – 537.25 mM	K_o = 1.80 x 10^{13} $molFe^{2+}.(molC.h)^{-1}$ E_a = 68.4 $kJ.mol^{-1}$ K_m' = 1.2 mM Fe^{2+} K_I' = 0.171 mM C β = 5.98 mM C α = 0.466 mM Fe^{2+}
Nemati & Webb	1998	$\frac{d[Fe^{2+}]}{dt}=\frac{K_0 e^{\frac{-Ea}{RT}}[X][Fe^{2+}]}{\left(1+\frac{[Fe^{3+}]}{K_I}\right)\left(K_m+[Fe^{2+}]\right)}$	[3.11]	Initial Rate T = 30 °C pH = 2.0 Fe_T =8.06 – 564.1 mM	K_o = 8.6 x 10^{12} $molFe^{2+}.(molC.h)^{-1}$ E_a = 68.4 $kJ.mol^{-1}$ K_m = 4.62 $mMFe^{2+}$ K_i = 36.89 $mMFe^{3+}$
Boon *et al.*	1999b	$\mu=\frac{\mu_{max}+m_0 Y_{ox}^{max}}{1+\frac{K_s}{[Fe^{2+}]-[Fe^{2+}]_t}+\frac{K_s}{K_i}.\frac{[Fe^{3+}]}{[Fe^{2+}]-[Fe^{2+}]_t}}-m_0 Y_{ox}^{max}$	[3.12]	Batch STR T= 30°C pH =1.8 Fe_T = 210 mM	μ^{max} =0.060-0.105 h^{-1} K_s = 0.2mM K_s/K_i = 0.06–0.10 Y_{ox}^{max}=0.012 $molC.(molFe^{2+})^{-1}$ m_o = 0.96 $molFe^{2+}.(molC.h)^{-1}$
Meruane *et al.*	2002	$q_{Fe^{2+}}=\frac{q_{max}-K_2\frac{[Fe^{3+}]}{[Fe^{2+}]}}{1+\frac{K_s}{[Fe^{2+}]}+K_I\frac{[Fe^{3+}]}{[Fe^{2+}]}}$	[2.15]	Electrochemical cell T= 30°C pH = 1.8 Fe_T = 0.90 – 17.9 mM	q^{max} = 6.128 $molFe^{2+}.(molC.h)^{-1}$ K_s = 1.31 $mMFe^{2+}$ K_I = 0.641 K_2 = 0.0248 $molFe^{2+}.(molC.h)^{-1}$
Meruane *et al.*	2002	$q_{Fe^{2+}}=\frac{K_1^*\exp\left[\frac{nF}{2RT}\left(E^m-E_h^0\right)\right]\left\{1-\exp\left[\frac{nF}{RT}\left(E^m-E\right)\right]\right\}}{1+\frac{K_2^*}{[Fe^{2+}]}+K_3^*\exp\left[\frac{nF}{RT}\left(E_h-E_h^0\right)\right]}$	[2.16]	Electrochemical cell T= 30°C pH = 1.8 Fe_T = 0.90 – 17.9 mM	K_1^* =0.447 $molFe^{2+}.(molC.h)^{-1}$ K_2^* = 1.31 $mMFe^{2+}$ K_3^* = 0.641 E^m = 639 mV (SHE)

Table 3.9. Published rate equations for ferrous iron oxidation with *Leptospirillum ferrooxidans*.

Author	Year	Rate Equation	Eqn No.	Conditions	Constants
Huberts	1994	$-r_{Fe^{2+}} = a_1\left(\frac{p_{O_2}}{k_B + p_{O_2}}\right)\left(\frac{[Fe^{2+}]}{[Fe^{2+}] + K_{Fe^{2+}}\left(1+\frac{[Fe^{3+}]}{K^*}\right)}\right)$	[2.19]	Continuous T= 30°C pH = 2.0	a_1 = 10.29 molFe^{2+}.(molC.h)$^{-1}$ K_b = 0.022 atm $K_{Fe^{2+}}$ = 0.021 mM Fe^{2+} K^* = 10.2 mM Fe^{3+}
van Scherpenzeel *et al.*	1998	$q_{O_2} = \frac{q_{O_2}^{max}}{1+K_{O_2}\frac{[Fe^{3+}]}{[Fe^{2+}]}}$	[2.13]	continuous T = 30 °C pH = 1.5-1.6 Fe_T = 210 mM	$q_{O_2}^{max}$ = 1.7 molO$_2$.(molC.h)$^{-1}$ K_{O2} = 0.0005 Y_{SX} = 0.011 molC.(molFe^{2+})$^{-1}$ m_{Fe2+} = 0.44 molFe^{2+}.(molC.h)$^{-1}$
Breed *et al.*	1999	$q_{Fe^{2+}} = \frac{q_{Fe^{2+}}^{max}}{1+K_{Fe^{2+}}\frac{[Fe^{3+}]}{[Fe^{2+}]}}$	[2.14]	continuous T = 30- 40 °C pH = 1.7 Fe_T = 210 mM	q_{Fe2+}^{max} = 8.65-13.58 molFe^{2+}.(molC.h)$^{-1}$ K_{Fe2+} = 0.0018-0.0033
Breed *et al.*	1999	$q_{Fe^{2+}} = \frac{1.204\times10^{7}\exp^{\frac{35.63}{RT}}}{1+(0.0002T-0.0453)\frac{[Fe^{3+}]}{[Fe^{2+}]}}$	[3.13]	continuous T = 30- 40 °C pH = 1.7 Fe_T = 210 mM	Y_{SX} =0.0059 molC.(molFe^{2+})$^{-1}$ m_{Fe2+} = 0.797 molFe^{2+}.(molC.h)$^{-1}$
Breed & Hansford	1999	$q_{Fe^{2+}} = \frac{15.53}{1+(0.0048pH-0.0043)\frac{[Fe^{3+}]}{[Fe^{2+}]}}$	[2.20]	continuous T = 40 °C pH = 1.1-1.7 Fe_T = 210 mM	Y_{SX} = 0.0074 molC.(molFe^{2+})$^{-1}$ m_{Fe2+} = 1.0029 molFe^{2+}.(molC.h)$^{-1}$
Norris *et al.*	1988	$\mu = \frac{\mu_{max}}{1+\frac{K_m}{[Fe^{2+}]}+\frac{K_m[Fe^{3+}]}{K_i[Fe^{2+}]}}$	[2.8]	Initial Rate T = 30 °C pH = 1.7 Fe_T = 50 – 60 mM	K_s = 0.25 mMFe^{2+} K_i = 42.8 mMFe^{3+}
van Scherpenzeel *et al.*	1998	$q_{O_2} = \frac{q_{O_2}^{max}}{1+K_{O_2}\frac{[Fe^{3+}]}{[Fe^{2+}]}}$	[2.13]	Initial rate T = 30 °C pH = 1.5-1.6 Fe_T = 210 mM	q_{O2}^{max} = 1.8-2.4 molO$_2$.(molC.h)$^{-1}$ K_{O2} = 7 x10^{-4}

The robustness of each rate equation proposed was tested by comparing their predictions to an independent set of data. The data set used was taken from Boon *et al.* (1999a): continuous iron oxidation by *At. ferrooxidans* at 30 °C, pH = 1.5, $[Fe]_i$ = 210 mM. This data set was chosen as it was one of the most complete data sets available, including steady state ferrous iron, ferric iron, and cell concentration data and specific rates of both growth and specific iron utilisation, all obtained in continuous culture over a wide range of dilution rates, from substrate-scarce conditions at low dilution rate (0.01 h^{-1}) to washout kinetics at high dilution rates (0.1 h^{-1}). The total iron concentration used (210 mM) was typical of iron concentrations found in commercial BIOX reactors. Each model's prediction of the specific growth and iron utilisation rates was compared to the experimentally determined rates using the kinetic and bioenergetic constants published with each model. Where rate equations were derived in terms of the specific growth rates, specific iron utilisation rates were calculated using their published yields (where available) and vice versa. Where kinetic constants had been determined at temperatures other than 30 °C, the maximum specific rate constant was modified using an Arrhenius expression, using an activation energy of 51.2kJ.mol^{-1}, derived from the data of MacDonald & Clark (1970).

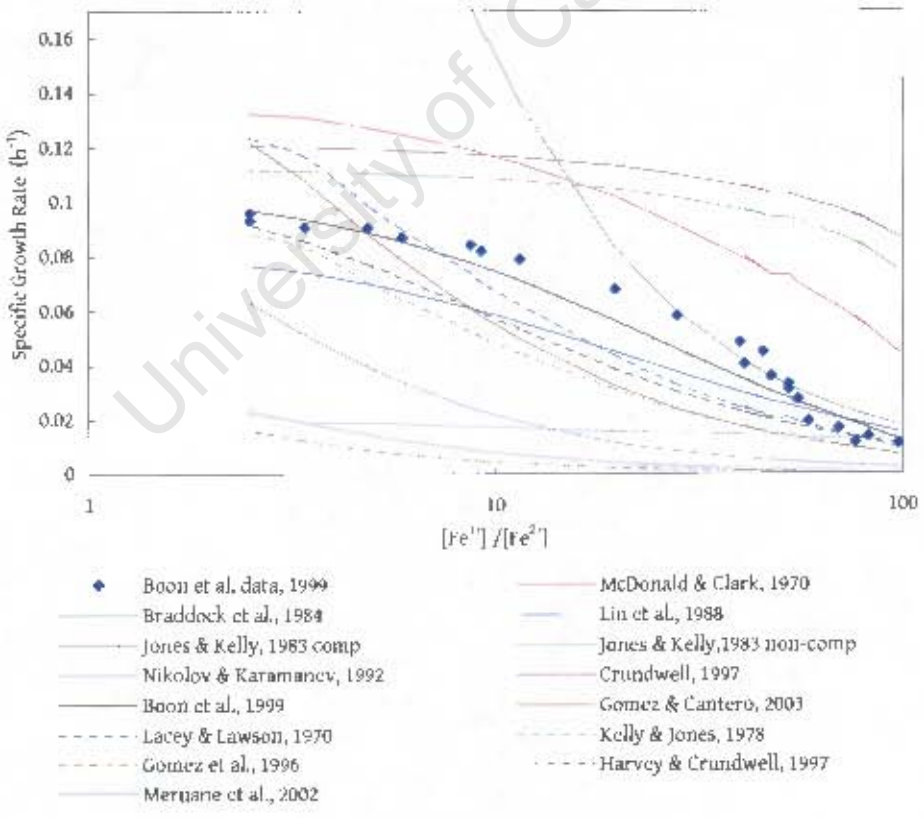

Figure 3.3 Predications of the specific growth rate by a number of kinetic models given the ferrous-iron, ferric iron and cell concentration data from Boon *et al.* (1999); continuous iron oxidation by *At. ferrooxidans* at 30 °C, pH = 1.5, $[Fe]_T$ = 210 mM. Solid lines represent models from continuous systems, dashed lines, batch systems and dotted lines, other techniques.

While each model undoubtedly fits the data from which it was generated, a great variety of response was observed when attempting to use these models to describe other data. This spread of results could not be attributed purely to the mode of operation, as the same range of responses was observed in batch, continuous and constant potential experiments.

Some models' predictions are not shown as their response was completely unrealistic. The model of Shrihari *et al.* (1990) predicted a negative rate due to an overemphasis in their model of "ferric poisoning". Other models such as that of Smith *et al.* (1988) predict much higher rates than those observed.

Other models predict similar maximum specific growth rates but at different ferric/ferrous iron ratios. This might in some instances be ascribed to differences in strain or species; Braddock *et al.* (1984) was using an arsenic-tolerant strain which may explain a lower substrate affinity particularly as the kinetics were extrapolated from threshold iron concentrations. Crundwell (1997) proposed a model for *At. ferrooxidans*, but used data from a *Leptospirillum* culture (Huberts, 1994) which explains the lower affinity observed. Gomez *et al.* (1996) and Gomez & Cantero (2003), both used a Rio Tinto strain. Both models are presented with normal maximum specific growth rates and high affinity coefficients, but a re evaluation of their data indicates that their substrate affinity was normal but their specific activity was lower than other systems. Nikolov & Karamenev (1992) used a re-suspended culture that they claimed had different properties, so different kinetic constants are not unexpected. Variations in temperature, pH, total iron concentration, and reactor configuration may also have contributed it the variability of the response.

Most models were focussed on predicting growth, and only a limited number provided sufficient yield information to predict substrate utilisation. The variation in the reported yield also produced even greater variation of results, with no other model predicting the specific substrate utilisation rates observed other than the model generated from the data itself. Liu *et al.* (1988) and MacDonald & Clark (1970) predict slightly higher rates, both of these models were generated at higher temperatures than the test system, so higher rates would be expected.

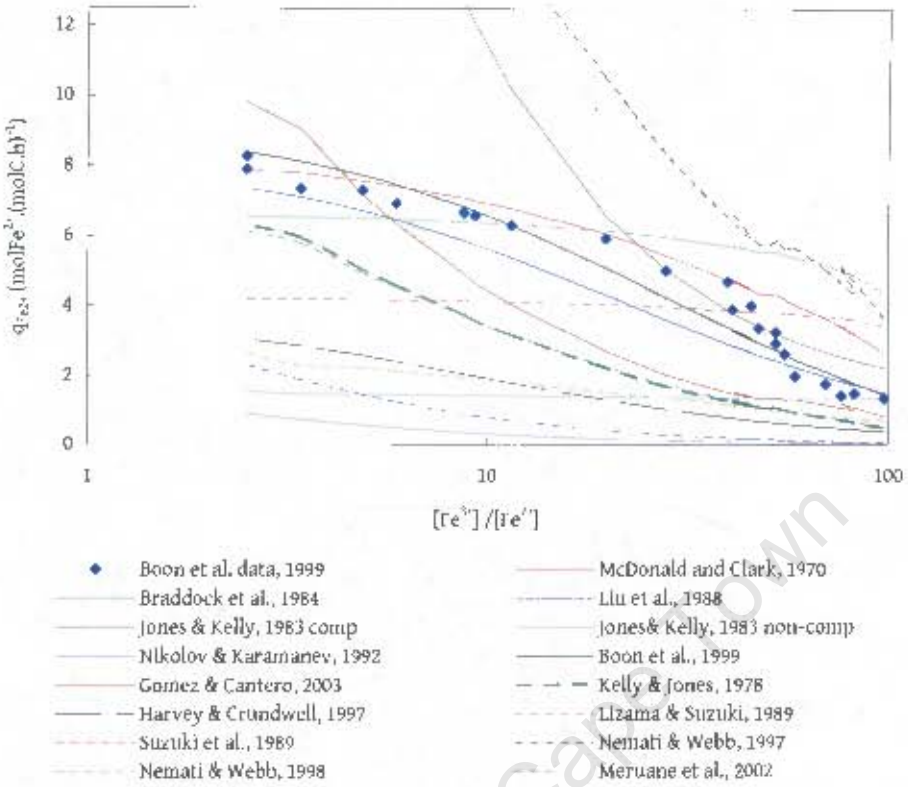

Figure 3.4 Predications of the specific iron utilisation rate by a number of kinetic models given the ferrous-iron, ferric iron and cell concentration data from Boon *et al.* (1999); continuous iron oxidation by *At. ferrooxidans* at 30 °C, pH = 1.5, $[Fe]_T$ = 210 mM. Solid lines represent models from continuous systems, dashed lines, batch systems and dotted lines, other techniques.

None of the kinetic constants generated from the initial O_2 uptake rate method (Nemati & Webb, 1997; Nemati & Webb, 1998; Lizama & Suzuki, 1989; Suzuki *et al.*, 1989) are able predict the observed data. This implies that the rates observed in initial rate studies are different to those observed in continuous studies and that the method is not suitable for generating data to predict continuous systems.

Models which were generated under conditions designed to test various inhibitions, be it cell concentration or substrate, tend to overemphasise the inhibition and model the stressed system and in so doing, fail to be able to model the unstressed system adequately.

3.3.2 Linear Transforms of Rate Equations

Despite the variety of models in Tables 3.8 and 3.9, most continuous data reviewed has been described using a rate equation derived from a simple Monod or competitive inhibition model. The kinetic parameters were classically determined by plotting reciprocal transforms of the kinetic data, e.g. a Lineweaver-Burk plot, and then by linear regression of the resultant trends. Although this

technique has been shown to be flawed as a method for determining parameters (Smith *et al.*, 1998), the transforms remain a valuable way to illustrating features of, and differences between, the various models. Reciprocal transforms of a number of simple rate equations are described in Table 3.10 and their behaviour as a function of the transformed variable is illustrated in Figures 3.5 and 3.7. This analysis has been performed on rate equations for specific growth rate, but remains valid for rate equations in terms of the specific iron utilisation rate.

In an iron oxidation system, the substrate, ferrous iron, is directly oxidised into the product, ferric iron. The ferrous and ferric iron concentrations and the ratio between the two are therefore not independent values but can all be defined by Equations 3.14 and 3.15 as functions of the ferrous and the total dissolved iron concentration.

$$[Fe^{3+}] = [Fe]_T - [Fe^{2+}] \qquad [3.14]$$

$$\frac{[Fe^{3+}]}{[Fe^{2+}]} = \frac{[Fe]_T - [Fe^{2+}]}{[Fe^{2+}]} \qquad [3.15]$$

Table 3.10 Transforms of a number of simple rate equations, showing the relationship between the inverse of the specific growth rate and the inverse of the substrate concentration.

Eqn No.	Rate Equation	Transform
2.7	$\mu = \frac{\mu_{max}[Fe^{2+}]}{K_s + [Fe^{2+}]}$	$\frac{1}{\mu} = \frac{K_s}{\mu_{max}}\frac{1}{[Fe^{2+}]} + \frac{1}{\mu_{max}}$
2.8	$\mu = \frac{\mu_{max}}{1 + \frac{K_S}{[Fe^{2+}]} + \frac{K_S[Fe^{3+}]}{K_p[Fe^{2+}]}}$	$\frac{1}{\mu} = \frac{K_s(K_1 - [Fe]_T)}{K_1\mu_{max}}\frac{1}{[Fe^{2+}]} + \frac{(K_1 - K_S)}{K_1\mu_{max}}$
3.16*	$\mu = \frac{\mu_{max}}{1 + K\frac{[Fe^{3+}]}{[Fe^{2+}]}}$	$\frac{1}{\mu} = \frac{K[Fe]_T}{\mu_{max}}\frac{1}{[Fe^{2+}]} - \frac{1-K}{\mu_{max}}$
2.11	$\mu = \frac{\mu_{max}([Fe^{2+}] - [Fe^{2+}]_{threshold})}{K_m + ([Fe^{2+}] - [Fe^{2+}]_{threshold})}$	$\frac{1}{\mu} = \frac{K_m}{\mu_{max}}\frac{1}{([Fe^{2+}] - [Fe^{2+}]_{threshold})} + \frac{1}{\mu_{max}}$
3.17†	$\mu = \frac{\mu_{max}[Fe^{2+}]}{[Fe^{2+}] + K_s + \frac{[Fe^{2+}]^2}{K_{SI}}}$	$\frac{1}{\mu} = \frac{K_s}{\mu_{max}}\frac{1}{[Fe^{2+}]} + \frac{[Fe^{2+}]}{\mu_{max}K_{SI}} + \frac{1}{\mu_{max}}$
2.9	$\mu = \frac{\mu_{max}}{\left(1 + \frac{[Fe^{3+}]}{K_p}\right)\left(\frac{K_s}{[Fe^{2+}]} + 1\right)}$	$\frac{1}{\mu} = \frac{(K_sFe_T + K_SK_1)}{K_1\mu_{max}}\frac{1}{[Fe^{2+}]} + \frac{(K_1 - K_S)}{K_1\mu_{max}} - \frac{[Fe^{2+}]}{K_1\mu_{max}}$
3.18†	$\mu = k_s\left(\frac{[Fe^{2+}][H^+]}{K_{Fe^{2+}} + [Fe^{2+}][H^+] + K_1[Fe^{2+}]}\right)^{0.5}\left(\frac{P_{O_2}}{K_B - P_{O_2}}\right)^{0.5}$	$\left(\frac{1}{\mu}\right)^2 = \frac{K_S[H^+](K_1 + [Fe]_T)}{K_1k^2\left(\frac{P_{O_2}}{K_B + P_{O_2}}\right)}\frac{1}{[Fe^{2+}]} - \frac{K_1 \quad K_S[H^+]}{K_1k^2\left(\frac{P_{O_2}}{K_B + P_{O_2}}\right)}$

*Equation 2.14 re-formulated in terms of specific growth rate, neglecting maintenance
†Equation 2.10 also includes a competitive inhibition term removed here
†Equation 2.23 neglecting maintenance

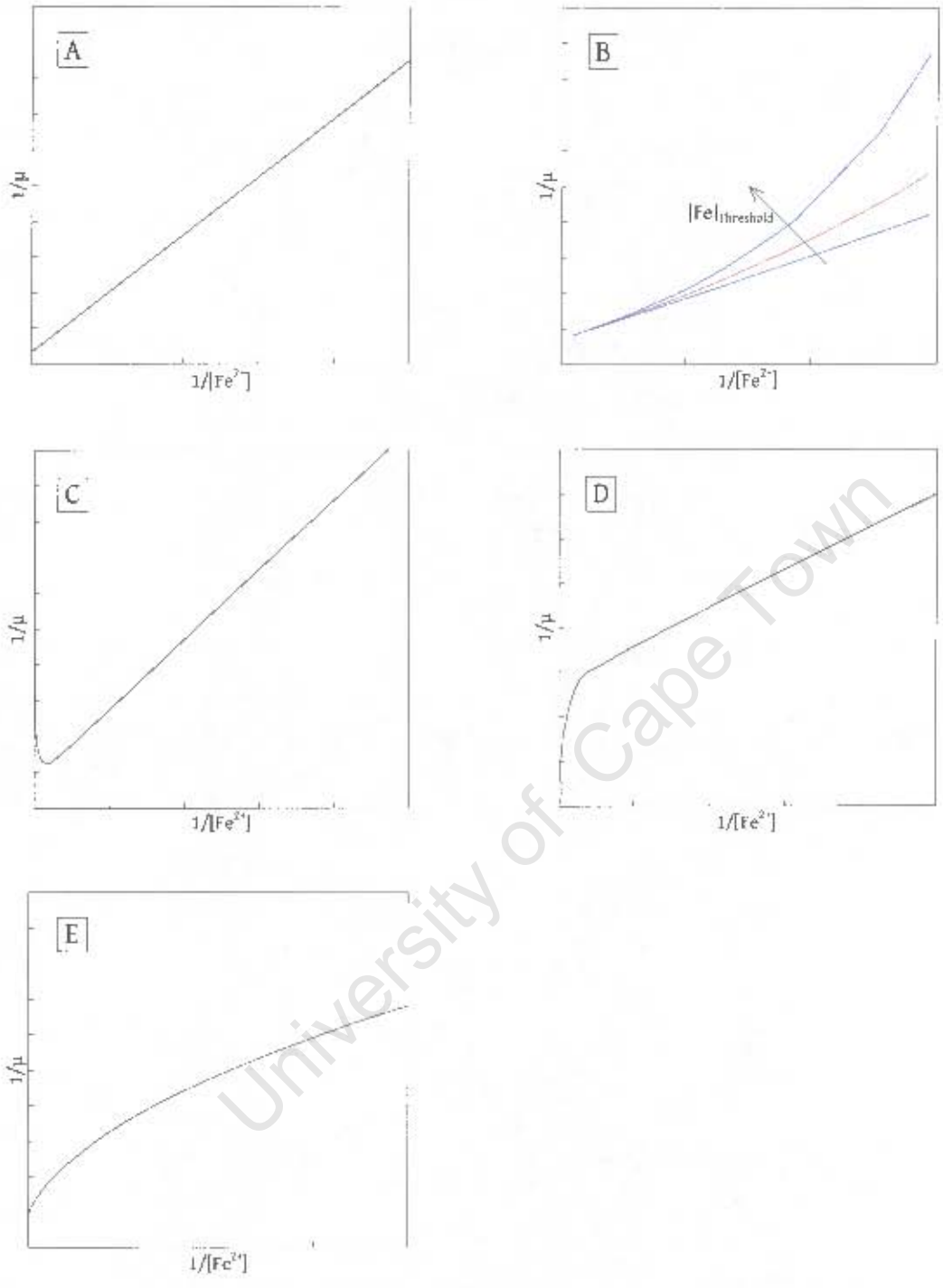

Figure 3.5 The inverse of the predicted specific growth rate as a function of the inverse of the substrate concentration as predicted by (A) Equations 2.7, 2.8 & 3.16; (B) Equation 2.11; (C) Equation 3.17 (substrate inhibition); (D) Equation 2.9 (non-competitive product inhibition); and (E) Equation 3.18.

These transforms show that the Monod model (Equation 2.7), the competitive inhibition model (Equation 2.8) and Equation 3.16 all predict a linear relationship between the inverse of the specific growth rate and the inverse of the substrate concentration. This implies that, given data from a

single set of fixed parameters (pH, temperature, total iron concentration, etc.) these models would fit equally well, as the closeness of fit in this instance only describes the linearity of the transformed data. Thus more than one set of fixed parameters are required to justify the use of a specific rate equation.

The threshold model (Equation 2.11) predicts a upwards deviation from linearity, with the degree of deviation dependent on the relative size of the threshold concentration, the model is only valid for substrate concentrations above the threshold concentration, as this concentration is defined as a boundary for growth. Both the substrate inhibition (Equation 3.17) and the non-competitive inhibition (Equation 2.9) models contain non-linear terms which only affect the predicted rate at high ferrous iron concentrations. The model proposed by Crundwell (1997) (Equation 3.18) predicts a parabolic relationship - a feature not found in any published data set, not even that published in Crundwell (1997).

The data sets presented in Figure 3.1 were transformed to test whether this form of analysis could be used to determine the appropriateness of rate equations.

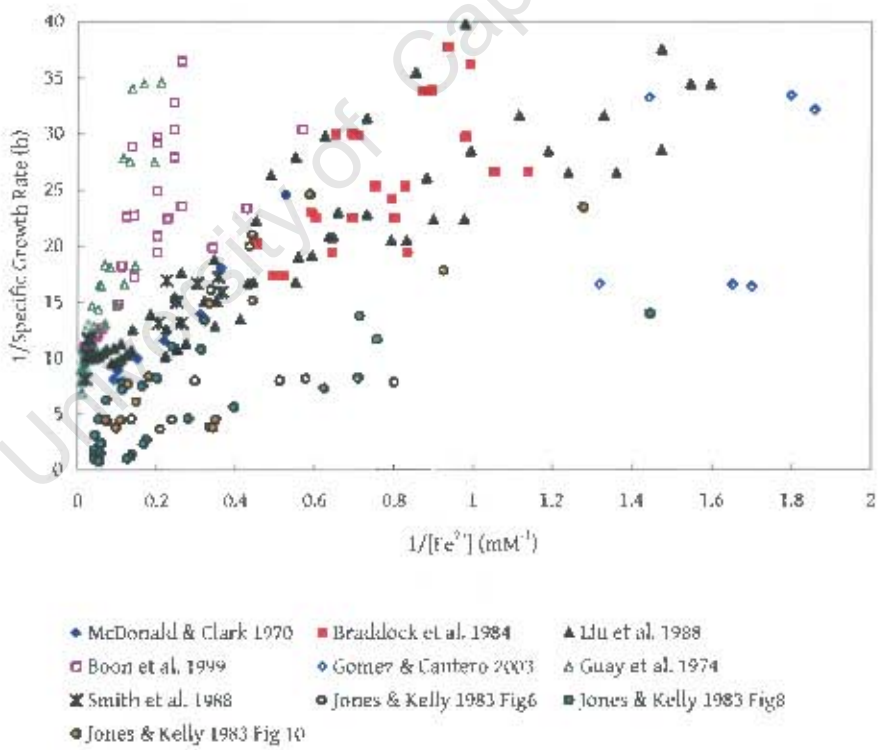

Figure 3.6 A Lineweaver Burk plot for the data presented in Figure 3.1, collating published data for *Acidithiobacillus ferrooxidans* in continuous culture.

The transformed plot shows that each set of data in which ferrous iron concentration is the only variable, shows a linear response to the change in concentration. Data sets that include other

variables such as changes in temperature or total iron concentration show multiple straight lines. The scatter in the observed data implies that there is little value in attempting to fit complicated rate equations.

Substrate inhibition (using inhibition constants from Nikolov & Karamenev (1992)) and non-competitive inhibition models (using inhibition constants presented by Jones & Kelly (1983)) show deviations from linearity only at high ferrous iron concentrations. As this is only found when operating with a very high total iron concentration or at very high dilution rates, approaching washout, very little data is available for confident fitting of these models.

This implies that the Monod model, Equation 3.16 (or its analogue Equation 2.14) and the competitive product inhibition model (Equation 2.8) are most appropriate for describing ferrous iron oxidation in continuous culture. Equation 2.14 was developed from the work of Boon (1996), who found the regression of data was insensitive to the $K_s/[Fe^{2+}]$ term in the competitive product inhibition model and that the term could be ignored.

Differences in slope may in some part be ascribed to differences in the total iron concentration, as can be seen from its influence on the slopes of the transforms of Equations 2.8, 3.16, 2.9 and 3.18. An alternative transform examining the relationship between the inverse of the specific rate and the ferric/ferrous-iron ratio, shows further differences between models with respect to the effect of the total iron concentration.

Table 3.11 An alternative transform relating the inverse of the specific growth to the ferric/ferrous-iron ratio.

	Model	Transform
[2.7]	Monod model	$\frac{1}{\mu} = \frac{K_s}{[Fe]_T \mu_{max}} \frac{[Fe^{3+}]}{[Fe^{2+}]} + \frac{K_s + [Fe]_T}{\mu_{max}}$
[2.8]	Competitive Inhibition model	$\frac{1}{\mu} = \frac{K_s(K_I + [Fe]_T)}{K_I [Fe]_T \mu_{max}} \frac{[Fe^{3+}]}{[Fe^{2+}]} + \frac{(K_s + [Fe]_T)}{[Fe]_T \mu_{max}}$
[3.16]	Equation 3.16*	$\frac{1}{\mu} = \frac{K}{\mu_{max}} \frac{[Fe^{3+}]}{[Fe^{2+}]} + \frac{1}{\mu_{max}}$

* Equation 2.14 re-formulated in terms of specific growth rate, neglecting maintenance

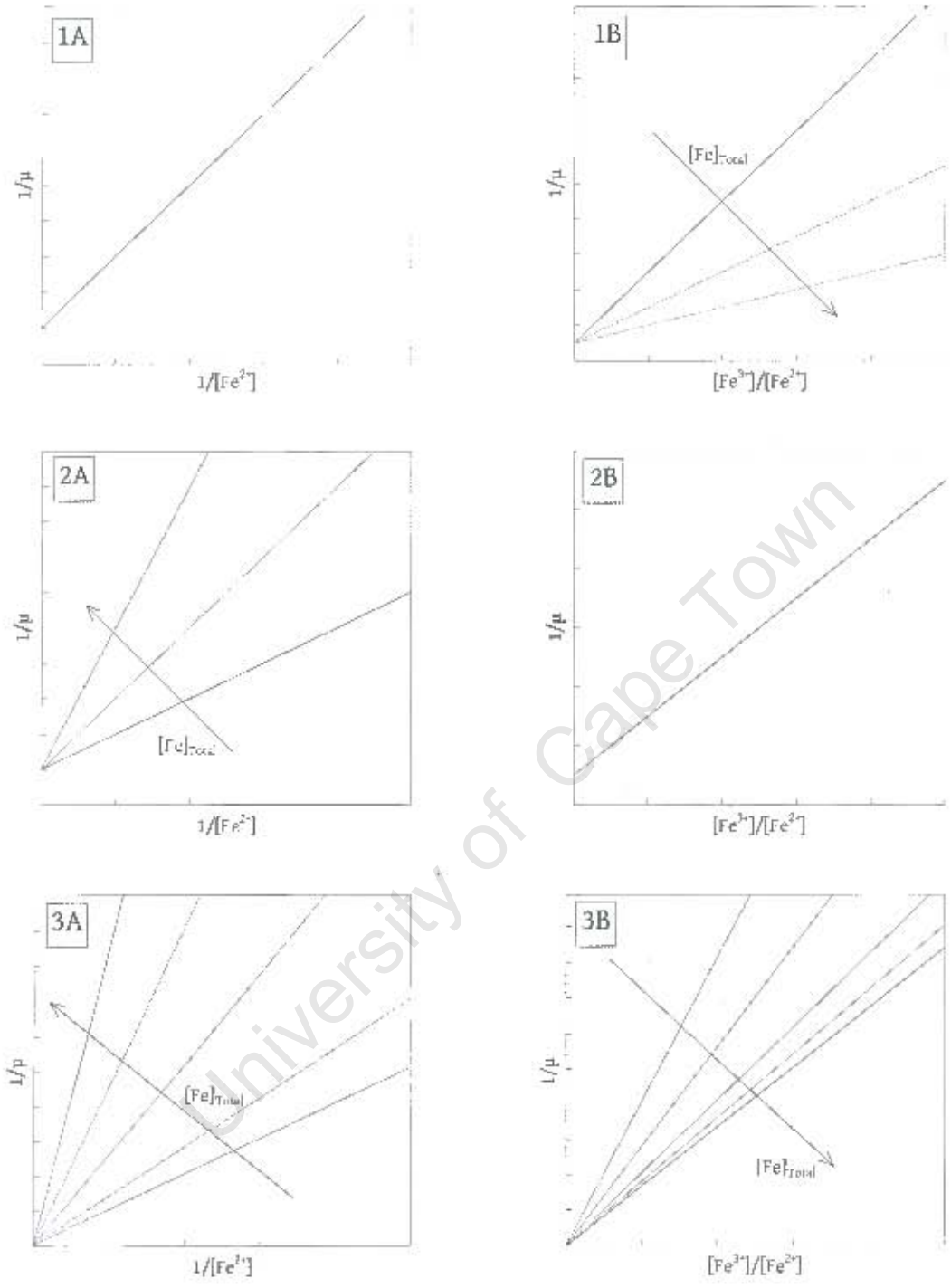

Figure 3.7 An illustration of the influence of the total iron concentration on the transforms of (1) the Monod model; (2) Equation 3.16 and (3) the Competitive Inhibition model with respect to (A) the inverse of the substrate concentration and (B) the ferric/ferrous-iron ratio.

The reciprocal transforms of the Monod model over a range of total iron concentrations has a constant slope with respect to the inverse of the substrate concentration and a decreasing slope with respect to the ferric/ferrous-iron ratio. The reciprocal transforms of Equation 3.16 shows the opposite trend, with an increasing slope with respect to the inverse of the substrate concentration

and a constant slope with respect to the ferric/ferrous-iron ratio. The reciprocal transforms of the competitive inhibition model has features of both of the other two transforms; with increasing slope with respect to the inverse of the substrate concentration and decreasing slope with respect to the ferric/ferrous-iron ratio.

The slopes of the reciprocal transforms in Figure 3.7 1B, 2A and 3A are all either directly or inversely proportional to the total iron concentration, indicating continued change of slope over all total iron concentrations. The slope of the reciprocal transform of the competitive inhibition model with respect to the ferric/ferrous-iron ratio (Figure 3.7 3B) has two total iron concentration terms which effectively cancel one another for total iron concentrations much greater than the inhibition constant K_i. This implies that at high total iron concentrations, the reciprocal transform with respect to the ferric/ferrous-iron ratio will not be a function of the total iron concentration and that both of the transforms of the competitive inhibition model will be indistinguishable from those of Equation 3.16. This implies that at low total iron concentrations, the system is controlled by ferrous iron limitation, and at high total iron concentrations, by ferric iron inhibition. This can be illustrated by looking at data from Liu *et al.* (1988) and Harvey & Crundwell (1997), both of which were originally fitted to the competitive inhibition model.

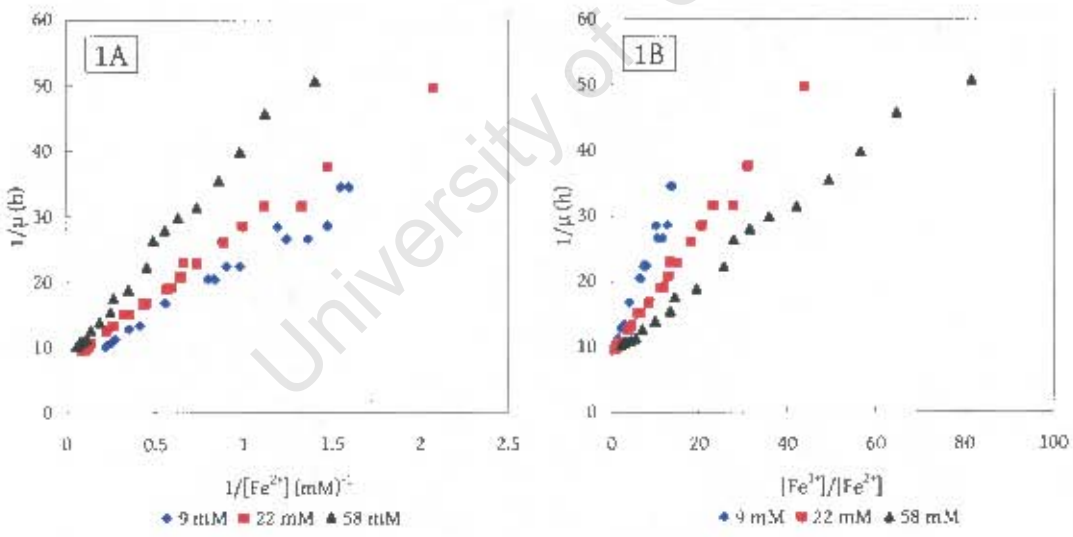

Figure 3.8 Reciprocal transforms of the data of (1) Liu *et al.* (1988) and (2) Harvey & Crundwell (1997) with respect to (A) the inverse of the substrate concentration and (B) the ferric/ferrous-iron ratio, for a range of total iron concentrations.

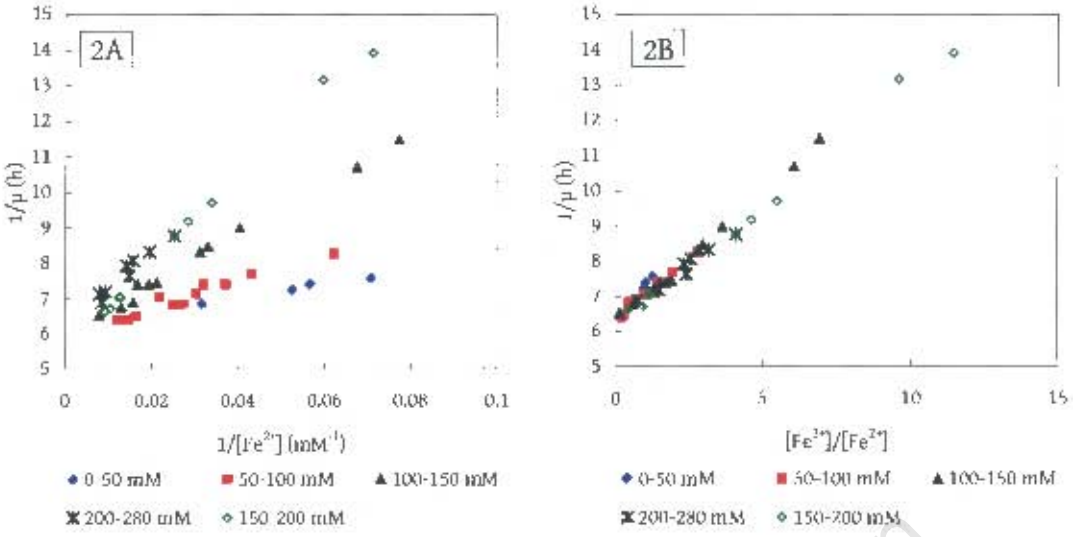

Figure 3.8 (continued) Reciprocal transforms of the data of (1) Liu *et al.* (1988) and (2) Harvey & Crundwell (1997) with respect to (A) the inverse of the substrate concentration and (B) the ferric/ferrous-iron ratio, for a range of total iron concentrations.

The transforms of both sets of data at high and low total iron concentration show variation in slope with respect to the inverse of the substrate concentration (Lineweaver-Burk plot), indicating that the Monod model is inadequate to model the system over a range of total iron concentrations.

Liu *et al.* (1988) varied the total iron concentration in a continuous reactor between 9 and 58mM and generated an inhibition constant of 50mM. The reciprocal plot (Figure 3.8 1B) shows a clear change of slope with changing total iron concentration. Harvey & Crundwell (1997) varied ferric and ferrous iron concentrations in a redox-controlled reactor, producing results that can be separated into ranges of total iron concentrations from 0-50mM to 150-200mM. The inhibition constant generated for these data was 16mM. The reciprocal plot (Figure 3.8 2B) shows no observable change in slope with respect to the ferric/ferrous-iron ratio with changing total iron concentration.

Thus, analysis of the reciprocal transforms of a number of simple kinetic models indicates that the competitive inhibition model is the most appropriate model for microbial ferrous iron oxidation, but that regression of data will not provide reliable values for the substrate affinity constant K_S at high total iron concentrations and that Equation 3.16 may be more useful under these conditions.

3.4 Conclusions

Results of published kinetic studies have been presented using a variety of different ways of measuring the biomass concentration. This makes comparison of even similar systems difficult. The conversion factors in Table 3.7 allow direct comparison of published results.

Studies have been done using many different modes of operation: including continuous stirred tank reactors, batch experiments in both stirred reactors and shake flasks, oxygen uptake experiments and controlled potential experiments. The disparate results of continuous and discontinuous experiments both in terms of the influence of reaction conditions and of the kinetic constants generated for similar models confirms that batch experiments are an unreliable way of generating kinetic data as the rapid change in solution conditions does not allow for a true response from the organisms.

While a large number of rate equations have been presented for microbial ferrous iron oxidation (Tables 3.8-9), the majority of results from studies in continuous culture have been fitted to relatively simple unstructured kinetic models. The data scatter in each data set further discourages attempts to fit more complicated models.

Analysis of the linear transforms of common simple rate equations shows similarities in the models' response to both the ferrous iron concentration and the ferric/ferrous-iron ratio. This means that the goodness of fit to a set of data obtained under a single set of experimental conditions does not imply the appropriateness of the model, and cannot be used to choose between models.

The effect of total iron concentration at low total iron concentrations on the slope of the transform shown in Figure 3.8A implies that the competitive inhibition model is more appropriate than the Monod equation. The linear transform of the competitive inhibition model in Table 3.10 shows that at low total iron concentrations, the system is controlled by substrate limitation and at high total iron concentration, by ferric iron inhibition. This implies that at high total iron concentrations, the competitive inhibition model may be approximated by Equation 3.16. The use of this approximation is validated by the results shown in Figure 3.8B.

Chapter 4

Theoretical and Experimental Methodology

The reaction kinetics of thermophilic ferrous iron oxidation was followed in continuous culture using a methodology developed for the analogous investigation of ferrous iron oxidation kinetics of the mesophile, *Acidithiobacillus ferrooxidans* (Boon, 1996), and the apparatus used was designed for the study of the kinetics of another dominant iron-oxidizing mesophile, *Leptospirillum ferrooxidans* (Breed *et al.* 1999; Breed and Hansford, 1999), using the same methodology. The kinetics were studied by on-line monitoring of off-gas oxygen and carbon dioxide concentrations over a range of dilution rates.

This chapter describes the experimental apparatus used and the experimental methods followed. It also describes how the desired reaction rates were determined from the measured off-gas concentrations, incorporating the effects of competing reactions and mass transfer limitations. This is followed by the procedure followed to fit rate equations to the observed rates.

4.1 Reactor Configuration

Experiments were performed in three uniform Applikon bioreactors (model Z61104CT04, Applikon Dependable Instruments, Schiedam, The Netherlands). The reactor vessels were borosilicate glass, water-jacketed for temperature control, with a stainless steel head-plate. The reactors had a maximum volume of 1.7L with an H/D ratio of approximately 1.3, and were run with a working volume of 1L.

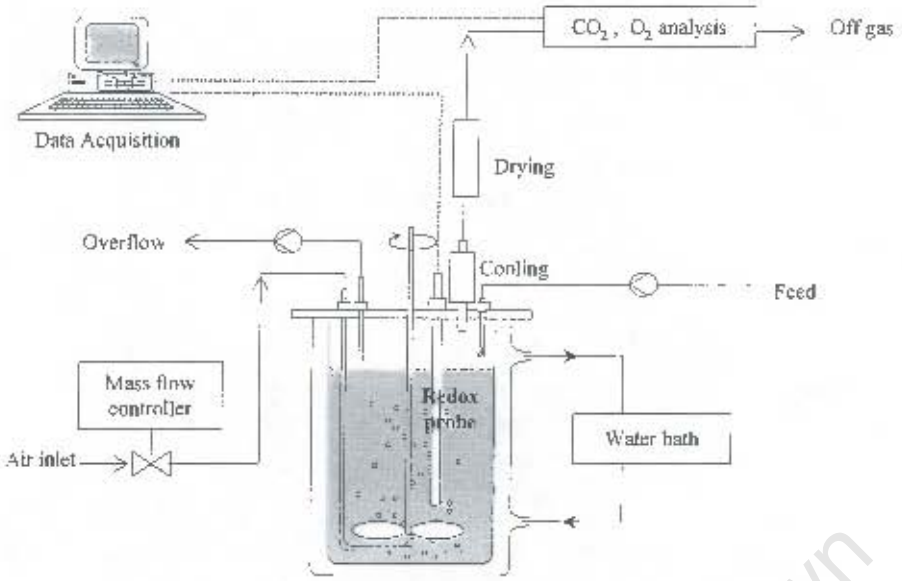

Figure 4.1 Diagram of apparatus used for continuous iron oxidation experiments (after Breed *et al.*, 1999).

The head-plate was 316 stainless steel and was fitted with a number of stainless steel accessories: a lip-sealed stirrer assembly, an L-shaped sparger, a condenser, a liquid sample port, three baffles, a liquid feed port, a liquid effluent port and several stoppered ports for introduction of redox and pH probes. The head-plate, when fully accoutered, hermetically sealed the reactor, allowing the measurement of the oxygen and carbon dioxide concentrations in the gas phase in the head-space above the reactor liquor.

Temperature in the reactor was maintained by circulating water through the reactor's water-jacket, pumped from a Grant waterbath (Y6 VFP, Grant Instruments, Cambridge, UK). The temperature was measured in the reactor, and the setpoint on the waterbath's controller was adjusted accordingly. Agitation and gas mixing was achieved by a Lightnin A315 impeller run at 400 rev.min^{-1} powered by an Applikon P100 motor controlled by an Applikon 1012 speed controller. Mixing was assisted by 3 stainless steel baffles, 220mm long and 10mm wide attached to the head-plate arranged at 120° to one another.

Compressed air was passed through a gas-chiller and a series of filters to obtain bone-dry medical quality air and fed into the reactor at a constant rate via a Brooks 5850S mass flow control valve (Brooks Instruments, Veenendal, The Netherlands), and sparged below the impeller. The air flow rate varied with reaction conditions from 300 to 400 mL.min^{-1} and was chosen to ensure a measurable difference in gas phase concentrations as is explained further in Section 4.8. Air leaving the reactor passed through a reflux condenser, which served the dual purpose of drying the gas before it enters the gas analysis system, and avoiding evaporative water loss in the reactor. An alternative would be to

feed saturated air to the reactor, but this affects the partial pressure of oxygen in the gas bubbles with a significant impact on the gas-liquid transfer rate.

The gas leaving the reactors passed to a gas manifold fitted with three-way valves which either vented the gas stream or passed it through the gas analysers. In the analyser system the off-gas was passed through a cloth filter and a Hartmann and Braun (ABB Automation) CGEK sample gas conditioner before entering the analysers. Oxygen concentration was measured by a Hartmann and Braun Magnos 6G paramagnetic oxygen analyser and carbon dioxide using a Hartmann and Braun Uras 4 infrared photometer.

The gas manifold consisted of 5 channels allowing the measurement of off-gas streams from four reactors and a reference stream, cycling each stream sequentially through the analysers with a sample period of six minutes. This produces a data point consisting of oxygen and carbon dioxide concentrations entering and leaving each reactor every half an hour. The gas sampling system and the data logging system hardware and software were designed in-house in the Department of Chemical Engineering of the University of Cape Town.

The fresh feed medium was dripped into the reactor via a peristaltic pump (Masterflex® 7521-57 L/S™ Variable-Speed Drive, Cole-Parmer, Vernon Hills, USA), fitted with a L/S™ 7013-20 Standard Pump Head and L/S™ 13 Norprene® food tubing. Reactor liquor was removed through a vertical tube placed at the liquid surface, connected to the same variable speed pump, the effluent stream was pumped through a L/S™ 7014-20 Standard Pump Head and L/S™ 14 Norprene® food tubing, which ensured that for any pump speed, the effluent pump had a greater capacity than the feed pump, which meant that, barring blockages, the reactor volume would stay constant.

4.2 Microbial Culture

Experiments were performed using a mixed thermophilic archaeal culture originally obtained from a BHP Billiton reactor and whichwas then thought to be predominantly *Sulfolobus metallicus*. From when it was obtained in 1998, it has been grown in a semi-continuous chalcopyrite stirred tank slurry reactor (3% w/v chalcopyrite concentrate in basal salt media media (Norris & Clark, 1996a), T = 70°C, pH = 1.5, 20% of the reactor contents withdrawn and replaced daily, resulting in an overall residence time of 5 days).

A sample was withdrawn from the chalcopyrite stock culture in 2001 and used to inoculate a continuous ferrous iron oxidation system, which ran for the duration of this work. The ferrous iron culture was allowed time to adapt to its new environment. Results reported in this thesis were obtained between 2002 and 2005 when it was assumed that the culture would have had ample time to have selected its dominant iron oxidising species.

Samples from both the continuous iron oxidation culture and the chalcopyrite stock culture were analysed to determine what species were present. Cells were collected from the samples by centrifugation at 13 000rpm for 10 minutes and re-suspended in 200 µL 1 x PBS buffer (Phosphate buffered solution). DNA was extracted using the High Pure PCR Template Prep Kit (Roche Diagnostics GmbH, Mannheim, Germany) and Polymerase Chain Reaction (PCR) analysis was performed directly on the prepared DNA. PCR amplifications of the 16S rRNA gene were carried out to generate a 1.0kb band on electrophoresis using primers pIJni-F (5'-CCGGATCCGTCGACGTGCCAGCXGCCGCGGTAA-3'), which contains cloning sites *Bam*HI and *Sal*I towards the 5' end, and primer prDD2 (5'-CAAAGCTTCTAGACGGXTACCTTGTTACGACTT-3'), which has *Hin*dIII and *Xba*I cloning sites. Approximately 100ng of chromosomal DNA was subject to amplification in a total volume of 50µl containing 20mM $(NH_4)_2SO_4$; 75mM Tris-HCl, (pH 8.8 at 25°C); 0.1% (v/v) Tween 20; 3mM $MgCl_2$; 2.5µM (each) deoxyribonucleotide (dATP, dCTP, dGTP, and dTTP), 0.25µM of each primer; and 2U Super-therm polymerase (Southern Cross Biotechnology, Cape Town, RSA). Denaturation was at 94°C for 60 s followed by 25 amplification cycles of 30 s at 94°C, 30 s at 52°C, 90 s at 72°C. An additional 120 s at 72°C and a cooling step at 4°C for 60 s completed the reaction. Reactions were carried out in a PCR Sprint cycler (ThermoHybaid, Middlesex, UK). PCR product restriction enzyme analysis was performed using *Eco*RV, *Stu*I, *Bam*HI, *Eco*RI, *Pst*I, *Sal*I and *Pvu*II in order to generate a discriminatory banding pattern on gel electrophoresis. The results of the restriction digests indicate that the cultures contain the following species

Table 4.1 The microbial species identified in the cultures used in this work.

Chalcopyrite culture	Iron culture
Metallosphaera sp. (most likely *hakonensis*)	*Metallosphaera* sp. (most likely *hakonensis*)
Ferroplasma sp.	*Ferroplasma* sp.
	Sulfobacillus sp. (most likely *yellowstonensis*)

The banding pattern from the *Stu*I digest was inconclusive and a subclone of the PCR product was sent for sequencing. The results of this indicated that the *Metallosphaera* species present was most like *Metallosphaera hakonensis* rather than *sedula* or *prunea*. Visual inspection of samples from the iron culture under a microscope indicated that the majority of the cells were small round cells with only occasional rod-shaped cells. From this it was concluded that the culture was predominantly *Metallosphaera hakonensis* and that the resultant reaction kinetics were similarly dominated by and representative of *Metallosphaera hakonensis*.

4.3 Growth Medium

The required macronutrients were supplied in a basal salt medium modified from that of Clark & Norris (1996a), adding iron as the growth substrate, and a reduced sulfur source.

Most experiments were run at a constant iron concentration of 0.210 M added as ferrous sulfate heptahydrate (12g.L^{-1} Fe^{2+}). Experiments testing the effect of the total iron concentration were run at concentrations between 0.0525 and 0.210 M.

Potassium tetrathionate was added as archaeal thermophiles appear unable to assimilate sulfate to provide sulfur for cell growth. (Norris & Barr, 1985) This inability was tested by removing the reduced sulfur supplement from the feed. The response was an immediate cessation in CO_2 uptake and a gradual decline in the overall rate of iron oxidation which corresponds to no growth and wash out of the existing cell mass. Potassium tetrathionate was preferred to cysteine and glutathoine as it contains no carbon and thus would not interfere with the CO_2 uptake measurements. Different concentrations are suggested by the literature. Norris & Barr (1985) used 1mM tetrathionate, Norris *et al.* (1986) replaced tetrathionate with the more economical sodium thiosulphate, using 0.2 g.L^{-1}, which is an equivalent amount of sulfur to 0.4 mM tetrathionate. Meruane *et al.* (2003) used 1.5 mM tetrathionate. A range of tetrathionate concentrations were tested to find an appropriate concentration that, while not growth-limiting, was also not high enough to promote significant growth of sulfur oxidisers. Concentrations ranging from 0.1 to 0.9 g.L^{-1} (0.3 – 3.0 mM) were found to have no effect on either the O_2 or the CO_2 uptake rates indicating that within that range the supplement was neither growth-limiting, nor acting as a second substrate. A concentration of 0.225 g.L^{-1} (0.75 mM) was used for the rest of the experiments.

Table 4.2 Growth medium (modified from Clark & Norris, 1996a).

Compound	Concentration
$MgSO_4$	0.50 g.L^{-1}
NH_4SO_4	0.40 g.L^{-1}
K_2HPO_4	0.20 g.L^{-1}
KCl	0.10 g.L^{-1}
$K_2S_4O_6$	0.225 g.L^{-1}
$FeSO_4$	32.64 g.L^{-1}

4.4 Abiotic Iron Oxidation

The contribution of abiotic ferrous iron oxidation by molecular oxygen, discussed in Section 2.4.6, was investigated by running a set of sterile batch tests under the appropriate conditions to determine the rate of abiotic ferrous iron oxidation.

The rate equations published for abiotic systems were mostly second order with respect to $[Fe^{2+}]$ deviating to first order at low iron concentrations (Verbaan & Crundwell, 1986); first order with respect to $[O_2]$; and varying with respect to $[H^+]$ depending on the pH of the system studied.

In the system of interest: acidophilic microbial ferrous iron oxidation at atmospheric pressure, where the pH is maintained at 1.5, temperature is held constant, and the partial pressure of O_2 remains between 20 and 21 kPa, the rate equation can be reduced to

$$-r_{Fe^{2+}} = r_{Fe^{3+}} = k[Fe^{2+}]^2 \qquad [4.1]$$

Batches were run in the stirred tank reactors described in Section 4.1 that were used in the microbial experiments. Experiments were performed at temperatures between 30 and 60°C, with initial ferrous iron concentrations between 0.53 and 0.21 mM. Batch experiments were chosen as the limited duration did not allow sufficient time for microbial contamination. No further attempt were made to ensure sterility, but the low reaction rates and visual inspection under the microscope showed no significant microbial growth.

The results were used to deduct the contribution of the abiotic component of the observed overall rate of iron oxidation to reveal the rate of microbial iron oxidation.

$$-r_{Fe^{2+},Microbial} = -r_{Fe^{2+},Total} - r_{Fe^{2+},Abiotic} \qquad [4.2]$$

4.5 Mass Transfer Limitation Considerations

As the solubility of oxygen and carbon dioxide decreases with increasing temperature, great care was taken to ensure that the system was not limited by the gas-liquid transfer of reaction species. As described in Section 2.4.4, the effect of the decreased solubility is offset by the concomitant increase in the overall transfer coefficient.

In continuous operation, at steady state, the oxygen utilisation rate is equal to the rate of transfer of oxygen into the liquid. The gas-liquid transfer rate is governed by

$$OUR = OTR = k_La([O_2]^* - [O_2]) \qquad [4.3]$$

where OUR = oxygen utilisation rate
OTR = oxygen transfer rate
k_La = overall transfer coefficient
$[O_2]^*$ = equilibrium oxygen concentration
$[O_2]$ = oxygen concentration in the bulk liquid

In this relation, k_La is a fixed parameter determined by the impeller type, reactor geometry, impeller speed and power, aeration rate and the solution conditions and the temperature. The equilibrium oxygen concentration can be determined from the measured concentration in the exiting gas stream, using Henry's Law.

$$p_i = H_i x_i \qquad [4.4]$$

where p_i = the partial pressure of component i in the gas phase (atm)

H_i = Henry's Law constant (atm)

x_i = the mole fraction of component i in the liquid phase

Henry's Law constants were calculated from a function of temperature correlated from an amalgamation of sources (Archer, 1997).

$$H = a + bT + cT^2 + dT^3 \qquad [4.5]$$

Table 4.3 Correlation coefficients for Henry's Law constants (atm x 10^{-4}) (after Archer, 1997).

Coefficient in Equation 4.5	O_2 (0-100°C)	CO_2 (0-80°C)
a	2.4788	0.0744
b	0.079	0.0024
c	$-1x10^{-4}$	$5x10^{-5}$
d	$-2x10^{-6}$	$-3x10^{-7}$

The oxygen transfer rate approaches its maximum as the oxygen concentration in the bulk liquid approaches zero, implying gas-liquid mass transfer limitation when the bulk liquid concentration drops below a lower threshold limit.

The use of a non-standard Lightnin impeller precluded the use of correlations to determine k_La, and instead values were estimated from measured oxidation rates in the stock culture using the same apparatus. The stock culture was maintained semi-continuously on chalcopyrite by daily addition of fresh concentrate, this culture supported a cell concentration much larger than any found in the continuous iron system, and hence with an oxygen and carbon dioxide demand commensurately higher. Shortly after fresh concentrate was added, the O_2 utilisation rate rose to a maximum of $7mM.h^{-1}$ and then declined, this rate was higher than any measured in continuous iron oxidation experiments and exhibited a discontinuity at the maximum that could indicate some form of limitation. If it is assumed that this represents the limit of gas-liquid mass transfer, then this maximum rate can be used to determine the value of k_La. If this rate is lower than OTR^{max} then this will result in an underestimate of k_La. In the same system, the maximum CO_2 utilisation rate observed was $0.12\ mM.h^{-1}$, occurring at the same time as the maximum O_2 utilisation rate.

Values of k_La_{CO2} can be estimated from k_La_{O2}, $k_La_{CO2} = 0.98k_La_{O2}$ (Boon & Heijnen, 1998). These values of k_La can be used to determine the liquid phase concentrations from each steady state utilisation rate. Limiting liquid phase concentrations were discussed in Section 2.4.4. An OTR^{max} of 7mM.h^{-1} with a gas phase concentration of 20.45% O_2, assuming a limiting concentration of 1 mg.L^{-1} (de Kock *et al.*, 2004) implies a k_La_{O2} of 49.9 h^{-1}. This predicts a k_La_{CO2} of 48.9 h^{-1}, which implies a limiting CO_2 concentration of 0.15 mg.L^{-1}. Liquid phase concentrations of O_2 and CO_2 above these limiting concentrations, implies no gas-liquid mass transfer limitation.

4.6 Steady State Continuous Operation

The microbial kinetics were measured in continuous culture, at dilution rates between 0.015 and 0.09 h^{-1}. The dilution rate was monitored by measuring the change of weight of the feed bottle.

$$D = \frac{(m_{i+1} - m_i)}{(t_{i+1} - t_i)\rho V} \qquad [4.6]$$

where m_i = the mass of the feed bottle at time t_i

ρ = the density of the feed = 1.034 g.L^{-1}

V = the working volume of the reactor = 1 L

Each data set was determined by setting the feed pump rate and waiting for a minimum of between 3 and 5 residence times for the system to reach steady state. System disturbances such as blockages in the feed and/or outlet pump lines and deviations from the desired pH often delayed reaching steady state. The system was assumed to be steady when the deviation from the mean measured rates of O_2 and CO_2 utilisation was less than 5% for a further residence time.

Deviations from ideal steady state continuous operation could be introduced by growth of micro-organisms attached to the reactor walls and internals (MacDonald & Clark, 1970). This was mediated by cleaning the reactors daily. During cleaning, the reactor contents were decanted and suspended precipitate was allowed to settle, the reactor walls were washed with dilute hydrochloric acid, and the stainless steel reactor internals scrubbed clean. After thorough rinsing, the liquor was returned to the reactor and continuous operation was resumed. Off-gas data gathered immediately after cleaning indicated that the system returned to steady state within 1 -2 hours, this data was ignored when determining the steady state reaction rates.

4.7 Iron Concentration

The total iron concentration was determined by titration with potassium dichromate, $K_2Cr_2O_7$ (Vogel, 1989) (method outlined in Appendix A1). Where viable, the ferrous iron concentration was determined by titration with cerium (IV) sulfate, $CeSO_4$ (Vogel, 1989). This was not possible for low

ferrous iron concentrations with high background ferric concentrations and the ferrous iron concentration calculated from the ferric/ferrous-iron ratio and the total iron concentration.

$$[Fe^{2+}] = \frac{[Fe]_T}{1+\frac{[Fe^{3+}]}{[Fe^{2+}]}} \quad [4.7]$$

The ferric/ferrous-iron ratio was determined from the solution redox potential using a Pt|Ag/$AgCl_2$ electrode (Mettler-Toledo combination redox electrode Pt4805-SC-DPAS-K85/225, Mettler-Toledo, Leicester, UK). The ferric/ferrous-iron ratio can be related to the redox potential via the Nernst equation, approximating activities as concentrations

$$E = E_0 + \frac{RT}{zF}\ln\left(\frac{[Fe^{3+}]}{[Fe^{2+}]}\right) \quad [4.8]$$

where E = solution redox potential (V)
E_0 = standard potential of the reaction (V)
z = the number of electrons in the reaction
F = Faraday's constant ($C.mol^{-1}$)

Probe- and temperature-specific parameters were determined by regression of the measured solution potential and the ferrous and total iron concentrations measured by titration. Calibration constants can be found in Appendix A2.

4.8 Off-gas Analysis

As described by Boon *et al.* (1995) and Boon *et al.* (1998), the rates of O_2 and CO_2 utilisation can be determined from the concentrations and flowrates of the gas streams entering and leaving the reactor.

$$-r_i = \frac{[i]_{IN}\Phi_{IN} - [i]_{OUT}\Phi_{OUT}}{V} \quad [4.9]$$

Where $-r_i$ = the rate of utilisation of substance i ($mM\ i.h^{-1}$)
Φ = the volumetric gas flowrate ($L.h^{-1}$)
V = the working volume (liquid) of the reactor (L)

The flowrates entering and leaving can be linked by using the mole fraction of the inert N_2 as a tie substance.

$$-r_{O_2} = \frac{\Phi_{OUT}}{V\times 22406}\left(x_{O_2,IN}\left(\frac{1-x_{O_2,OUT}-x_{CO_2,OUT}}{1-x_{O_2,IN}-x_{CO_2,IN}}\right)-x_{O_2,OUT}\right) \quad [4.10]$$

and

$$-r_{CO_2} = \frac{\Phi_{OUT}}{V\times 22406}\left(x_{CO_2,IN}\left(\frac{1-x_{O_2,OUT}-x_{CO_2,OUT}}{1-x_{O_2,IN}-x_{CO_2,IN}}\right)-x_{CO_2,OUT}\right) \quad [4.11]$$

Where $-r_{O2}$ = the rate of utilisation of O_2 ($mM\ O_2.h^{-1}$)
$-r_{CO2}$ = the rate of utilisation of CO_2 ($mM\ CO_2.h^{-1}$)

Φ_{OUT} = the volumetric flowrate of gas leaving the reactor ($L.h^{-1}$)
V = the working volume (liquid) of the reactor (L)
$x_{O2,IN}$ = mole fraction of O_2 in the gas stream entering the reactor
$x_{O2,OUT}$ = mole fraction of O_2 in the gas stream leaving the reactor
$x_{CO2,IN}$ = mole fraction of CO_2 in the gas stream entering the reactor
$x_{CO2,OUT}$ = mole fraction of CO_2 in the gas stream leaving the reactor

As the offgas measurement is dependent on the gas concentrations in the headspace of the reactor, the measurement was disrupted every time the reactor was opened for sampling and/or cleaning. Opening the reactor for sampling does not affect the system, only the measurement, and the data point obtained immediately after sampling was ignored. Washing the reactor resulted in a greater disturbance of the observed activity as the reactor contents spent some time without aeration, feed and heating, and the data for several hours after washing was hence ignored. As the time spent recovering from disturbances is proportionally larger at short residence times (high dilution rate), it can be seen that the system is more difficult to maintain at steady state under these conditions.

4.9 Determining Reaction Rates

Using the unstructured approach outlined in Section 2.3, microbial growth by the oxidation of ferrous iron can be modelled by an energy-producing reaction oxidising ferrous iron, and an energy-consuming reaction producing biomass.

In microbial ferrous iron oxidation, ferrous iron is oxidized to ferric iron. Whilst the reaction may be split into its constituent half-reactions, occurring on opposite sides of the cell membrane and the electron may follow an indirect route through a cytochrome chain to its final acceptor, the overall redox reaction follows the following reaction stoichiometry:

$$4Fe^{2+} + 4H^+ + O_2 \xrightarrow{\text{microbes}} 4Fe^{3+} + 2H_2O \qquad [2.1]$$

and the energy produced is used autotrophically, assimilating CO_2 as the sole carbon source, and NH_4^+ as the nitrogen source, to form biomass, which can be approximated as the stoichiometric formula $CH_{1.8}O_{0.5}N_{0.2}$ (Roels, 1983).

$$CO_2, H_2O, NH_4^+ \longrightarrow CH_{1.8}O_{0.5}N_{0.2} \qquad [2.6]$$

The coefficients of the macrochemical balance produced by combining these two reactions can be determined by simultaneous solution of the element and charge balances (Boon, 1996). The simultaneous solution may be simplified by adding the degree-of-reduction balance (Roels, 1983) to the set. The degree-of-reduction (γ) is defined as the number of electrons liberated in a redox half reaction converting 1 C-mole for organic compounds, or 1 mole of the compound, to H+, CO_2, H_2O,

N-source, SO_4^{2-} or Fe^{3+} (which all have a degree-of-reduction defined as zero). The degree-of-reduction balance is an alternative way of expressing that electrons are also conserved in the system.

$$\sum_{i=0}^{i} \gamma_i r_i = 0 \qquad [4.12]$$

Hence the balance becomes:

$$-r_{Fe^{2+}} = -4r_{O_2} + 4.2r_X \qquad [4.13]$$

In an autotrophic system, the only carbon source is atmospheric carbon dioxide, and thus, when cell mass is described in terms of the amount of carbon present, the carbon dioxide utilisation rate can be used to follow the growth kinetics.

$$r_X = -r_{CO_2} \qquad [4.14]$$

Combining Equations 4.13 and 4.14, the rate of iron utilisation can be determined from the measured rates of consumption of O_2 and CO_2 from the analysis of the off-gas stream.

$$-r_{Fe^{2+}} = -4r_{O_2} - 4.2r_{CO_2} \qquad [4.15]$$

Table 4.4 Element and charge balances for a microbial iron oxidation system.

Compound	C	H	O	N	Fe^{2+}	Fe^{3+}	charge	Degree of reduction
Fe^{2+}	-	-	-	-	1	-	2+	1
Fe^{3+}	-	-	-	-	-	1	3+	0
H^+	-	1	-	-	-	-	1+	0
H_2O	-	2	1	-	-	-	-	0
O_2	-	-	2	-	-	--	-	-4
CO_2	1	-	2	-	-	-	-	0
NH_4^+	-	4	-	1	-	-	1+	0
$CH_{1.8}O_{0.5}N_{0.2}$	1	1.8	0.5	0.2	-	-	-	4.2

Simultaneous solution of the balances in Table 4.4 yields the macrochemical balance in terms of the biomass yield on substrate (Y_{sx})

$$CO_2 + 0.2NH_4^+ + \left[\frac{1-4.2Y_{SX}}{4Y_{SX}}\right]O_2 + \frac{1}{Y_{SX}}Fe^{2+} + \left[\frac{1}{Y_{SX}} - 0.2\right]H^+ \rightarrow CH_{1.8}O_{0.5}N_{0.2} + \frac{1}{Y_{SX}}Fe^{3+} + \left[\frac{1}{2Y_{SX}} - 0.6\right]H_2O \qquad [4.16]$$

The performance equation of a continuous stirred tank reactor can be manipulated to show that in the absence of significant cell death, the dilution rate (D) is equal to the specific growth rate (μ). This can be combined with Equation 4.14 to provide a non-invasive on-line measurement of the cell concentration (c_x), in terms of moles of carbon fixed.

$$c_x = \frac{-r_{CO_2}}{D} \qquad [4.17]$$

where c_x = the steady state cell concentration (molC.L^{-1})

D = the dilution rate (h^{-1})

This can be used to determine the cell specific substrate utilisation rate (q_{Fe2+})

$$q_{Fe^{2+}} = \frac{-r_{Fe^{2+}}}{c_X} \quad [4.18]$$

where q_{Fe2+} = the specific iron utilisation rate ($molFe^{2+}.molC^{-1}.h^{-1}$)

The specific iron utilisation rate is used as the primary indicator of microbial activity and the variable of interest in the rate equations tested.

4.10 Theoretical Yield

For thermophilic ferrous iron oxidation, the macrochemical balance

$$CO_2 + 0.2NH_4^+ + \left[\frac{1-4.2Y_{SX}}{4Y_{SX}}\right]O_2 + \frac{1}{Y_{SX}}Fe^{2+} + \left[\frac{1}{Y_{SX}} - 0.2\right]H^+ \rightarrow CH_{1.8}O_{0.5}N_{0.2} + \frac{1}{Y_{SX}}Fe^{3+} + \left[\frac{1}{2Y_{SX}} - 0.6\right]H_2O \quad [4.19]$$

$$\Delta G_R = \sum_{i=0}^{i} a_i \Delta G_{if}^0 = \left(\frac{D_S^{01}}{r_X}\right) = 3500 \quad [4.20]$$

Where ΔG_R = Gibbs free energy of reaction

ΔG_{if}^0 = Gibbs free energy of formation of component *i* under standard conditions

a_i = the stoichiometric coefficient of component *i* in the macrochemical balance

This method predicts a theoretical maximum yield of 0.011 molC.$(molFe^{2+})^{-1}$. (Calculation can be found in Appendix D)

4.11 Determining Rate Equation Constants

Rate equations were written in terms of a predicted specific iron utilisation rate, and the predicted specific rates were compared to the measured rates. The kinetic constants were determined by minimising the sum of the squared error between the experimental and the predicted value.

$$SSE = \Sigma(y - y_{reg})^2 \quad [4.21]$$

where y = the measured value

y_{reg} = the value of y determined from the non-linear regression

Confidence in the fit was expressed in terms of R^2:

$$R^2 = \frac{\Sigma(y - y_{reg})^2}{\Sigma(y - y_{mean})^2} \quad [4.22]$$

where y_{mean} = the mean value of y in the measured data set.

Chapter 5

Results and Discussion - Abiotic Ferrous Iron Oxidation

In abiotic systems, specifically solutions containing iron but no active, iron-oxidising microorganisms, ferrous iron is oxidized chemically by molecular oxygen. In microbial systems, this abiotic oxidation continues as a parallel reaction. The focus of this study is microbial oxidation and thus it becomes necessary to quantify the contribution made by the abiotic reaction to the overall oxidation rate. In bioleaching systems, the abiotic rate is greatly retarded by the low pH and the consequent low oxygen solubility, and hence neglected in mesophilic systems. Increasing the temperature to the thermophilic range studied in this microbial oxidation investigation will produce a corresponding increase in the competing abiotic rate. Batch experiments were performed to determine whether abiotic oxidation was significant in a bioleaching system over the temperature range of 60 – 80 °C.

5.1 Rate Equations for Abiotic Iron Oxidation

Abiotic iron oxidation has been identified as a significant reaction in the study of acid mine drainage, pressure leaching and geochemistry (Kirby *et al.*, 1999; Chmielewski & Charewicz, 1984; Verbaan & Crundwell, 1986), and rate equations have been proposed that describe the rate of reaction in these systems.

A number of these rate equations relate the rate of oxidation to the concentration of the reactants in the oxidation reaction.

$$4Fe^{2+} + 4H^{+} + O_2 \rightarrow 4Fe^{3+} + 2H_2O \qquad [2.1]$$

Table 5.1 Published rate equations for abiotic iron oxidation.

Authors		Rate equation	System investigated
Keenan	1970	$r_{Fe^{3+}} = k\frac{[Fe^{2+}]^2[O_2]}{[H^+]^{0.33}}\exp\left(\frac{-94.1}{RT}\right)$	Uranium Leaching
Verbaan & Crundwell	1986	$r_{Fe^{3+}} = k\frac{[Fe^{2+}]^2[O_2]}{[H^+]^{0.36}}\exp\left(\frac{-68.6}{RT}\right)$	Pressure leaching
Chmielewski & Charewicz	1984	$r_{Fe^{3+}} = k[Fe^{2+}]^2 P_{O_2} \exp\left(\frac{-56.9}{RT}\right)$	Pressure leaching
Kirby *et al.*	1999	$r_{Fe^{3+}} = k\frac{[Fe^{2+}][O_2]}{[H^+]^2}$	Acid mine drainage

The equations were mostly second order with respect to $[Fe^{2+}]$; first order with respect to $[O_2]$; and varying with respect to $[H^+]$ depending on the pH of the system studied.

The difference in reaction conditions between these systems and those found in bioleaching systems hinders the direct use of these rate equations and rate constants. In pressure leach systems the reaction is subjected to extreme temperatures and pressures (T = 40-135°C, P_{O2} = 200-1000kPa, Chmielewski & Charewicz, 1984; T = 25-85°C, P_{O2} = 1-4.5 bar, Verbaan & Crundwell, 1986). Acid mine drainage systems are often less acidic than bioleach systems and with much lower iron concentrations (pH =2 – 6.5, Johnson, 2005). This may cause a change in the dominant iron species present, and a change in reaction mechanism.

If these rate equations can be applied to the system of interest: acidophilic microbial ferrous iron oxidation at atmospheric pressure, where the pH is maintained at 1.5, temperature is held constant, and the partial pressure of O_2 remains between 20 and 21 kPa, assuming that the rate is second order with respect to the ferrous iron concentration, then the rate equation can be reduced to

$$-r_{Fe^{2+}} = r_{Fe^{3+}} = k[Fe^{2+}]^2 \quad [5.1]$$

Values predicted for the rate constant in Equation 5.1 under the required conditions, using the constants associated with the rate equations presented in Table 5.1 vary by an order of magnitude, from 2.43×10^{-5} (Keenan, 1970) to 1.36×10^{-4} $mM^{-1}.h^{-1}$(Chmielewski & Charewicz, 1984). This variance means that these kinetic constants cannot be used to predict abiotic oxidation under bioleaching conditions with any confidence and that the required constants would have to be determined experimentally.

5.2 Abiotic Ferrous Iron Oxidation Kinetics under Bioleaching Conditions

Batch experiments were performed using the same apparatus and liquid media as the microbial oxidation investigation described in Chapter 6. Batches were run at constant temperatures ranging from 30 to 80°C, and with initial ferrous iron and total iron concentrations from 0.11 to 0.21mM (6-12g.L^{-1}). The kinetics were followed by monitoring the change in iron concentration with time. Kinetic constants were determined by minimising the sum-of-squared-errors of actual and predicted concentrations in each run. This was found to be a more effective regression technique than attempting to compare actual and predicted rates directly as it avoided the problem of accurately determining the measured rate from discrete data points.

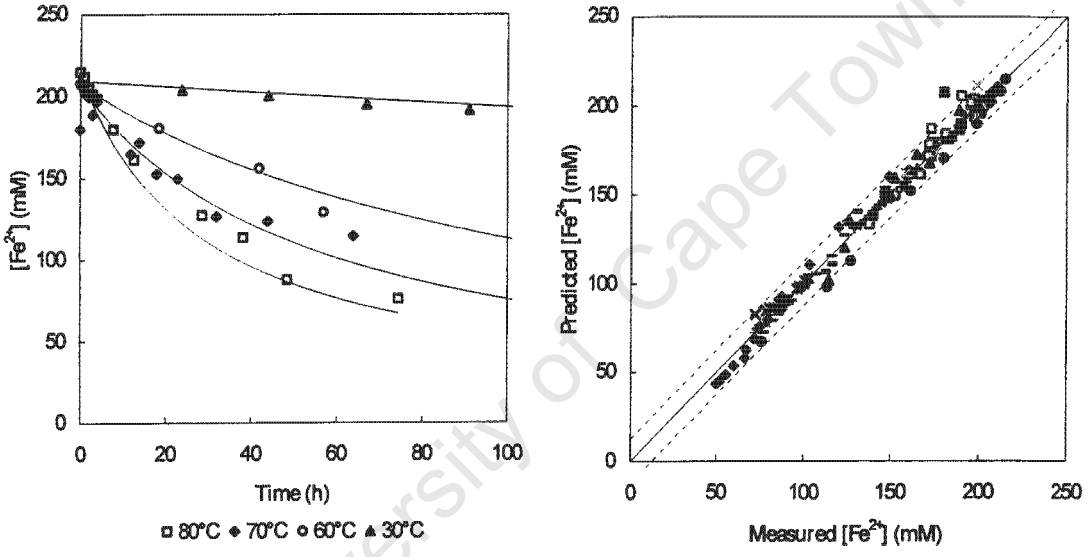

Figure 5.1 Prediction of $[Fe^{2+}]$ by Equation 5.1 in abiotic batch experiments run at $[Fe]_T$ = 12g.L^{-1}, pH = 1.5 and temperatures varying from 30 to 80°C, using constants determined for each run, and a parity chart for all batches run.

Table 5.2 Rate constants for Equation 5.1 determined by regression of the concentration-time profiles.

Run	Temperature °C	$[Fe^{2+}]_{Initial}$ mM	k_0 mM^{-1}.h^{-1}	R^2
1	70	210	8.42×10^{-5}	0.99
2	70	210	8.00×10^{-5}	0.98
3	70	91	8.00×10^{-5}	0.98
4	70	91	8.29×10^{-5}	0.99
6	70	102	8.00×10^{-5}	0.93
7	80	214	1.53×10^{-4}	0.97
8	30	209	3.92×10^{-6}	0.99
9	60	208	4.08×10^{-5}	0.97

Run	Temperature °C	$[Fe^{2+}]_{Initial}$ mM	k_0 $mM^{-1}.h^{-1}$	R^2
10	60	210	3.30×10^{-5}	0.99
11	70	208	5.67×10^{-5}	0.98
13	60	207	4.01×10^{-5}	0.88
14	70	207	8.00×10^{-5}	0.97
15	80	211	2.00×10^{-4}	0.97

The results show good agreement between the model and the observed iron concentrations, with consistent rate constants determined for each operating temperature examined. Differences between the observed and predicted concentrations were more pronounced in runs that experienced greater iron precipitation. The parity chart indicates that over all conditions tested, the rate equation predicts the measured iron concentration within 5%. Differences in the total iron concentration had no effect on the rate constants produced. Experiments run with an initial ferrous iron concentration of 100mM oxidised iron at the same rate as experiments started at 210 mM Fe^{2+}, at corresponding residual iron concentrations. Further experiments started at 50 mM Fe^{2+} showed no discernable oxidation at all.

The results do provide an acceptable fit to second-order reaction kinetics, and this is in agreement with the literature surveyed. These results do not in themselves prove that the reaction is second-order with respect to $[Fe^{2+}]$ – there being an insignificant difference between first-, second- and third-order fits to the data over the range of concentrations measured. Pressure leaching systems, run at much higher temperatures and elevated oxygen partial pressures, produced much faster reactions and achieved greater variation in initial and final iron concentrations allowing for a better understanding of reaction order. Results in pressure leach systems indicate that the reaction is second-order, deviating to first order at low iron concentrations (Verbaan & Crundwell, 1986), in bioleach systems, the rate at low iron concentrations is negligible and the rate can be modelled in terms of a second order rate equation.

5.1.1 The Effect of Temperature

Increasing temperature produced faster reactions and consequently larger rate constants. The effect of temperature was modelled by fitting the determined k values to an Arrhenius function. This allows the rate equation to be expanded to

$$-r_{Fe^{2+}} = r_{Fe^{3+}} = k_0[Fe^{2+}]^2 \exp\left(\frac{-E_a}{RT}\right) \qquad [5.2]$$

This allows all data collected to be predicted using a single set of kinetic constants, $k_o = 7.58 \times 10^5$ $mM.^{-1}h^{-1}$, $E_a = 65.5$ $kJ.mol^{-1}$. The calculated and reviewed activation energies show similarity lending confidence to the results obtained.

This allows all data collected to be predicted using a single set of kinetic constants, k_o = 7.58 x10^5 mM.$^{-1}$h^{-1}, E_a = 65.5 kJ.mol^{-1}. The calculated and reviewed activation energies show similarity lending confidence to the results obtained.

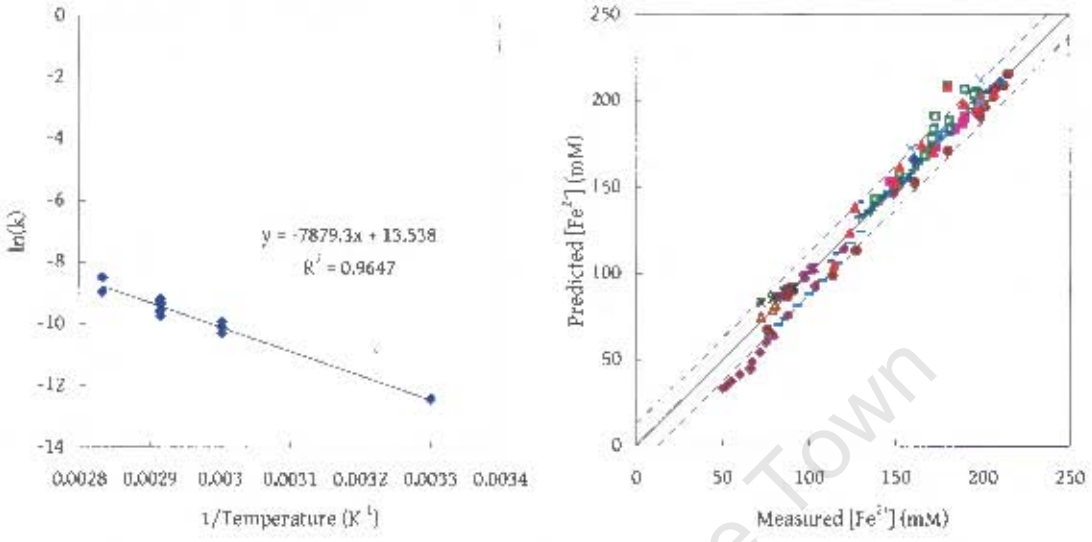

Figure 5.2 Arrhenius fit for k values determined for runs run between 30 – 80°C, and a parity chart for the prediction of concentration data with Equation 5.2.

Figure 5.2 shows that the Arrhenius function adequately describes the effect of temperature on the rate constant, k, and the parity chart shows that the use of a common rate constant does not adversely affect the overall fit.

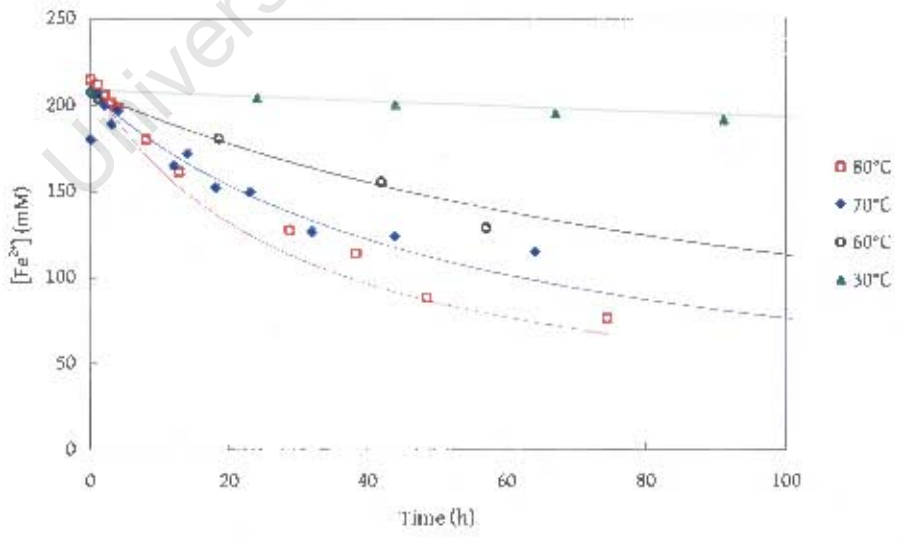

Figure 5.3 Prediction of [Fe^{2+}] by Equation 5.2 in abiotic batch experiments run at [Fe]$_T$ = 12g.L^{-1}, pH = 1,5 and temperatures varying from 30 to 80 °C, using constants corrected for temperature.

Table 5.3 Comparison of calculated and published rate constants, converted to common units and conditions of T= 70°C, pH = 1.5, $[O_2]$ = 1.68 x10^{-4} M.

Author		k_o mM^{-1}.h^{-1}	E_a kJ.mol^{-1}
Equation 5.2		7.58 x10^{7}	65.5
Huffman & Davidson*	1956	not calc	67.9
Keenan	1970	4.9 x10^{9}	94.1
Mathews & Robins*	1972	not calc	73.7
Iwai *et al.**	1982	not calc	51.6
Chmielewski & Charewicz†	1984	3.21 x10^{41}	55.0†
Verbaan & Crundwell	1986	4.36 x10^{6}	68.6

* cited in Verbaan & Crundwell (1986)
† re-calculated from Chmielewski & Charewicz (1984) Table 2

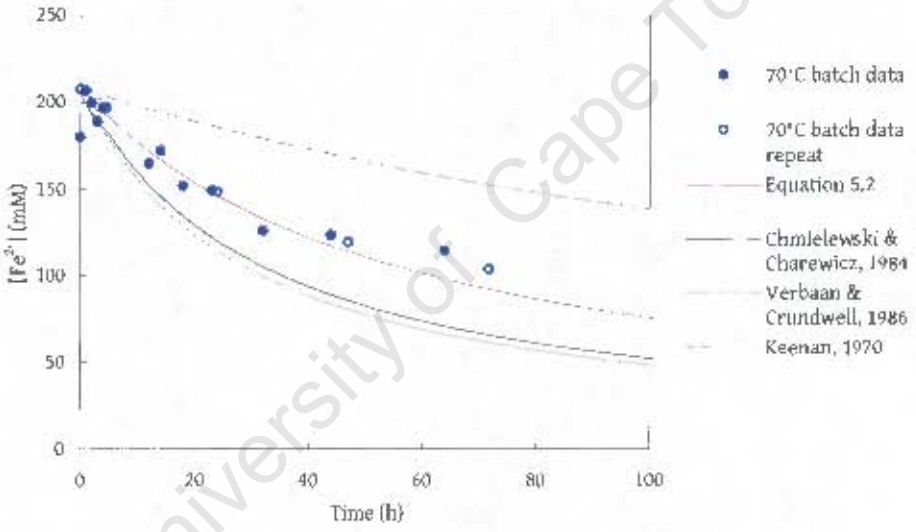

Figure 5.4 A comparison of the predictions of various published rate equations with currently determined parameters.

Attempts to fit measured data using published kinetic rate equations indicate that systems developed for pressure leaching over-predict the rate of abiotic iron oxidation in atmospheric systems. The results imply that the best results will be obtained by using the kinetic rate equation developed here for further iron oxidation experiments using thermophilic microorganisms, where the microbial oxidation rate can be deduced by subtracting the predicted abiotic rate from the measured overall rate.

$$-r_{Fe^{2+}}\Big|_{Bio} = -r_{Fe^{2+}}\Big|_{Total} - \left(k_o[Fe^{2+}]^2 \exp^{\left(\frac{-E_a}{RT}\right)}\right) \qquad [5.3]$$

5.3 Conclusions

The rate of abiotic ferrous iron oxidation was determined under the conditions found in thermophilic bioleaching systems. Rate equations developed for abiotic iron oxidation in pressure leach systems, and acid mine drainage systems were applicable to bioleach conditions, but the associated kinetic constants could not provide accurate predictions of the observed concentrations.

Sterile batch experiments were performed in the same apparatus as the microbial investigation, using the same basal salt media. The rate was found to be second order with respect to the ferrous iron concentration, and increases exponentially with an increase in temperature.

Thus, while the abiotic oxidation rate is negligible in mesophilic iron oxidation systems, at the elevated temperatures found in thermophilic iron oxidation systems, abiotic iron oxidation has a significant effect at high ferrous iron concentrations, and needs to be accounted for when investigating microbial iron oxidation under these conditions. Equation 5.3 provides an adequate description of the contribution of abiotic ferrous iron oxidation to the overall rate of oxidation measured in the microbial system investigated in Chapter 6.

Chapter 6

Results and Discussion - Thermophilic Microbial Ferrous Iron Oxidation Kinetics

The review of the relevant literature in Chapter 2 showed that thermophilic microbial ferrous iron oxidation is an integral process in high temperature bioleaching, and also showed a lack of published data concerning thermophilic microbial growth and iron oxidation kinetics. This investigation was performed to provide this data and to propose rate equations to describe the system, as it would be of interest in the further development of a comprehensive model for thermophilic bioleaching.

This chapter reports the findings of an investigation of the kinetics of ferrous iron oxidation by a thermophilic archaeal culture, predominantly *Metallosphaera hakonensis*. The investigation was run in continuous culture, at a pH of 1.5, and an influent iron concentration of 210mM (12 $gFe^{2+}.L^{-1}$), fed as ferrous sulfate. Temperature was varied between 60 and 80°C. The results of the investigation were used to determine kinetic constants for an appropriate rate equation describing the specific rate of iron utilisation as a function of the iron concentrations present and an appropriate expression describing the cell yield.

The measured steady state data as a function of the dilution rate is presented first, followed by variables such as cell concentration and specific growth and substrate utilisation rates that can be calculated from the measured data. These variables will be analysed to determine rate-controlling parameters, and this analysis will be used to propose appropriate rate equations and yield parameters to model the system.

6.1 Steady State Data

Experiments were run in three identical reactors, each run under conditions of constant temperature, influent iron concentration and pH. Experiments were run in two sets. Run 1 was performed in 2002, and the reactors were operated at 65, 70 and 75°C. Run 2 was performed in 2004 and the reactors were operated at 60, 70 and 80°C, extending the temperature range investigated and testing the reproducibility of the 70°C results. The dilution rate was varied stepwise through each experiment allowing the system to reach steady state at each step. Details of the experimental methodology can be found in Chapter 4. The steady state rates of oxygen and carbon dioxide utilisation; the total iron and ferrous iron concentrations and the solution redox potential are presented in Figures 6.2-6.4 as a function of the dilution rate for each experiment run from 60 to 80°C. A summary of all steady state data can also be found in Appendix B.

6.1.1 Oxygen and Carbon Dioxide Utilisation Rates

As described in Section 4.8, the rates of oxygen and carbon dioxide utilisation rates were calculated from the difference of concentration between the influent and effluent gas streams and were used to follow the growth and substrate utilisation reaction kinetics.

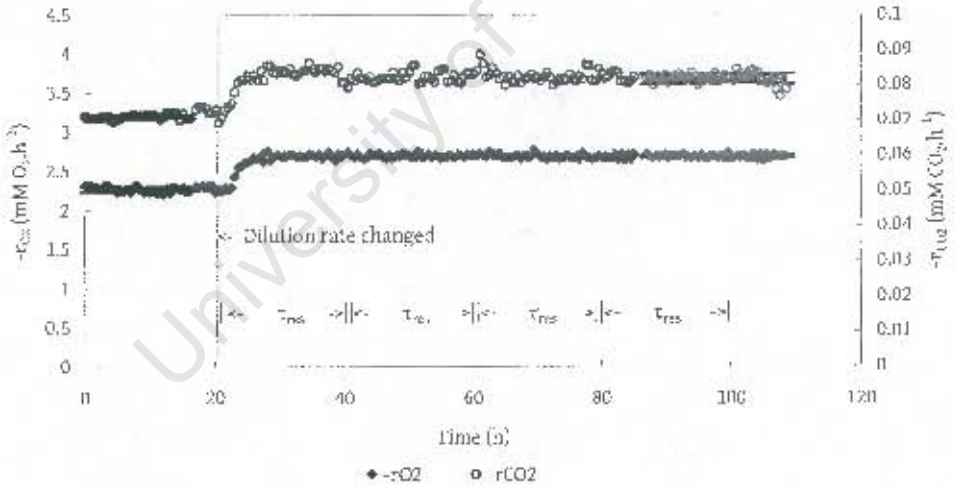

Figure 6.1 The change in measured oxygen and carbon dioxide utilisation rate data determined for continuous iron oxidation as the residence time was changed from 25 to 20 hours. T = 65°C, pH = 1.5, $[Fe]_T$ = 214 mM, Run 1 (2002).

Figure 6.1 shows an example of the measured steady state data captured. At time =0, the system is at steady state for a dilution rate of 0.04 h^{-1}. At t=20h, the dilution rate was changed to 0.05h^{-1}, the oxygen and carbon dioxide utilisation rates then smoothly increased to their new steady state rates. As described in Section 4.6, the system was then left at the new dilution rate for 3 -5 residence times before the new steady state was measured. The intermediate data was then discarded. Standard

deviations for all data sets for the rate of oxygen utilisation ranged from 0.7 to 2.9 % and for carbon dioxide, from 0.8 to 4.7 %. Steady state oxygen and carbon dioxide utilisation rates were determined for each dilution rate from 0.02 h^{-1} to washout.

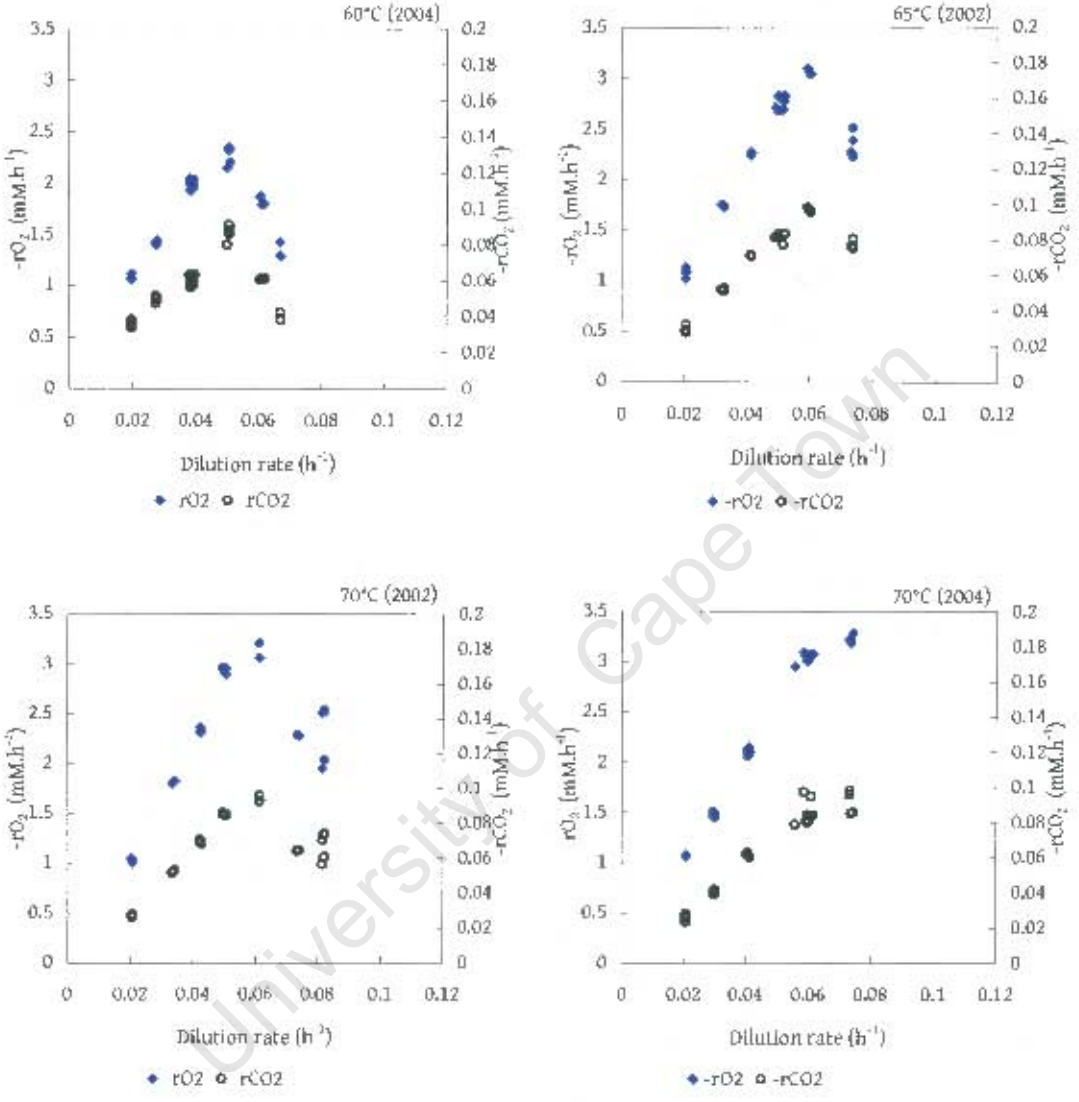

Figure 6.2 Oxygen and carbon dioxide utilisation rates determined for continuous iron oxidation at T = 60 - 80°C, pH = 1.5, $[Fe]_T$ = 214 mM. (continued overleaf)

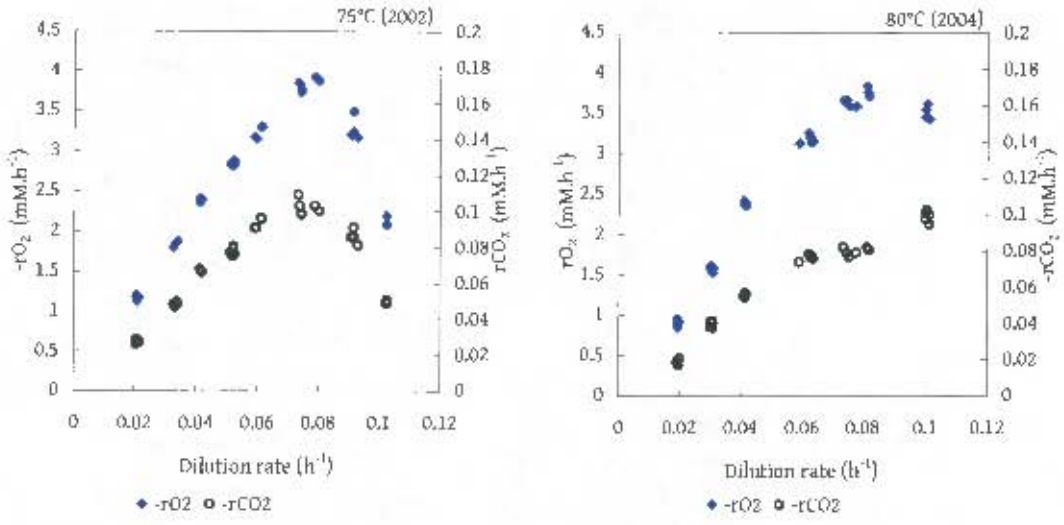

Figure 6.2 (continued) Oxygen and carbon dioxide utilisation rates determined for continuous iron oxidation at T = 60 - 80°C, pH = 1.5, $[Fe]_T$ = 214 mM.

The rates of oxygen and carbon dioxide utilisation show very similar trends over the range of dilution rates used. The change in rate with changing dilution rate displays the same pattern for all measured temperatures between 60 and 80°C, the rates are low at low dilution rate, increasing to an intermediate maximum and then decreasing as the system approaches washout. The low rates at low dilution rate are expected, as the substrate concentration is low under these conditions. The increase of rate with increasing dilution rate corresponds to the increased availability of substrate. These characteristics can be described by simple Monod kinetics. The decrease of the gas utilisation rates at high dilution rate implies a decrease in the steady state cell concentration. This may be explained in terms of a bioenergetic change, either an increased maintenance energy requirement, or an increased rate of cell death or a change in the efficiency of energy assimilation, or a combination of effects.

The maximum rates of oxygen and carbon dioxide observed, increased with increasing temperature, indicating that the temperature range investigated was within the normal operating range of the micro-organism studied, and that the predominant effect of temperature was an increase of the intermediate reaction steps rather than an increase in thermal deactivation. The effect of temperature is illustrated further in Figure 6.3.

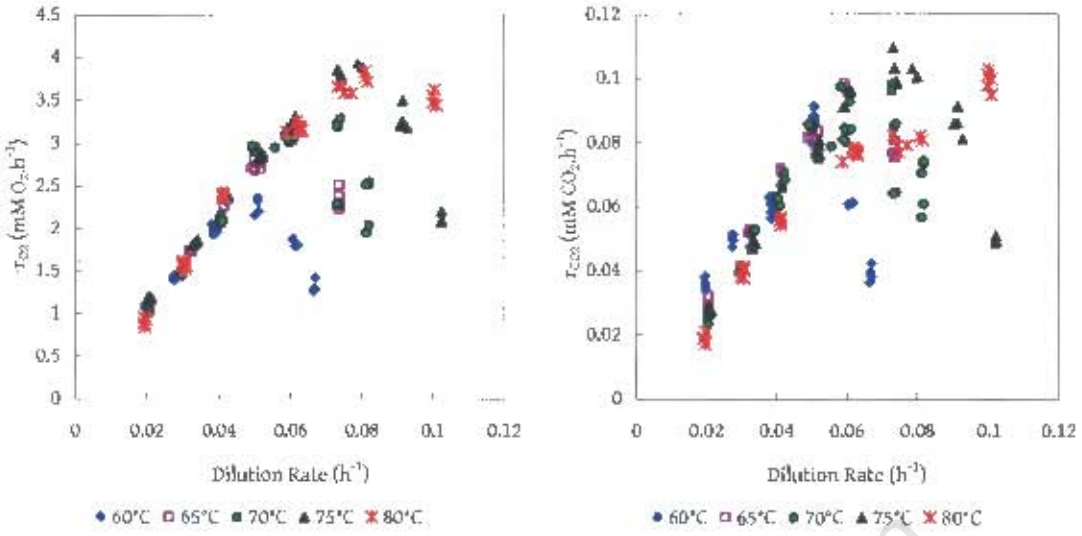

Figure 6.3 Oxygen and carbon dioxide utilisation rates as a function of temperature, determined for continuous iron oxidation at T = 60 - 80°C, pH = 1.5, $[Fe]_T$ = 214 mM.

The rate of oxygen utilisation at low dilution rate is constant as a function of temperature. The rates pass through a maximum and then decline towards washout. The maximum rate observed increases with increasing temperature and also is observed at higher dilution rates at higher temperature.

The rate of carbon dioxide uptake at low dilution rate decreases with increasing temperature, and thereafter follows a similar trend to the oxygen utilisation rate. This can be attributed to an increase in the proportion of the energy generated by iron oxidation being diverted from cell growth to cell maintenance with increased temperature.

6.1.2 Iron Concentrations

The reactors were run with a continuous feed containing 214 mM of ferrous iron fed as ferrous sulfate. The steady state iron concentrations were determined by titration versus cerium sulfate for ferrous iron and potassium dichromate for total iron concentrations. The solution redox potential was measured *in situ* with a combination Pt|Ag/AgCl2 electrode. The ferrous iron concentrations at low dilution rates proved to be close to the detection limit of the titrametric technique, and further analysis of the kinetic data was performed using the ferrous iron concentrations and the ferric/ferrous-iron ratios calculated from the redox potential using probe- and temperature-dependent calibration parameters as described in Appendix A2.

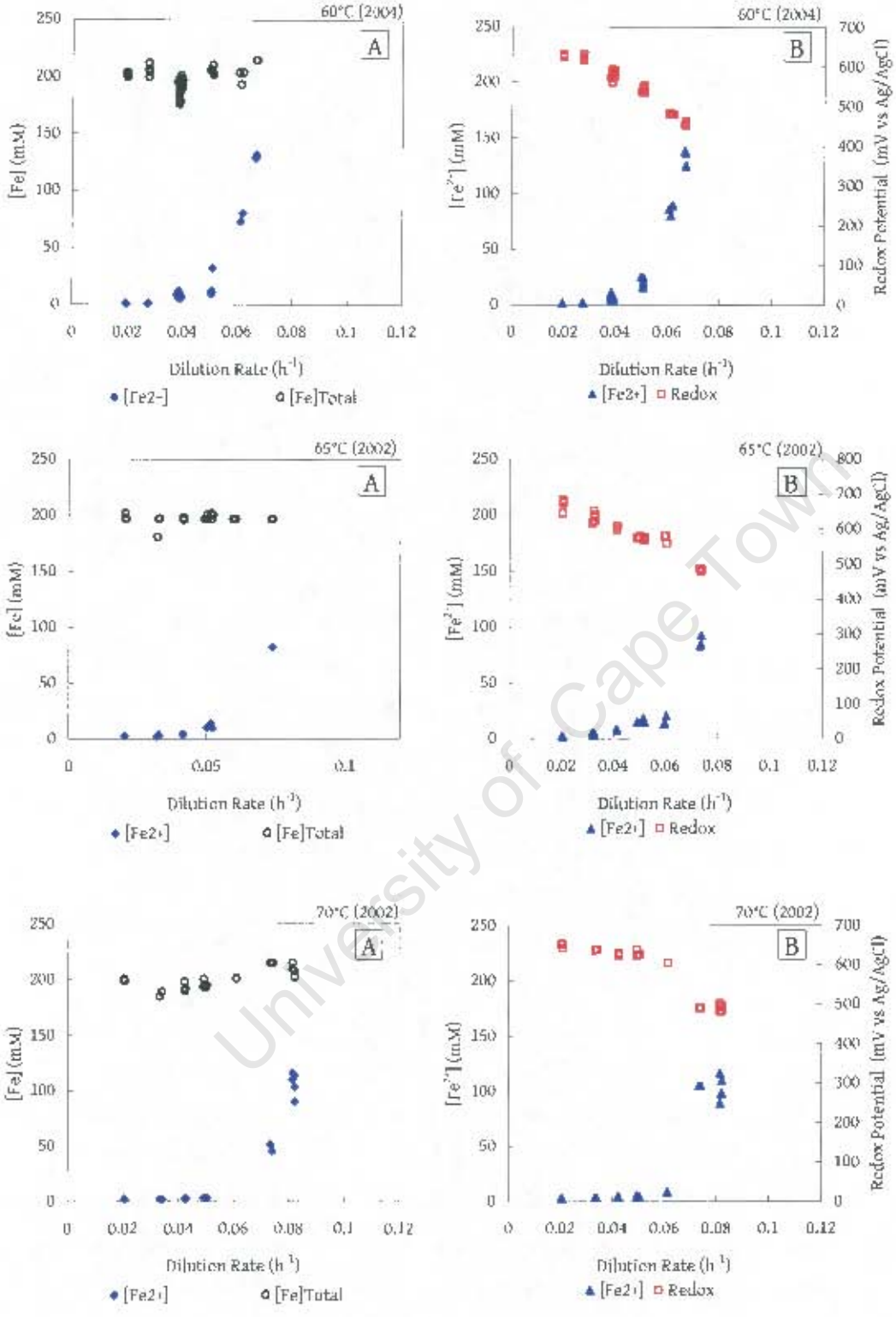

Figure 6.4 (A) Ferrous and total iron concentrations measured by titration at each steady state and (B) the redox potential measured by a combination Pt|Ag/AgCl2 electrode and the ferrous iron concentration calculated from the redox potential for continuous iron oxidation at T = 60 - 80°C, pH = 1.5, $[Fe]_T$ = 210 mM.

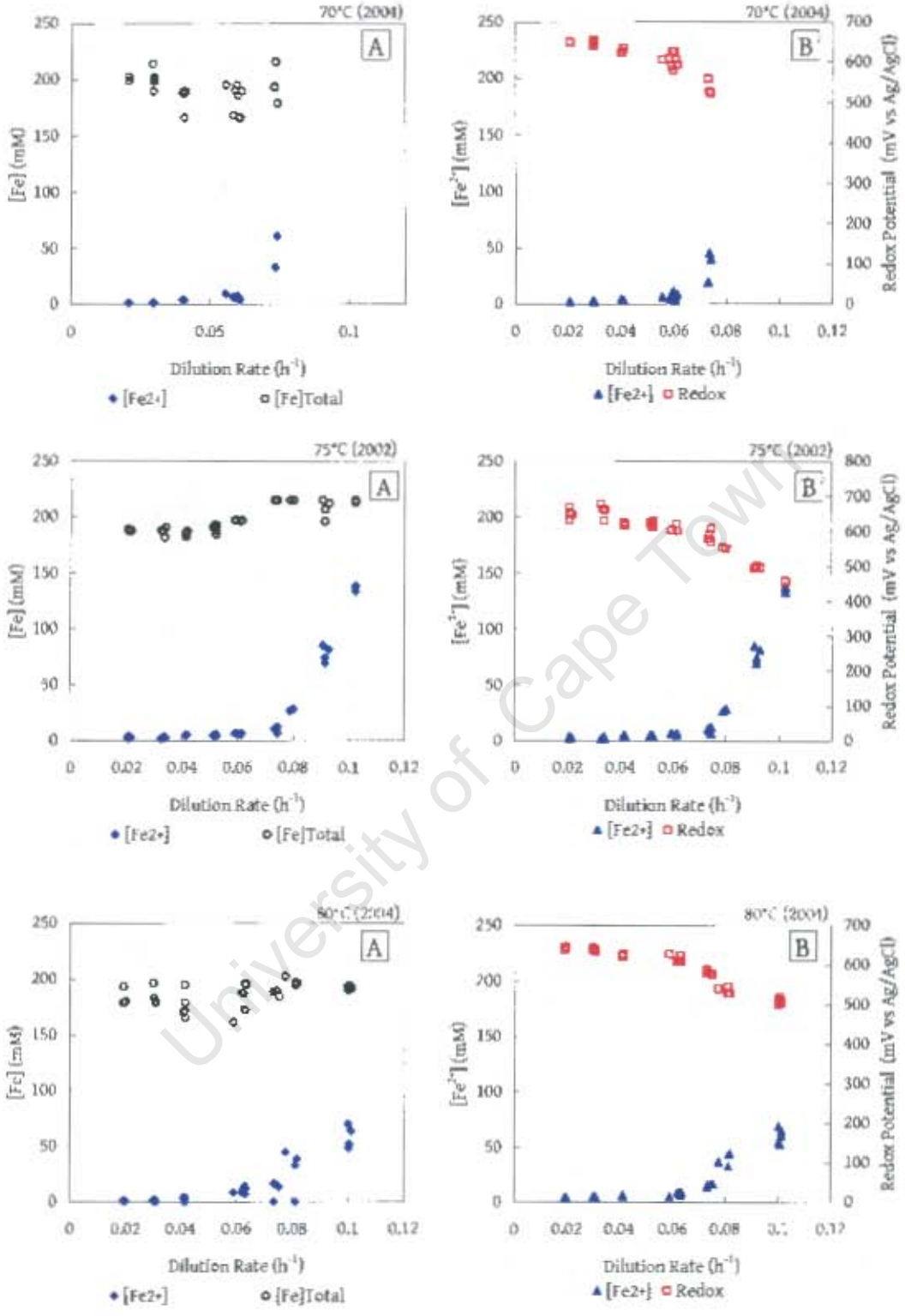

Figure 6.4 (continued) (A) Ferrous and total iron concentrations measured by titration at each steady state and (B) the redox potential measured by a combination Pt|Ag/AgCl2 electrode and the ferrous iron concentration calculated from the redox potential for continuous iron oxidation at T = 60 – 80°C, pH = 1.5, $[Fe]_T$ = 210 mM.

The steady state total iron concentration was measured to vary between 180 and 210mM. The difference leaves the reactor as a solid precipitate, either ferric hydroxide or various forms of jarosite. This precipitation is impossible to avoid when operating at elevated temperatures and high iron concentrations. The precipitate leaves the reactor either in suspension in the liquid effluent, or is removed when the reactor is cleaned. As the precipitates contain predominantly ferric iron rather than ferrous iron, all iron lost in the precipitate was assumed to have been oxidised before it precipitated. Precipitation was more prevalent at long residence times and at higher temperatures. The precipitation reaction is a strong function of pH and has a buffering effect on the solution pH. In this study the pH was externally controlled and kept constant, and the precipitate was removed regularly and was assumed to have no further impact on the reaction kinetics studied.

The ferrous iron concentration at all temperatures was low at long residence times and increased as dilution rate increased. This is in agreement with Monod continuous culture theory. The increase in concentration was matched by a corresponding drop in solution redox potential. The low but non-zero concentration at long residence times implies that in continuous culture, a minimum concentration of substrate is required for sustained growth. The lowest measured concentration increased with increasing temperature (1.4 – 3.6mM, for T = 60 - 80°C) which correlates with the expected increased maintenance energy requirement. This effect was also observed in experiments with *Leptospirillum* cultures (0.08 – 0.15mM, for T = 30 - 40°C, Breed *et al.* (1999)), but the absolute values observed are closer to those from experiments with *Acidithiobacillus ferrooxidans* (1.76mM at T = 30°C, Boon *et al.* (1999)).

The data sets presented thus far represent all measured steady states, many of which were obtained under identical conditions. These may be averaged without introducing significant additional error. Further results will be presented in terms of these average values, however all calculations will still be performed on the full data set.

6.1 Processed Data

6.1.1 Reproducibility of 70°C Data

Two identical experiments were performed at 70°C, the first in 2002, and the second in 2004. These two data sets were compared.

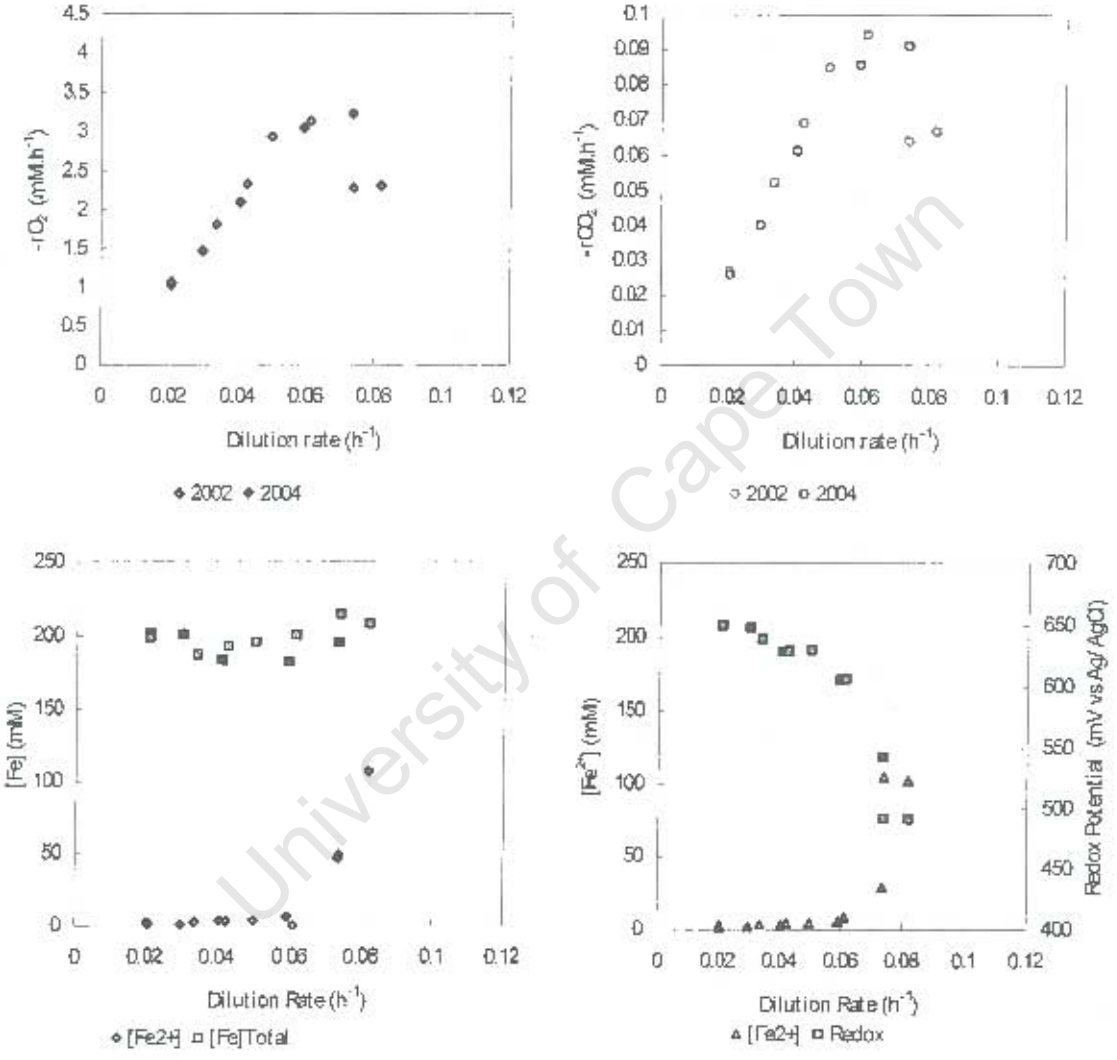

Figure 6.5 A comparison of data obtained under the same conditions in two experimental runs, Run 1, 2002 (green), and Run 2, 2004 (red). T = 70°C, pH = 1.5, $[Fe]_T$ = 210 mM.

It can be seen that the same results were obtained in the two experiments. This implies that the experimental methodology followed is sound and the results are reproducible. It also confirms that the microbial culture used did not vary during the investigation. The two data sets can thus be evaluated as a single data set.

6.1.2 Validation of Off-gas Data

The rate of ferrous iron oxidation was calculated from the rates of oxygen and carbon dioxide, using the relation determined from the degree-of-reduction balance derived in Section 4.9.

$$-r_{Fe^{2+}} = -4r_{O_2} - 4.2r_{CO_2} \qquad [4.15]$$

The derivation of Equation 6.5 was shown in Chapter 4. This was checked against a rate calculated from the iron mass balance over the reactor.

$$-r_{Fe^{2+}} = D\left([Fe^{2+}]_{IN} - [Fe^{2+}]_{OUT}\right) \qquad [6.1]$$

The microbial component of both of these rates was determined by removing the abiotic component determined in Chapter 5. As the same value is deducted from both rates, this does not affect the parity chart at all.

$$-r_{Fe^{2+}}\Big|_{Bio} = -r_{Fe^{2+}}\Big|_{Total} - 7.58\times10^{5}\left[Fe^{2+}\right]^{2} e^{-\frac{555}{RT}} \qquad [5.3]$$

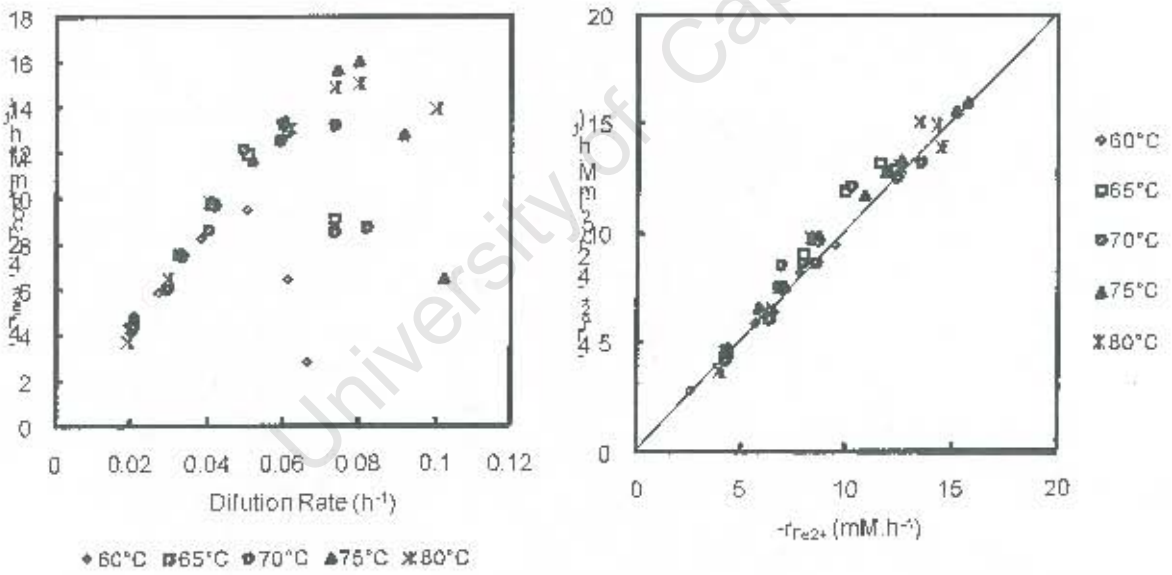

Figure 6.6 The rates of microbial ferrous iron oxidation determined by analysis of gas phase concentrations and the degree-of-reduction balance for T = 60-80°C, and a parity plot comparing these rates to rates determined from the iron mass balance. $[Fe]_T$ = 214 mM, pH = 1.5, T = 60-80°C.

The trend of the ferrous iron oxidation rate with respect to temperature mirrors that of the oxygen utilisation rate, with similar rates at low dilution rate, rising to a temperature specific maximum and declining towards washout.

that the underlying macroscopic chemical reaction scheme is valid for a thermophilic iron oxidation system.

6.2.3 Cell Concentration

As described in Section 4.9, the cell concentration, in terms of moles of carbon fixed, was determined from the rate of CO_2 uptake, assuming that all CO_2 assimilated is incorporated into viable biomass and that the rate of death is negligible. If the rate of death is negligible then the steady state specific growth rate in continuous culture is equal to the dilution rate (from the performance equation of a CSTR), and hence the cell concentration can be determined from the rate of carbon uptake.

$$c_x = \frac{r_x}{\mu} = \frac{-r_{CO_2}}{D} \qquad [4.17]$$

This method of measuring cell concentration was chosen as it is an indirect method, allowing continuous monitoring without affecting the steady state operation of the reactor. Other common techniques for the quantification of biomass were hampered by the reaction conditions. Direct cell counts, dry weight and turbidity measurements were complicated by the presence of precipitates, while protein assays were difficult at low pH and rendered varying results (Moon, 1995). The amount of biomass carbon present determined by carbon dioxide uptake was found to compare well with a total organic carbon assay (Boon, 1996).

One limitation of the method is that it does not differentiate between carbon assimilated to produce active biomass and carbon assimilated to form any other carbon containing compound. As these micro-organisms are known to produce an extracellular polymeric substance (EPS) layer (Harniet *et al.*, 2006), this limitation may be significant. However the function of this layer is linked to the attachment to mineral surfaces and much less is produced by iron-grown cells (Gehrke *et al.*, 1998). The elemental analysis of the composition of bioleaching micro-organisms reviewed in Table 3.2 would have included this layer, and the results did not show any deviation from a general formula proposed for all biomass (Roels, 1983). As long as the proportion of EPS per cell remains constant then it should not affect the analysis of data further.

The influence of growth of cells attached to surfaces in the reactor was minimised by regular scrubbing of the reactor walls and internals and removal of jarosite precipitates. This ensured that the residence time of the biomass was the same as the hydraulic residence time.

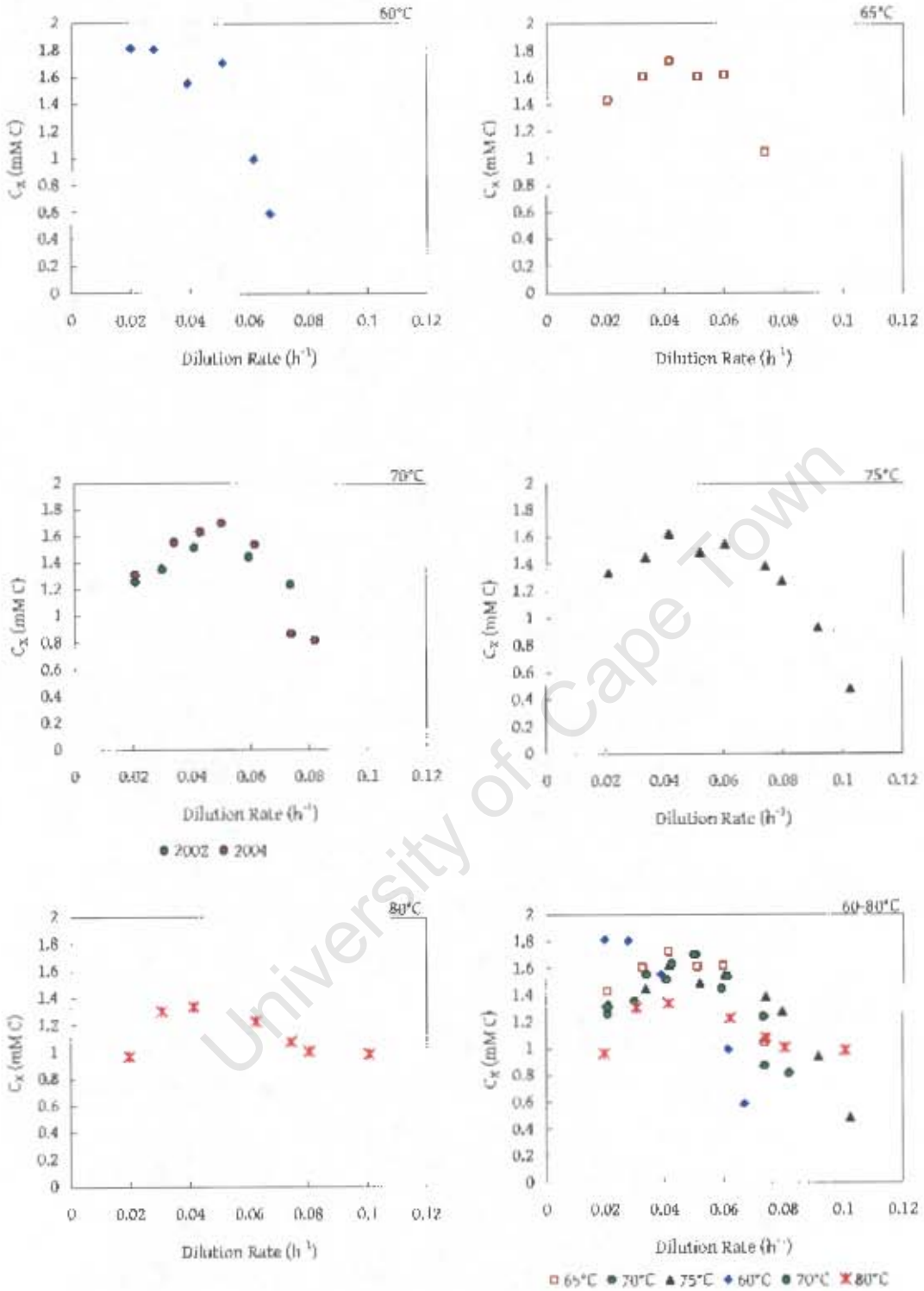

Figure 6.7 Steady state cell concentrations as moles of carbon fixed determined by offgas analysis for each dilution rate investigated. $[Fe]_T$ = 214 mM, pH = 1.5, T = 60 80°C.

The lower cell concentration at low dilution rate, i.e. specific growth rate, can be attributed to an increased proportion of energy assimilated being required for cell maintenance under substrate-

conditions. This effect is enhanced by increasing temperature as the cell concentration is highest at the lowest measured temperature and decreases with increasing temperature as the maintenance requirement increases. At intermediate dilution rates, all systems show similar cell concentrations, implying that the growth yield is not a strong function of temperature. At high dilution rates, the opposite trend was observed with respect to temperature with the highest cell concentrations observed at 80 °C. This will be discussed further in Section 6.3.3.

Washout was observed at dilution rates from 0.075 to 0.110 h^{-1}, with the washout dilution rate increasing with increasing temperature. This is expected, as washout occurs when the dilution rate exceeds the maximum specific rate at which the cell mass can replace itself, this maximum rate, μ_{max} is expected to increase with temperature. A gradual drop in cell concentration was observed from dilution rates of approximately $0.06h^{-1}$ to the washout dilution rate. This gradual or incomplete washout implies that the yield changes with dilution rate, either by a change in the maintenance requirement or a change in the efficiency of energy assimilation. Yield and cell maintenance will be discussed further in Section 6.5. The gradual washout could also be an artefact caused by a small amount of wall growth that may become more significant under conditions of rapid cell growth and less frequent washing relative to the residence time (The reactors were washed daily – this corresponds to twice a residence time at 50 hours, but only once every two residence times at 14 hours).

6.1.1 Specific Growth Rates

The specific growth rate was determined from the dilution rate and studied as a function of the ferric/ferrous-iron ratio and the concentration of ferrous iron.

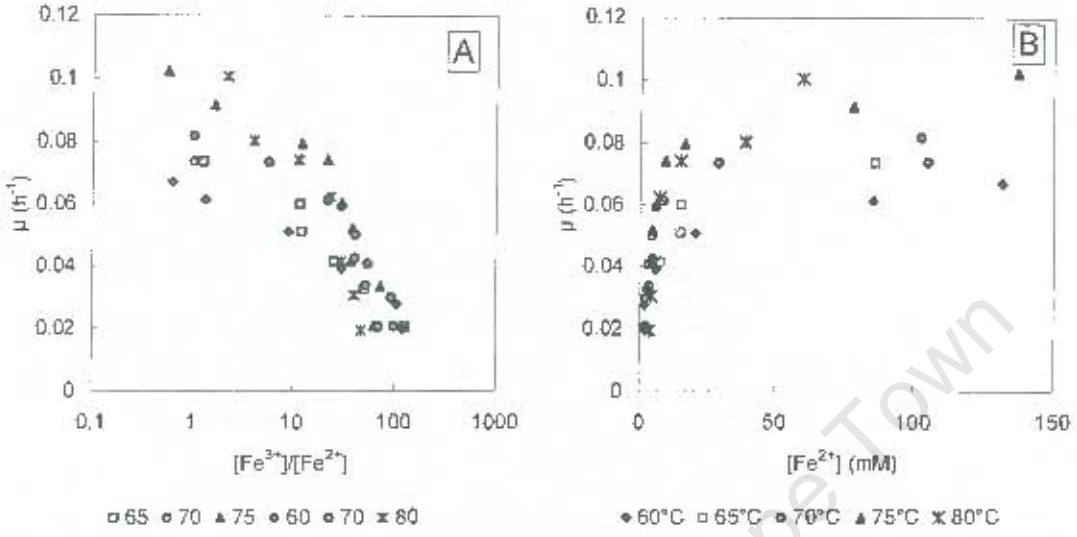

Figure 6.8 Specific growth rate studied as a function of (A) the ferric/ferrous-iron ratio and (B) the ferrous iron concentration. $[Fe]_T$ = 214 mM, pH = 1.5, T = 60-80°C.

The results at all temperatures show low specific growth rates under substrate-poor conditions, increasing to a maximum as the amount of substrate available increases, as would be expected for simple substrate-limited growth. The maximum observed specific growth rate increased with increasing temperature. Results above 70°C were more adversely affected by low substrate availability or a high ferric/ferrous-iron ratio, than experiments run at lower temperature. This can be attributed to an increased maintenance energy requirement under the combined stresses of high temperature and scarce substrate.

6.1.2 Specific Iron Utilisation Rates

The specific rates of iron oxidation were determined from

$$q_{Fe^{2+}} = \frac{r_{Fe^{2+}}}{C_X} \qquad [4.18]$$

and plotted as a function of the ferric/ferrous-iron ratio. The results show a reverse sigmoidal curve, characteristic of Michaelis-Menten kinetics, with a steady increase in the maximum rate with increasing temperature. The rates drop from the maximum at ferric/ferrous-iron ratios of

approximately 100, implying a greater similarity to *Acidithiobacillus ferrooxidans* ($[Fe^{3+}]/[Fe^{2+}]$ = 50; Boon *et al.*, 1999) than to *Leptospirillum* ($[Fe^{3+}]/[Fe^{2+}]$ = 1000; Breed *et al.*, 1999). In a bioleach system, this would be manifested by a lower operating range of the solution redox potential, a feature that may in some part explain the thermophiles' success in chalcopyrite bioleaching systems. This hypothesis was discussed by Hansford *et al.* (1999) and is based on the cycling of iron by various reactions of the multiple sub-process mechanism, where the operating redox potential is determined by the combination of ferrous iron consumption by microbial oxidation and ferrous iron production by ferric iron attack. Ferric leaching of pyrite is favoured at high potential, and so micro-organisms like *Leptospirillum ferrooxidans* that generate high redox potentials are favoured. Re-analysis of the ferric leaching data published by Kametani & Aoki (1985) showed that the rate of ferric leaching of chalcopyrite decreased at high potential (Hansford *et al.*, 1999) and that there was a narrow redox range available for effective leaching. This narrow range corresponds to the potential or ferric/ferrous-iron ratio where the thermophiles change activity, indicating their capacity to control leaching within the active potential range.

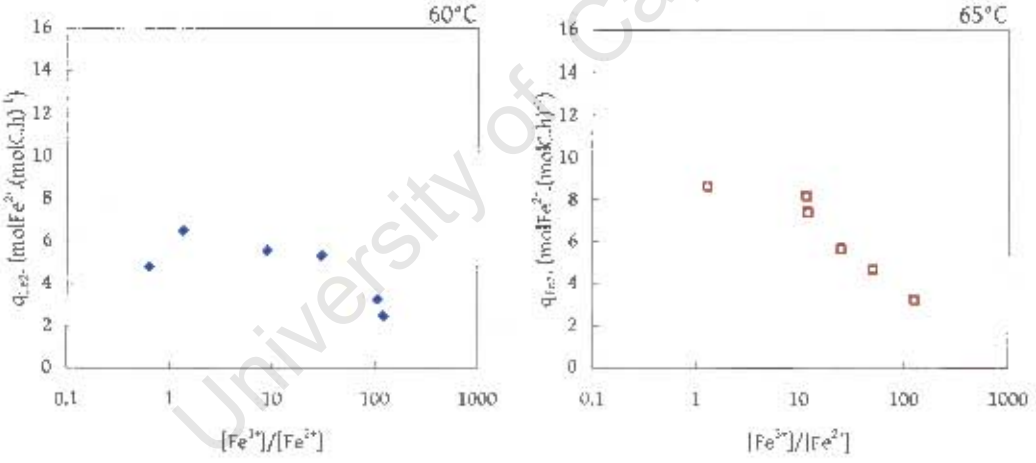

Figure 6.9 Specific microbial iron oxidation rates as a function of the ferric/ferrous-iron ratio in continuous culture. $[Fe]_T$ = 214 mM, pH 1.5, T 60-80°C.

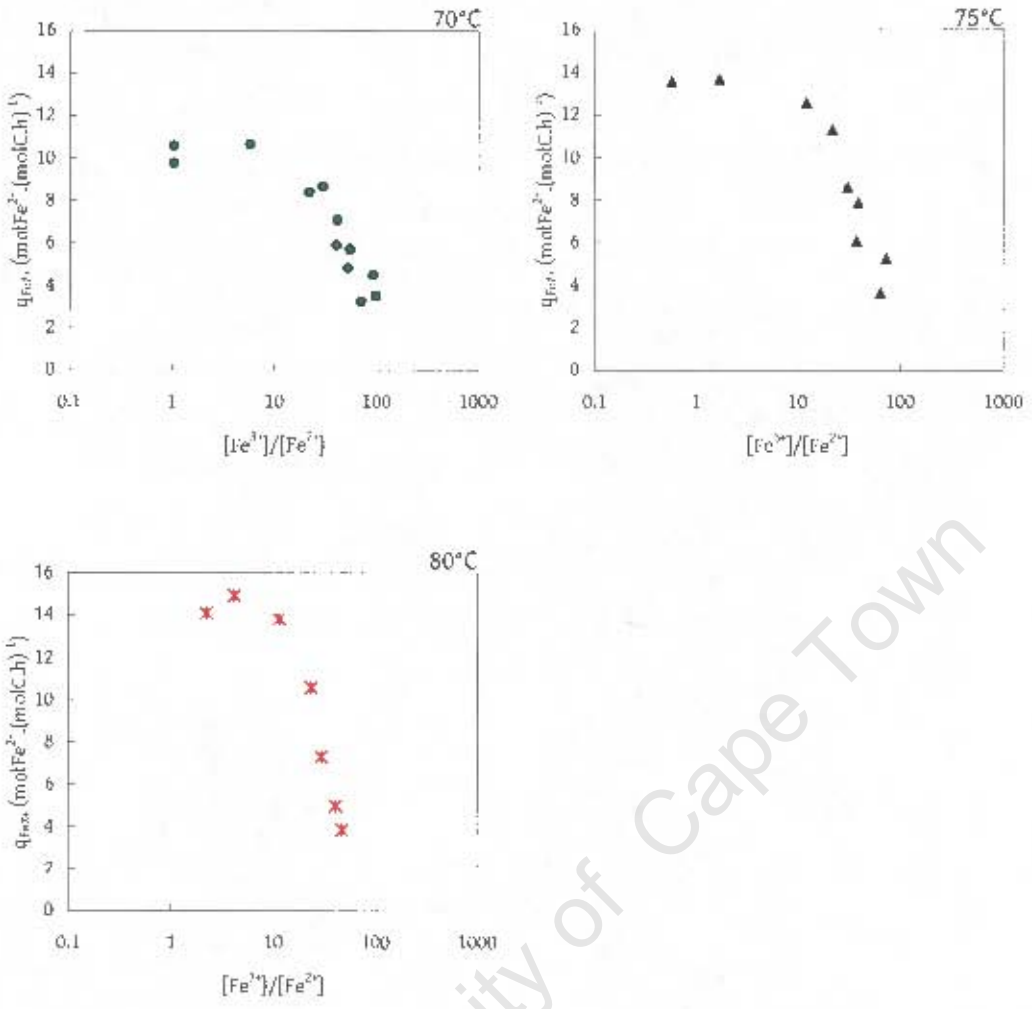

Figure 6.9 (continued) Specific microbial iron oxidation rates as a function of the ferric/ferrous-iron ratio in continuous culture. $[Fe]_t$ = 214 mM, pH = 1.5, T = 60-80°C.

The rates showed a marked increase with increasing temperature, similar to that observed in the specific growth rates in Section 6.2.4. Several of the data sets show a decrease in specific rate at low ferric/ferrous-iron ratios, corresponding to experiments run at high dilution rates. This may be an artefact of the experimental set-up caused by incomplete mixing or bypassing at high feed rates. If a portion of the feed bypasses the reactor then it could affect the results in two ways, firstly by increasing the effluent ferrous iron concentration, and secondly by interfering with the calculation of the dilution rate. If the actual dilution rate is lower than that calculated from the feed rate, then this will over-predict the cell concentration and consequently under-predict the specific iron utilisation rate. An actual decrease in the specific utilisation rate under these conditions could also be caused by substrate inhibition, indicating that the culture is inhibited by ferrous iron concentrations above 100mM Fe^{2+}. Insufficient data was captured at these iron concentrations to test this hypothesis, but batch experiments run with initial concentrations of 214mM Fe^{2+} did not

exhibit an extended lag phase, as would be expected if the culture was substrate inhibited under these conditions.

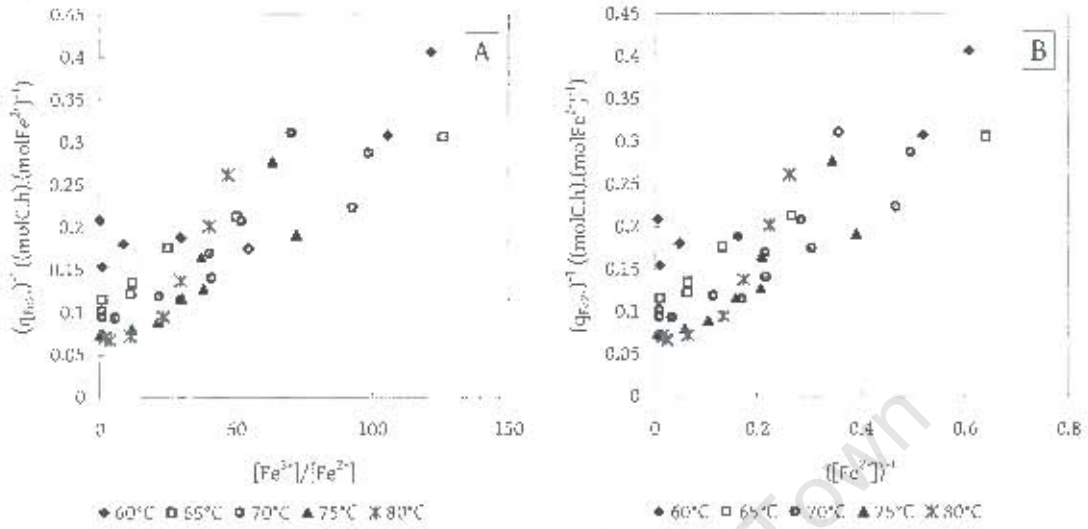

Figure 6.10 Reciprocal plots for the specific iron utilisation rate studied as a function of (A) the ferric/ferrous-iron ratio and (B) the ferrous iron concentration. $[Fe]_t$ = 214 mM, pH = 1.5, T = 60-80°C.

Reciprocal plots of the specific iron utilisation data show deviations from linearity at both high and low residual ferrous iron concentrations. The deviation at high ferrous iron concentration is characteristic of substrate inhibition, as discussed before, and the deviation at low iron concentrations is characteristic of a threshold substrate concentration, i.e. a limiting ferrous iron concentration below which no further oxidation occurs. Reciprocal plots of the specific growth rate shows a similar deviation at low iron concentrations confirming that it is a threshold effect separate from the diversion of energy for cell maintenance. Similar threshold effects were found in mesophilic systems and incorporated into the relevant rate equations (Braddock *et al.*, 1984; Boon, 1996).

6.3 Modelling Thermophilic Microbial Ferrous Iron Oxidation

6.3.1 Specific Iron Utilisation Rates

It was established in Chapter 3 that mesophilic microbial ferrous iron oxidation kinetics were most readily described by a simple rate equation describing the specific substrate utilisation rate and an expression of the cell yield. The most appropriate rate equation was found to be Equation 2.14, which related the rate to a Michaelis-Menten expression governed by the ferric/ferrous-iron ratio.

$$q_{Fe^{2+}} = \frac{q^{max}_{Fe^{2+}}}{1 + K_{Fe^{2+}} \cdot \frac{[Fe^{3+}]}{[Fe^{2+}]}} \qquad [2.14]$$

The predominantly linear behaviour of the reciprocal plots in Figure 6.10 indicated that the simple rate equations used in the mesophilic microbial iron oxidation would still be applicable for thermophiles. The application of Equation 2.14 to the thermophilic regime was tested by fitting the specific rates determined in Section 6.2.5, generating a set of temperature-specific kinetic constants,

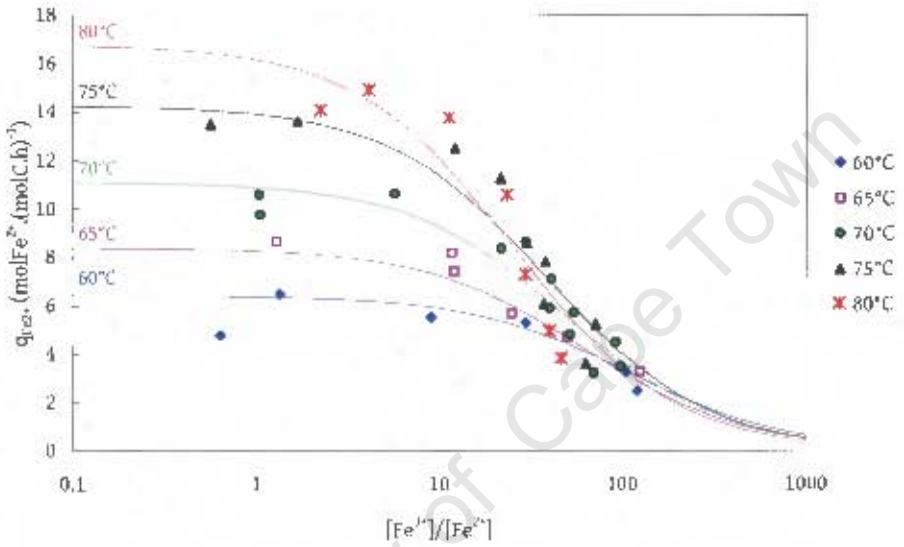

Figure 6.11 Specific microbial iron oxidation rates as a function of the ferric/ferrous-iron ratio in continuous culture. $[Fe]_T$ = 214 mM, pH = 1.5, T = 60-80°C. Lines represent fits to Equation 2.14 using the kinetic constants in Table 6.1.

Table 6.1 Kinetic constants for Equation 2.14 fitting specific iron utilisation data for $[Fe]_T$ = 214 mM, pH = 1.5, T = 60-80°C.

Temperature (°C)	q_{max} (molFe^{2+}.(molC.h^{-1}))	$K_{Fe^{2+}}$ (-)	R^2
60	6.43	0.0090	0.89
65	8.38	0.0158	0.89
70	11.11	0.0201	0.86
75	14.27	0.0254	0.87
80	16.79	0.0391	0.84

The maximum specific iron utilisation rates predicted increased with temperature. The values produced were slightly higher than those predicted for mesophilic bacteria. Breed *et al.* (1999) found q_{max} values from 8.65 to 13.65 molFe^{2+}.(molC.h)$^{-1}$ for oxidation between 30 and 40°C for *Leptospirillum*. The q_{max} values were compared to other published thermophilic kinetic constant (see

Table 2.6) and at 70 °C, the q_{max} of 11.11 molFe^{2+}(.molC.h)$^{-1}$ is very similar to that published for *Metallosphaera sedula* of 11.9 and *Sulfolobus metallicus* BC of 9.9 molFe^{2+}(.molC.h)$^{-1}$ (Norris, 1992).

The similarity between the microbial iron oxidation rates in mesophilic and thermophilic systems shows that the advantage that thermophiles enjoy in bioleaching is not due to vastly higher iron oxidation rates, but is rather more attributable to the improvement of the chemical leaching reactions and the removal of diffusional limitations. This in turn implies that the quest for a "superbug", a species that oxidises iron faster, is unlikely to provide significant improvement to bioleaching.

Values for K_{Fe2+} (comparable to K_s/K_i) between 0.009 and 0.0391 show no similarity to any of the published constants that varied from 0.02 to 3.8 (Norris, 1992; Meruane *et al.*, 2003) though it may be significant that none of the preceding thermophilic studies were performed in continuous culture. In comparison to mesophilic constants the range produced lies directly between values for *Acidithiobacillus ferrooxidans* (0.04 at 30°C; Boon, 1996) and *Leptospirillum ferrooxidans* (0.0018 – 0.0034 30-40°C; Breed *et al.*, 1999) though closer to *At. ferrooxidans* than *L. ferrooxidans*. This indicates that the culture will not generate high operating redox potentials as discussed in Section 6.2.5.

The data was also fitted to a number of other simple rate equations discussed in Chapter 3. The kinetic constants generated are tabulated in Appendix C. Fits to the Monod equation (Equation 2.7) produced similar q_{max} values to those of Equation 2.14 and K_s values between 1.62 and 7.24 mM Fe^{2+}, and similar regression coefficients to those of Equation 2.14 as predicted by the discussion in Section 3.3.2. The limitations of the Monod equation will be discussed later in Section 6.5. Regression to determine constants to Equation 2.8 for competitive product inhibition produced two solutions in which either K_s or K_i, regressed to zero, and the remaining constants produced matched either those of the Monod equation or Equation 2.14. This matches the observation made by Boon (1996) for *At. ferrooxidans*, that regression of continuous oxidation data was not sensitive to the Ks/[Fe2+] term in the competitive inhibition rate equation and that Equation 2.14 is an adequate approximation.

The reciprocal plots in Figure 6.10 shows an upward deviation in many of the data sets, characteristic of a threshold iron concentration, the exception being the 65°C data which is notably linear. Equation 2.14 was modified to include a threshold term and the constants were determined by regression.

$$q_{Fe^{2+}} = \frac{q^{max}_{Fe^{2+}}}{1 + K_{Fe^{2+}} \dfrac{[Fe^{3+}]}{[Fe^{2+}] - [Fe^{2+}]_{Threshold}}} \qquad [6.2]$$

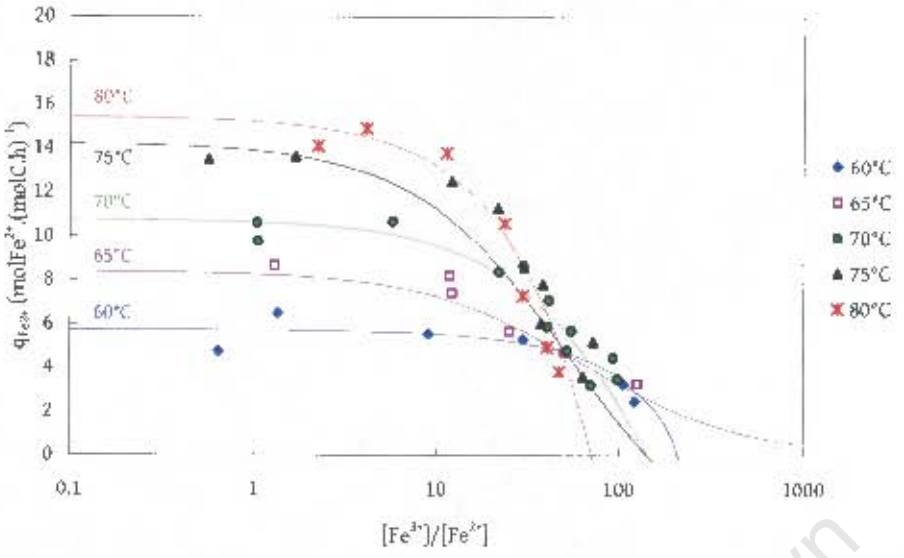

Figure 6.12 Specific microbial iron oxidation rates as a function of the ferric/ferrous iron ratio in continuous culture. $[Fe]_T$ = 214 mM, pH = 1.5, T 60-80°C. Lines represent fits to Equation 6.2 using the kinetic constants in Table 6.2.

Table 6.2 Kinetic constants for Equation 6.2 fitting specific iron utilisation data for $[Fe]_T$ = 214 mM, pH = 1.5, T = 60-80°C.

Temperature (°C)	q_{max} (molFe^{2+}.(molC.h^{-1}))	K_{Fe2+} ( )	$[Fe^{2+}]_{Threshold}$ (mMFe^{2+})	R^2
60	5.73	0.0033	0.99	0.79
65	8.38	0.0158	0	0.89
70	10.74	0.0113	1.46	0.89
75	14.24	0.0248	1.50	0.88
80	15.43	0.0146	2.96	0.94

Equation 6.2 predicts an increase in the threshold concentration with increasing temperature. This may be a consequence of complexing reactions forming ionic species that are not available for microbial oxidation. The inclusion of the threshold term provides an explanation for the changing slope of the q versus the ferric/ferrous-iron ratio plots in Figure 6.9. The results do show an improved fit with respect to the regression coefficients, but not enough to warrant the inclusion of another constant into the rate equation. The $[Fe]_{Threshold}$ values obtained were higher than those found in mesophilic systems: 0.5mM (*At. ferrooxidans* (Boon *et al.*, 1999)); 0.25mM (*At. ferrooxidans* (Braddock *et al.*, 1984)) and 0.054-0.268mM (*L. ferrooxidans* (Breed *et al.*, 1999)).

Regression was also attempted using rate equations proposed by Meruane *et al.* (2002) (Equation 2.15) and Crundwell (1997) (Equation 2.23). Equation 2.15 produced improved regression coefficients but with no consistency with respect to the constants produced for different data sets.

not fit the data. Adding a substrate inhibition term to Equation 2.14 produced improved fits for 60 and 80°C data sets, but did not fit any of the other data sets.

6.1.1 Yield and Maintenance

As described in Section 2.5.6, the microbial growth kinetics can be coupled to the iron oxidation kinetics via a description of the cell yield. One common yield expression is the constant maintenance Pirt equation (Pirt, 1965), which states that the energy produced by substrate utilisation is divided between cell synthesis and cell maintenance.

$$-r_{Fe^{2+}} = \frac{r_X}{Y_{SX}^{max}} + C_X m_S \qquad [6.3]$$

This can be manipulated a number of ways for linear regression of the Pirt parameters.

$$q_{Fe^{2+}} = \frac{\mu}{Y_{SX}^{max}} + m_S \qquad [2.33]$$

$$\frac{1}{Y_{SX}} = \frac{m_S}{\mu} + \frac{1}{Y_{SX}^{max}} \qquad [6.4]$$

It can be seen that from Equation 2.33 and 6.4, a plot of specific iron utilisation rate, q_{Fe2+}, versus the specific growth rate, μ (= dilution rate) yields a straight line with a slope of $1/Y_{SX}^{max}$ and an intercept of m_S, while plotting the reciprocal of the observed yield against the reciprocal of the specific growth rate should produce a linear trend with a slope of m_S and an intercept of $1/Y_{SX}^{max}$. These plots were attempted in Figure 6.13.

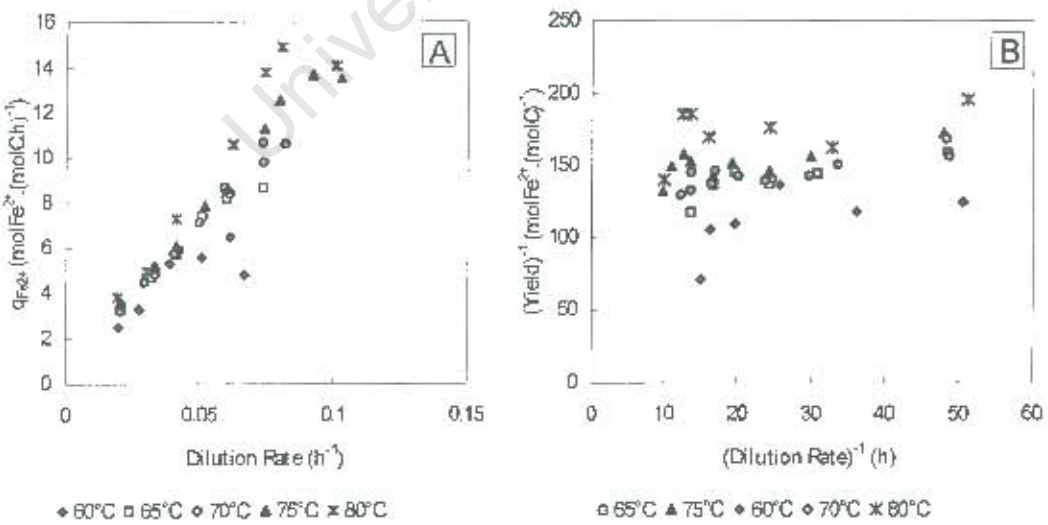

Figure 6.13 Plots of (A) the specific iron utilisation rate versus the specific growth rate (=dilution rate); and (B) the reciprocal of the observed yield versus the reciprocal of the specific growth rate (= residence time), used to determine the Pirt parameters; Y_{SX}^{max} and m_S.

The slopes of the data sets in Figure 6.13(A) show that Y_{SX}^{max} does not change greatly with temperature, but that the scatter in the data makes m_S impossible to determine with any confidence. This scatter extends to Figure 6.13(B) as m_S is small compared to $1/Y_{SX}$ and no value of m_S was obtained.

The Pirt parameters were obtained by substituting Equation 2.33 into Equation 2.14, producing

$$\mu = \frac{Y_{SX}^{max} q_{Fe^{2+}}^{max}}{1 + K_{Fe^{2+}} \frac{[Fe^{3+}]}{[Fe^{2+}]}} - Y_{SX}^{max} m_S \qquad [6.5]$$

and using the kinetic constants q_{Fe2+}^{max} and K_{Fe2+} from Table 6.1, to determine Y_{SX}^{max} and m_S by regression of the specific growth rate versus the ferric/ferrous-iron ratio data as a function of temperature.

Table 6.3 Bioenergetic constants for Equation 6.5 fitting specific growth data for $[Fe]_T$ = 214 mM, pH = 1.5, T = 60-80°C.

Temperature (°C)	Y_{SX}^{max} (molC.(molFe^{2+})$^{-1}$)	m_S (molFe^{2+}.(molC.h)$^{-1}$)	R^2
60	0.0092	0.626	0.90
65	0.0088	0.713	0.88
70	0.0083	1.08	0.89
75	0.0078	1.18	0.89
80	0.0072	1.84	0.91

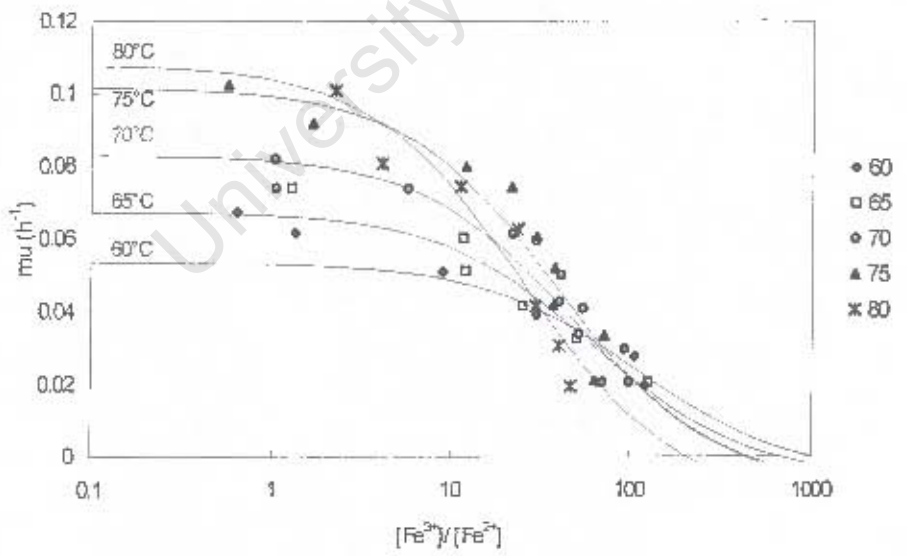

Figure 6.14 Plot of specific growth rate versus the ferric/ferrous-iron ratio, showing the fit of Equation 6.5, using kinetic constants from Tables 6.1 and 6.3, to thermophilic data with $[Fe]_T$ = 214 mM, pH = 1.5, T = 60-80°C.

The bioenergetic constants generated produced fits to the specific growth rate data that were comparable to fitting a μ-based rate equation to the data directly. The values for Y_{SX}^{max} lie between those published for *At. ferrooxidans* (0.012 molC.(molFe^{2+})$^{-1}$; Boon, 1996) and *L. ferriphilum* (0.0075 molC.(molFe^{2+})$^{-1}$; Breed *et al.*, 1999). The theoretical maximum yield based on the Gibbs free energy dissipated under standard conditions (Heijnen, lecture notes) is predicted to be 0.011 molC.(Fe^{2+})$^{-1}$, this is very close to the values deduced from the data. Calculation of this theoretical yield is shown in Appendix D.

Very little information concerning thermophilic archaeal cell yields exists in the literature, as studies in non-growing systems like oxygen uptake experiments and electrochemical cell systems do not produce yield information. Nemati & Harrison (2000) published a cell yield of between 1.9 x10^{13} and 2.2 x10^{14} cells/kgFe^{2+} and Konishi *et al.* (1995) a yield of 2.05 x10^{13} cells/kgFe^{2+}, both for *Acidianus brierleyi*. Conversion of these yields using the conversions in Table 3.7 produces yields between 0.0068 and 0.072 molC.(molFe^{2+})$^{-1}$.

The maintenance coefficients in Table 6.3 are higher than those found in mesophilic systems, indicating that the thermophiles spend a greater portion of their energy on processes other than cell synthesis, as would be expected from the more extreme environment that they exist in. Maintenance coefficients of between 0.36 and 1.06 mol Fe^{2+}.(molC.h)$^{-1}$ were found for *L. ferrooxidans* for temperatures between 30 and 40 °C (Breed *et al.*, 1999), showing a similar trend with respect to temperature, but not a continuous increase across species.

Y_{SX}^{max} showed a linear decrease with increasing temperature. This is counter-intuitive as Y_{SX}^{max} represents the maximum amount of energy available from the oxidation per mole of ferrous iron to ferric iron, which thermodynamically would be expected to increase with increasing temperature. This could mean that there is some proportion of the maintenance that varies with growth rate. Neijssel & Tempest (1976) and Pirt (1982) proposed variable maintenance models, which were reviewed in Section 2.5.6. It can be seen from Equation 2.34, that the trend in Y_{SX}^{max} can be explained by Y_{SX}^{max} itself remaining almost constant as predicted thermodynamically, and the variable maintenance term increasing with increasing temperature.

$$q_{Fe^{2+}} = \frac{\mu}{Y_{SX}^{max}} + m_S^V \mu + m_S \qquad [6.6]$$

where m_S^V – variable maintenance coefficient (mol Fe^{2+}.(molC.h)$^{-1}$

Fitting Equation 6.6 to the specific growth data, assuming that Y_{SX}^{max} remains constant at the value determined theoretically from the dissipation of Gibbs free energy under standard conditions, 0.011molC.(molFe^{2+})$^{-1}$, produces the following maintenance coefficients.

Table 6.4 Bioenergetic constants for Equation 6.6 fitting specific growth data for $[Fe]_T$ = 214 mM, pH = 1.5, T = 60-80°C, Y_{SX}^{max} = 0.011 $(molC.molFe^{2+})^{-1}$.

Temperature (°C)	m_s^v $(molFe^{2+}.(molC)^{-1})$	m_s $(molFe^{2+}.(molC.h)^{-1})$	R^2
60	17.91	0.626	0.90
65	23.20	0.713	0.88
70	30.00	1.08	0.89
75	37.84	1.18	0.89
80	47.32	1.84	0.91

Equation 6.6 produces identical regression coefficients to Equation 2.33 and identical constant maintenance coefficients, m_s. The values produced for the variable maintenance coefficients are dependent on the value assumed for Y_{SX}^{max}, and this analysis does not validate the assumed value, it merely provides a more reasonable explanation of how and why the observed yield changes with temperature, postulating a component of the energy usage of the cell, linked to the rate at which it grows, that increases exponentially with increasing temperature.

6.3.3 Prediction of the Cell Concentration

Cell concentrations can be predicted as a function of the dilution rate from a combination of a rate equation describing the specific iron utilisation rate and an expression describing the cell yield.

Assuming that the specific iron utilisation rate may be described by Equation 2.14, and that the constant maintenance Pirt equation (Equation 2.33) (Pirt, 1982) holds, then the steady state cell concentration will be predicted by

$$C_X = \frac{\mu[Fe^{2+}]_{IN}}{\frac{\mu}{Y_{SX}^{max}} + m_s} - \frac{\mu[Fe]_T K_{Fe^{2+}}}{q^{max} - \left(1 - K_{Fe^{2+}}\right)\left(\frac{\mu}{Y_{SX}^{max}} + m_s\right)} \qquad [6.7]$$

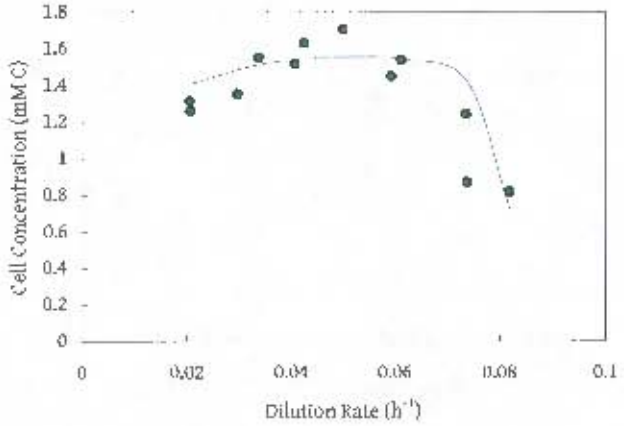

Figure 6.15 Prediction of steady state cell concentrations as moles of carbon fixed ($[Fe]_T$ = 214 mM, pH = 1.5, T = 70°C) by Equation 6.7.

This relationship between cell concentration and dilution rate is illustrated in Figure 6.15, using previously determined kinetic constants from Tables 6.1 and 6.3. The model predicts the behaviour observed in the experimental results. This affirms the appropriateness of the rate equations chosen to model the data.

At low dilution rates, the cell concentration is low due to the effect of the cell maintenance requirement, m_s. The cell concentration reaches an intermediate maximum before decreasing to zero as the dilution rate approaches washout, where steady state is unattainable and the cell concentration drops to zero.

6.4 The Effect of Temperature

Increased temperature was observed to produce an increase in reaction rate. The effect of temperature on the kinetic constants for the rate equations and yield relation was investigated further.

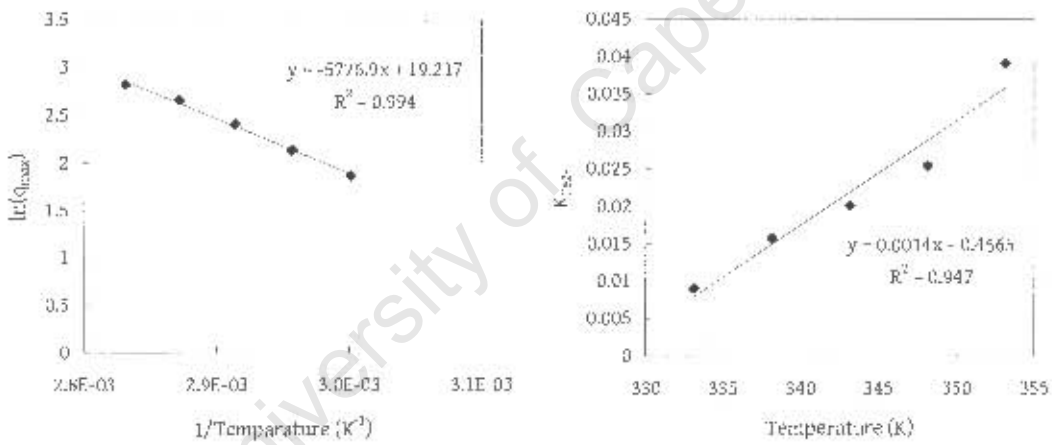

Figure 6.16 The effect of temperature on the kinetic constants, q_{max} and K_{Fe2+} from Table 6.1. $[Fe]_T$ = 214 mM, pH = 1.5, T = 60-80°C.

The results show that the effect of temperature on the maximum specific iron utilisation rate could be described by an Arrhenius function as described in Section 2.5.5, such that

$$q_{Fe^{2+}}^{max} = q_0 e^{-E_A/RT} \qquad [6.8]$$

where q_0 = 2.22×10^5 molFe^{2+}.molC^{-1}.h^{-1}
E_A = 48.0 kJ.mol^{-1}
R^2 0.99

The activation energy can be compared to other published values in Table 2.4, these vary from 33.9 to 89 kJ.mol^{-1} for a variety of iron-oxidising micro-organisms. The activation energy obtained, 48.0 kJ.mol^{-1}, is similar to the values obtained for *At. ferrooxidans* by MacDonald & Clark (1970) and

Okereke & Stevens (1991), and comparable to the values obtained for *Sulfobacillus thermosulfooxidans* (Franzmann *et al.*, 2005) and *Sulfolobus* JP1 and 2 (Plumb *et al.*, 2002).

The effect of temperature could also be described by a Ratkowsky function.

$$\sqrt{q_{Fe^{2+}}^{max}} = b(T - T_0) \qquad [6.9]$$

where $b = 0.0801$ $(molFe^{2+}.molC^{-1}.h^{-1}.K^{-1})^{0.5}$
$T_0 = 305.4$ K
$R^2 = 0.99$

This implies that the culture is able to remain active down to 305.7 K. This is unlikely and can be attributed to the temperature range studied being limited to within the viable range, where accurate fits to the Ratkowsky equation requires data at temperature that are close to the limit of viability for the species investigated.

Values found for K_{Fe2+} showed a broadly linear increase with temperature, similar to that found by Breed *et al.* (1999) for *Leptospirillum*.

$$K_{Fe^{2+}} = 1.39 \times 10^{-3} T - 0.457 \qquad [6.10]$$

where $R^2 = 0.95$

Therefore the effect of temperature can be incorporated into Equation 6.2 thus

$$q_{Fe^{2+}} = \frac{q_0 e^{-E_A/RT}}{1 + (1.39 \times 10^{-3} T - 0.457)\frac{[Fe^{3+}]}{[Fe^{2+}]}} \qquad [6.11]$$

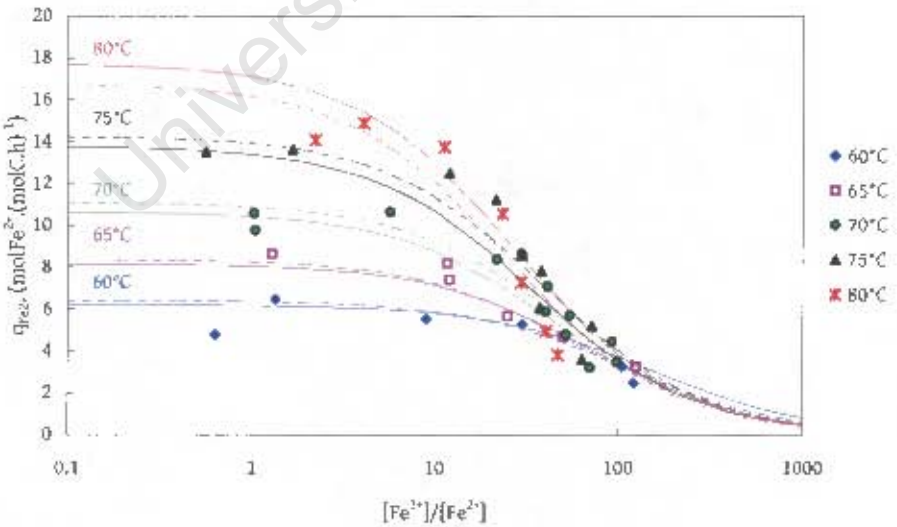

Figure 6.17 Specific microbial iron oxidation rates as a function of the ferric/ferrous-iron ratio in continuous culture. $[Fe]_T$ = 214 mM, pH = 1.5, T = 60-80°C. Dotted lines represent fits to Equation 2.14 using the kinetic constants in Table 6.1, and solid lines represent fits to Equation 6.11.

Figure 6.17 shows that very little difference in the predicted specific rate is introduced by replacing Equation 2.14 with Equation 6.11.

As discussed earlier, the bioenergetic constants for the constant maintenance Pirt equation were influenced by the temperature, with Y_{sx}^{max} displaying an unexpected decrease with increasing temperature, and the maintenance coefficient displaying an exponential increase with temperature.

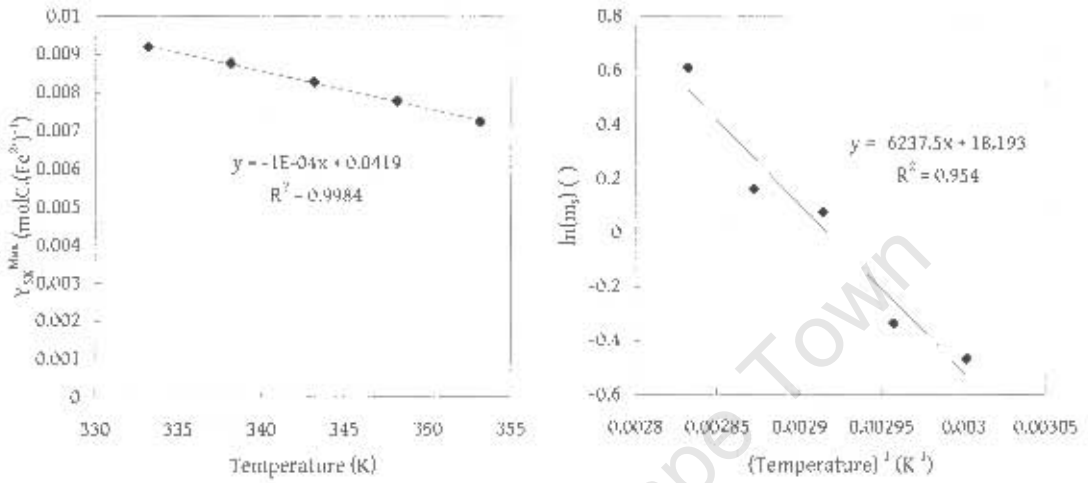

Figure 6.18 The effect of temperature on the bioenergetic parameters Y_{sx}^{max} and m_s from Table 6.3. $[Fe]_T$ = 214 mM, pH = 1.5, T = 60-80°C.

The maintenance coefficient m_s was found to be a strong function of temperature as predicted by its effect on the observed cell concentration in Section 6.3, and in agreement with the correlation developed by Tijhuis *et al.* (1993), (Equation 2.38). The effect of temperature on the bioenergetic parameters can be included in the overall yield expression, by replacing Y_{sx}^{max} by a linear function of temperature, and m_s by an Arrhenius function.

$$Y_{SX}^{max} = Y_{SX\,0}^{max} - cT \qquad [6.11]$$

where $c = 1 \times 10^{-4}$
$Y_{sx}^{max}{}_0 = 0.0418$
$R^2 = 0.998$

and

$$m_S = m_{S0} e^{-E_a/RT} \qquad [6.12]$$

where $m_{S0} = 7.97 \times 10^7 molFe^{2+}.molC^{-1}.h^{-1}$
$E_a = 51.9\ kJ.mol^{-1}$
$R^2 = 0.954$

Equations 6.11 and 6.12 can be substituted into Equation 2.33 to produce Equation 6.13.

$$q_{Fe^{2+}} = \frac{\mu}{Y_{SX}^{max}{}_0 - cT} + m_{S0} e^{-E_a/RT} \qquad [6.13]$$

The activation energy for the maintenance coefficient is very similar to that found for the specific iron utilisation rate. This is an expected result, as neither are true activation energies for single defined chemical reactions, but rather represent a composite of the biochemical reactions that make up the overall iron oxidation reaction. Both are specific rates of iron utilisation, where the specific rate of iron utilised to produce energy for maintenance functions is a subset of the overall specific rate of iron utilisation.

6.5 Effect of Total Iron Concentration

A limited study was performed investigating the influence of the total iron concentration on the oxidation kinetics. A reactor was run at a 17 hour residence time and the influent iron concentration fed as ferrous sulfate was varied from 214 to 53 mM Fe^{2+}.

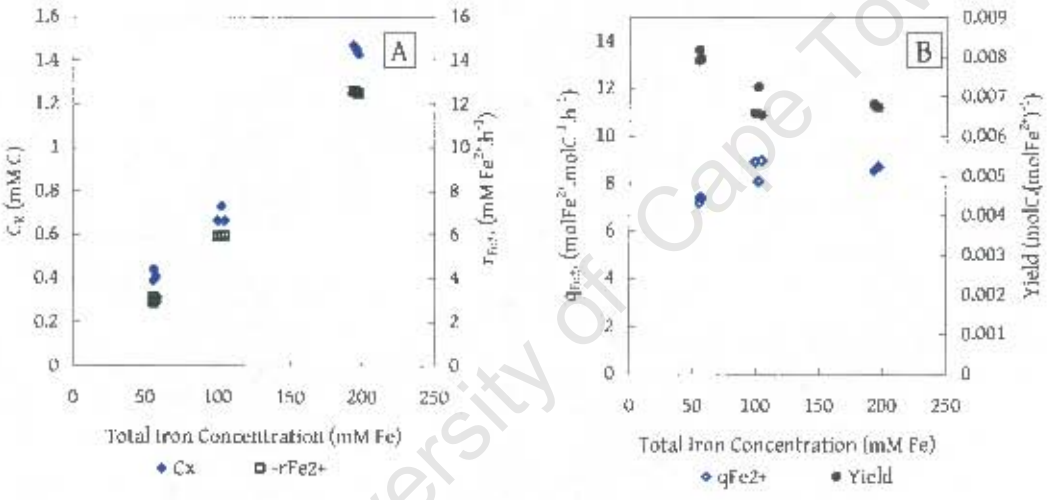

Figure 6.19 The effect of total iron concentration on (A) the cell concentration and the overall iron utilisation rate and (B) the specific iron utilisation rate and the cell yield.

Both the cell concentration and the rate of iron utilisation show a linear decline with decreasing total iron concentration, but of different proportions. This translates into a decrease in specific rate and an increase in the cell yield with decreasing total iron concentration. The decrease in specific iron utilisation rate is predicted by all of the rate equations discussed in Section 3.3.2 as both the steady state ferrous iron concentration and the ferric/ferrous-iron ratio in the reactor decreased with decreased total iron entering the reactor. The increase in yield however, implies that some limitation or inhibition is lifted when the iron load is reduced, which further implies that the K_s constants determined for the Monod model in Section 6.4.2 are not true substrate affinity constants but are modified by total iron or ferric iron inhibition.

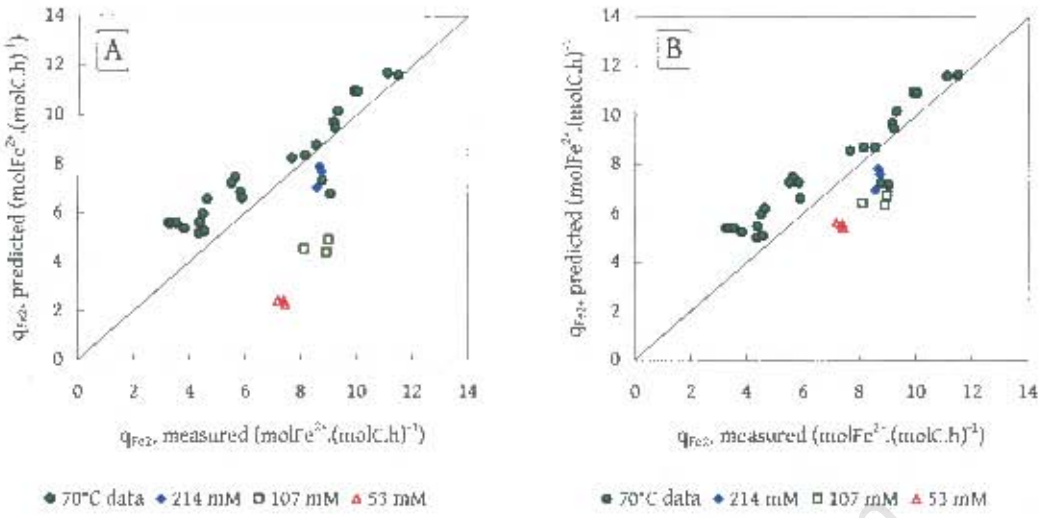

Figure 6.20 Parity plots for (A) the Monod equation and (B) Equation 2.14, showing the ability of each rate equation to predict the measured specific iron utilisation rate, using the kinetic constants determined using the 70°C data from Section 6.2.5 (Tables 6.1 and C.1). The additional data evaluated is denoted by its total iron concentration. T = 70 °C, pH = 1.5, $[Fe]_T$ = 53 - 214 mM Fe.

Figure 6.20 confirms that the Monod equation is increasingly incapable of predicting the measured specific iron utilisation rate as the conditions move further away from those used to determine the constants, and that the observed kinetics are influenced by the presence of ferric iron, hence Equation 2.14 is a more appropriate rate equation to describe the kinetics of the system.

6.6 Conclusions

The microbial oxidation of ferrous iron by a thermophilic archaeal culture was studied in continuous culture in a well-mixed, well-aerated, pH-controlled system over a temperature range of 60 to 80°C.

The reaction kinetics were followed by analysis of the off-gas oxygen and carbon dioxide concentrations and the measured redox potential. The rate of ferrous iron oxidation was determined from the gas utilisation rates via the degree-of-reduction balance. A comparison of this ferrous iron oxidation rate with rates determined from the iron mass balance showed good agreement, confirming the validity of the methodology.

The observed kinetics could be described by a rate equation describing the specific iron utilisation rate in terms of the ferric/ferrous-iron ratio (Boon, 1996), coupled to a yield expression in terms of a maximum yield and a constant maintenance coefficient (Pirt, 1965).

Scatter in the data contributing to low overall correlation coefficients for fits to the proposed rate equations can be ascribed to difficulties in maintaining constant pH and total iron oxidation over the time frame required for continuous experiments. The periodic stopping and cleaning of reactor surfaces due to iron precipitation and wall growth also contributed to the scatter.

A number of rate equations discussed in Chapter 3 were fitted to the data. As predicted by the discussion in Section 3.3.2, rate equations based on the Monod equation (Equation 2.7), competitive product inhibition (Equation 2.8) and Equation 2.14 produced similar fits for experiments investigating the effect of temperature. Experiments investigating the effect of total iron concentration showed that the equation constants determined for Equation 2.7 were not true substrate affinity constants and were modified by the presence of ferric iron. The results also showed that the regression was not sensitive to the $[Fe^{3+}]/K_i$ term in Equation 2.8, and hence that Equation 2.14 is the most appropriate rate equation to use to describe the data.

The inclusion of a threshold ferrous iron concentration term into Equation 2.14 improved the overall correlation at the cost of adding another kinetic constant to the overall model.

The effect of temperature on the system could be described by simple functions of the kinetic constants determined for each data set. Both the maximum specific iron utilisation rate, q_{Fe2+}^{max}, and the maintenance coefficient, m_s, increased exponentially with temperature and could be described by Arrhenius functions. The activation energies of these functions were similar, which explains the similarity of the overall performance of the reactors for all temperatures at low dilution rates. The maximum yield Y_{sx}^{max} was found to be similar to the predicted theoretical thermodynamic yield based on dissipation of Gibbs free energy. The observed decrease in Y_{sx}^{max} with increasing temperature was explained by postulating a growth-rate-dependent maintenance function that increased linearly with temperature.

Chapter 7

Conclusions and Recommendations

The objective of this work was to describe the kinetics of ferrous iron oxidation by thermophilic bioleaching micro-organisms. This was achieved by applying rate equations developed for mesophilic microbial ferrous iron oxidation to data gathered from an experimental investigation of thermophilic ferrous iron oxidation performed in continuous culture, to produce a set of rate expressions and kinetic constants that describe the rates of specific iron oxidation and microbial growth as a function of bulk solution conditions.

7.1 Re-evaluation of Mesophilic Iron Oxidation Data and Rate Equations

The unstructured nature of the Michaelis-Menten reaction mechanism that underpins many of the mesophilic rate equations allows their use to describe thermophilic systems, as the mechanism is governed by bulk solution conditions and is not affected by the differences of cell structure or components of the electron transport chain that exist between the mesophilic bacteria and the thermophilic archaea, treating the cell as a black box.

Direct comparison of published mesophilic kinetic data was hindered by the range of units and measurements used to present experimental results, specifically the variety of ways of expressing the amount of biomass present. The data was converted to a common basis, expressing rates in terms of moles per hour and cell concentrations in terms of moles of carbon present using a table of conversion factors (Table 3.7) compiled from the literature.

Comparison of a number of investigations of iron oxidation by the mesophile *Acidithiobacillus ferrooxidans* in continuous culture showed similar specific growth and iron oxidation rates with respect to the ferric/ferrous-iron ratio. This confirms that the concentrations of ferrous and ferric

iron and the ratio of the two are key parameters in controlling the rate of growth and oxidation. The influence of the ferric/ferrous-iron ratio is in accord with the chemiosmotic mechanism proposed for energy assimilation (Ingledew, 1982). The similarity of rates at common ratios but different total iron concentrations implies that rate equations in terms of the ferrous iron only will be inadequate to describe reaction rates in systems at other total iron concentrations than that used to determine the kinetic constants.

The disparate results of continuous and discontinuous experiments both in terms of the influence of reaction conditions and of the kinetic constants generated for similar models confirms that batch experiments are an unreliable way of generating kinetic data as the rapid change in solution conditions does not allow for a true response from the organisms.

While a large number of rate equations have been presented for microbial ferrous iron oxidation (Tables 3.8-9), the majority of results from studies in continuous culture have been fitted to relatively simple unstructured kinetic models. The data scatter in the results further discourages attempts to fit more complicated models. Analysis of the linear transforms of these simple rate equations shows similarities in the models' response to both the ferrous iron concentration and the ferric/ferrous-iron ratio. This means that the goodness of fit to a set of data obtained under a single set of experimental conditions does not imply the appropriateness of the model, and cannot be used to choose between models. Further analysis of transforms of the continuous data shows that microbial ferrous iron oxidation is best described by a rate equation derived from Michaelis-Menten reaction kinetics with competitive product inhibition, and that this rate equation may be simplified to a Monod-form equation in terms of the ferric/ferrous-iron ratio at total iron concentrations found in commercial bioleaching stirred tank reactor systems.

7.2 Abiotic Ferrous Iron Oxidation

The rate of abiotic oxidation of ferrous iron by molecular oxygen was investigated to determine whether it made a significant contribution to the overall rate of iron oxidation in thermophilic bioleaching systems. The contribution is largely ignored in mesophilic bioleaching systems, as the low temperature, low oxygen pressure and low pH retard the abiotic rate to levels that are negligible in comparison to microbial oxidation rates. As the rate was expected to increase with increasing temperature, a negligible contribution from abiotic oxidation could no longer be assumed.

Rate equations developed for abiotic oxidation in pressure leach systems and acid mine drainage systems were examined. The form of the equations were similar but the kinetic constants differed

widely, this was attributed to the different conditions of temperature, oxygen pressure and pH in each system – none of which were directly appropriate for thermophilic bioleaching.

Abiotic oxidation batch experiments in a well-mixed, well-aerated stirred tank reactor were run at constant pH using sterile feed from the microbial investigation over temperatures from 30 to 80 °C. The results showed that the reaction was second order with respect to the ferrous iron concentration, and increased in rate with increasing temperature. The results confirm that the rate of abiotic oxidation is negligible at 30°C, but becomes significant at thermophilic temperatures at high ferrous concentrations. These conditions occur in microbial systems at high dilution rates and may cause unstable behaviour near washout.

The contribution of abiotic ferrous iron oxidation to the overall rate of iron oxidation can be described by

$$-r_{Fe^{2+}}\Big|_{Total} = -r_{Fe^{2+}}\Big|_{Bio} - 7.58 \times 10^{5}[Fe^{2+}]^{2}\, e^{-\frac{65.5}{RT}} \qquad [5.4]$$

7.3 Microbial Ferrous Iron Oxidation

The microbial oxidation of ferrous iron by a thermophilic archaeal culture was studied in continuous culture in a well-mixed, well-aerated, pH-controlled system over a temperature range of 60 to 80°C.

The reaction kinetics were followed by analysis of the off-gas oxygen and carbon dioxide concentrations and the measured redox potential. The rate of ferrous iron oxidation was determined from the gas utilisation rates via the degree-of-reduction balance. A comparison of this ferrous iron oxidation rate with rates determined from the iron mass balance showed good agreement, confirming the validity of the methodology.

The observed kinetics could be described by a rate equation describing the specific iron utilisation rate in terms of the ferric/ferrous-iron ratio (Boon, 1996), coupled to a yield expression in terms of a maximum yield and a constant maintenance coefficient (Pirt, 1965).

Scatter in the data contributing to low overall correlation coefficients for fits to the proposed rate equations can be ascribed to difficulties in maintaining constant pH and total iron oxidation over the time frame required for continuous experiments. The periodic stopping and cleaning of reactor surfaces due to iron precipitation and wall growth also contributed to the scatter.

The effect of temperature on the system could be described by simple functions of the kinetic constants determined for each data set. Both the maximum specific iron utilisation rate, q_{Fe2+}^{max}, and the maintenance coefficient, m_s, increased exponentially with temperature and could be described

by Arrhenius functions, whilst K_{Fe2+} and Y_{SX}^{max} could be replaced by linear functions of temperature. This allows Equations 3.16 and 6.13 to be replaced by

$$q_{Fe^{2+}} = \frac{k_0 e^{-E_A/RT}}{1 + (aT - b)\frac{[Fe^{3+}]}{[Fe^{2+}]}} \quad [6.11]$$

$$q_{Fe^{2+}} = \frac{\mu}{Y_{SX}^{max}{}_0 - cT} + m_{S0} e^{-E_B/RT} \quad [6.13]$$

where k_0 = 2.22 x 10^8 molFe^{2+}.molC^{-1}.h^{-1}
E_A = 48.0 kJ.mol^{-1}
a = 1.39 x 10^{-3} T^{-1}
b = 0.457
c = 1 x10^{-4} T^{-1}
$Y_{SX}^{max}{}_0$ = 0.0418
m_{S0} = 7.97 x10^7molFe^{2+}.molC^{-1}.h^{-1}
E_B = 51.9 kJ.mol^{-1}

producing a model that describes thermophilic microbial ferrous iron oxidation as a function of the ferric/ferrous-iron ratio over a range of temperature from 60-80°C.

7.4 Recommendations for Future Work

This work was limited in scope to well-mixed, well-aerated system, with parameters chosen (pH, iron concentration, reactor configuration) that resemble conditions found in commercial bioleaching stirred tank systems. In less easily controlled systems such as heaps and dumps, the parameters are less likely to remain around the optimum, and the model will need to be expanded to be able to predict microbial behaviour over a much wider range of conditions.

As the experiments were run in well-aerated laboratory-scale stirred tank reactors, the reaction kinetics were not influenced by the concentration of oxygen or carbon dioxide. In industrial scale systems the supply of sufficient air is more difficult, and the effect of the oxygen concentration on the kinetics needs further study, both in terms of overcoming gas-liquid mass transfer limitations and in terms of directly affecting the microbial reaction kinetics.

All experiments were performed at pH 1.5, as this provided a suitable environment for the micro-organisms present and limited the amount of iron lost to precipitation. pH is a key parameter in microbial ferrous iron oxidation and further work in this area would need to develop an understanding of the influence of pH on the generation of a proton-motive force, on the rate of precipitation and the species formed, the cell membrane stability and the formation of different iron complexes and whether they are available as microbial substrate.

The parameters determined in Table 6.2 showed evidence of a threshold level of ferrous iron below which no cell growth was possible. This could be investigated further using lower total iron concentrations and longer residence times to confirm the threshold concentration and to determine whether it is a true threshold, or an artefact caused by the formation of iron complexes that were not available for use as substrate.

The rates predicted by the proposed model deviated from the observed data at high dilution rates near wash-out dilution rate. This corresponded to conditions of high ferrous concentrations and high specific rates. The data shows an apparent decrease in the specific iron utilisation rate and rapid drop in the observed yield. It is unclear whether this decrease is real (possibly substrate inhibition) or whether it is caused by deviations from ideal CSTR behaviour, or an over-prediction of the contribution of abiotic iron oxidation (the abiotic experiments were performed under well-oxygenated conditions).

The yield expression used in this work provides an adequate description of the relationship between the specific iron utilisation rate and the growth rate, however the parameters have little physical meaning: all energy utilisation not related to carbon assimilation is lumped under "maintenance" without necessarily having being used for maintenance function, and the maximum yield decreases with increasing temperature, whilst the theoretical amount of energy available per mole of substrate should increase with temperature. This may be explained by introducing a growth rate related component to the maintenance requirement, but this needs to be investigated further to establish what functions require more energy per cell when growing faster. This may be more suited to the development of a structured model that differentiates the cell according to function: electron transport apparatus, cell replication, protein synthesis, formation of extracellular polysaccharides, and maintenance of osmotic gradients.

The effect of temperature could be described by an Arrhenius function as the range of temperatures investigated lay within the operating range of the micro-organism used. If the temperature range was increased beyond the maximum tolerated by the organism then the increase in the rate of cell formation will be superseded by the increase in the rate of cell death, and the Arrhenius expression will no longer adequately describe the effect of temperature. As temperatures cannot be tightly controlled in a heap leaching system, it would be valuable to be able to understand what happens to a culture at temperatures both below and above its normal operating temperature, both physiologically and with respect to the effect on the oxidation reaction kinetics.

Chapter 8

List of References

1) Ahonen L, Tuovinen OH. 1989. Microbiological oxidation of ferrous iron at low temperatures. Appl Environ Microbiol 55(2): 312-16.

2) Anemüller S, Luebben M, Schaefer G. 1985. The respiratory system of *Sulfolobus acidocaldarius*, a thermoacidophilic archaebacterium. FEBS Lett 193(1): 83-7.

3) Barr DW, Ingledew WJ, Norris PR. 1990. Respiratory chain components of iron-oxidizing, acidophilic bacteria. FEMS Microbiol Lett 70(1): 85-9.

4) Barron JL, Lueking DR. 1990. Growth and maintenance of *Thiobacillus ferrooxidans* cells. Appl Environ Microbiol 56(9): 2801-6.

5) Batty JD, Rorke GV. 2006. Development and commercial demonstration of the BioCOP thermophile process. Hydrometallurgy 83(1-4): 83-89.

6) Baumeister W, Lembcke G. 1992. Structural features of archaebacterial cell envelopes. J Bioenerg Biomembr 24: 567-575.

7) Bhakta P, Arthur B. 2002. Heap bio-oxidation and gold recovery at Newmont Mining: first-year results. JOM 54(10): 31-34.

8) Blake RC II, McGinness S. 1993. Electron-transfer proteins of bacteria that respire on iron. Biohydrometall Technol, Proc Int Biohydrometall Symp 2: 615-28.

9) Blight KR, Ralph DE. 2004. Effect of ionic strength on iron oxidation with batch cultures of chemolithotrophic bacteria. Hydrometallurgy 73(3-4): 325-334.

10) Boogerd FC, Bos P, Kuenen JG, Heijnen JJ, Van der Lans RGJM. 1990. Oxygen and carbon dioxide mass transfer and the aerobic, autotrophic cultivation of moderate and extreme

thermophiles: a case study related to the microbial desulfurization of coal. Biotechnol Bioeng 35(11): 1111-19.

11) Boon M, Meeder TA, Thone C, Ras C, Heijnen JJ. 1999a. The ferrous iron oxidation kinetics of *Thiobacillus ferrooxidans* in continuous cultures. Appl Microbiol Biotech 51(6): 820-826.

12) Boon M, Heijnen JJ, Hansford GS. 1995. Recent developments in modelling bio-oxidation kinetics part i: measurement methods. In: Proceedings of the Engineering Foundation Conference "Minerals Processing II", Snowbird, Utah, July 10-15, 1995. 41-61.

13) Boon M, Luyben KChAM, Heijnen JJ. 1998. The use of online off-gas analyses and stoichiometry in the bio-oxidation kinetics of sulfide minerals. Hydrometallurgy 48(1): 1-26.

14) Boon M, Ras C, Heijnen JJ. 1999b. The ferrous iron oxidation kinetics of *Thiobacillus ferrooxidans* in batch cultures. Appl Microbiol Biotech 51(6):813-819.

15) Boon M. 1996. Theoretical and experimental methods in the modelling of bio-oxidation kinetics of sulphide minerals. Ph.D. Thesis, Delft University of Technology, The Netherlands.

16) Bouffard SC, Dixon DG. 2004. Heap biooxidation of refractory gold ores: Current state of the art. Miner Process Extr Metall Rev 25(3): 159-192.

17) Braddock JF, Luong HV, Brown E. 1984. Growth kinetics of *Thiobacillus ferrooxidans* isolated from arsenic mine drainage. Appl Environ Microbiol 48: 48-55.

18) Brasseur G, Levican G, Bonnefoy V, Holmes D, Jedlicki E, Lemesle-Meunier D. 2004. Apparent redundancy of electron transfer pathways via bc1 complexes and terminal oxidases in the extremophilic chemolithoautotrophic *Acidithiobacillus ferrooxidans*. Biochim Biophys Acta 1656(2-3): 114-126.

19) Breed AW, Dempers CJN, Searby GE, Gardner MN, Rawlings DE, Hansford GS. 1999. The effect of temperature on the continuous ferrous iron oxidation kinetics of a predominantly *Leptospirillum ferrooxidans* culture. Biotechnol Bioeng 65(1): 44-53.

20) Breed AW, Hansford GS. 1999. Effect of pH on ferrous iron oxidation kinetics of *Leptospirillum ferrooxidans* in continuous culture. Biochem Eng J 3(3): 193-201.

21) Breed AW. 2000. Studies on the mechanism and kinetics of bioleaching with special reference to the bioleaching of refractory gold-bearing arsenopyrite/pyrite concentrates. Ph.D. Thesis, University of Cape Town, South Africa.

22) Bridge TAM, Johnson DB. 1998. Reduction of soluble iron and reductive dissolution of ferric iron-containing minerals by moderately thermophilic iron-oxidizing bacteria. Appl Environ Microbiol 64(6): 2181-2186.

23) Brierley JA, Brierley CL. 2001. Present and future commercial applications of biohydrometallurgy. Hydrometallurgy 59(2-3): 233-239.

24) Brierley JA, Norris PR, Kelly DP, Le Roux NW. 1978. Characteristics of a moderately thermophilic and acidophilic iron-oxidizing *Thiobacillus*. Eur J Appl Microbiol Biotechnol 5(4): 291-9.

25) Brierley JA. 1997. Heap leaching of gold-bearing deposits: theory and operational description. In: Rawlings DE. (ed) Biomining: Theory, Micro-organisms and Industrial Processes. Springer-Verlag, Berlin 103-115.

26) Brierley JA. 1978. Thermophilic iron-oxidizing bacteria found in copper leaching dumps. Appl Environ Microbiol 36(3): 523-5.

27) Brock TD, Brock KM, Belly RT, Weiss RL. 1972. *Sulfolobus*: A new genus of sulfur-oxidizing bacteria living at low pH and high temperature. Arch Mibrobiol 84: 54-68.

28) Brock TD, Cook S, Petersen S, Mosser JL. 1976. Biogeochemistry and bacteriology of ferrous iron oxidation in geothermal habitats. Geochim Cosmochim Acta 40(5): 493-500.

29) Brock TD. 1978. Thermophilic Micro-organisms and Life at High Temperatures. Springer-Verlag, New York.

30) Burton NP, Williams TD, Norris PR. 1999. Carboxylase genes of *Sulfolobus metallicus*. Arch Microbiol 172(6): 349-53.

31) Bustos S, Castro S, Montealegre R. 1993. The Sociedad Minera Pudahuel bacterial thin-layer leaching process at Lo Aguirre. FEMS Microbiol Rev 11(1-3): 231-235.

32) Chmielewski, T Charewicz, WA. 1984. The oxidation of iron(II) in aqueous sulfuric acid under oxygen pressure. Hydrometallurgy 12(1): 21-30.

33) Clark DA, Norris PR. 1996a. Oxidation of mineral sulfides by thermophilic microorganisms. Miner Eng 9(11): 1119-1125.

34) Clark DA, Norris PR. 1996b. *Acidimicrobium ferrooxidans* gen. nov., sp. nov.: mixed-culture ferrous iron oxidation with *Sulfobacillus* species. Microbiol 142(4): 785-90.

35) Coram NJ, Rawlings DE. 2002. Molecular relationship between two groups of the genus *Leptospirillum* and the finding that *Leptospirillum ferriphilum* sp. nov. dominates South African commercial biooxidation tanks that operate at 40 °C. Appl Environ Microbiol 68(2): 838-45.

36) Crundwell FK. 1997. The kinetics of the chemiosmotic proton circuit of the iron-oxidizing bacterium *Thiobacillus ferrooxidans*. Bioelectrochem Bioenerg 43: 115-122.

37) de Kock SH, Barnard P, du Plessis CA. 2004. Oxygen and carbon dioxide kinetic challenges for thermophilic mineral bioleaching processes. Biochem Soc Trans 32(2): 273-275.

38) De Rosa M, Gambacorta A, Bu'lock JD. 1975. Extremely thermophilic acidophilic bacteria convergent with *Sulfolobus acidocaldarius*. J Gen Microbiol 86(1): 156-64.

39) De Rosa M, Trincone A, Nicolaus B, Gambacorta A. 1991. Archaebacteria: lipids, membrane structures, and adaptions to environmental stresses. In: Prisco G (ed) Life under extreme conditions. Springer, Berlin Heidelberg New York. 61-87.

40) Dempers CJN, Breed AW, Hansford GS. 2003. The kinetics of ferrous-iron oxidation by *Acidithiobacillus ferrooxidans* and *Leptospirillum ferrooxidans*: effect of cell maintenance. Biochem Eng J 16(3): 337-346.

41) Dempers CJN. 2000. An investigation into the use of batch experiments in the determination of the kinetics of ferrous-iron oxidation by *Leptospirillum ferrooxidans*. MSc Dissertation, University of Cape Town, South Africa.

42) Dew DW, Van Buuren C, McEwan K, Bowker C. 1999. Bioleaching of base metal sulfide concentrates: a comparison of mesophile and thermophile bacterial cultures. Process Metallurgy 9A(Biohydrometallurgy and the Environment Toward the Mining of the 21st Century, Pt. A) 229-238.

43) Dopson M, Baker-Austin C, Hind A, Bowman JP, Bond PL. 2004. Characterization of *Ferroplasma* isolates and *Ferroplasma acidarmanus* sp. nov., extreme acidophiles from acid mine drainage and industrial bioleaching environments. Appl Environ Microbiol 70(4): 2079-2088.

44) Edwards KJ, Bond PL, Gihring TM, Banfield JF. 2000. An Archaeal iron-oxidizing extreme acidophile important in acid mine drainage. Science 287(5459): 1796-1799.

45) Ehrlich HL. 2001. Past, present and future of biohydrometallurgy. Hydrometallurgy 59(2-3): 127-134.

46) Eneroth E, Bender Koch C. 2004. Fe-hydroxysulphates from bacterial Fe^{2+} oxidation. Hyperfine Interact 156/157(1-4): 423-429.

47) Esener AA, Roels JA, Kossen NWF. 1983. Theory and applications of unstructured growth models: kinetic and energetic aspects. Biotechnol Bioeng 25(12): 2803-41.

48) Franzmann PD, Haddad CM, Hawkes RB, Robertson WJ, Plumb JJ. 2005. Effects of temperature on the rates of iron and sulfur oxidation by selected bioleaching bacteria and archaea: Application of the Ratkowsky equation. Miner Eng 18(13-14): 1304-1314.

49) Fuchs T, Huber H, Burggraf S, Stetter KO. 1996. 16S rDNA-based phylogeny of the archaeal order *Sulfolobales* and reclassification of *Desulfurolobus ambivalens* as *Acidianus ambivalens* comb. nov.. Syst Appl Microbiol 19(1): 56-60.

50) Fuchs T, Huber H, Teiner K, Burggraf S, Stetter KO. 1995. *Metallosphaera prunae*, sp. nov., a novel metal-mobilizing, thermoacidophilic *Archaeum*, isolated from a uranium mine in Germany. Syst Appl Microbiol 18: 560-566.

51) Gehrke T, Telegdi J, Thierry D, Sand W. 1998. Importance of extracellular polymeric substances from *Thiobacillus ferrooxidans* for bioleaching. Appl Environ Microbiol 64(7): 2743-2747.

52) Giudici-Orticoni MT, Guerlesquin F, Bruschi M, Nitschke W. 1999. Interaction-induced redox switch in the electron transfer complex rusticyanin-cytochrome c(4). J Biol Chem 274(43): 30365-9.

53) Golovacheva RS, Golyshina OV, Karavaiko GI, Dorofeev AG, Chernykh NA. 1992. The new iron-oxidizing bacterium *Leptospirillum thermoferrooxidans* sp. nov. Mikrobiologiya 61(6): 1056-65.

54) Golovacheva RS, Karavaiko GI. 1978. *Sulfobacillus*, a new genus of thermophilic sporeforming bacteria. Mikrobiologiya 47(5): 815-22.

55) Golovacheva RS, Valiejo-Roman KM, Troitskii AV. 1987. *Sulfurococcus mirabilis* gen. nov. sp. nov., a new thermophilic archaebacterium oxidizing sulfur. Mikrobiologiya 56(1): 100-7.

56) Golyshina OV, Pivovarova TA, Karavaiko GI, Kondrat'eva TF, Moore ERB, Abraham W-R, Lunsdorf H, Timmis KN, Yakimov MM, Golyshin, PN. 2000. *Ferroplasma acidiphilum* gen. nov., sp. nov., an acidophilic, autotrophic, ferrous-iron-oxidizing, cell-wall-lacking, mesophilic member of the *Ferroplasmaceae* fam. nov., comprising a distinct lineage of the Archaea. Int J Sys Evol Microbiol 50(3): 997-1006.

57) Gomez E, Lopez AI, Marin I, Amils R. 1993. Isolation and characterization of novel bioleaching microorganisms from Rio Tinto. Biohydrometall. Technol., Proc. Int. Biohydrometall. Symp. 2: 479-86.

58) Gomez JM, Cantero D. 1998. Modelling of ferrous sulfate oxidation by *Thiobacillus ferrooxidans* in discontinuous culture: influence of temperature, pH and agitation rate. J Ferment Bioeng 86(1): 79-83.

59) Gomez JM, Cantero D. 2003. Kinetic study of biological ferrous sulphate oxidation by iron-oxidising bacteria in continuous stirred tank and packed bed bioreactors. Proc Biochem 38(6): 867-875.

60) Gomez JM, Caro I, Cantero D. 1996. Kinetic equation for growth of *Thiobacillus ferrooxidans* in submerged culture over aqueous ferrous sulfate solutions. J Biotechnol 48(1,2): 147-152.

61) Gormely LS, Duncan DW. 1974. Estimation of *Thiobacillus ferrooxidans* concentrations. Can J Microbiol 1453-1455.

62) Grogan D, Palm P, Zillig W. 1990. Isolate B12, which harbours a virus-like element, represents a new species of the archaebacterial genus *Sulfolobus*, *Sulfolobus shibatae*, sp. nov.. Arch Microbiol 154: 594-599.

63) Guay R, Silver M, Torma AE. 1977. Ferrous iron oxidation and uranium extraction by *Thiobacillus ferrooxidans*. Biotechnol Bioeng 19(5): 727-40.

64) Haddadin J, Dagot C, Fick M. 1995. Models of Microbial Leaching. Enzyme Microb Technol 17(April): 290-305.

65) Halfmeier H, Schafer-Treffenfeldt W, Reuss M. 1993. Potential of *Thiobacillus ferrooxidans* for Waste Gas Purification. Part 1. Kinetics of Continuous ferrous Iron Oxidation. Appl Microbiol Biotechnol 40: 416-420.

66) Hallberg KB, Lindstrom EB. 1994. Characterization of *Thiobacillus caldus* sp. nov., a moderately thermophilic acidophile. Microbiology (Reading, United Kingdom) 140(12): 3451-6.

67) Hallberg KB. 1995. Role of arsenic toxicity to, and resistance of thermophilic bioleaching micro-organisms. Ph.D. Thesis, Umeå University, Umeå, Sweden.

68) Hallmann R, Friedrich A, Koops HP, Pommerening-Roeser A, Rohde K, Zenneck C, Sand W. 1992. Physiological characteristics of *Thiobacillus ferrooxidans* and *Leptospirillum ferrooxidans* and physicochemical factors influence microbial metal leaching. Geomicrobiol J 10(3-4): 193-206.

69) Han CJ, Park SH, Kelly RM. 1997. Acquired thermotolerance and stressed-phase growth of the extremely thermoacidophilic archaeon *Metallosphaera sedula* in continuous culture. Appl Environ Microbiol 63(6): 2391-2396.

70) Hansford GS, Furamera TA, Jaffer MA, Searby GE. Preliminary results of an investigation on the mechanism of bioleaching of chalcopyrite. In: ALTA COPPER 1999 Copper Sulphides Symposium and Copper Hydrometallurgy Forum, Technical Proceedings of the 5th Annual Forum on Copper Sulphides and Copper Hydrometallurgy, ALTA Metallurgical Services, Melbourne, Australia.

71) Hansford GS, Vargas T. 2001. Chemical and electrochemical basis of bioleaching processes. Hydrometallurgy 59(2-3): 135-145.

72) Hansford GS. 1997. Recent developments in modeling the kinetics of bioleaching. In: Rawlings DE. (ed) Biomining: Theory, Micro-organisms and Industrial Processes. Springer-Verlag, Berlin 153-175.

73) Harneit K, Goeksel A, Kock D, Klock J-H, Gehrke T, Sand W. 2006. Adhesion to metal sulfide surfaces by cells of *Acidithiobacillus ferrooxidans, Acidithiobacillus thiooxidans and Leptospirillum ferrooxidans*. Hydrometallurgy 83(1-4): 245-254.

74) Harvey PI, Crundwell FK. 1997. Growth of *Thiobacillus ferrooxidans*: a novel experiment design for batch growth and bacterial leaching studies. Appl Environ Microbiol 63(7): 2586-2592.

75) Harvey TJ, Bath M. 2003. The Development of the first Commercial GEOCOAT® Heap Leach For Refractory Gold at the Agnes Mine, Barberton South Africa. In: Proceedings of the 15th International Biohydrometallurgy Symposium (IBS 2003) held 14-19th September 2003, Athens, Greece.

76) Hawkes RB, Franzmann PD, Plumb JJ. 2006. Moderate thermophiles including "Ferroplasma cupricumulans" sp. nov. dominate an industrial-scale chalcocite heap bioleaching operation. Hydrometallurgy 83(1-4): 229-236.

77) He ZG, Zhong H, Li, Y. 2004. *Acidianus tengchongensis* sp. nov., a new species of acidothermophilic archaeon isolated from an acidothermal spring. Curr Microbiol 48: 159-163.

78) Heijnen JJ, Van Dijken JP. 1992. In search of a thermodynamic description of biomass yields for the chemotrophic growth of microorganisms. Biotechnol Bioeng 39(8): 833-58.

79) Herbert D, Elsworth R, Telling RC. 1956. The continuous culture of bacteria; a theoretical and experimental study. J Gen Microbiol 14(3): 601-22.

80) Hinshelwood C, Dean ACR. 1966. Growth, function and regulation in bacterial cells. Oxford at the Clarendon Press.

81) Hippe H. 2000. *Leptospirillum* gen. nov. (ex Markosyan 1972), nom. rev., including *Leptospirillum ferrooxidans* sp. nov. (ex Markosyan 1972), nom. rev. and *Leptospirillum thermoferrooxidans* sp. nov. (Golovacheva *et al.*, 1992). Int J Sys Evol Microbiol 50(2): 501-3.

82) Hiraishi A, Nagashima KVP, Matsuura K, Shimada K, Takaichi S, Wakao N, Katayama Y. 1998. Phylogeny and photosynthetic features of *Thiobacillus acidophilus* and related acidophilic

bacteria: its transfer to the genus *Acidiphilium* as *Acidiphilium acidophilum* comb. nov. Int J Sys Bacteriol 48(4): 1389-1398.

83) Huber G, Stetter KO. 1991. *Sulfolobus metallicus*, sp. nov., a novel strictly chemolithoautotrophic thermophilic archaeal species of metal-mobilizers. Syst Appl Microbiol 14: 372-378.

84) Huber, G, Spinnler C, Gambacorta A, Stetter, KO. 1989. *Metallosphaera sedula* gen. and sp. nov. represents a new genus of aerobic, metal-mobilising, thermophilic archaebacteria. Sys Appl Microbiol 12: 38-47.

85) Huberts R. 1994. Modelling of ferrous sulphate oxidation by iron-oxidising bacteria: a chemiosmotic and electrochemical approach. Ph.D. Thesis, University of the Witwatersrand, Johannesburg, South Africa.

86) Huffman RE, Davidson N. 1956. Kinetics of the ferrous iron-oxygen reaction in sulfuric acid solution. J Am Chem Soc 78 :4836-42. (cited in Verbaan & Crundwell, 1986).

87) Hugenholtz P, Pitulle C, Hershberger KL, Pace NR. 1998. Novel division level bacterial diversity in a Yellowstone hot spring. J Bacteriol 180(2): 366-76.

88) Hugler M, Krieger RS, Jahn M, Fuchs G. 2003. Characterization of acetyl-CoA/propionyl-CoA carboxylase in *Metallosphaera sedula*. Carboxylating enzyme in the 3-hydroxypropionate cycle for autotrophic carbon fixation. Eur J Biochem 270(4): 736-744.

89) Imai K, Sugio T, Tsuchida T, Tano T. 1975. Effect of heavy metal ions on the growth and iron-oxidizing activity of Thiobacillus ferrooxidans. Agric Biol Chem 39(7): 1349-54.

90) Ingledew WJ. 1982. *Thiobacillus ferrooxidans*. The bioenergetics of an acidophilic chemolithotroph. Biochim Biophys Acta 683(2): 89-117.

91) Ingledew WJ. 1986. Ferrous iron oxidation by *Thiobacillus ferrooxidans*. Biotechnol Bioeng Symp 16 (Biotechnol. Min. Met.-Refin. Fossil Fuel Process. Ind.) 23-33.

92) Ishii M, Miyake T, Satoh T, Sugiyama H, Oshima Y, Kodama T, Igarashi Y. 1996. Autotrophic carbon dioxide fixation in *Acidianus brierleyi*. Arch Microbiol 166(6): 368-71.

93) Itoh T. 2003. Taxonomy of nonmethanogenic hyperthermophilic and related thermophilic Archaea. J Biosci Bioeng 96(3): 203-212.

94) Iwai M, Majima H, Awakura Y. 1982. Oxidation of iron(II) in sulfuric acid solutions with dissolved molecular oxygen. Metall Trans B 13B(3): 311-18. (cited in Verbaan & Crundwell, 1986)

95) Jan R-L, Wu J, Chaw S-M, Tsai C-W, Tsen S-D. 1999. A novel species of thermoacidophilic archaeon, *Sulfolobus yangmingensis* sp. nov.. Int J Sys Bacteriol 49(4): 1809-1816.

96) Jensen AB, Webb C. 1995. Ferrous Sulphate Oxidation Using *Thiobacillus ferrooxidans*: a Review. Process Biochem 30(3): 225-236.

97) Johnson DB. 1998. Biodiversity and ecology of acidophilic microorganisms. FEMS Microbiol Ecol 27(4): 307-317.

98) Johnson DB. 2005. Biohydrometallurgy and the Environment: Intimate and Important Interplay. In: Proceedings of the 16th International Biohydrometallurgy Symposium IBS 2005, held 25-29th September 2005, Cape Town, South Africa.

99) Jones CA, Kelly DP. 1983. Growth of *Thiobacillus ferrooxidans* on ferrous iron in chemostat culture: influence of product and substrate inhibition. J Chem Technol Biotechnol 33B(4): 241-61.

100) Kametani H, Aoki A. 1985. Effect of suspension potential on the oxidation rate of copper concentrate in sulphuric acid solution. Metall Trans B 16B(Dec): 695-705.

101) Kandler O. 1992. Where next with the archaebacteria? Biochemical Society Symposia 58 (Archaebact: Biochem Biotechnol): 195-207.

102) Karavaiko GL, Golyshina OV, Troitsky AV, Valieho-Roman KM, Golovacheva RS, Pivovarova TA. 1994. *Sulfurococcus yellowstonii* sp. nov.-a new sulfur-oxidizing thermoacidophilic archaebacteria. Mikrobiologiya 63(4): 668-82.

103) Kawabe Y, Inoue C, Suto K, Chida T. 2003. Inhibitory effect of high concentrations of ferric ions on the activity of *Acidithiobacillus ferrooxidans*. J Biosci Bioeng 96(4): 375-379.

104) Keenan EA. 1969. Bacterial Beneficiation of Uranium Materials, Ph.D. Thesis, University of New South Wales. cited in Verbaan & Crundwell, 1986; Chmielewski & Charewicz, 1984; and Lacey & Lawson, 1970.

105) Kelly DP, Wood AP. 2000. Reclassification of some species of *Thiobacillus* to the newly designated genera *Acidithiobacillus* gen. nov., *Halothiobacillus* gen. nov. and *Thermithiobacillus* gen. nov.. Int J Sys Evol Microbiol 50(2): 511-6.

106) Kelly DP, Jones CA. 1978. Factors affecting metabolism and ferrous iron oxidation in suspensions and batch cultures of *Thiobacillus ferrooxidans*: relevance to ferric iron leach solution regeneration. In: Murr LE, Torma AE, Brierley JA. (eds.) Metallurgical Applications of Bacterial Leaching and Related Microbiological Phenomena. Academic Press Inc., New York 19-44.

107) Kinnunen PH-M, Robertson WJ, Plumb JJ, Gibson JAE, Nichols PD, Franzmann PD, Puhakka JA. 2003. The isolation and use of iron-oxidizing, moderately thermophilic acidophiles from the Collie coal mine for the generation of ferric iron leaching solution. Appl Microbiol Biotechnol 60(6): 748-53.

108) Kirby CS, Thomas HM, Southam G, Donald R. 1999. Relative contributions of abiotic and biological factors in Fe(II) oxidation in mine drainage. Applied Geochemistry 14(4): 511-530.

109) Koffler H, Johnson FH, Wilson PW. 1947. Combined influence of temperature and urethan on the respiration of *Rhizobium*. J Am Chem Soc 69: 1113-17.

110) König H. 1988. Archaeobacterial cell envelopes. Can J Microbiol 34: 395-406.

111) Konishi Y, Yoshida S, Asai S. 1995. Bioleaching of pyrite by acidophilic thermophile *Acidianus brierleyi*. Biotechnol Bioeng 48(6): 592-600.

112) Kovarova-Kovar K, Egli T. 1998. Growth kinetics of suspended microbial cells: from single-substrate-controlled growth to mixed-substrate kinetics. Microbiol Mol Biol Rev 62(3): 646-66

113) Kuenen JG. 1979. Growth yields and "maintenance energy requirement" in *Thiobacillus* species under energy limitation. Arch Microbiol 122(2): 183-8.

114) Kurosawa N, Itoh YH, Itoh T. 2003. Reclassification of *Sulfolobus hakonensis* Takayanagi *et al.* 1996 as *Metallosphaera hakonensis* comb. nov. based on phylogenetic evidence and DNA G+C content. Int. J. Syst. Evol. Microbiol 53: 1607-1608.

115) Lacey DT, Lawson F. 1970. Kinetics of the Liquid-Phase Oxidation of Acid Ferrous Sulfate by the Bacterium *Thiobacillus ferrooxidans*. Biotechnol Bioeng 12: 29-50.

116) Lazaroff N, Sigal W, Wasserman A. 1982. Iron oxidation and precipitation of ferric hydroxysulfates by resting *Thiobacillus ferrooxidans* cells. Appl Environ Microbiol 43(4): 924-38.

117) Le Roux NW, Wakerley DS. 1988. Leaching of chalcopyrite (CuFeS2) at 70°C using *Sulfolobus*. In: Norris PR, (eds) Proceedings of Biohydrometall. Proc. Int. Symp. 1987, 305-17.

118) Leduc LG, Ferroni GD. 1994. The chemolithotropic bacterium *Thiobacillus ferrooxidans*. FEMS Microbiol Rev 14(2): 103-20.

119) Li Y, Liu G, Zhong H. 1994. A new species of *Thermoplasma*. (in Chinese). *Wei Sheng Wu Hsueh Pao* 34: 255-260

120) Liu MS, Branion RMR, Duncan DW. 1988. The effects of ferrous iron, dissolved oxygen, and inert solids concentrations on the growth of *Thiobacillus ferrooxidans*. Can J Chem Eng 66(3): 445-51.

121) Liu Y. 1998. Energy uncoupling in microbial growth under substrate-sufficient conditions. Appl Microbiol Biotechnol 49(5): 500-505.

122) Lizama HM, Suzuki I. 1989. Synergistic competitive inhibition of ferrous iron oxidation by *Thiobacillus ferrooxidans* by increasing concentrations of ferric iron and cells. Appl Environ Microbiol 55(10): 2588-91.

123) Lundgren DG, Andersen KJ, Remsen CC, Mahoney RP. 1964. Culture, structure, and physiology of the chemoautotroph *Ferrobacillus ferrooxidans*. Dev Ind Microbiol 6: 250-259.

124) Macalady JL, Vestling MM, Baumler D, Boekelheide N, Kaspar CW, Banfield JF. 2004. Tetraether-linked membrane monolayers in *Ferroplasma* spp: A key to survival in acid. Extremophiles 8(5): 411-419.

125) MacDonald DG, Clark RH. 1970. The oxidation of aqueous ferrous sulphate by *Thiobacillus ferrooxidans*. Can J Chem Eng 482: 669-676.

126) Mandl M. 1984. Growth and respiration kinetics of *Thiobacillus ferrooxidans* limited by carbon dioxide and oxygen. Biologia (Bratislava, Slovakia) 39(4): 429-34.

127) Marsh RM, Norris PR. 1983. Mineral sulfide oxidation by moderately thermophilic acidophilic bacteria. Biotechnol Lett 5(9): 585-90.

128) Mathews CT, Robins RG. 1972. Oxidation of aqueous ferrous sulfate solutions by molecular oxygen. Proc Aust Inst Min Metall 242: 47-56. (cited in Verbaan & Crundwell, 1986)

129) Menendez C, Bauer Z, Huber H, Gad'on N, Stetter KO, Fuchs G. 1999. Presence of acetyl coenzyme A (CoA) carboxylase and propionyl-CoA carboxylase in autotrophic Crenarchaeota and indication for operation of a 3-hydroxypropionate cycle in autotrophic carbon fixation. J Bacteriol 181(4): 1088-98.

130) Meruane G, Carcamo C, Vargas T. 2003. Kinetics of ferrous iron oxidation with *Sulfolobus metallicus* at 70°C. In: Proceedings of the 15th International Biohydrometallurgy Symposium (IBS 2003), held 14-19th Sept 2003, Athens, Greece.

131) Meruane G, Salhe C, Wiertz J, Vargas T. 2002. Novel electrochemical-enzymatic model which quantifies the effect of the solution Eh on the kinetics of ferrous iron oxidation with *Acidithiobacillus ferrooxidans*. Biotechnol Bioeng 80(3): 280-288.

132) Meruane G, Vargas T. 2003. Bacterial oxidation of ferrous iron by *Acidithiobacillus ferrooxidans* in the pH range 2.5-7.0. Hydrometallurgy 71(1-2): 149-158.

133) Mier JL, Ballester A, Gonzalez F, Blazquez ML, Gomez E. 1996. The influence of metallic ions on the activity of *Sulfolobus BC*. J Chem Technol Biotechnol 65(3): 272-80.

134) Miller JD, Portillo HD. 1981. Silver catalysis in ferric sulphate leaching of chalcopyrite. In: Lawskoski J. (ed) *XIII Mineral Processing Congress Proceedings. Part A*, Elsevier, Amsterdam, 851-899.

135) Miller KW, Risanico SS, Risatti JB. 1992. Differential tolerance of *Sulfolobus* strains to transition metals. FEMS Microbiol Lett 93(1): 69-73.

136) Mitchell P. 1966. Chemiosmotic coupling in oxidative and photosynthetic phosphorylation. Biol Rev Cambridge Phil Soc 41(3): 445-502.

137) Moll R, Schaefer G. 1988. Chemiosmotic proton cycling across the plasma membrane of the thermoacidophilic archaebacterium *Sulfolobus acidocaldarius*. FEBS Lett 232(2): 359-63.

138) Monod J. 1949. The growth of bacterial cultures. Ann Rev Microbiol 3: 371-94.

139) Moon JA. 1995. The quantification of biomass in a biooxidation system. MSc. Dissertation, University of Cape Town, South Africa.

140) Morin D, d'Hugues P, Mugabi, M. 2003. Bioleaching of metallic sulphide concentrate in continuous stirred reactors at industrial scale – Experience and lessons. In: Proceedings of the 15th International Biohydrometallurgy Symposium (IBS 2003) held 14-19th September 2003, Athens, Greece.

141) Nagpal S. 1997. A structured model for *Thiobacillus ferrooxidans* growth on ferrous iron. Biotechnol Bioeng 53(3): 310-319.

142) Neijssel OM, Tempest DW. 1976. Bioenergetic aspects of aerobic growth of *Klebsiella aerogenes* NCTC 418 in carbon-limited and carbon-sufficient chemostat culture. Arch Microbiol 107(2): 215-21.

143) Nemati M, Harrison STL, Hansford GS, Webb C. 1998. Biological oxidation of ferrous sulphate by *Thiobacillus ferrooxidans*. Biochem Eng J 1: 171-190.

144) Nemati M, Harrison STL. 2000. A comparative study on thermophilic and mesophilic biooxidation of ferrous iron. Min Eng 13(1): 19-24.

145) Nemati M, Webb C. 1997. A kinetic model for biological oxidation of ferrous iron by *Thiobacillus ferrooxidans*. Biotechnol Bioeng 53(5): 478-486.

146) Nemati M, Webb C. 1998. Inhibition effect of ferric iron on the kinetics of ferrous iron biooxidation. Biotechnol Lett 20(9): 873-877.

147) Nichols PD, Franzmann PD. 1992. Unsaturated diether phospholipids in the Antarctic methanogen *Methanococcoides burtonii*. FEMS Microbiol Lett 98(1-3): 205-8.

148) Nikolov LN, Karamanev DG. 1992. Kinetics of the ferrous iron oxidation by resuspended cells of *Thiobacillus ferrooxidans*. Biotechnol Prog 8(3): 252-5.

149) Norris PR, Barr DW. 1985. Growth and iron oxidation by acidophilic moderate thermophiles. FEMS Microbiol Lett 28(3): 221-4.

150) Norris PR, Ballester A, Gonzalez F, Blazquez ML, Mier JL. 1990. Bioleaching of chalcopyrite by thermophilic organisms. 7th Congr Nac Cienc Tecnol Metal 1: 407-16.

151) Norris PR, Barr DW, Hinson D. 1988. Iron and mineral oxidation by acidophilic bacteria: affinities for iron and attachment to pyrite. Biohydrometall Proc Int Symp 1987 43-59.

152) Norris PR, Burton NP, Foulis NAM. 2000. Acidophiles in bioreactor mineral processing. Extremophiles 4(2): 71-76

153) Norris PR, Clark DA, Owen JP, Waterhouse S. 1996. Characteristics of *Sulfobacillus acidophilus* sp. nov. and other moderately thermophilic mineral-sulfide-oxidizing bacteria. Microbiology (Reading, United Kingdom) 142(4): 775-83.

154) Norris PR, Owen JP. 1993. Mineral sulfide oxidation by enrichment cultures of novel thermoacidophilic bacteria. FEMS Microbiol Rev 11(1-3): 51-6.

155) Norris PR, Parrott L, Marsh RM. 1986. Moderately thermophilic mineral-oxidizing bacteria. Biotechnol Bioeng Symp 16(Biotechnol. Min. Met.-Refin. Fossil Fuel Process. Ind.): 253-62.

156) Norris PR. 1992. Thermoacidophilic archaebacteria: potential applications. In: Biochemical Society Symposia 1991 58(Archaebact.: Biochem. Biotechnol.): 171-80.

157) Norris PR. 1997. Thermophiles and bioleaching. In: Rawlings DE. (ed) Biomining: Theory, Micro-organisms and Industrial Processes. Springer-Verlag, Berlin 247-258.

158) Norris PR, Johnson DB. 1998. Acidophilic Microorganisms. In: Horikoshi K, Grant WD (eds.) Extremophiles (Microbial Life in Extreme Environments). Wiley. 133-153.

159) Nyavor K, Egiebor NO, Fedorak PM. 1996. The effect of ferric iron on the rate of ferrous oxidation by *Thiobacillus ferrooxidans*. Appl Microbiol Biotechnol 45: 688-691.

160) Okereke A, Stevens SE Jr. 1991. Kinetics of iron oxidation by *Thiobacillus ferrooxidans*. Appl Environ Microbiol 57(4): 1052-1056.

161) Olson GJ, Brierley JA, Brierley CL. 2003. Bioleaching review part B: Progress in bioleaching: applications of microbial processes by the minerals industries. Appl Microbiol Biotechnol 63(3): 249-257.

162) Peeples TL, Kelly RM. 1995. Bioenergetic response of the extreme thermoacidophile *Metallosphaera sedula* to thermal and nutritional stresses. Appl Environ Microbiol 61(6): 2314-21.

163) Pesic B, Oliver DJ, Wichlacz P. 1989. An electrochemical method of measuring the oxidation rate of ferrous to ferric iron with oxygen in the presence of *Thiobacillus ferrooxidans*. Biotechnol Bioeng 33(4): 428-39.

164) Pirt SJ. 1965. The maintenance energy of bacteria in growing cultures. Proc R Soc London Series B 163(991): 224-31.

165) Pirt SJ. 1975. Principles of Microbe and Cell Cultivation. Blackwell Scientific Publications, London.

166) Pirt SJ. 1982. Maintenance energy: a general model for energy-limited and energy-sufficient growth. Arch Microbiol 133(4): 300-2.

167) Plumb JJ, Gibbs B, Stott MB, Robertson WJ, Gibson JAE, Nichols PD, Watling HR, Franzmann PD. 2002. Enrichment and characterization of thermophilic acidophiles for the bioleaching of mineral sulphides. Miner Eng 15(11): 787-794.

168) Raja SB. 2005. The effect of particulate-induced hydrodynamic stress on the bioleaching of chalcopyrite by a *Sulfolobus*-like culture. Ph.D. Thesis, University of Cape Town, South Africa.

169) Ratkowsky DA, Lowry RK, McMeekin TA, Stokes AN, Chandler RE. 1983. Model for bacterial culture growth rate throughout the entire biokinetic temperature range. J Bacteriol 154(3): 1222-1226.

170) Ratkowsky DA, Olley J, McMeekin TA, Ball A. 1982. Relationship between temperature and growth rate of bacterial cultures. J Bacteriol 149(1): 1-5.

171) Ratkowsky DA, Olley J, Ross T. 2005. Unifying temperature effects on the growth rate of bacteria and the stability of globular proteins. J Theor Biol 233(3): 351-362.

172) Rawlings DE, Coram NJ, Gardner MN, Deane SM. 1999. *Thiobacillus caldus* and *Leptospirillum ferrooxidans* are widely distributed in continuous flow biooxidation tanks used to treat a variety of metal containing ores and concentrates. Process Metall 9A(Biohydrometallurgy and the Environment Toward the Mining of the 21st Century, Pt. A) 777-786.

173) Rawlings DE, Dew D, du Plessis C. 2003. Biomineralization of metal-containing ores and concentrates. Trends Biotechnol 21(1): 38-44.

174) Rawlings DE, Tributsch H, Hansford GS. 1999. Reasons why "*Leptospirillum*"-like species rather than *Thiobacillus ferrooxidans* are the dominant iron-oxidizing bacteria in many commercial processes for the biooxidation of pyrite and related ores. Microbiology (Reading, United Kingdom) 145(1): 5-13.

175) Rawlings DE. 2002. Heavy metal mining using micro-organisms. Ann Rev Microbiol 56: 65-91.

176) Rawlings DE. 2005. Characteristics and adaptability of iron- and sulfur-oxidizing microorganisms used for the recovery of metals from minerals and their concentrates. Microb Cell Factories 4 No pp. given.

177) Rawlings, DE. (ed) 1997. Biomining: Theory, Micro-organisms and Industrial Processes. Springer-Verlag, Berlin.

178) Roels JA. 1983. Energetics and kinetics in biotechnology. Elsevier Biomedical Press, Amsterdam, 20-31.

179) Rohwerder T, Gehrke T, Kinzler K, Sand W. 2003. Bioleaching review part A. Progress in bioleaching: Fundamentals and mechanisms of bacterial metal sulfide oxidation. Appl Microbiol Biotechnol 63(3): 239-248.

180) Rohwerder T, Sand W. 2003. The sulfane sulfur of persulfides is the actual substrate of the sulfur-oxidizing enzymes from *Acidithiobacillus* and *Acidiphilium* spp. Microbiology (Reading, United Kingdom) 149(7): 1699-1709.

181) Rossi G. 1990. Biohydrometallurgy. McGraw Hill Book Co., Hamburg.

182) Sand W, Gehrke T, Jozsa P-G, Schippers A. 2001. (Bio) chemistry of bacterial leaching-direct vs. indirect bioleaching. Hydrometallurgy 59(2-3): 159-175.

183) Savic DS, Veljkovic VB, Lazic ML, Vrvic MM, Vucetic JI. 1998. Effects of the oxygen transfer rate on ferrous iron oxidation by *Thiobacillus ferrooxidans*. Enzyme Microb Technol 23(7/8): 427-431.

184) Schippers A, Sand W. 1999. Bacterial leaching of metal sulfides proceeds by two indirect mechanisms via thiosulfate or via polysulfides and sulfur. Appl Environ Microbiol 65(1): 319-321.

185) Schoolfield RM, Sharpe PJH, Magnuson CE. 1981. Nonlinear regression of biological temperature-dependent rate models based on absolute reaction-rate theory. J Theor Biol 88(4): 719-31.

186) Searby GE, Hansford GS. 2003. The kinetics of thermophilic ferrous-iron oxidation. In: Proc Int Biohydrometall Symp, IBS 2003, September 2003, Athens, Greece.

187) Segerer A, Neuner AM, Kristjansson JK, Stetter KO. 1986. *Acidianus infernus* gen. nov., sp. nov., and *Acidianus brierleyi* comb. nov.: facultatively aerobic, extremely acidophilic thermophilic sulfur-metabolizing archaebacteria. Int J Syst Bacteriol 36: 559-564.

188) Shrihari, Kumar R, Gandhi KS. 1990. Modelling of Fe^{2+} Oxidation by *Thiobacillus ferrooxidans*. Appl Environ Microbiol 33: 524-528.

189) Silverman MP, Lundgren DG. 1959. The chemoautotrophic iron bacterium *Ferrobacillus ferrooxidans*. II. Manometric studies. J Bacteriol 78: 326-31.

190) Sinclair CG, Topiwala HH. 1970. Model for continuous culture which considers the viability concept. Biotechnol Bioeng 12(6): 1069-1079.

191) Smith JR, Luthy RG, Middleton AC. 1988. Microbial ferrous iron oxidation in acidic solution. J WPCF 60(4): 518-530.

192) Smith LH, Mccarty PL, Kitanidis PK. 1998. Spreadsheet method for evaluation of biochemical reaction rate coefficients and their uncertainties by weighted nonlinear least-squares analysis of the integrated Monod equation. Appl Environ Microbiol 64(6): 2044-2050.

193) Steudel R. 1996. Mechanism for the formation of elemental sulfur from aqueous sulfide in chemical and microbiological desulfurization processes. Ind Eng Chem Res 35(4): 1417-23.

194) Stott MB, Watling HR, Franzmann PD, Sutton D. 2000. The role of iron-hydroxy precipitates in the passivation of chalcopyrite during bioleaching. Miner Eng 13(10-11): 1117-1127.

195) Suzuki I, Lizama HM, Tackaberry PD. 1989. Competitive inhibition of ferrous iron oxidation by *Thiobacillus ferrooxidans* by increasing concentrations of cells. Appl Environ Microbiol 55(5): 1117-21.

196) Tempest DW. 1978. The biochemical significance of microbial growth yields: a reassessment. Trends Biochem Sci 3(8): 180-4.

197) Temple KL, Colmer AR. 1951. The autotrophic oxidation of iron by a new bacterium, *Thiobacillus ferrooxidans*. J Bacteriol 62(5): 605-11.

198) Tijhuis L, van Loosdrecht MCM, Heijnen JJ. 1993. A thermodynamically based correlation for maintenance Gibbs energy requirements in aerobic and anaerobic chemotrophic growth. Biotechnol Bioeng 42(4): 509-19.

199) Topiwala H, Sinclair CG. 1971. Temperature relationship in continuous culture. Biotechnol Bioeng 13(6): 795-813.

200) Toro L, Paponetti B, Cantalini C. 1988. Precipitate formation in the oxidation of ferrous ions in the presence of *Thiobacillus ferrooxidans*. Hydrometallurgy 20(1): 1-9.

201) Tributsch H. 2001. Direct versus indirect bioleaching. Hydrometallurgy 59(2-3): 177-185.

202) Tuovinen OH, Kelly DP. 1973. Studies on the growth of *Thiobacillus ferrooxidans*. I. Use of membrane filters and ferrous iron agar to determine viable numbers, and comparison with $^{14}CO_2$- fixation and iron oxidation as measures of growth. Arch. Mikrobiol. 88: 285-298

203) Tuovinen OH, Niemela SI, Gyllenberg HG. 1971. Tolerance of *Thiobacillus ferrooxidans* to some metals. Antonie van Leeuwenhoek 37(4): 489-96.

204) van de Vossenberg JLCM, Driessen AJM, Konings WN. 1998. The essence of being extremophilic: the role of the unique archaeal membrane lipids. Extremophiles 2(3): 163-170.

205) van Scherpenzeel DA, Boon M, Ras C, Hansford GS, Heijnen JJ. 1998. Kinetics of ferrous iron oxidation by *Leptospirillum* bacteria in continuous cultures. Biotechnol Prog 14(3): 425-433.

206) Verbaan B, Crundwell FK. 1986. An electrochemical model for the leaching of a sphalerite concentrate. Hydrometallurgy 16(3): 345-59.

207) Vogel AI. 1989. Vogel's Textbook of Quantitative Chemical Analysis. 5th ed. (eds.) GH Jeffrey, J Bassett, J Mendham, and RC Denney. Longman Scientific and Technical, Essex, England

208) Vogelaar JCT, Klapwijk A, Van Lier JB, Rulkens WH. 2000 Temperature effects on the oxygen transfer rate between 20 and 55□°C. Water Res 34(3): 1037-1041.

209) Wood AP, Kelly DP. 1983. Autotrophic and mixotrophic growth of three thermoacidophilic iron-oxidizing bacteria. FEMS Microbiol Lett 20(1): 107-12.

210) Yarzabal A, Brasseur G, Bonnefoy V. 2002b. Cytochromes c of *Acidithiobacillus ferrooxidans*. FEMS Microbiol Lett 209(2): 189-95.

211) Yarzabal A, Brasseur G, Ratouchniak J, Lund K, Lemesle-Meunier D, DeMoss JA, Bonnefoy V. 2002a. The high-molecular-weight cytochrome c Cyc2 of *Acidithiobacillus ferrooxidans* is an outer membrane protein. J Bacteriol 184(1): 313-317.

212) Zillig W, Stetter KO, Wunderl S, Schulz W, Priess H, Scholz I. 1980. The *Sulfolobus*-"*Caldariella*" group: taxonomy on the basis of the structure of DNA-dependent RNA polymerases. Arch Mikrobiol 125: 259-269.

213) Zwietering MH, de Koos JT, Hasenack BE, de Witt JC, van't Riet K. 1991. Modeling of bacterial growth as a function of temperature. Appl Environ Microbiol 57(4): 1094-1101.

214)

215) Web pages and electronic resources:

216) http://www.thecdi.com/cdi/images/news_pdf/Cobalt_News_April_06.pdf

217) http://www.engineeringnews.co.za/eng/features/environment/?show=13436

218) ScanIt 1.0: www.amsterchem.com/?scanit/

Appendix A

Iron Concentrations

A.1 Methods for the Determination of Iron concentrations by Titration

Filter sample prior to titration if solids and/or precipitates present. Titrations are usually performed on 5 mL aliquots. 10 mL aliquots may be used for greater accuracy at lower concentrations (< 1.0g.L^{-1}).

A.1.1 Reagents

Cerium (IV) Sulfate (Usually 0.05M)

- Although the cerium (IV) sulfate solutions purchased are standardised using sodium oxalate, the concentrations of the solutions may vary significantly and they need to be standardised again.

1,10-phenanthroline ferrous complex solution (Feroin Indicator)

Spekker acid

- Measure out 1200 ml distilled water in a 5l beaker and agitate.
- Slowly and carefully add 450 ml concentrated (98%) sulphuric acid and then 450 ml concentrated (85%) phosphoric acid.
- Allow to cool before transferring to storage bottle

CAUTION! The heat of mixing may cause localised boiling if the acid (particularly the concentrated sulfuric acid) is added too fast.

Potassium Dichromate ($K_2Cr_2O_7$) Solution (0.0149M)

- Dry 10g of $K_2Cr_2O_7$ (MW = 294.20 g.mol^{-1})in an oven at 105 – 110 °C for 1-2 hours. Cool in a dessicator.

- Weigh out accurately 8.780g of the dried $K_2Cr_2O_7$ in a 100mL beaker.
- Transfer quantitatively into a 2 L beaker using distilled water
- Add 1.5 L of distilled water and agitate till the salt has completely dissolved.
- Transfer quantitatively into a 2 L volumetric flask. Make up volume with distilled water and mix thoroughly. Makes solution with concentration = 0.01492M

Ferric acid

- Measure out 1200 mL distilled water in a 5 L beaker and agitate.
- Slowly and carefully add 300 mL Spekker acid solution and then 600 mL concentrated (32%) hydrochloric acid.
- Allow to cool before transferring to storage bottle

Stannous Chloride ($SnCl_2$) Solution

- Weigh out 30g stannous chloride in a 200 mL beaker
- Add 100 mL conc HCl and agitate at 50 °C until completely dissolved.
- Cool and transfer to storage vessel dilute with 200mL distilled water
- add a small amount of granular tin to retard precipitation

Mercuric Chloride ($HgCl_2$) Solution (saturated)

- Weigh out 50g mercuric chloride in a 1 L beaker
- Add 1 L of distilled water and agitate for 2 hours
- If all the $HgCl_2$ has dissolved, add a spatula tip more and stir for a further 2 hours

Barium Diphenylamine Sulphonate $C_{24}H_{20}BaN_2O_6S_2$ Indicator

- Weigh out 1.0g barium diphenylamine sulphonate in a 250 mL beaker
- Add 100 mL of concentrated (98%) sulphuric acid and agitate until the salt has completely dissolved

A.1.2 Determination of ferrous-iron concentration by titration versus cerium (IV) sulfate

- Pipette the required aliquot of solution into a 50ml - 100ml conical flask. (5ml is usually used)
- Add 10ml spekker acid solution and 1-2 drops of ferroin indicator solution.
- Titrate with the cerium (IV) sulfate solution until the first colour change from orange/red to blue is obtained.

Iron concentration can be calculated from

$$[Fe^{2+}] = \frac{[CeSO_4] \times V_T \times 55.84}{V_{sol}} \qquad [A.1]$$

Where: $[Fe^{2+}]$ = Ferrous-iron concentration ($g.L^{-1}$)
C_{Ce} = Ce (IV) sulfate solution concentration (M)
V_T = Titre (mL)
V_{sol} = Sample aliquot (mL)

A.1.3 Determination of ferrous-iron concentration by titration versus potassium dichromate

- Pipette the required aliquot of solution into a 50mL - 100mL conical flask. (5mL is usually used)
- Add 4-8 drops of barium diphenyl sulphonate indicator solution.
- Titrate with the potassium dichromate solution until the first colour change from yellow/green to intense purple is obtained.
- The ferrous iron concentration can be calculated from

$$[Fe^{2+}] = \frac{[K_2Cr_2O_7] \times V_T \times 55.84 \times 6}{V_{sol}} \qquad [A.2]$$

Where: $[Fe_T]$ = Total iron concentration ($g.L^{-1}$)
$[K_2Cr_2O_7]$= potassium dichromate concentration (M)
V_T = Titre (mL)
V_{sol} = Sample aliquot (mL)

A.1.4 Determination of the total iron concentration by titration versus potassium dichromate

- Pipette the required aliquot of solution into a 50mL - 100mL conical flask. (5mL is usually used)
- Add 30 mL of ferric acid solution and heat to boiling point
- Add stannous chloride dropwise until yellow colour completely disappears. Add one extra drop and record amount of stannous chloride used
- Allow the solution to cool to room temperature and add 10mL mercuric chloride solution. A silky white precipitate should form. If no precipitate forms then insufficient stannous chloride has been added earlier, if the precipitate is heavy and grey/black, then too much stannous chloride has been added, in either case, abort the titration and repeat.
- Add 4-8 drops of barium diphenyl sulphonate indicator solution.
- Titrate with the potassium dichromate solution until the first colour change from yellow/green to intense purple is obtained.
- The total iron concentration can be calculated from

$$[Fe_T] = \frac{[K_2Cr_2O_7] \times V_{\bar{}} \times 55.84 \times 6}{V_{sol}} \qquad [A.3]$$

Where: $[Fe_T]$ – Total iron concentration ($g.L^{-1}$)
$[K_2Cr_2O_7]$= potassium dichromate concentration (M)
$V_{\bar{}}$ = Titre (mL)
V_{sol} = Sample aliquot (mL)

CAUTION! Potassium chromate and mercuric chloride are toxic, while the sulphuric, phosphoric and hydrochloric acid mixtures are corrosive. Additional care should be taken when analysing samples that may contain arsenic as this may be converted to volatile and toxic arsine gas AsH_3 during stannous chloride reduction.

A.2 Determining the ferric/ferrous iron ratio from the solution redox potential

As discussed in Section 3.6, the ferric/ferrous iron ratio is related to the solution redox potential via the Nernst Equation (Equation [3.2]). It was assumed that the ratio of the activities could be approximated by the ratio of the concentrations of the iron species.

$$E = E_0' + kT \ln\left(\frac{[Fe^{3+}]}{[Fe^{2+}]}\right) \qquad [A.4]$$

where E = measured solution redox potential (mV)
E_0' and k = calibration parameters

Problems due to voltage drops in the cabling and the data capturing system, probe idiosyncrasies and the effect of elevated temperature were avoided by generating a set of probe-specific constants for Equation A.4 using the concentrations of ferrous and the total iron measured in the course of the kinetic studies. The equation parameters were determined by minimising the sum of the squared error between the measured and the predicted ferrous iron concentration.

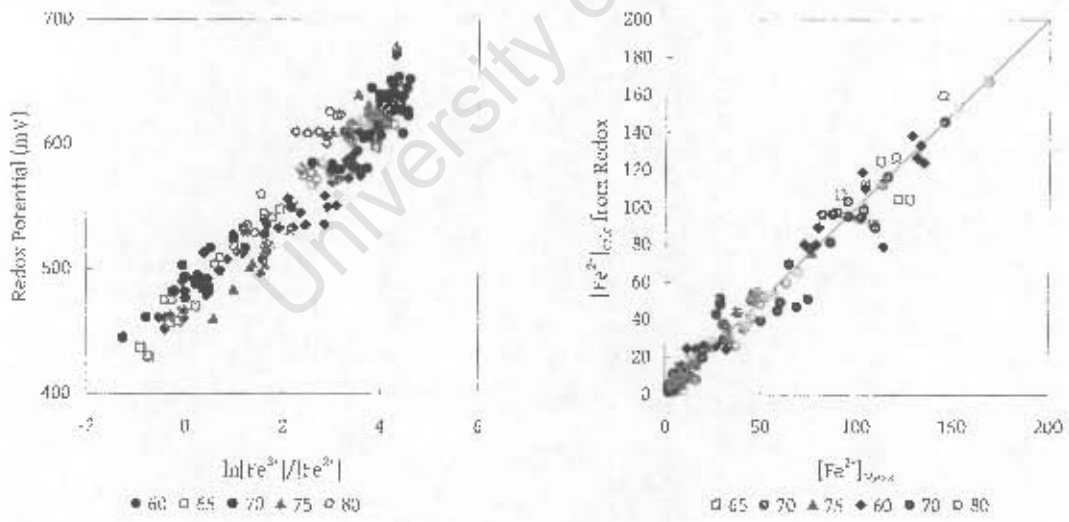

Figure A.1 Calibration curves for a Mettler-Toledo combination redox Pt|Ag/AgCl, electrode (Pt4805-SC-DPAS-K85/225) at $[Fe]_t$ = 17g.L^{-1}, T = 60 - 80°C, pH = 1.5

Table A.1 Probe-specific calibration parameters determined for the redox probes used in this investigation.

	Temperature (°C)	E_0' (mV)	k (-)	R^2
Probe 1	65	473.1	0.1204	0.97
	70	490.3	0.1092	0.99
	75	429.6	0.1484	0.98
Probe 2	60	471.0	0.0966	0.97
	70	476.2	0.1106	0.94
	80	473.1	0.1265	0.95

Appendix B

Steady State Data

B.1 Steady State Oxygen and Carbon Dioxide Utilisation Rates

As described in Section 4.6 and 6.1.1, steady state oxygen and carbon dioxide utilisation rates were determined from the mean of rates calculated from off-gas concentrations measured over an extended period of time. The measured rates are presented here for each steady state obtained.

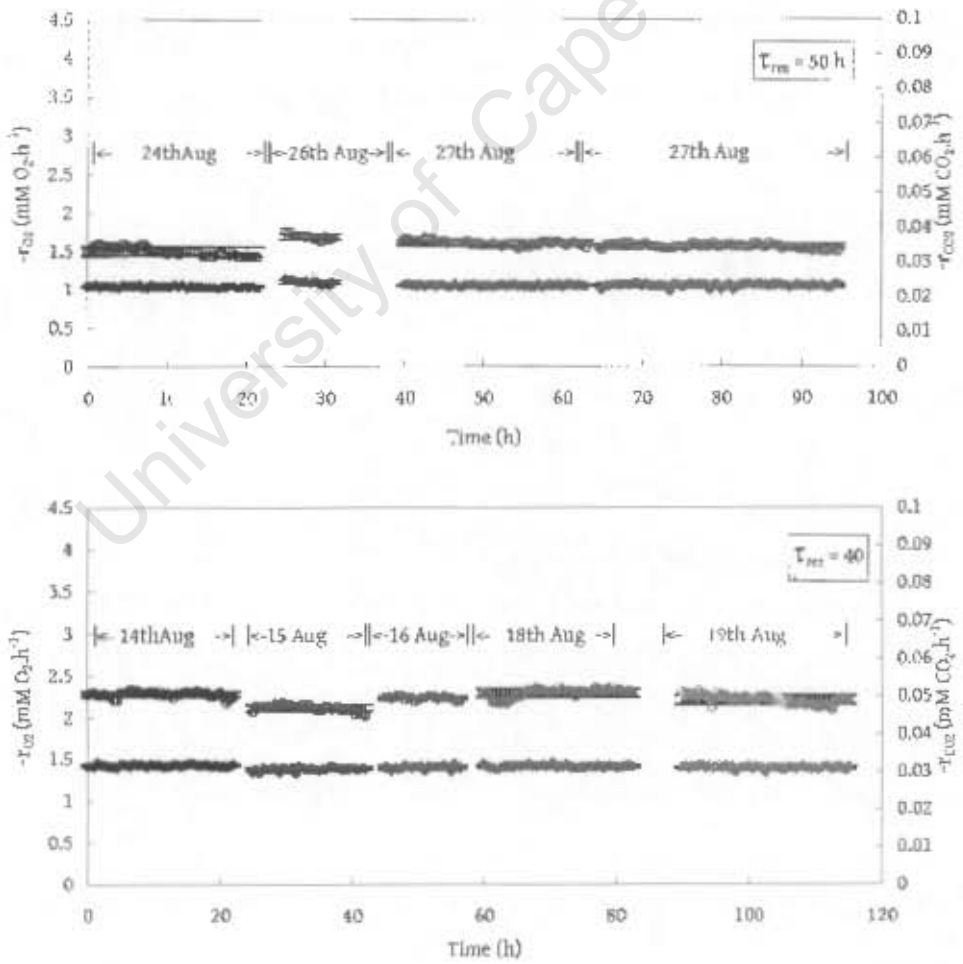

Figure B.1 Measured oxygen and carbon dioxide utilisation rate data determined for continuous iron oxidation. T = 60°C, pH = 1.5, $[Fe]_T$ = 210 mM, Run 2 (2004).

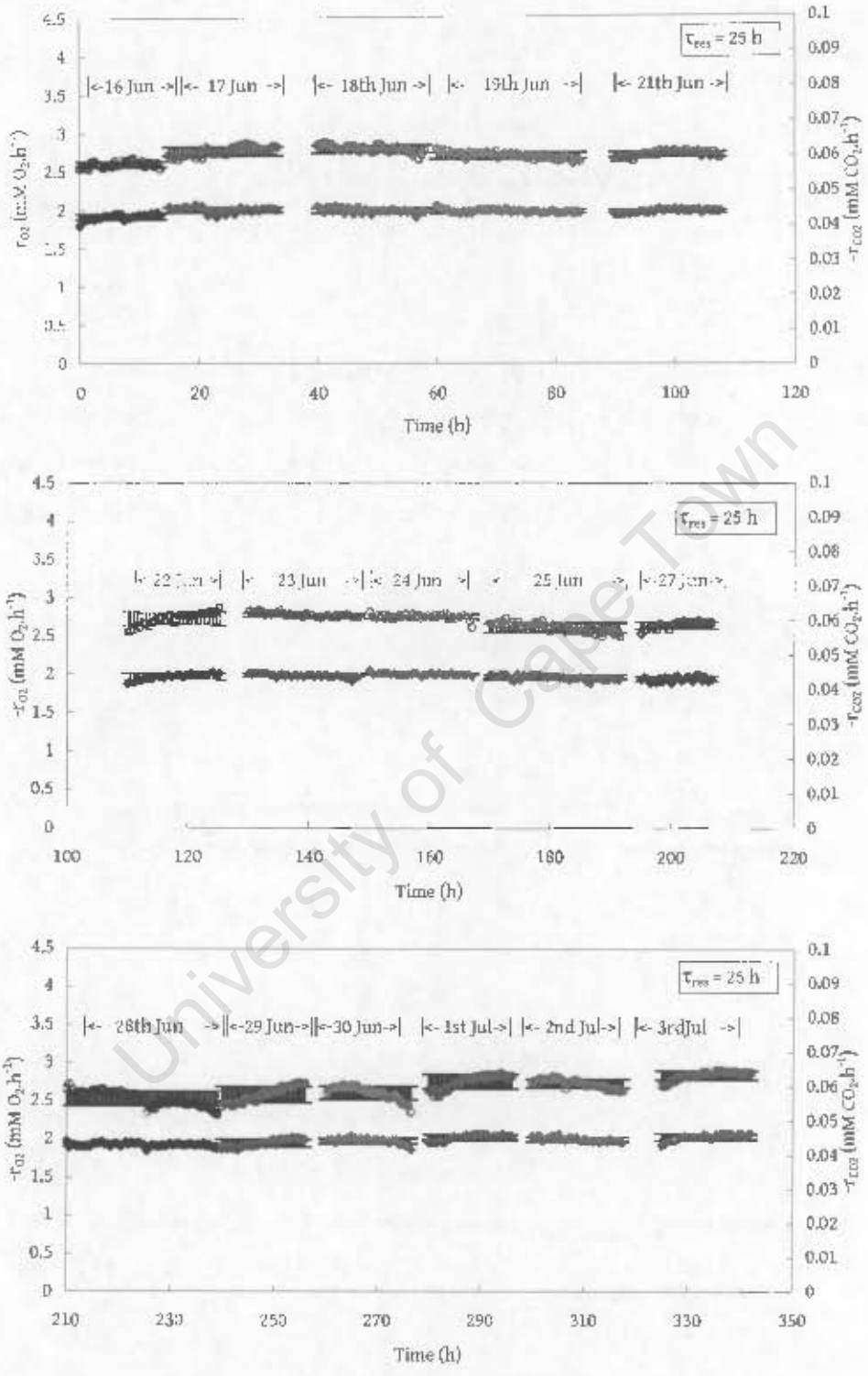

Figure B.1 **(continued)** Measured oxygen and carbon dioxide utilisation rate data determined for continuous iron oxidation. T = 60°C, pH = 1.5, $[Fe]_T$ = 210 mM, Run 2 (2004).

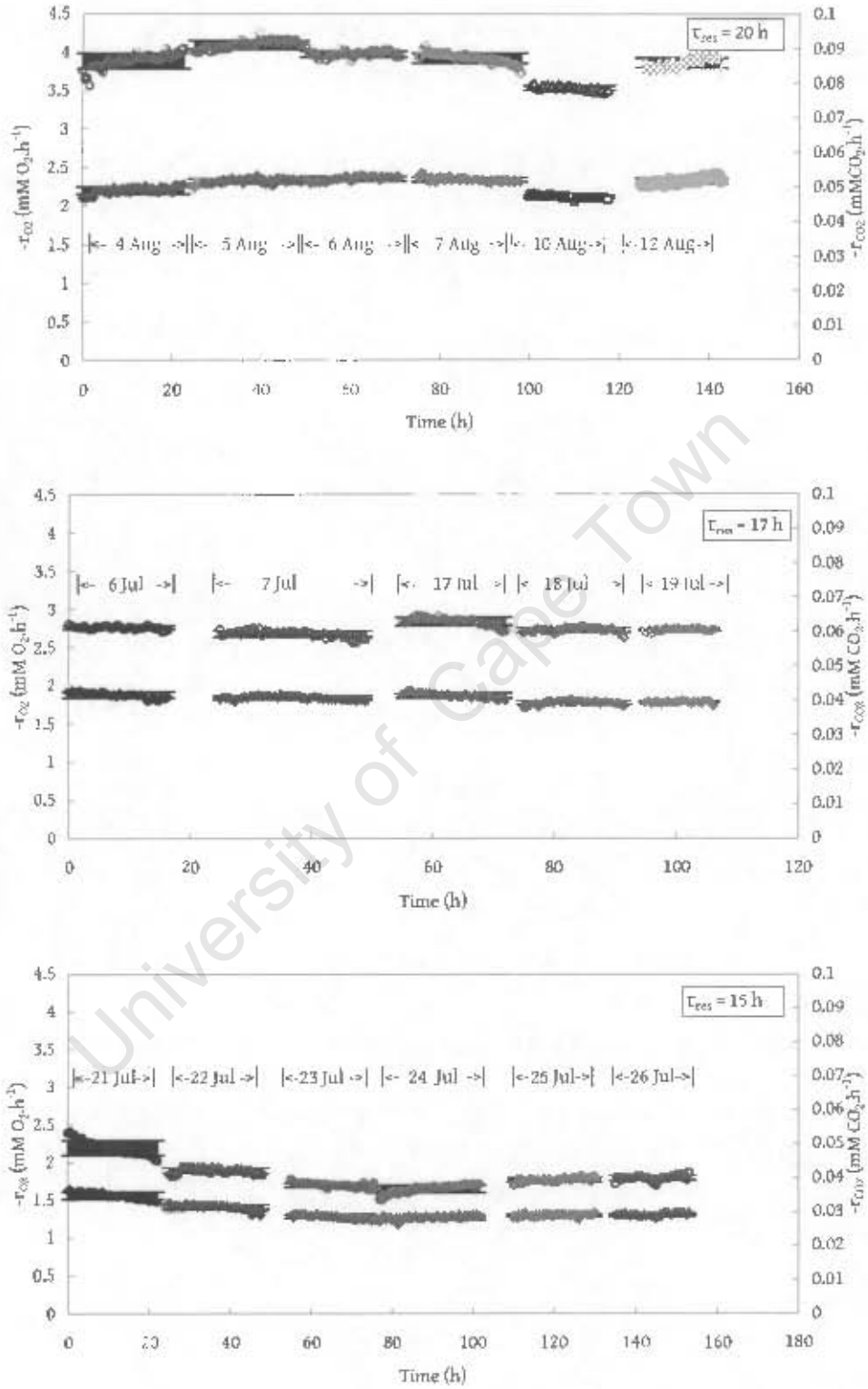

Figure B.1 **(continued)** Measured oxygen and carbon dioxide utilisation rate data determined for continuous iron oxidation. T = 60°C, pH = 1.5, $[Fe]_T$ = 210 mM, Run 2 (2004).

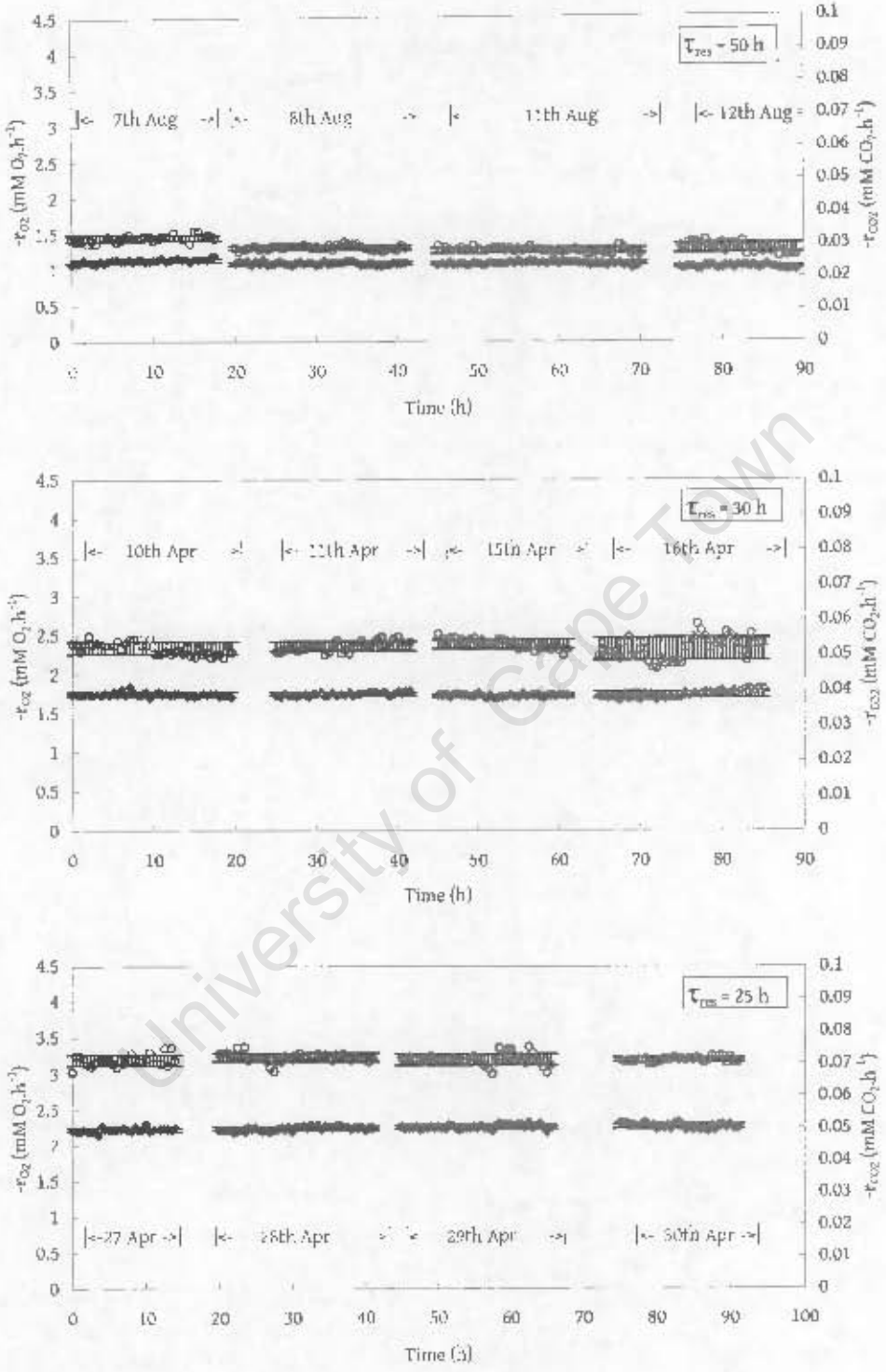

Figure B.2 Measured oxygen and carbon dioxide utilisation rate data determined for continuous iron oxidation. T = 65°C, pH = 1.5, $[Fe]_T$ = 210 mM, Run 1 (2002).

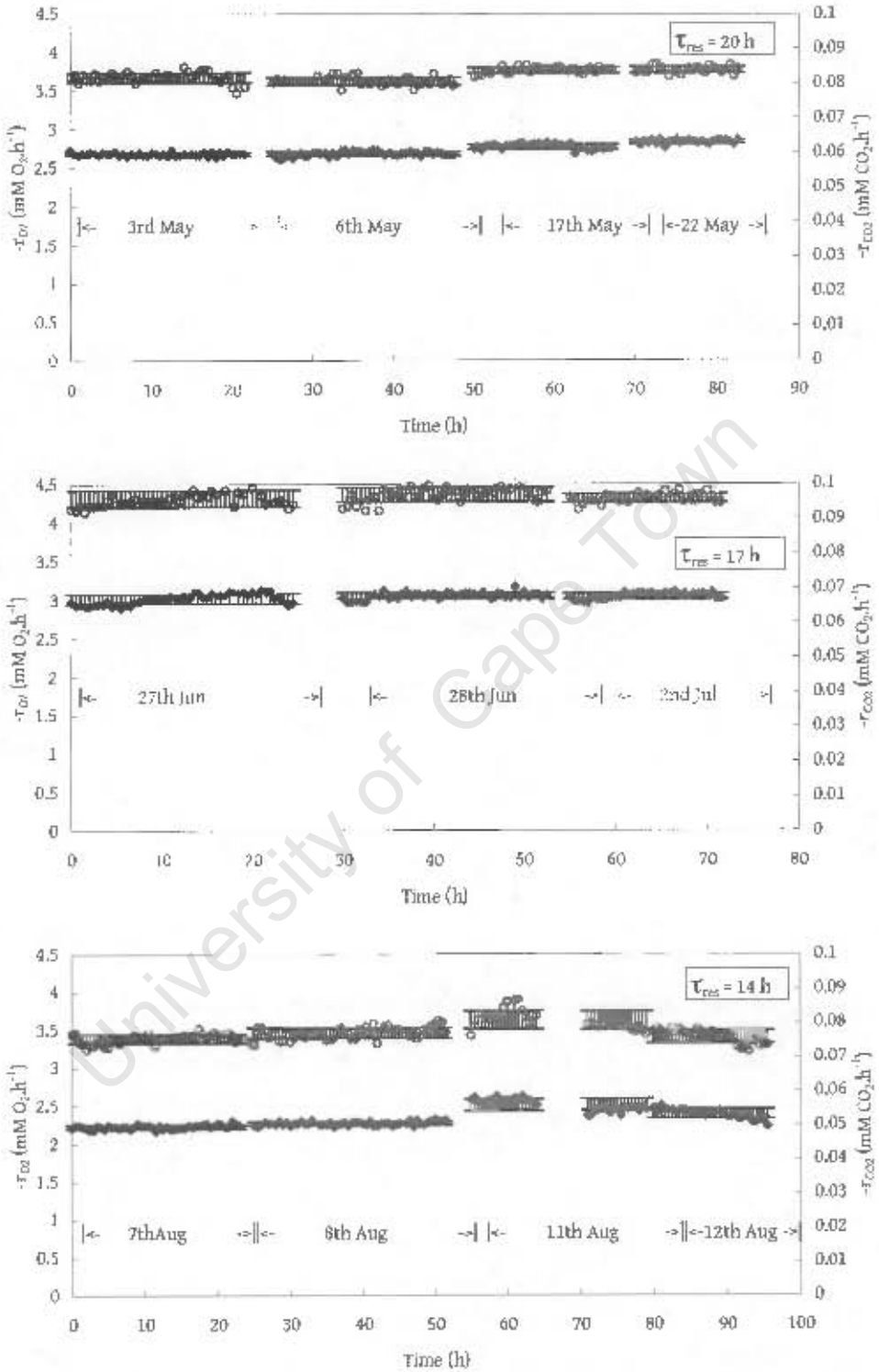

Figure B.2 **(continued)** Measured oxygen and carbon dioxide utilisation rate data determined for continuous iron oxidation. T = 65°C, pH = 1.5, $[Fe]_T$ = 210 mM, Run 1 (2002).

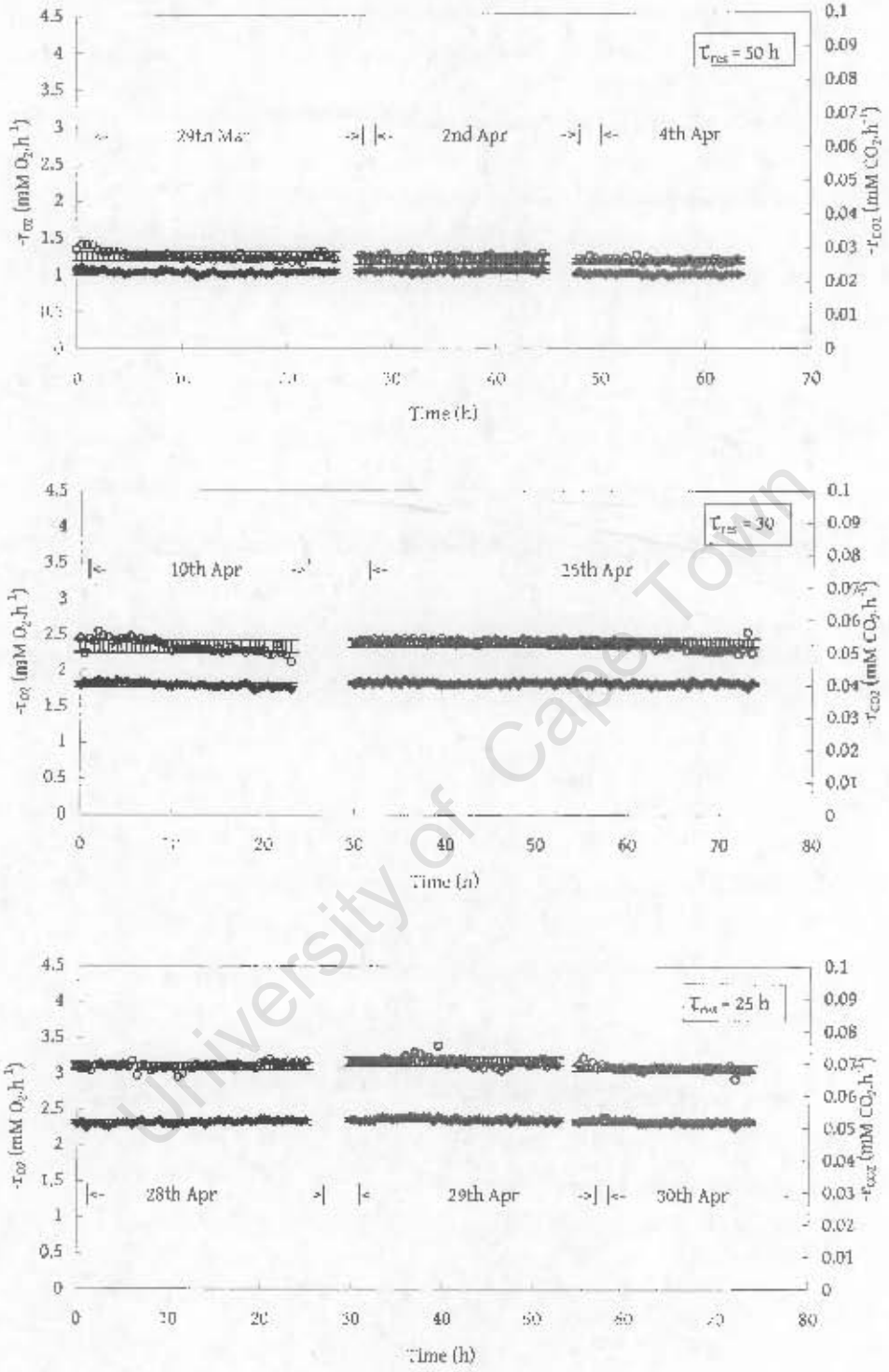

Figure B.3 Measured oxygen and carbon dioxide utilisation rate data determined for continuous iron oxidation. T = 70°C, pH = 1.5, $[Fe]_T$ = 210 mM, Run 1 (2002).

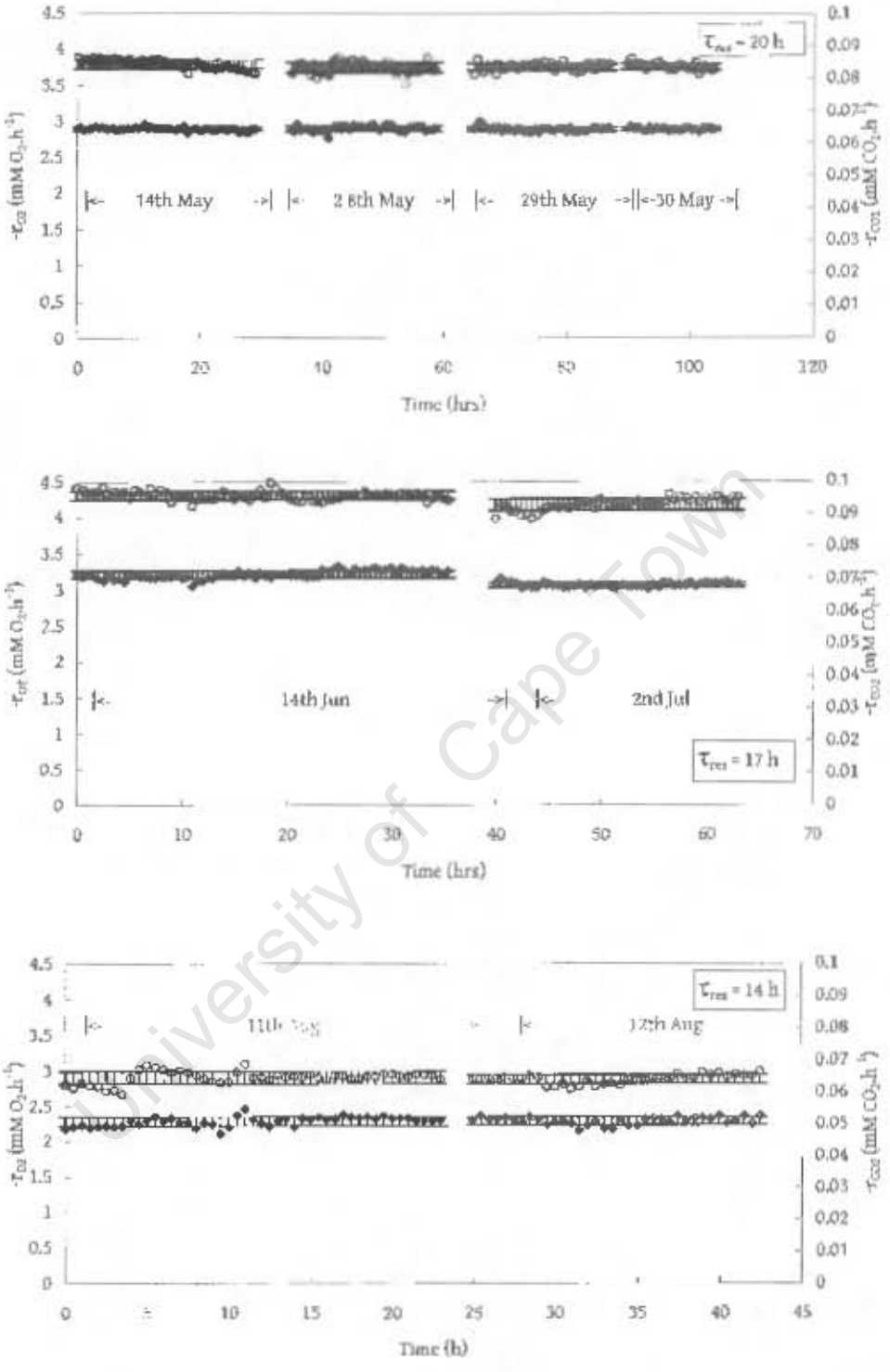

Figure B.3 **(continued)** Measured oxygen and carbon dioxide utilisation rate data determined for continuous iron oxidation, T = 70°C, pH = 1.5, $[Fe]_T$ = 210 mM, Run 1 (2002).

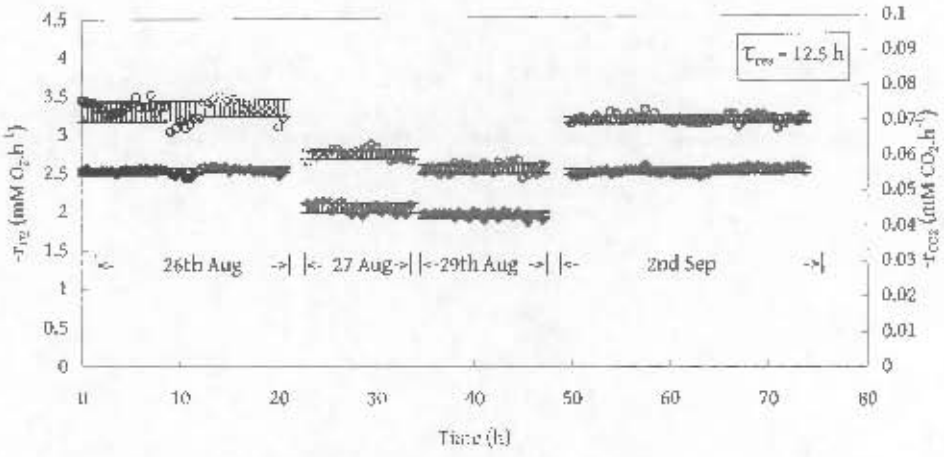

Figure B.3 **(continued)** Measured oxygen and carbon dioxide utilisation rate data determined for continuous iron oxidation. T = 70°C, pH = 1.5, $[Fe]_T$ = 210 mM, Run 1 (2002).

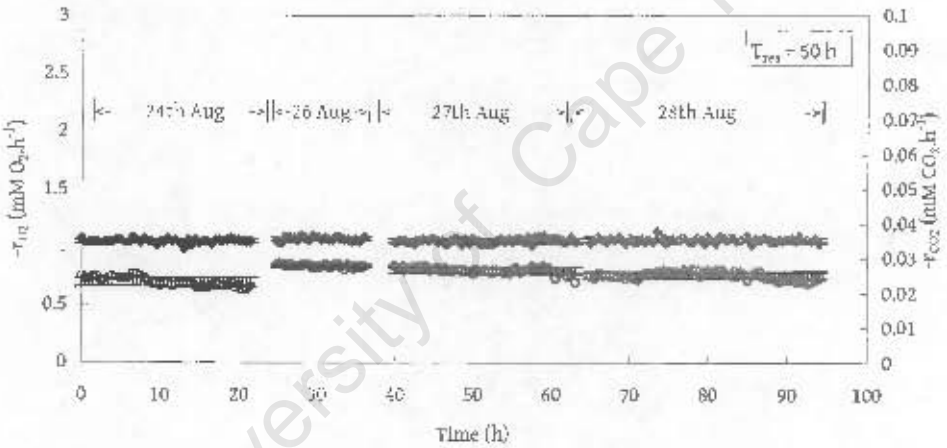

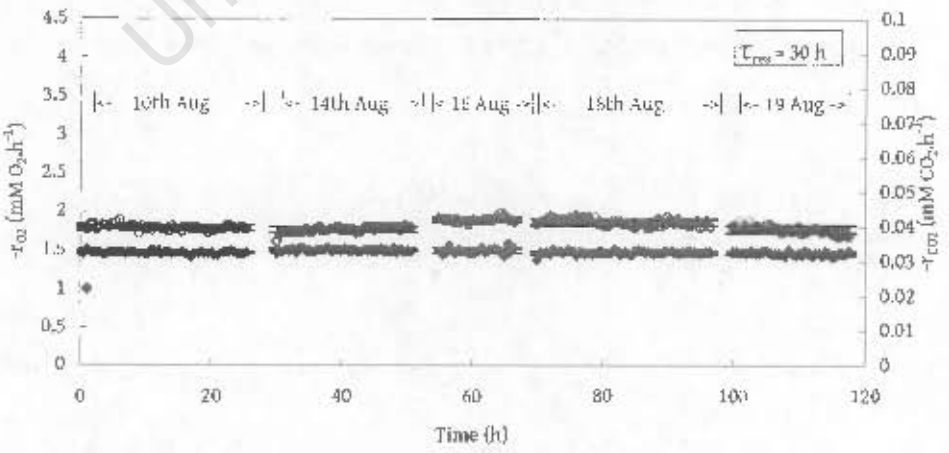

Figure B.4 Measured oxygen and carbon dioxide utilisation rate data determined for continuous iron oxidation. T = 70°C, pH = 1.5, $[Fe]_T$ = 210 mM, Run 2 (2004).

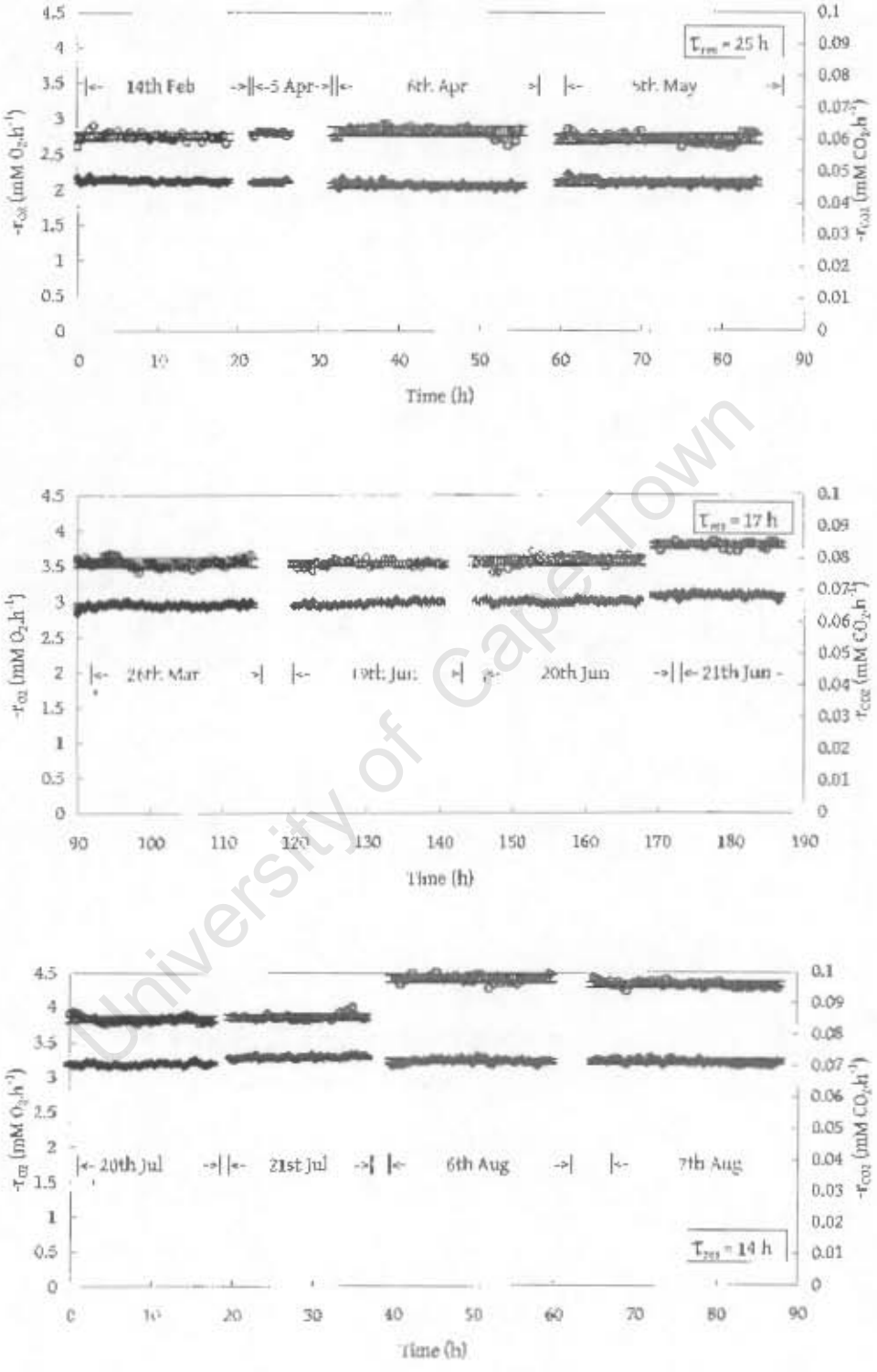

Figure B.4 **(continued)** Measured oxygen and carbon dioxide utilisation rate data determined for continuous iron oxidation. T = 70°C, pH = 1.5, $[Fe]_T$ = 210 mM, Run 2 (2004).

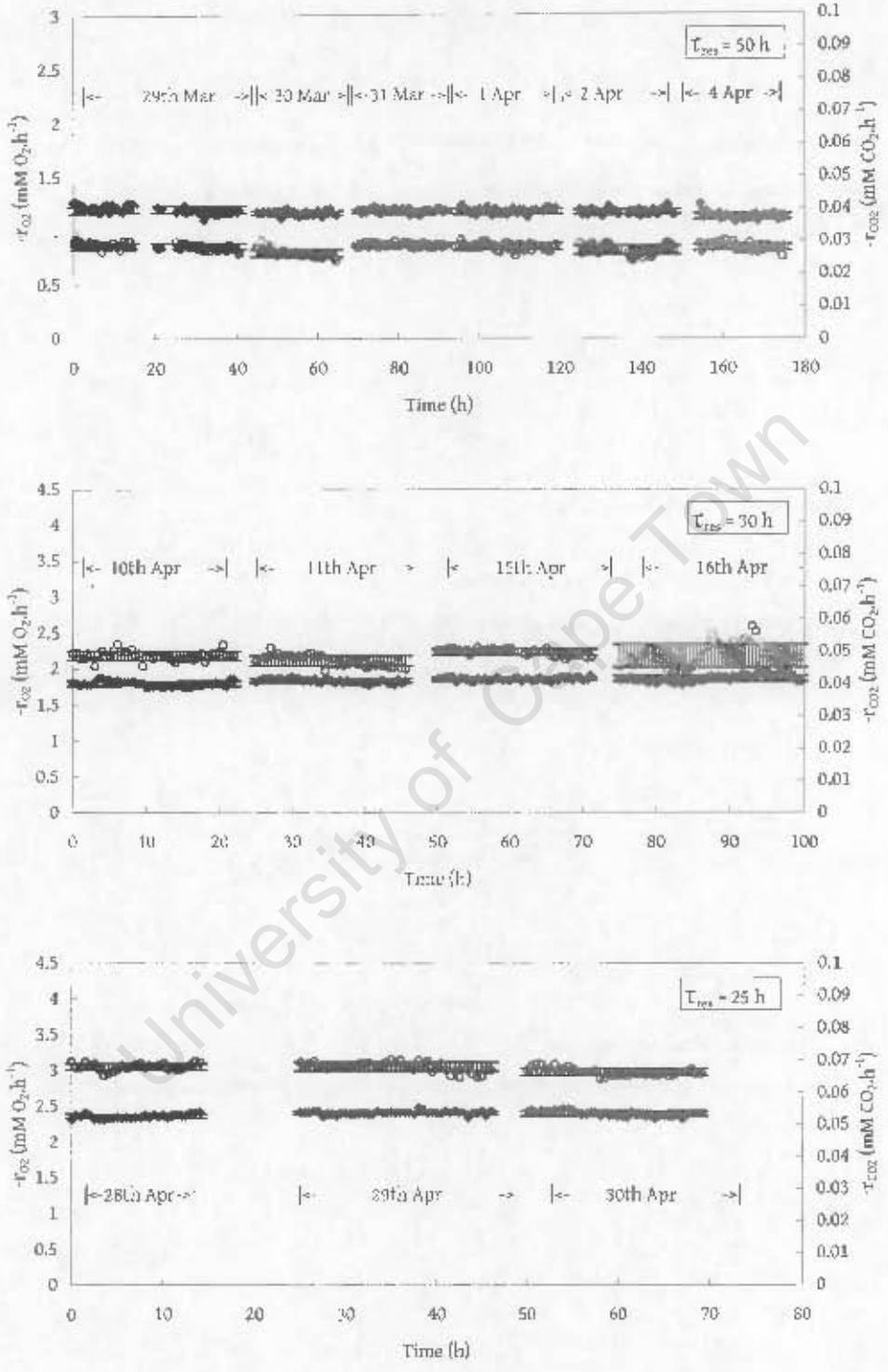

Figure B.5 Measured oxygen and carbon dioxide utilisation rate data determined for continuous iron oxidation. T = 75°C, pH = 1.5, $[Fe]_T$ = 210 mM, Run 1 (2002).

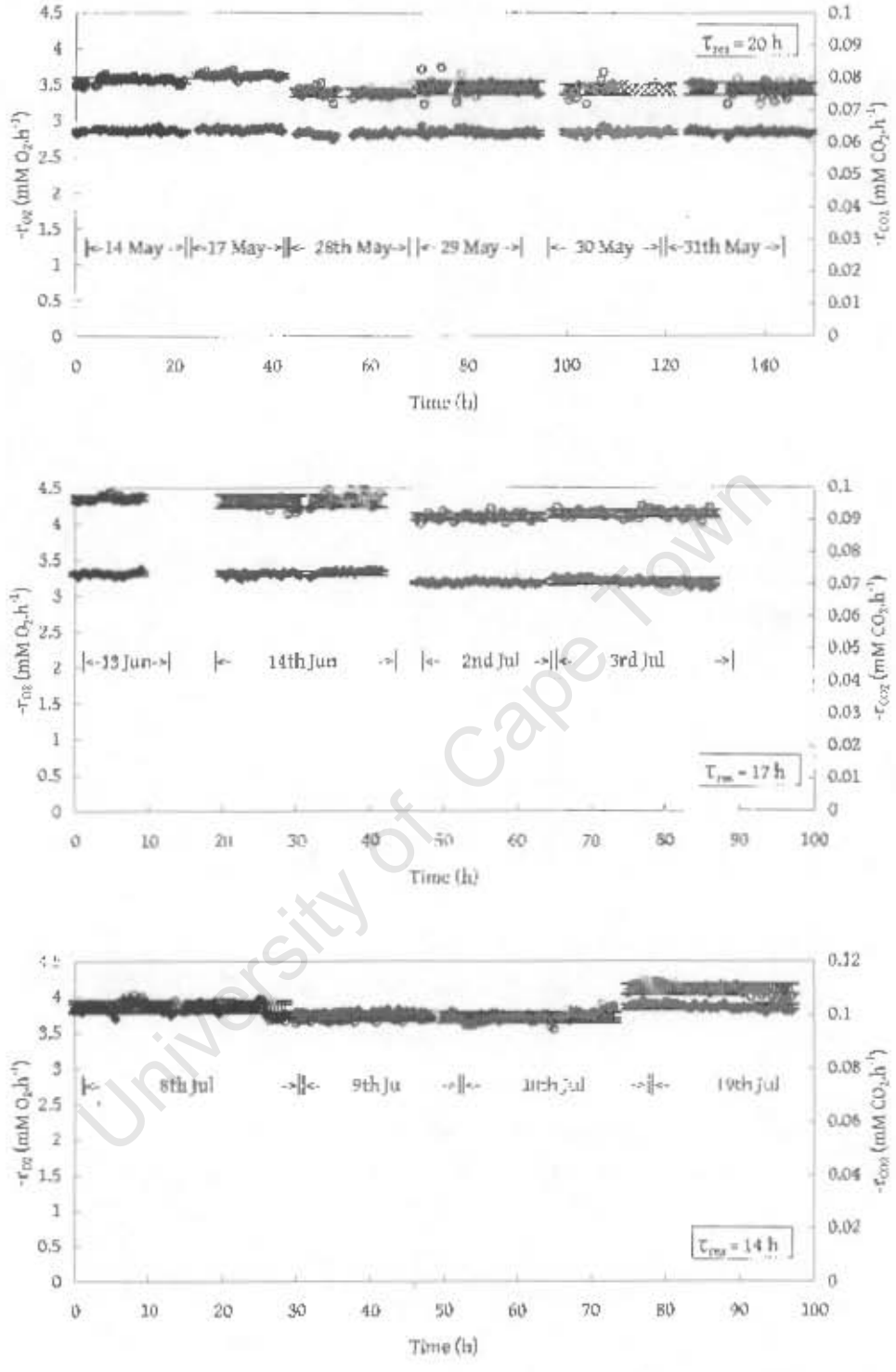

Figure B.5 **(continued)** Measured oxygen and carbon dioxide utilisation rate data determined for continuous iron oxidation. T = 75°C, pH = 1.5, $[Fe]_T$ = 210 mM, Run 1 (2002).

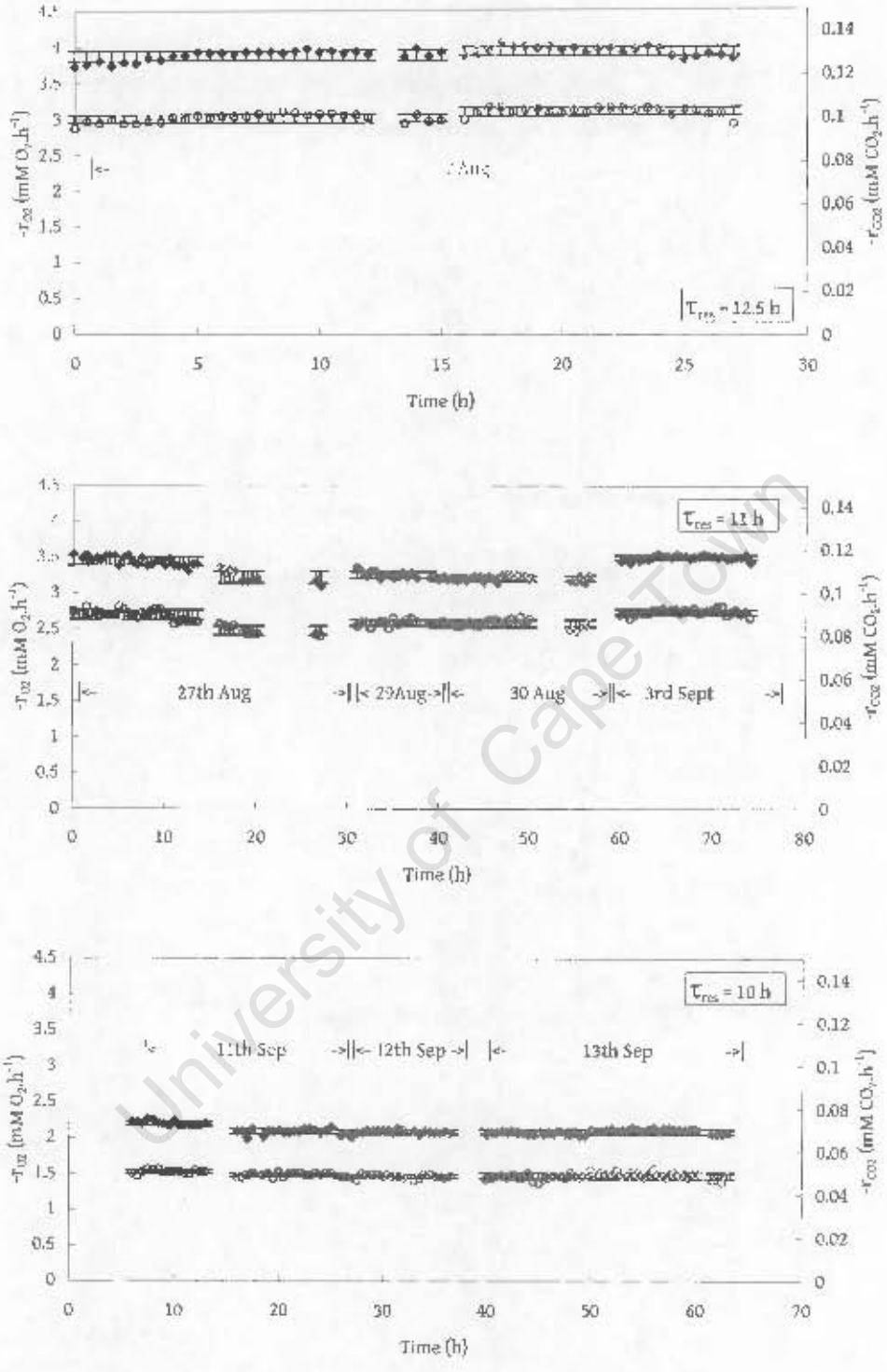

Figure B.5 **(continued)** Measured oxygen and carbon dioxide utilisation rate data determined for continuous iron oxidation. T = 75°C, pH = 1.5, $[Fe]_T$ = 210 mM, Run 1 (2002).

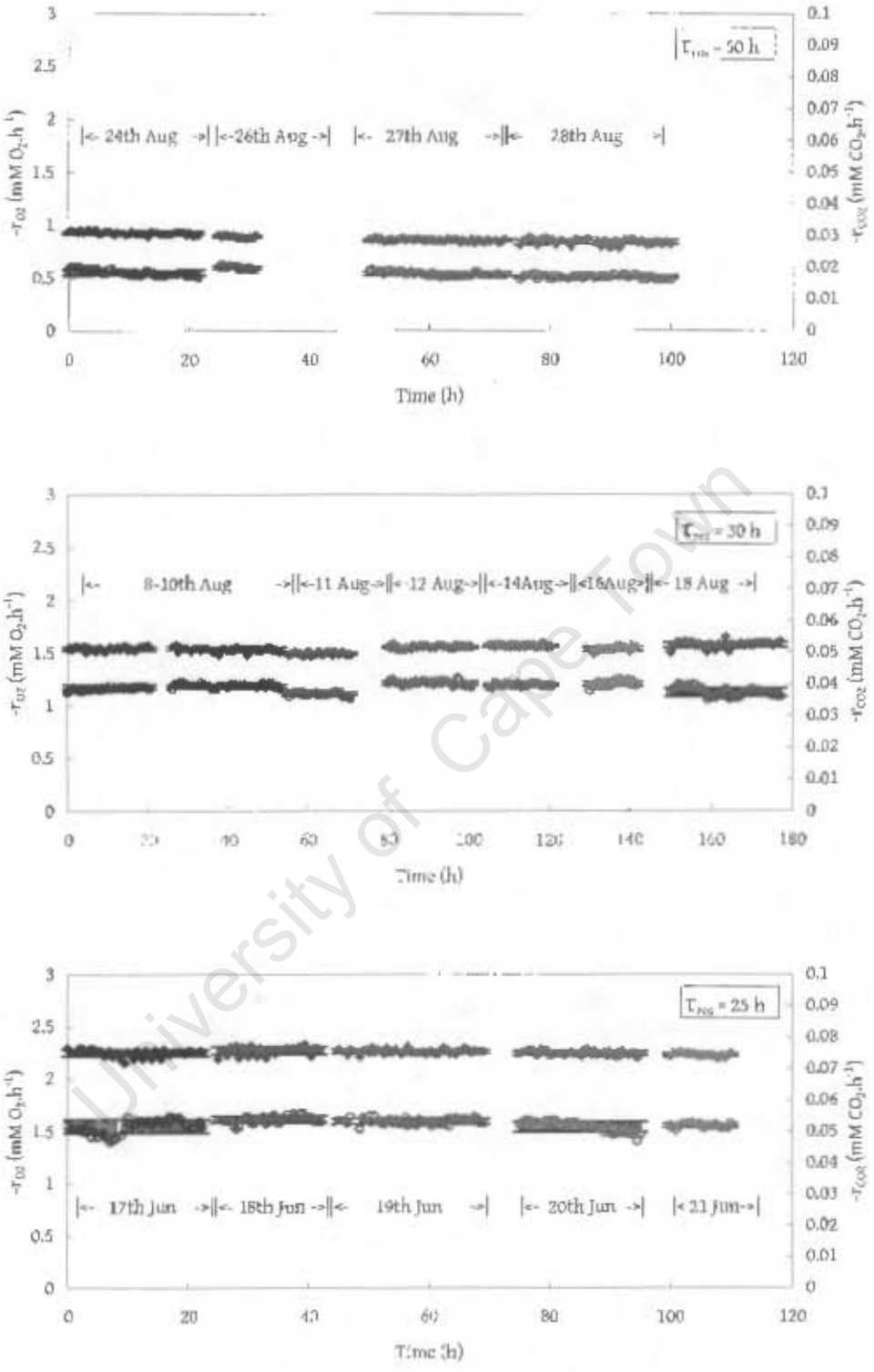

Figure B.6 Measured oxygen and carbon dioxide utilisation rate data determined for continuous iron oxidation. T = 80°C, pH = 1.5, $[Fe]_T$ = 210 mM, Run 2 (2004).

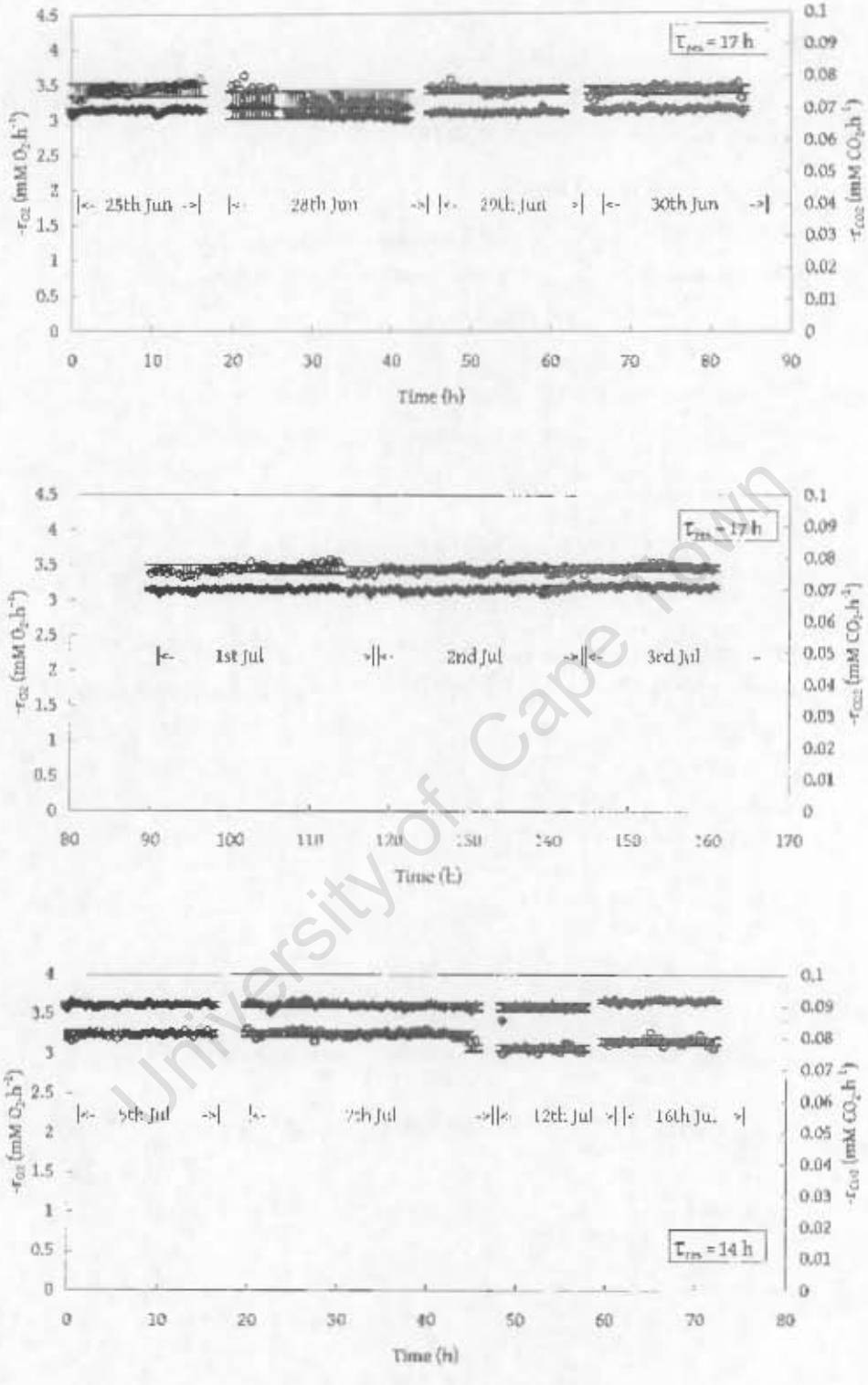

Figure B.6 **(continued)** Measured oxygen and carbon dioxide utilisation rate data determined for continuous iron oxidation. T = 80°C, pH = 1.5, $[Fe]_T$ = 210 mM, Run 2 (2004).

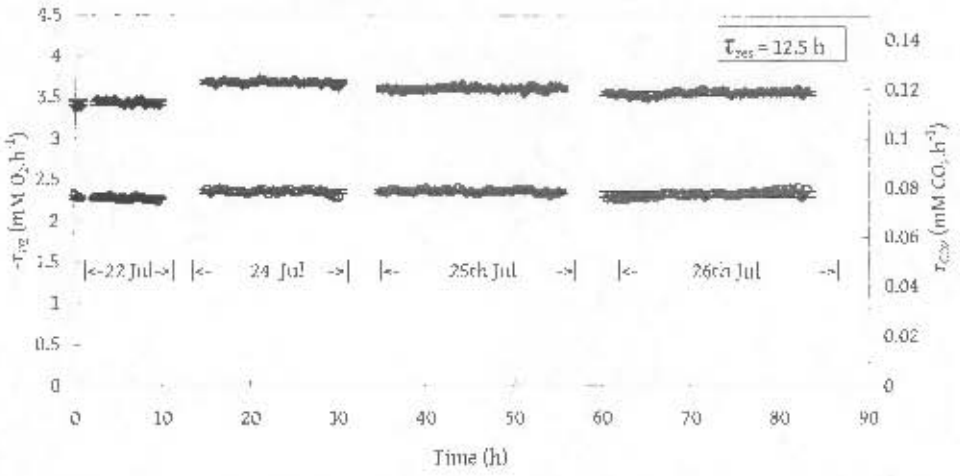

Figure B.6 **(continued)** Measured oxygen and carbon dioxide utilisation rate data determined for continuous iron oxidation. T = 80°C, pH = 1.5, $[Fe]_T$ = 210 mM, Run 2 (2004).

B.2 Tabulated Steady State Data

Each data point presented in Chapter 6 is the result of a continuous experiment in which the conditions are set and the system is allowed to attain steady state. The reaction conditions and the steady state data captured for each experiment are tabulated here.

Table B.1 Steady state data collected for a continuous reactor run at T = 60 °C, $[Fe^{2+}]_{IN}$ = 214mM, Run 2 (2004).

Date	Feed Rate ($L.h^{-1}$)	pH	Temp (degC)	Volume (L)	$-r_{O2}$ ($mMO_2.h^{-1}$)	$-r_{CO2}$ ($mMCO_2.h^{-1}$)	Eh (mV)	Fe(II) (mM)	Fe_T (mM)
24-Aug-04	1.957E-02	1.53		0.98	1.038	0.0333	622	0.90	199.68
26-Aug-04	1.955E-02	1.52		0.98	1.095	0.0374	622	0.90	201.47
27-Aug-04	1.953E-02	1.55		0.98	1.051	0.0355	628	0.90	204.15
28-Aug-04	1.952E-02	1.55		0.98	1.050	0.0346	630		202.01
14-Aug-04	2.712E-02	1.65		0.99	1.426	0.0507	630	0.90	204.15
15-Aug-04	2.696E-02	1.58		0.99	1.387	0.0470	620	0.90	206.84
16-Aug-04	2.699E-02	1.6		0.99	1.401	0.0496	620	0.90	205.05
18-Aug-04	2.700E-02	1.53		0.99	1.411	0.0509	614	0.90	212.21
19-Aug-04	2.700E-02	1.59		0.99	1.395	0.0490	621	0.90	199.68
16-Jun-04	3.772E-02	1.66	59.9	0.99	1.919	0.0578	584		198.78
17-Jun-04	3.788E-02	1.54	60	0.99	2.008	0.0615	574	11.64	198.78
18-Jun-04	3.788E-02	1.74	59.2	0.99	1.995	0.0621	580	8.95	187.14
19-Jun-04	3.781E-02	1.54	60.5	0.99	1.981	0.0599	582	6.09	193.41
21-Jun-04	3.775E-02	1.46	60.8	1	1.975	0.0602	577		196.99
22-Jun-04	3.840E-02	1.51	60.7	0.96	1.964	0.0605	572	8.42	195.20
23-Jun-04	3.839E-02	1.46	60.5	1	1.978	0.0617	584	6.09	192.51
24-Jun-04	3.788E-02	1.51	60.4	0.99	1.997	0.0611	587	6.45	179.08
25-Jun-04	3.784E-02	1.43	60.5	0.99	1.954	0.0579	588	6.09	176.40
27-Jun-04	3.765E-02	1.42	60.6	1	1.933	0.0587	581	6.09	190.72
28-Jun-04	3.736E-02	1.62	60.8	1	1.928	0.0562	559	10.03	183.56
29-Jun-04	3.815E-02	1.66	60.5	1	1.948	0.0574	575	8.06	189.83
30-Jun-04	3.823E-02	1.35	60.7	0.99	1.975	0.0580	579	10.03	197.89
01-Jul-04	3.833E-02	1.31	60.7	0.99	2.022	0.0614	584	6.98	201.47
02-Jul-04	3.814E-02	1.15	60.6	0.98	1.992	0.0602	592	6.09	196.10
03 Jul-04	3.846E-02	1.43	60.5	1	2.033	0.0633	590	6.45	196.99

Date	Feed Rate ($L.h^{-1}$)	pH	Temp (degC)	Volume (L)	$-r_{O_2}$ ($mMO_2.h^{-1}$)	$-r_{CO_2}$ ($mMCO_2.h^{-1}$)	Eh (mV)	Fe(II) (mM)	Fe_T (mM)
04-Aug-04	4.950E-02	1.52		1	2.202	0.0863	535	32.23	202.36
05-Aug-04	4.926E-02	1.69		1	2.323	0.0910	543		203.62
06-Aug-04	4.924E-02	1.63		1	2.355	0.0884	551	8.95	203.26
07-Aug-04	4.904E-02	1.51		1	2.343	0.0872	550	10.74	205.95
10-Aug-04	4.924E-02	1.61		0.985	2.116	0.0786	535		205.95
12-Aug-04	4.931E-02	1.61		1	2.324	0.0859	536	11.64	210.42
07-Jul-04	5.988E-02	1.47		0.98	1.839	0.0594	481		203.62
18-Jul-04	5.992E-02	1.52		0.99	1.772	0.0605	482	73.07	193.41
19-Jul-04	6.068E-02	1.5		0.99	1.778	0.0605	479	80.23	204.15
22-Jul-04	6.553E-02	1.33		0.99	1.408	0.0420	461	131.45	214.90
23-Jul-04	6.557E-02	1.3		0.99	1.279	0.0379	460		214.90
24-Jul-04	6.460E-02	1.5		1	1.259	0.0364	452	128.94	214.90
26-Jul-04	6.472E-02	1.47		1	1.302	0.0397	453		214.90

Table B.2 Steady state data collected for a continuous reactor run at T = 65 °C, $[Fe^{2+}]_{in}$ = 214mM, Run 1 (2002).

Date	Feed Rate ($l.h^{-1}$)	pH	Temp (degC)	Volume (L)	$-r_{O_2}$ ($mMO_2.h^{-1}$)	$-r_{CO_2}$ ($mMCO_2.h^{-1}$)	Eh (mV)	Fe(II) (mM)	Fe_T (mM)
29-Mar-02	2.000E-02	1.49	65.1	1	1.133	0.0321	673		196.99
30-Mar-02	2.000E-02	1.5	64.8	1	1.089	0.0291	682		196.99
31 Mar 02	2.000E-02			1	1.079	0.0280	680		196.99
04-Apr-02	1.980E-02	1.57	64.8	1	1.023	0.0286	645	2.51	201.47
10-Apr-02	3.096E-02	1.52	64.8	1	1.748	0.0519	616	2.51	180.87
11-Apr-02	3.145E-02	1.54	64.8	1	1.747	0.0524	652		196.99
15-Apr-02	3.174E-02	1.49	64.9	1	1.726	0.0530	623	3.58	196.99
16 Apr 02	3.175E 02	1.49	64.8	1	1.739	0.0516	640		196.99
28-Apr-02	4.000E-02	1.58	64.8	1	2.241	0.0718	598	3.94	196.99
29-Apr-02	4.000E-02	1.54	64.7	1	2.259	0.0711	608	4.48	197.89
30-Apr-02	4.016E-02	1.52	65	1	2.268	0.0710	607	3.94	196.10
03 May-02	4.854E-02	1.52	64.8	1	2.677	0.0816	577		196.99
06-May-02	4.808E-02	1.56	64.9	0.99	2.680	0.0805	574		196.99
17-May-02	5.025E-02	1.54	64.9	1	2.771	0.0837	573		196.99
22-May-02	5.025E-02	1.56	64.8	1	2.833	0.0838	577		196.99
28-May-02	5.025E-02	1.51	64.9	1.005	2.833	0.0838	576	9.85	200.57
29-May 02	5.000E 02	1.53	64.9	1	2.691	0.0775	567	14.33	201.47
30-May-02	5.000E-02	1.53	64.7	0.97	2.742	0.0810	578	9.85	200.57
27-Jun-02	5.882E-02	1.53	65.2	0.985	3.011	0.0958	580		196.99
28-Jun-02	5.848E-02	1.5	65.1	0.985	3.047	0.0969	580		196.99
02 Jul-02	5.848E-02	1.54	65.1	1	3.038	0.0958	560		196.99
07-Aug-02	7.143E 02	1.54		1	2.276	0.0753	478		196.99
08-Aug-02	7.097E-02	1.58	65	1	2.269	0.0769	486		196.99
11-Aug-02	7.143E-02	1.55	64.8	1	2.510	0.0807	485	82.38	196.99
17-Aug-02	7.143E-02	1.52	64.7	1	2.385	0.0759	485		196.99

Table B.3 Steady state data collected for a continuous reactor run at T = 70 °C, $[Fe^{2+}]_{in}$ = 214mM, Run 1 (2002).

Date	Feed Rate ($L.h^{-1}$)	pH	Temp (degC)	Volume (L)	$-r_{O2}$ ($mMO_2.h^{-1}$)	$-r_{CO2}$ ($mMCO_2.h^{-1}$)	Eh (mV)	Fe(II) (mM)	Fe_T (mM)
29-Mar-02	2.000E-02	1.54	70.3	1	1.037	0.0279	643		200.57
02-Apr-02	1.969E-02	1.43	69.9	1	1.046	0.0269	652		200.57
04-Apr-02	2.000E-02	1.44	69.6	1	1.003	0.0262	654	2.51	198.78
10-Apr-02	3.226E-02	1.52	69.8	1	1.800	0.0519	637	2.51	185.35
15-Apr-02	3.300E-02	1.48	70	1	1.824	0.0529	640	2.51	188.93
28-Apr-02	4.098E-02	1.51	70.1	1	2.317	0.0689	625	3.04	197.89
29-Apr-02	4.098E-02	1.54	70.2	1	2.362	0.0705	630	3.04	189.83
30-Apr-02	4.115E-02	1.52	70.1	1	2.332	0.0685	632	3.04	191.62
14-May-02	4.878E-02	1.49	70	1	2.894	0.0847	627	3.58	195.20
28-May-02	4.975E-02	1.5	70	0.98	2.897	0.0833	627	3.58	193.41
29-May 02	4.878E-02	1.52	69.9	0.98	2.887	0.0835	625	3.58	200.57
30-May-02	4.902E-02	1.51	70	0.975	2.893	0.0836	640	3.58	193.41
14-Jun-02	5.917E-02	1.5	69.8	1	3.209	0.0957	605		200.57
02-Jul-02	5.917E-02	1.51		1	3.060	0.0928	607		200.57
11-Aug-02	7.174E-02	1.57	69.9	1	2.279	0.0645	492	46.02	214.90
12-Aug-02	7.092E-02			1	2.290	0.0641	492	51.76	214.90
26-Aug-02	7.937E-02	1.65	69.6	1	2.521	0.0733	494	103.87	207.74
26-Aug-02	7.937E-02	1.55	69.5	1	2.540	0.0742	495	90.44	207.74
27-Aug-02	7.937E-02	1.59		1	2.042	0.0608	484	113.72	202.36
29-Aug-02	7.874E-02	1.57	69.4	1	1.949	0.0566	482	116.40	209.53
02-Sep-02	7.874E-02	1.55	69.2	1	2.506	0.0704	503	110.14	214.90

Table B.4 Steady state data collected for a continuous reactor run at T = 70 °C, $[Fe^{2+}]_{IN}$ = 234mM, Run 2 (2004).

Date	Feed Rate ($L.h^{-1}$)	pH	Temp (degC)	Volume (L)	$-r_{O2}$ ($mMO_2.h^{-1}$)	$-r_{CO2}$ ($mMCO_2.h^{-1}$)	Eh (mV)	Fe(II) (mM)	Fe_T (mM)
24 Aug 04	2.026E-02	1.52		0.985	1.047	0.0232	652	0.90	198.78
26-Aug-04	2.023E-02	1.56		0.99	1.068	0.0278	650	0.90	202.36
27-Aug-04	2.024E 02	1.57		0.99	1.054	0.0266	650	0.90	202.36
28 Aug 04	2.024E-02	1.56		0.99	1.063	0.0255	650		202.36
10-Aug-04	2.873E-02	1.55		1	1.461	0.0397	643		189.83
14-Aug-04	2.879E-02	1.59		0.99	1.495	0.0391	640	0.90	214.00
16-Aug-04	2.880E-02	1.55		1.005	1.488	0.0420	649	0.90	198.78
18-Aug-04	2.881E 02	1.51		1	1.465	0.0413	655	0.90	200.57
19-Aug-04	2.897E-02	1.55		1	1.453	0.0394	654	0.90	202.36
14-Feb-04	3.975E-02	1.6	70.1	0.99	2.125	0.0611	627	3.58	166.55
05-Apr-04	3.891E-02	1.42	69.9	1	2.107	0.0621	624	3.58	188.93
06-Apr-04	3.932E 02	1.46	69.9	1	2.058	0.0627	627	3.58	188.04
05-May-04	3.976E-02	1.62	70.1	1	2.094	0.0603	635		189.83
13-Feb-04	5.656E 02	1.55	70.3	1	3.090	0.0973	609	6.27	168.34
14 Feb 04	5.882E-02	1.64	70.3	1	3.077	0.0949	607	3.58	166.55
21-May-04	5.848E-02	1.59	70.3	1	3.045	0.0838	628	5.37	166.55
25-May-04	5.770E-02	1.57	69.8	1	3.006	0.0844	627		195.20
26 May 04	5.388E-02	1.6	70.2	1	2.947	0.0789	607	8.95	195.20
19-Jun-04	5.917E-02	1.6	70.2	0.98	2.971	0.0785	580	7.52	186.25
20-Jun-04	5.841E 02	1.41	70.3	0.98	2.990	0.0793	590	5.55	190.72
21-Jun-04	5.938E-02	1.59	69.9	1	3.073	0.0842	594		189.83
20 Jul 04	7.317E-02	1.49		1	3.189	0.0851	527	32.95	215.80
21-Jul-04	7.174E-02	1.49		1	3.285	0.0858	524	60.53	179.08
06-Aug-04	7.077E 02	1.55		1	3.225	0.0981	559		193.41
07-Aug-04	7.062E-02	1.58		1	3.211	0.0961	560		193.41

Table B.5 Steady state data collected for a continuous reactor run at T = 75 °C, $[Fe^{2+}]_{IN}$ = 214mM, Run 1 (2002).

Date	Feed Rate ($L.h^{-1}$)	pH	Temp (degC)	Volume (L)	$-r_{O_2}$ ($mMO_2.h^{-1}$)	$-r_{CO_2}$ ($mMO_2.h^{-1}$)	Eh (mV)	Fe(II) (mM)	Fe_T (mM)
29-Mar-02	2.000E-02	1.5	75.1	1	1.201	0.0286	649		188.04
30-Mar-02	2.000E-02	1.49	75.4	1	1.169	0.0264	655		188.04
31-Mar-02	2.000E-02			1	1.185	0.0288	670		188.04
01-Apr-02	2.039E-02	1.45	75.3	1	1.183	0.0284	650	2.51	188.04
02-Apr-02	2.088E-02	1.5	69.7	1	1.175	0.0272	649	2.51	188.04
04-Apr-02	2.000E-02	1.47	74.8	1	1.130	0.0280	635	2.51	188.93
10-Apr-02	3.165E-02	1.5	74.9	1	1.795	0.0485	679	3.04	188.04
11-Apr-02	3.215E-02	1.5	75	1	1.836	0.0469	663		188.04
15-Apr-02	3.268E-02	1.44	75	1	1.858	0.0496	631	3.04	181.77
16-Apr-02	3.300E-02	1.45	74.9	1	1.867	0.0485	662	3.04	190.72
28-Apr-02	4.000E-02	1.47	75	1	2.359	0.0679	616	3.04	185.35
29-Apr-02	4.000E-02	1.51	74.7	1	2.409	0.0679	625	6.09	182.66
30-Apr-02	4.049E-02	1.52	74.9	1	2.397	0.0663	620		187.14
14-May-02	5.051E-02	1.48	75	1	2.862	0.0792	619	5.37	184.46
17-May-02	5.051E-02	1.49	75.2	1	2.882	0.0807	612	4.30	188.04
28-May-02	5.025E-02	1.53	75	1	2.820	0.0753	619	4.48	192.51
29-May-02	4.950E-02	1.58	75.2	1	2.836	0.0769	626		190.72
30-May-02	5.071E-02	1.5	74.9	1	2.840	0.0764	631	6.27	192.51
31-May-02	5.000E-02	1.5	74.9	1	2.840	0.0766	622		192.51
13-Jun-02	5.917E-02	1.5	75.4	1	3.303	0.0964	620		196.10
14-Jun-02	5.952E-02	1.46	75.4	1	3.311	0.0959	601		196.99
02-Jul-02	5.714E-02	1.46	74.9	1	3.177	0.0909	604		196.99
03-Jul-02	5.714E-02	1.53	75.4	1.01	3.187	0.0919	605		196.99
08-Jul-02	7.143E-02	1.47	75.5	1	3.839	0.1032	592		214.90
09-Jul-02	7.194E-02	1.49	75.9	1	3.779	0.0984	609		214.90
10-Jul-02	7.194E-02	1.45	75.7	1	3.738	0.0990	571		214.90
19-Jul-02	7.092E-02	1.52	75.1	1	3.859	0.1095	580		214.90

Date	Feed Rate ($L.h^{-1}$)	pH	Temp (degC)	Volume (L)	$-r_{O2}$ ($mMO_2.h^{-1}$)	$-r_{CO2}$ ($mMCO_2.h^{-1}$)	Eh (mV)	Fe(II) (mM)	Fe_T (mM)
07-Aug-02	7.752E-02	1.51	74.3	1	3.882	0.1003	552	37.07	214.90
07-Aug-02	7.634E-02			1	3.928	0.1031	555	43.52	214.90
27-Aug-02	8.850E-02	1.51	74.5	1.015	3.222	0.0825	498		212.21
29 Aug 02	8.850E-02	1.57	74.6	1	3.254	0.0861	502	32.41	206.84
30-Aug-02	8.772E-02	1.58	74.7	1	3.207	0.0858	496	76.83	214.90
03-Sep-02	8.850E-02	1.52	74.7	1	3.495	0.0912	503		196.10
11-Sep-02	9.901E-02	1.54	74.7	1	2.198	0.0509	460		213.11
11-Sep-02	9.901E-02	1.56	74.7	1	2.090	0.0496	458		214.90
12 Sep 02	9.901E-02	1.54	74.7	1	2.080	0.0489	457		214.90
13-Sep-02	9.901E-02	1.55	74.6	1	2.088	0.0492	457		214.90

Table B.6 Steady state data collected for a continuous reactor run at T = 80 °C, $[Fe^{2+}]_{IN}$ = 214mM, Run 2 (2004).

Date	Feed Rate ($L.h^{-1}$)	pH	Temp (degC)	Volume (L)	$-r_{O2}$ ($mMO_2.h^{-1}$)	$-r_{CO2}$ ($mMCO_2.h^{-1}$)	Eh (mV)	Fe(II) (mM)	Fe_T (mM)
24 Aug 04	1.923E-02	1.48		0.97	0.928	0.0185	640	0.90	193.41
26-Aug-04	1.986E-02	1.52		0.97	0.894	0.0201	646	0.90	179.98
27-Aug-04	1.923E-02	1.5		0.97	0.860	0.0180	648	0.90	179.08
28-Aug-04	1.901E-02	1.46		1	0.843	0.0170	646		179.08
10 Aug 04	3.052E-02	1.51		0.98	1.535	0.0393	635		179.08
11-Aug-04	3.047E-02	1.51		0.98	1.489	0.0370	636	1.43	179.98
12-Aug-04	3.037E-02	1.53		0.98	1.551	0.0404	637	1.07	179.08
14-Aug-04	3.016E-02	1.56		0.98	1.571	0.0400	639	1.25	182.66
16-Aug-04	2.973E-02	1.53		0.98	1.531	0.0401	644	0.90	196.10
18 Aug-04	2.970E-02	1.49		0.98	1.568	0.0373	639	0.90	196.99
17-Jun-04	4.259E-02	1.5	80.2	0.93	2.248	0.0515	624	3.58	170.13
18 Jun-04	4.228E-02	1.62	80.2	0.95	2.273	0.0538	623	3.58	165.65

Date	Feed Rate ($l.h^{-1}$)	pH	Temp (degC)	Volume (L)	$-r_{O2}$ ($mMO_2.h^{-1}$)	$-r_{CO2}$ ($mMCO_2.h^{-1}$)	Eh (mV)	Fe(II) (mM)	Fe_t (mM)
19-Jun-04	4.225E-02			0.95	2.262	0.0532	626	3.04	171.92
20-Jun-04	4.203E-02	1.4	79.9	0.95	2.244	0.0514	623	3.58	195.20
21-Jun-04	4.219E-02	1.42		0.95	2.230	0.0517	627		179.08
25-Jun 04	6.173E 02	1.43	80.3	0.99	3.144	0.0763	624	6.98	171.92
28-Jun-04	5.757E-02	1.58	80.2	0.99	3.095	0.0732	627	8.06	161.17
29-Jun-04	6.135E-02	1.55	80.1	0.99	3.105	0.0759	610	9.13	172.82
30-Jun-04	6.139E-02	1.33	80	1	3.143	0.0759	610	12.00	195.20
01-Jul-04	6.105E-02	1.31	79.8	1	3.154	0.0765	609	15.04	196.10
02-Jul-04	6.150E-02	1.2	80	0.985	3.145	0.0763	610	11.46	187.14
03-Jul-04	6.112E-02	1.47	79.8	0.98	3.187	0.0767	609	8.06	188.04
05-Jul-04	7.158E-02			0.99	3.616	0.0812	581	16.48	188.93
07-Jul-04	7.168E-02	1.5		0.99	3.615	0.0813	588		188.04
12-Jul-04	7.289E-02	1.5		1	3.584	0.0767	577	13.07	184.46
16-Jul-04	7.205E 02	1.55		1	3.665	0.0789	579	15.94	189.83
22-Jul 04	7.813E-02	1.39		0.96	3.436	0.0759	541	44.95	202.36
24-Jul-04	8.170E-02	1.55		0.96	3.684	0.0785	545	33.13	195.20
25-Jul-04	8.170E-02	1.61		0.96	3.611	0.0786	530		196.99
26-Jul-04	8.237E-02	1.53		0.96	3.560	0.0775	529	38.50	196.99
03-Aug-04	9.775E-02	1.45		1	3.436	0.0947	509	63.57	193.41
04-Aug-04	9.775E 02	1.54		0.99	3.424	0.0965	500	69.84	193.41
05-Aug-04	9.785E 02	1.6		1	3.428	0.0996	504	63.57	191.62
05-Aug-04	9.785E 02	1.55		0.99	3.513	0.0999	514	48.35	190.72
06-Aug-04	9.814E-02	1.51		0.99	3.586	0.1016	518	51.93	194.31

Table B.7 Steady state data collected for a continuous reactor run at T = 70 °C, τ_{res} = 17h, varying feed iron concentration. (2003).

Date	Feed Rate	pH	Temp	Volume	$-r_{O_2}$	$-r_{FeII}$	Eh	Fe(II)	Fe_T
	($L.h^{-1}$)		(°C)	(L)	($mMO_2.h^{-1}$)	($mMO_2.h^{-1}$)	(mV)	(mM)	(mM)
06 Jun-03	215	1.52	70.1	1	3.063	0.085	607	5.01	195.20
07 Jun-03	215	1.63	69.8	1	3.063	0.086	618	3.94	193.41
09 Jun-03	215	1.48	70	1	3.035	0.084	610	3.94	196.99
13 Jun-03	107	1.51	69.9	1	1.44	0.043	625	2.51	102.08
14 Jun 03	107	1.5	70.2	1	1.44	0.039	626	3.04	99.39
15 Jun 03	107	1.51	69.9	1	1.45	0.039	621	1.97	104.76
19-Jun-03	54	1.49	69.8	1	0.703	0.023	638	1.43	55.52
20-Jun-03	54	1.47	70	1	0.73	0.024	636	1.43	57.31
21-Jun-03	54	1.53	69.9	1	0.767	0.026	635	1.43	55.52

Appendix C

Kinetic Constants

As discussed in Section 6.3.1, a number of rate equations were examined to determine which would describe the observed data most effectively. The kinetic constants determined by regression for each data set in Figure 6.14.

C.1 Monod Equation

$$q_{Fe^{2+}} = \frac{q_{Fe^{2+}}^{max}}{\frac{K_S}{[Fe^{2+}]} + 1} \qquad [C.1]$$

Table C.1 Kinetic constants for the Monod equation (C.1).

Temperature (°C)	q_{max} (molFe^{2+}.(molC.h^{-1}))	K_s (mM Fe^{2+})	R^2
60	5.96	1.36	0.85
65	8.52	3.16	0.89
70	11.31	3.92	0.86
75	14.56	4.99	0.89
80	17.25	7.25	0.84

C.2 Competitive Inhibition

$$q_{Fe^{2+}} = \frac{q_{Fe^{2+}}^{max}}{\frac{K_S}{[Fe^{2+}]} + \frac{K_S [Fe^{3+}]}{K_I [Fe^{2+}]} + 1} \qquad [C.2]$$

Table C.2 Kinetic constants for the competitive inhibition model (Equation 2.8).

Temperature (°C)	q_{max} (molFe^{2+}.(molC.h^{-1}))	K_s (mM Fe^{2+})	K_I (mM Fe^{3+})	R^2
60	5.92	6.84×10^{-3}	0	0.85
65	8.52	0	3.16	0.89
70	11.11	2.01×10^{-2}	0	0.86
75	14.56	0	4.99	0.89
80	16.79	3.91×10^{-2}	0	0.84

C.3 Substrate Inhibition

$$q_{Fe^{2+}} = \frac{q^{max}_{Fe^{2+}}}{1 + K_{Fe^{2+}} \frac{[Fe^{3+}]}{[Fe^{2+}]} + \frac{[Fe^{2+}]}{K_{SI}}} \quad [C.3]$$

Table C.3 Kinetic constants for the substrate inhibition equation (C3).

Temperature (°C)	q_{max} ($molFe^{2+}.(molC.h^{-1})$)	K_{Fe2+} (-)	K_{SI} (mM Fe^{3+})	R^2
60	6.88	0.0107	391	0.87
65	8.41	0.0159	23092	0.89
70	13.61	0.0300	354	0.89
75	16.98	0.0352	517	0.88
80	48.78	0.176	27	0.93

C.4 Meruane *et al.*, 2002

$$q_{Fe^{2+}} = \frac{q_{max} - K_2 \frac{[Fe^{3+}]}{[Fe^{2+}]}}{1 + \frac{K_S}{[Fe^{2+}]} + K_1 \frac{[Fe^{3+}]}{[Fe^{2+}]}} \quad [2.15]$$

Table C.4 Kinetic constants for Equation 2.15 (Meruane *et al.*, 2002).

Temperature (°C)	q_{max} ($molFe^{2+}.(molC.h^{-1})$)	K_1	K_S	K_2 (-)	R^2
60	6.07	8.74×10^{-4}	0	0.024	0.92
65	8.38	1.57×10^{-2}	1	0	0.89
70	10.74	4.33×10^{-3}	0	0.079	0.90
75	14.07	250	3.49	0.070	0.88
80	15.60	0	0	0.250	0.94

Appendix D

Calculation of the Theoretical Yield

For thermophilic ferrous iron oxidation, the Gibbs free energy of reaction of Equation 4.16: the macrochemical balance written per mole of biomass formed (solving the element and charge balances in Table 4.4)

$$CO_2 + 0.2NH_4^+ + \left[\frac{1-4.2Y_{SX}}{4Y_{SX}}\right]O_2 + \frac{1}{Y_{SX}}Fe^{2+} + \left[\frac{1}{Y_{SX}} - 0.2\right]H^+ \rightarrow CH_{1.8}O_{0.5}N_{0.2} + \frac{1}{Y_{SX}}Fe^{3+} + \left[\frac{1}{2Y_{SX}} - 0.6\right]H_2O \qquad [4.16]$$

is equal to the energy dissipated per mole of biomass, which for systems performing reverse electron transport across the cell membrane is equal to 3500 kJ.molC^{-1}

$$\Delta G_R - \sum_{i=0}^{i} a_i \Delta G_{fi}^{o} = -\left(\frac{D_S^{01}}{r_X}\right) = -3500 \qquad [4.22]$$

Where ΔG_R = Gibbs free energy of reaction
ΔG_{fi}^{o} = Gibbs free energy of formation of component *i* under standard conditions
a_i = the stoichiometric coefficient of component *i* in the macrochemical balance

Table D.1 Gibbs energy of formation (aqueous pH=7) in thermodynamic reference.

Compound	ΔG^o_f	Stoichiometric coefficient
CO_2	-394.359	-1
NH_4^+	-79.37	-0.2
O_2	0	$-[(1-4Y_{SX})/4Y_{SX}]$
Fe^{2+}	78.87	$-1/Y_{SX}$
H^+	-39.87	$-[1/Y_{SX}-0.2]$
$CH_{1.8}O_{0.5}N_{0.2}$	-237.18	1
Fe^{3+}	-4.6	$1/Y_{SX}$
H_2O	-237.18	$1/(2Y_{SX})-0.6$

Solving Equation 4.22 for Y_{SX}^{max} under standard conditions (T = 25°C, liquid concentrations = 1 M, gas partial pressures = 1 atm) yields,

Y_{SX}^{max} = 0.011 molC.(mol Fe^{2+})$^{-1}$.